Contribution to the study of mechanical behaviour and the durability of multi-material wood-concrete structures with glued joints

Mohammed Shehada

RÉPUBLIQUE FRANÇAISE
Liberté Égalité Fraternité

Université de Toulouse

Doctorat de l'Université de Toulouse

préparé à l'INSA Toulouse

Contribution à l'étude du comportement mécanique des structures bois-béton avec joints collés

---

Thèse présentée et soutenue, le 12 juillet 2024 par

Mohammed SHEHADA

École doctorale
MEGEP - Mécanique, Energétique, Génie civil, Procédés

Spécialité
Génie civil

Unité de recherche
LMDC - Laboratoire Matériaux et Durabilité des Constructions de Toulouse

Thèse dirigée par
Frederic DUPRAT et Zakaria Ilyes DJAMAI

Composition du jury
Mme Evelyne TOUSSAINT, Présidente, Université Clermont Auvergne
M. David BIGAUD, Rapporteur, University of Angers
M. Abdelhamid BOUCHAIR, Rapporteur, Université Clermont Auvergne
Mme Francesca LANATA, Examinatrice, Ecole Superieure du Bois
M. Yannick SIEFFERT, Examinateur, Université Grenoble Alpes
M. Anaclet TURATSINZE, Examinateur, Université Toulouse III - Paul Sabatier
M. Frederic DUPRAT, Directeur de thèse, INSA Toulouse
M. Zakaria Ilyes DJAMAI, Co-directeur de thèse, INSA Toulouse

Membres invités
Mme Caroline Morin, GA Smart Building
M. Husam WADI, Grundig Akademie

Abstract

English version

This thesis explores the mechanical behaviour of adhesively bonded TCC joints and beams Through experimental and numerical investigations.

The mechanical behaviour of the adhesively bonded joints between timber (GL24h) and self-compacting concrete (SCC) set by the dry or wet bonding process is investigated. For this purpose, double push-out shear tests on TCC joints bonded by epoxy resin of adhesives were performed. Several variables were considered for both fabrication processes. These parameters were: variation of moisture content (MC.) of timber, adhesive type, adhesive thickness, sand addition, concrete surface treatment, and scale of bonding length. The results showed that glueing seems to be a feasible alternative to mechanical means for producing dry and wet TCC joints. Under dry conditions of timber elements, the shear strength can be considered highly satisfactory, with a mean value range of 6-8MPa. The failure mode is primarily affected by concrete and timber failure. However, the findings confirm the hypothesis that increasing the moisture content of the timber before the glueing process significantly reduces the shear strength of adhesively bonded TCC joints by approximately 30% in certain instances.

An experimental investigation of the failure characteristics, interface slip, strain distribution, and load-deflection response of adhesively bonded timber-concrete composite (TCC) beams fabricated using wet or dry processes was conducted. A total of six full-scale adhesively bonded TCC beams were produced with a span of 3.2 m and subjected to four-point bending tests. Wet and dry fabricated TCC beams revealed distinct failure modes. The results emphasized the critical role of bonding integrity in ensuring effective composite action and shared contribution mechanism. Wet-fabricated TCC beams exhibited a rigid bonding characterized by a consistent neutral axis alignment and load distribution along the beam span, while dry-fabricated beams experienced interface separation and compromised load-shared contribution, resulting in a significant reduction of the ultimate bending capacity of TCC beams. The outcomes showed that wet and dry TCC beams exhibited comparable load-to-mid-span deflection responses before failure, highlighting uniform behaviour and alignment with fully composite characteristics under the imposed loads.

Furthermore, an analytical model for calculating TCC beams is presented and validated. The foundation of the analytical model is established upon the γ-method derived from Eurocode 5. The analytical model is compared with experimental results, highlighting its reliability and precision. Load-deflection responses, bending strain distributions, and ultimate failure loads are accurately captured, affirming the model's capability to anticipate the TCC beam behaviour.

Additionally, a 3D non-linear Finite Element (FE) model for adhesively bonded Timber-Concrete Composite (TCC) beams is presented. The model analyzes the deformation behaviour, bending stress distribution, ultimate capacity, and failure characteristics of TCC beams. Despite the challenges that arose in cases of bonding failure, leading to exceptional deviations in behaviour, the results revealed a remarkable agreement between the predictions of the FE model and the outcomes of experimental tests. The FE model accurately predicted the degree of composite action. Notably, the FE model and analytical model based on the γ-method exhibit comparable predictive performance in terms of deformation. Bending stress distribution findings highlighted a strong correspondence between FE simulations and experimental data. Furthermore, the FE model demonstrated efficacy in predicting the ultimate capacity of TCC beams and consistently captured failure modes, indicating its consistency in simulating the complex behaviour of TCC beams.

French version

Cette thèse explore le comportement mécanique de poutres en composite bois-béton (TCC) collés par adhésif à travers des investigations expérimentales et numériques.

Le comportement mécanique des joints collés par adhésif entre le bois (GL24h) et le béton auto-plaçant (SCC), dans un processus de collage à sec ou humide a été étudié. À cette fin, des essais de cisaillement double push-out ont été réalisés sur des joints TCC collés par de la résine époxy. Le rôle de plusieurs variables a été pris en compte pour les deux processus de fabrication. Ces paramètres étaient : la variation de la teneur en humidité du bois, le type d'adhésif, l'épaisseur de l'adhésif, l'addition de sable, le traitement de surface du béton et l'effet d'échelle de surface de la liaison. Les résultats ont montré que le collage semble être une bonne alternative aux moyens mécaniques pour produire des joints TCC secs ou humides. Dans des conditions de bois sec, la résistance au cisaillement peut être considérée comme très satisfaisante, avec une plage de valeurs moyennes de 6 à 8 MPa. Le mode de rupture est principalement influencé par la rupture cohesive du béton ou du bois. Cependant, les résultats confirment l'hypothèse selon laquelle l'augmentation de la teneur en humidité du bois avant le processus de collage réduit significativement la résistance au cisaillement des joints TCC collés par adhésif d'environ 30% dans certains cas.

Une investigation expérimentale de poutres TCC en flexion sur une portée de 3.2 m a été menée. L'analayse du glissement de l'interface, de la distribution des contraintes et de la réponse charge-déformation des poutres (produites par voie humide ou seche) en composite bois-béton collées a été investigué. Les poutres en composite bois-béton fabriquées par voie humide ou sèche ont révélé des modes de rupture distincts. Les résultats ont souligné le rôle critique de l'intégrité du collage pour garantir une action composite efficace. Les poutres en composite bois-béton fabriquées par voie humide ont présenté un

comportement rigide caractérisé par un axe neutre à l'interface bois/béton et avec preservation de l'intégrité du collage bois/béton jusqu'à rupture totale des poutres, tandis que les poutres fabriquées par voie sèche ont connu un délaminage à l'interface et une rupture prématurée. Les résultats ont montré que les poutres en composite bois-béton fabriquées par voie humide ou sèche présentaient des réponses similaires avant occurrence des ruptures mettant en evidence le comportement quasi-parfait de la section composite avant occurrence du délaminage pour les poutres fabriquées par voie seche.

De plus, un modèle analytique pour le calcul des poutres en composite bois-béton est présenté et validé. La base du modèle analytique est établie sur la méthode du coefficient γ, dérivée de l'Eurocode 5. Le modèle analytique est comparé aux résultats expérimentaux, mettant en évidence sa pertinence et sa précision. Les réponses charge-flèche, les distributions des contraintes de flexion et les charges de rupture ultimes sont estimées avec précision, affirmant la capacité du modèle à prévoir le comportement des poutres en composite bois-béton.

En outre, un modèle aux éléments finis non linéaire tridimensionnel (FE) pour les poutres en composite bois-béton collées par adhésif est présenté. Le modèle analyse le comportement de déformation, la distribution des contraintes de flexion, la capacité ultime et les caractéristiques de rupture des poutres. Malgré les défis rencontrés en cas de rupture du collage, entraînant des déviations exceptionnelles du comportement, les résultats ont révélé un bon accord entre les prédictions du modèle FE et les résultats des essais expérimentaux. Le modèle FE a prédit avec précision le degré d'action composite. Notamment, le modèle FE et le modèle analytique basé sur la méthode γ présentent une performance prédictive comparable en termes de déformation. Les résultats de la distribution des contraintes de flexion ont mis en évidence une correspondance étroite entre les simulations FE et les données expérimentales. De plus, le modèle FE a démontré son efficacité dans la prédiction de la capacité ultime des poutres en composite bois-béton et a capturé de manière cohérente les modes de rupture, indiquant sa fiabilité dans la simulation du comportement complexe des poutres en composite bois-béton.

Dedication

I would like to dedicate this work to my parents for their unwavering support, my wife, Hanna, for her boundless encouragement, and my beloved daughters, Amal and Mona. I extend my gratitude to my brothers, sisters, and family members who have always stood by me. Special thanks to everyone who contributed to the completion of this study.

Acknowledgement

First and foremost, I extend my deepest gratitude to Allah, the compassionate and the merciful, for granting me the patience, perseverance, and strength necessary to make this accomplishment possible.

I would like to express my sincere gratitude to my advisors, Prof. Frederic Duprat and Dr. Zakaria Djamai, for their unwavering scientific support, expert guidance, and diligent review of this thesis. I am grateful for their valuable suggestions, discussions, and provision of essential data that have contributed significantly to the completion of this study.

Great thanks are extended to technicians from the National Institute of Applied Sciences of Toulouse and GA Smart Building Company for their assistance during the experimental works. The appreciation would also be extended to SIKA Co. for gracefully supplying resins and discussing the mechanical performance of used resins.

Finally, I express my heartfelt gratitude and appreciation to my family for their endless support, encouragement, and understanding throughout this journey.

Table of Contents

List of Tables

List of Figures

List of Abbreviations

CDP	Concrete Damage Plasticity
CFRP	Carbon Fiber-Reinforced Polymer
CHS	Circular Hollow Section
CLT	Cross Laminated Timber
CO2	Carbon Dioxide
COV	Coefficient of Variation
DCA	Degree of Composite Action
DIC	Digital Image Correlation
FE	Finite Element
FEA	Finite Element Analysis
FSFM	Frozen Shear Force Method
GL	Glulam
HBV	Holz-Beton-Verbundsystem
HSC	High Strength Concrete
LMDC	Laboratoire Matériaux et Durabilité des Constructions
LVDT	Linear Voltage Displacement Transducer
LVL	Laminated Veneer Lumber
MC	Moisture Content
NSC	Normal Strength Concrete
NSM	Near-Surface Mounted
OC	Ordinary Concrete
PRF	Phenol Resorcinol Formaldehyde
PUR	Polyurethane
PVC	Polyvinyl Chloride
RH	Relative Humidity
SCC	Self Compacting Concrete
SLS	Serviceability Limit State
TCC	Timber-Concrete Composite

UC	Universal Column
UF	Urea-Formaldehyde
UHPC	Ultra-High-Performance Concrete
UHPFRC	Ultra-High-Performance Fiber-Reinforced Concrete
ULS	Ultimate Limit State
WCC	Wood Chip Concrete

Introduction

Introduction

1. Background

Timber-concrete composite (TCC) structure is a construction technique comprised of a timber deck or beam connected to an upper concrete slab utilizing different types of shear connectors. These connectors can be either mechanically or adhesively bonded, with the primary purpose of reducing relative slip between the components, thus strengthening and stiffness upgrading of the structures.

Today, prioritizing innovative solutions in construction is crucial while also considering the environmental impact of our structures. Concrete, one of the most commonly used building materials globally, plays a significant role in construction practices. It offers numerous advantages, such as high compressive strength, familiarity with construction methods, and durability. However, concrete production comes with significant ecological impacts. It's crucial to reevaluate our construction practices, integrating sustainability throughout the entire building process, from conception to completion, to minimize environmental footprint. While numerous new standards for concrete construction aim to achieve this objective, it is also important to consider innovative solutions that combine concrete with timber.

Given its relatively high strength/density ratio, timber naturally competes with concrete and steel as an efficient structural material. Under convenient conditions of production and use, as recommended in standards, structural floor systems made from these materials offer satisfactory and similar durability and reliability, provided that an appropriate maintenance policy is followed. Environmental considerations are now giving wood a greater prominence as a material with a lower carbon footprint. However, the impact of climate change on forestry systems raises concerns about their sustained capacity to meet long-term demand [1]. Unlike concrete and steel, timber is highly deformable, which is likely its main disadvantage. Thus, innovative structural solutions that smartly combine these materials can be utilized to address the challenges encountered by today's builders, for example, in fields such as seismic design [2].

Timber-concrete composite (TCC) structures have hence gained popularity during the last four decades as an efficient construction technique, combining the best qualities of timber and concrete to enhance structural strength and stiffness [3]. TCC floor systems optimize the placement of concrete in the compression area of the section and timber in the tension area, which efficiently benefits both materials, offering several advantages over traditional reinforced concrete or timber-only floors. The literature review chapter thoroughly covers the benefits of TCC structures, including increased stiffness, improved sound insulation, enhanced thermal mass, reduced load on foundations, and lower CO2 emissions [4–6].

Adhesive bonding has gained attention as a promising method for connecting timber and concrete elements in TCC structures, particularly in heavily loaded or large-span TCC beams and slabs where there is an increased demand for high-shear strength connections. This bonding technique offers a rigid bonding between timber and concrete components, ensuring efficient load-shared contribution and enhancing the overall stiffness of the composite system [7].

2. Research motivation

The motivation for this research stems from several considerations in adhesively bonded TCC structures.

Firstly, the integrity of adhesively bonded TCC elements heavily relies on the performance of the glue connection, making the investigation of shear bonding strength essential. The conducted research on glued connections as shear connectors is still in its early stages but developing. There is a lack of research that dedicates itself to understanding the comprehensive influence of various parameters on the bonding performance of wet and dry TCC joints, such as timber moisture content, adhesive type, adhesive layer thickness, sand addition, sandblasting of pre-fabricated concrete, and bonding scale effect. By examining the influence of these factors, we seek to enhance the understanding of the bonding behaviour and inform improvements in design and manufacturing techniques.

Additionally, in line with the need to reduce the carbon footprint of constructions, there is a pressing requirement to find an optimal balance between timber and concrete, considering both environmental and structural requirements. In this pursuit, achieving a relatively higher timber-to-concrete ratio in the TCC floor system cross-section could be targeted. However, this attempt must ensure that it does not compromise the structural performance, which is often reached when both materials are pushed to their limits. This aspect was rarely addressed in the literature, as most surveys focused only on the structural behaviour of the proposed floor systems. While acknowledging the complexity of achieving the optimal trade-off between climate impact and structural performance, the present research approaches this challenge by utilizing a thin concrete slab connected to a timber beam. The present research aims to extend the current state-of-the-art in adhesive-bonded TCC structures by comprehensively evaluating the load-carrying capacity, stiffness, interface slip, and deformation of an exceptionally light floor system. Through this investigation, we aim to identify and promote innovative solutions that align with the global objective of a low-carbon footprint construction.

Similar to the experimental body of work, there is a notable scarcity of studies dedicated to developing 3D non-linear finite element models for adhesively bonded TCC structures. The current research aims to address this gap by pioneering the creation and evaluation of 3D non-linear finite element models for

adhesively bonded TCC systems, offering a novel perspective on investigating their behaviour and performance.

3. Research objectives

The primary objectives of this research are outlined as follows:

- To explore the impact of various parameters on the bonding process of wet and dry TCC joints, such as moisture content of timber, adhesive type and thickness, sand addition, surface treatment of concrete, and bonding scale effect.
- To investigate the mechanical performance and failure characteristics of adhesively bonded TCC joints.
- To assess the load-bearing capacity, stiffness, interface slip, and deformation of adhesively bonded TCC beams with a thin concrete slab.
- To develop analytical and numerical models to predict the behaviour of adhesively bonded TCC beams and validate these models against experimental results.

4. Thesis structure

The thesis starts with a thorough literature review in **Chapter 1**, delving into the fundamental theory surrounding TCC composite structures. It initially explores the historical background and benefits of TCC structures before turning into topics such as standards, design methods, and structural aspects of TCC. Furthermore, the review discusses various connection types, connection efficiency, and structural behaviour of TCC systems. Finally, the chapter summarizes modeling approaches to predict TCC composite beams' behaviour.

Chapter 2 will delve into the bonding performance of wet and dry TCC joints, presenting findings from push-out tests, discussing experimental specimen design, and detailing the methodology and setup of double-shear push-out tests.

Chapter 3 will present the findings obtained from four-point bending tests, shifting from the scale of push-out tests on adhesive-bonded TCC joints to a structural investigation of adhesive-bonded TCC beams. It will outline the experimental setup for bending tests, including specimen design, loading configuration, and analysis of structural behaviour and failure mechanisms.

Chapter 4 delves into analytical modeling, exploring its role in predicting the behaviour of adhesive-bonded TCC beams. Furthermore, it will present the development and validation of a full non-linear 3D FE model, accompanied by a comparative analysis of experimental results.

Finally, the thesis will end with a general conclusion in which perspectives will be proposed.

Chapter 1
Literature Review

Chapter 1 Literature Review

1.1 Introduction

Timber-concrete composite (TCC) structures have been increasingly used in recent years. These structures combine the strengths of both timber and concrete materials, resulting in a composite system with superior properties compared to individual materials. For instance, the part of the self-weight in the load-bearing capacity is reduced compared to that of a full concrete structure. The fire resistance and the serviceability regarding deflection and vibration are improved compared to that of a full timber structure. The composite action between the materials is crucial to ensure the optimal performance of the TCC structures. Researchers have investigated various aspects of TCC structures in this context. This literature review aims to provide an up-to-date overview of the current knowledge of TCC structures. The review covers the historical background and advantages of TCC structures, the principles of composite action, shear connection testing, adhesives, bonding in civil engineering, connection types, full-scale experimental tests, and modeling approaches used to predict their behaviour.

1.2 Historical overview

TCC structure is a construction technique comprised of a timber deck or beam connected to an upper concrete slab utilizing different types of shear connectors, mechanically or adhesively bonded, thus strengthening and stiffness upgrading of the structures. TCC systems' popularity was owing to the shortage of steel after World War I and II [8]. The TCC system is used either for new constructions or rehabilitation of old buildings by increasing the strength and stiffness of existing floors; it was used for new public and residential building floors, bridges, and prefabricated walls and floors.

Müller et al. [9] patented the first official record of using TCC with nail and steel braces as a shear connector between the two components. A second patent was in 1939 and used steel Z-profiles and I-profiles as shear connectors [8]. There was a gap in the development of TCC systems during the early 20th century. Research into the systems began to increase in the 1960s. During this period, new joint techniques were developed, and researchers started using calculations to better understand TCC systems' behaviour. This allowed them to design more efficient and effective systems and optimize the use of materials.

In the 1990s, the interest in TCC systems increased, resulting in high utilization of TCC systems in bridge construction, timber floor upgrading, and new building constructions. More specifically, the use of TCCs in renovating and rehabilitating existing structures has appeared to be an innovative and effective solution that offers many benefits. By incorporating TCCs into the renovation process, it is possible to strengthen the structure and extend its lifespan while preserving its historical and architectural value.

For instance, Poštulka et al. 1997 [10] reports that over 10,000 m² of timber floors were renovated using TCCs by connecting the timber and concrete with nails spaced throughout the beams [11]. This large-scale application demonstrated the effectiveness of TCCs in upgrading existing structures. Similarly, Rilem et al. [12] describes a renovation project involving more than 1,000 m² of timber floors in Lodz, which also utilized nailed joints [11]. This method is more cost-effective than installing a completely new system, making it a popular option for renovation projects. In addition, using steel dowels installed in oversized holes and bonded to the timber with glue is another effective method for rehabilitating historical buildings using TCCs [8,11].

Examples of applications of new TCC residential floor structures are given by Natterer et al. [13], which describes the use of post-stressed dowels shared with concrete notches to create strong and durable floors for multi-story residential buildings in Switzerland. This method utilizes nail-laminated slabs and log slabs, which are combined with TCCs to create a reliable and efficient flooring system. Kuhlmann et al. [14] discuss the application of TCCs in multiple-family houses using a similar approach to Natterer et al. [13]. The first TCC road traffic bridge was completed in 1997, with a span of 15 meters long. The bridge used three timber beams of different height sections that were bonded to a concrete slab with glued-in steel bars. This innovative construction method created a lightweight bridge that could be used in areas with weight restrictions or other environmental concerns [11].

The Life Cycle Tower in Austria, which was built in 2012, is a great example of how TCCs have been used in modern full-scale structures. The tower uses prefabricated TCC slabs fixed to a timber frame, allowing for quick and efficient construction. Webb Yates is also a leader in using TCC structures in the UK, and their 15 Clerkenwell Close project showcases how TCC floors can be used in a modern, mixed-use building. The building's TCC floors provide a durable and long-lasting foundation for both residential and commercial spaces. Additionally, the use of TCCs in the construction of Peavy Hall at Oregon State University shows how this material can be used in conjunction with structural health monitoring systems to ensure the safety and longevity of a building. TCCs have the potential to revolutionize the construction industry with their many benefits, and it's exciting to see how they're being used in innovative ways worldwide [15].

1.3 TCC systems

1.3.1 Advantages of TCC

Traditional light timber frame floors may suffer severe deflection, vibration weakness, low fire resistance, and inadequate acoustic insulation. These problems may be overcome by using the TCC system. The best qualities of the two TCC components can be exploited, with the concrete placed in the compression

area of the section and the timber in the tension area. TCC systems offer several advantages over reinforced concrete or timber-only floors. It is possible to achieve the following benefits for new construction buildings: i) increased stiffness: by combining timber and concrete, TCC systems can achieve a higher stiffness than timber-only floors. It can allow for larger spans and reduce the need for intermediate supports; ii) enhanced sound insulation: TCC systems provide better sound insulation than all-timber floors. The concrete layer helps dampen sound vibrations and reduce noise transmission between floors; iii) increased thermal mass: TCC systems offer greater thermal mass than timber-only floors. That means they can absorb and store heat, which can help to regulate indoor temperature and reduce the energy consumption required for building conditioning. Other advantages of TCC systems include their versatility and flexibility, as they can be used for a wide range of building types and applications. They are also relatively lightweight and can be prefabricated off-site, reducing construction time and costs. Additionally, TCC systems can be designed to be fire-resistant, which is an important consideration for many construction projects.

Furthermore, by replacing the ineffective lower section of reinforced concrete under tensile stresses with timber joists, the following advantages could be attained: i) quick fabrication of the timber part, especially with off-site prefabricated parts, ii) reduced transferred load on foundations, iii) reduce mass, thus enhance seismic resistance, iv) using the timber as a decorative ceiling lining, v) reduce CO_2 by reducing the demand on cement manufacturing. For the rehabilitation of old buildings, the following advantages can be gathered by connecting approximately 50 mm of a concrete topping with a timber floor: i) improved stiffness and load-bearing capacity, ii) protection of historical buildings, and iii) improved seismic performance, due to the improved diaphragm action. TCC floors are considerably lighter and more cost-effective compared to their equals, steel-concrete composite and reinforced concrete floors, which are considered a nonregenerative manufacturing process with high energy consumption and high environmental emissions of carbon dioxide [16].

1.3.2 TCC theory

The shear connection forms a significant role in a composite system to determine the efficiency and the performance of the TCC system; therefore, they should form an efficient joint with enough strength to be able to transmit the shear loads developed in the bonding line and stiff enough to reduce the slip between concrete and timber. Composite action is the governing theory of TCC structures; there are three theoretical cases of the TCC: fully composite action, partially composite action, and no composite action. These three cases of composite action are shown in **Fig. 1-1.**

- Fully composite action refers to the rigid connection between concrete and timber with no interlayer slip, resulting in the two materials behaving as one material. This type of connection enables the transfer of both shear and moment forces between the timber and concrete components, allowing the composite

element to resist bending and other loads more effectively. In a fully composite system, the timber component primarily experiences tension stresses, while the concrete component experiences compression stresses. These stresses are distributed uniformly across the composite component, resulting in lower deformations.

- No composite action; in a non-composite system, there is no rigid connection between the timber and concrete components, resulting in a large slip between them. As a result, the two materials act independently and offer separate resistance to bending loads. The lack of composite action leads to the development of compression and tension stresses in both materials. The magnitude of these stresses depends on the load distribution and the relative stiffness of the timber and concrete components. The separate response of the two materials also leads to increased deformations.
- In partially composite action, the connection between the timber and concrete elements allows for some degree of interlayer slip, resulting in an intermediate level of flexural behaviour. The amount of slip and deflection in the composite beam depends on the strength and stiffness of the connection system. In this case, both materials contribute to resisting the bending loads, but not to the same extent as in the fully composite action.

In reality, achieving a fully composite action in TCC beams with mechanical connectors is challenging due to the need for connectors with greater stiffness than composite materials. As a result, most TCC beams with mechanical connectors behave under the assumption of partial composite action. In contrast, TCC beams with glue connections may exhibit fully composite behaviour, where the connection system's stiffness and strength determine the composite action level.

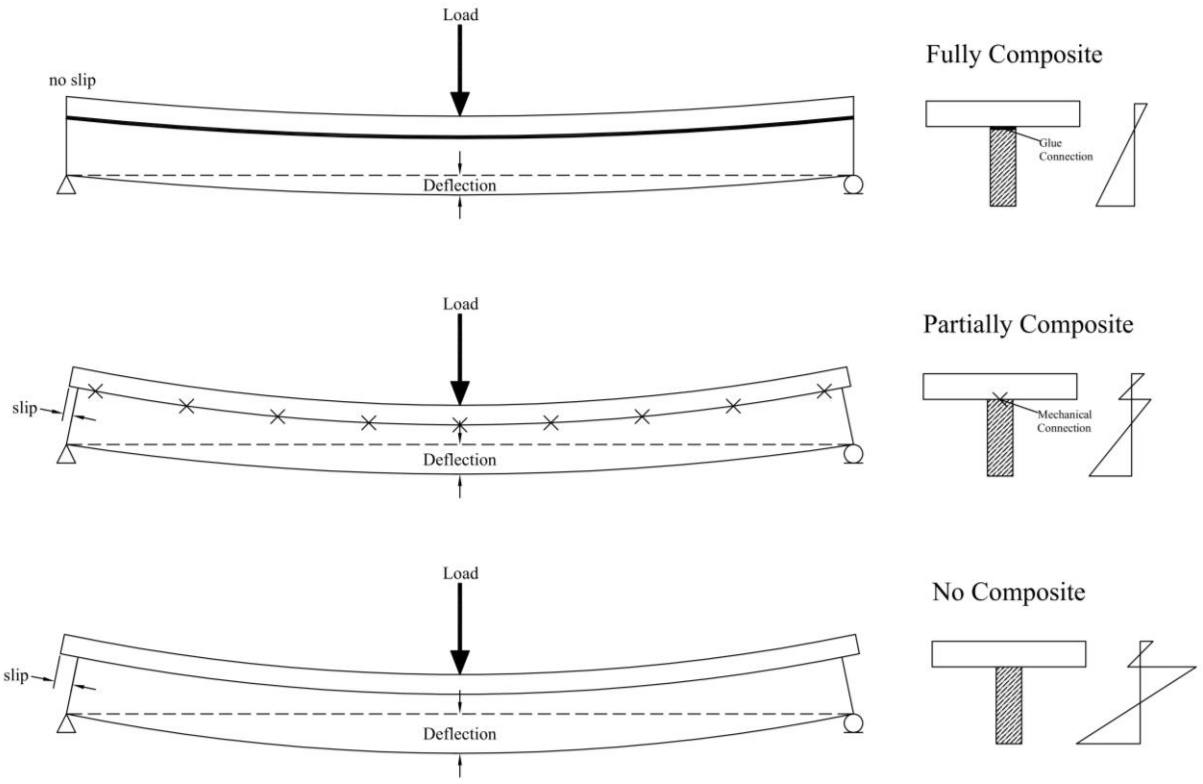

Fig. 1-1 Stresses and deformations distribution for fully, partially, and no composite action connections

1.3.3 Standards and design methods

The design of TCC structures is not comprehensively addressed by most timber standards worldwide, except for Eurocode 5, Part 2 [17]. The design of TCC structures must consider two main phenomena: (1) the partial composite action resulting from the flexibility of the shear connection in the case of mechanical connectors and (2) the time-dependent properties of the component materials. This includes considerations for creep, mechano-sorption, drying shrinkage, thermal, and hygroscopic strains. Two approaches have been proposed to address the partial composite action phenomenon: the linear-elastic method and the elastoplastic method [16]. More details are provided in the section 1.7.1.

Ceccotti et al. [18] proposed the effective modulus method to address the creep deformation of different materials in TCC structures. This method replaces the elastic and slip moduli with effective moduli. These effective moduli are calculated by dividing the elastic and slip moduli of concrete, timber, and connection by one plus the pure creep coefficient of the material at the end of the service life. This coefficient is defined as the ratio between the delayed and the elastic strain in a test under sustained, constant load. However, it's worth mentioning that this approach neglects the effect of environmental strains caused by the different thermal expansion and shrinkage of concrete and timber on the internal forces and the deflection of TCC

structures. As a result, there is a tendency to underestimate the deflection at the end of the service life when using the effective modulus method.

To address this issue, Fragiacomo et al. [19] developed accurate solutions to consider the effects of environmental strains and drying shrinkage of concrete on TCC structures. Additionally, Fragiacomo et al. [20] proposed formulas to convert environmental strains and drying shrinkage of concrete into equivalent uniformly distributed loads, which are then used in design formulas such as the gamma method proposed by Eurocode 5 [17].

1.3.4 Structural aspects of TCC

Table 1-1 emphasizes the most significant structural aspects of TCC and how the different technical connection solutions illustrate them more or less efficiently. The table highlights the key structural aspects of TCC construction, including load transfer, initial shear/flexural stiffness under short-term loading, the resistance of initial stiffness decrease due to Creep, maximum shear/flexural capacity, and failure mode. It then lists some common connection solutions, including mechanical fasteners, notched connections, metal plate connections, and glued connections. Finally, it assigns each technical solution an efficiency rating based on how effectively it achieves the desired structural aspect, with high efficiency being the most effective and low efficiency being the least effective. For example, the table shows that glued connections are highly efficient in achieving load transfer, initial shear/flexural stiffness, and maximum shear/flexural capacity, while notched connections and mechanical fasteners are less efficient in these aspects. However, notched connections are more efficient than glued connections in resisting stiffness decrease due to creep. Metal plate connections are also effective in achieving load transfer and maximum shear/flexural capacity, but they are less efficient than glued connections in achieving initial stiffness under short-term loading. It is worth mentioning that the efficiency ratings for each technical solution in the table are based on general trends and may vary depending on the specific design parameters and materials used in each application. The selection of the shear connector is a critical factor that can significantly impact the behaviour and load response of specimens. Although no single "best" type of connector exists, selecting the most suitable one can depend on various structural requirements. Several criteria have been proposed to identify the most appropriate connector type. Dowel connectors are suggested when ductility is a crucial requirement but may not provide adequate slip stiffness and strength. In such cases, glued or notched connections are highly recommended. Furthermore, conducting thorough analysis and testing is crucial to ensure that the chosen connection solution meets the specific requirements.

Table 1-1 Structural aspects of TCC and how the different technical connection solutions illustrate them more or less efficiently

	load transfer	Initial stiffness (Shear/Flexural) under short-term loading	Resistance of initial stiffness (Shear/Flexural) decreases due to creep	Maximum Shear/Flexural capacity	Failure modes
Mechanical Fasteners	Moderate	Moderate	Low	Low	ductile
Notched Connections without dowels reinforcement	Moderate	Moderate	High	Moderate	brittle
Notched Connections with dowel reinforcement	High	High	High	Moderate	ductile
Metal Plates Connection	Moderate	Moderate	Moderate	Moderate	ductile
Glued Connection	High	High	Moderate	High	brittle

1.4 Connection types

Many types of connection systems have been developed for timber-concrete composite structures. These systems can involve mechanical fasteners (dowels, nails, screws, bolts, etc.), notched timber (with or without screws or dowels, horizontal shear connectors, etc.), adhesives, steel mesh, nail plates, and other Connectors. Connectors can be categorized as continuous or discrete and vertical or inclined based on their arrangement along the beam. Additionally, depending on how they are installed in the timber, they can be classified as glued or non-glued and prestressed or non-prestressed [16].

The location and spacing of the connectors depend on the magnitude and distribution of the shear forces along the beam. The connectors are typically arranged in a pattern that ensures uniform distribution of the load between the timber and the concrete, as well as the desired composite action. In general, the connectors are placed closer together near the supports where the shear forces are highest and farther apart towards the center of the span where the shear forces are lower. This arrangement helps to optimize the load transfer between the timber and the concrete, resulting in a more efficient and effective composite system.

Each connection system exhibits a unique load-slip response, and their stiffness and strength can be determined through push-out tests. These tests provide the load-slip response under shear loads. **Fig. 1-2** presents a typical load-slip curve for several connection systems.

From an ideal perspective, connection systems should be: 1) strong enough to be able to resist the horizontal shear force along with the interface; 2) sufficiently stiff before yielding, resulting in a high degree of composite action; and 3) sufficiently ductile after a yielding point, providing overall ductility to TCC system.

In this section, we will delve deeper into adhesive bonding as shear connectors in TCC structures. We will explore the bonding mechanism, types of adhesives used, ageing properties, the necessity for surface treatment, bonding failure mechanisms, and mechanical tests on adhesive bonding.

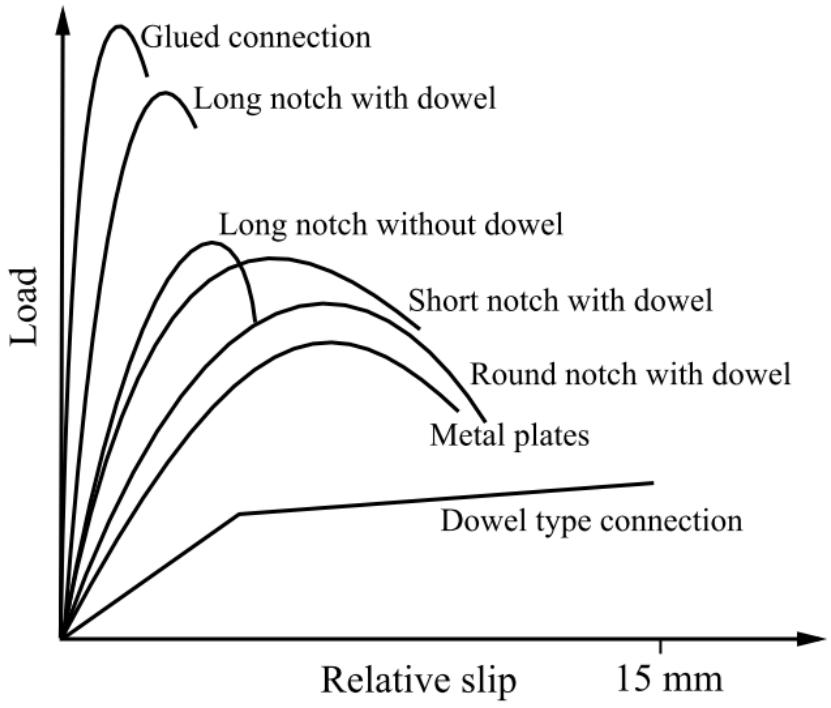

Fig. 1-2 Typical load-slip behaviour for several types of joints, Deresa et al. [21]

1.4.1 Mechanical fasteners

Dowel-type fasteners are among the most commonly used connection systems in timber structures and have naturally become a popular choice for timber-concrete composite (TCC) connections. These fasteners, including screws, nails, bolts, staples, and dowels, are characterized by their ability to transmit loads predominantly in bending and shear. It's worth noting that inclined fasteners, such as screws and glued-in rods, are also considered part of this group [16,22].

Among these, screws are the most commonly used due to their high axial load-bearing capacity. In TCC systems, this axial load-bearing capacity can be crucial for improving shear load transfer and preventing potential separation between the timber and concrete, making screws particularly well-suited for this application [22].

1.4.2 Notched connections

Notched connections in TCC structures can be achieved through various methods, including drilling holes in timber members, cutting out sections of timber, or attaching glued blocks to the structural timber member. Typically, the first two approaches are preferred due to their simplicity and lower cost. Notched connections offer an excellent balance between simplicity and mechanical performance, especially in terms of stiffness. However, they do have some disadvantages, such as a tendency for brittle failure and a relatively low axial load-carrying capacity. To address these issues, notched connections are often reinforced with steel fasteners, which add both ductility and axial load-carrying capacity to the connection system. Depending on the configuration, particularly the dimensions in proportion to the notch size, the additional steel fastener can provide additional shear capacity, axial load-carrying capacity, and ductility [21,22].

1.4.3 Metal plate connections

Metal plate connections are used to connect timber and concrete components in TCC structures. These connections typically consist of a metal plate that is fixed to the timber component using screws, nails, or bolts. The metal plate is then embedded into the concrete component during the construction process. Metal plate connections offer several advantages in TCC structures, including ease of installation and high strength. They also provide a high level of flexibility in the design of TCC structures, allowing for various configurations and load-bearing capacities. Several types of metal plate connections are used in TCC structures, including perforated/mesh plate connectors, toothed plates, and split-ring connectors. These connectors offer different levels of shear resistance, stiffness, and ductility depending on their design and installation method [21].

1.4.4 Adhesive bonding

The use of adhesive bonding in civil engineering requires careful consideration of the properties of the adhesive and the substrate materials, as well as the service conditions and loads the bond will sustain. Proper surface preparation and bonding techniques are also critical for a strong and durable bond. Knowing the properties of the adhesive used to join the two substrates is important but insufficient. An essential step is to mechanically test the bonded assemblies at the glue joint to investigate how they behave in real life and to study the sensitivity of the assembly to variations in temperature and humidity.

1.4.4.1 Adhesion mechanisms

Adhesive bonding is a complex technology that uses an adhesive layer to connect two solid surfaces (the substrates). Generally, mechanical interlocking or anchoring, diffusion, electrostatic (contact charging), and adsorption/surface reaction theories have been assumed to illustrate adhesion mechanisms. More recently, other assumptions on the relevant actions have been set to explain this mechanism, such as wettability (the capacity to spread on the solid) and chemical bonding, as described in **Fig. 1-3**. It is challenging to ascribe adhesive bonding to a unique mechanism. Assigning adhesive bonding to a single mechanism is difficult, as it is likely that a combination of several mechanisms is responsible for bonding within a particular adhesive system. Furthermore, the degree to which each mechanism contributes to bonding may vary for different adhesive systems [23].

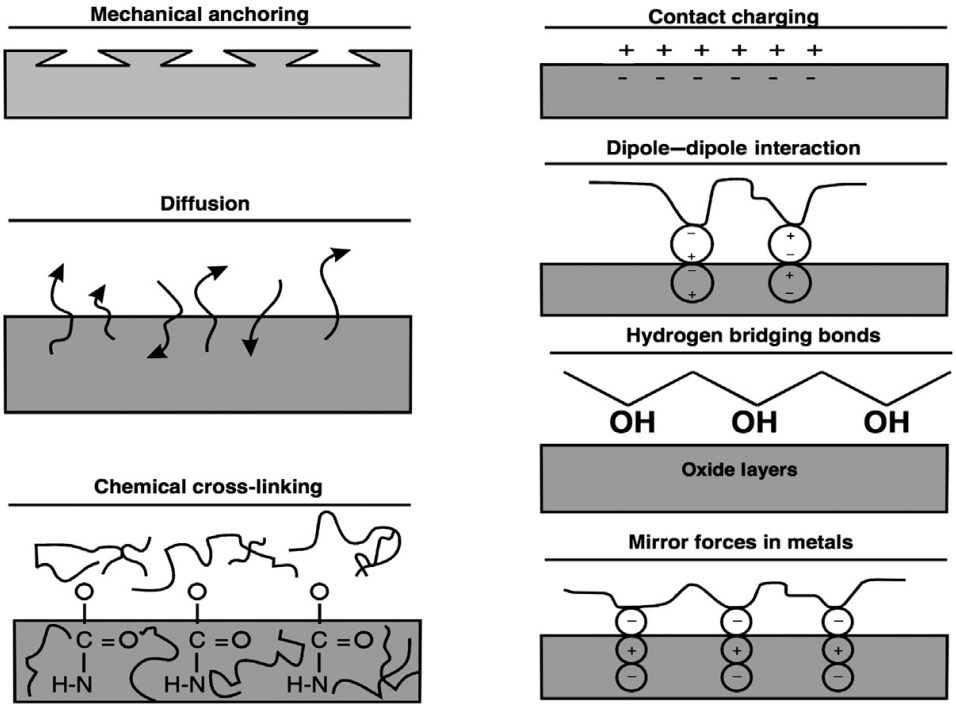

Fig. 1-3 Physical and chemical causes for the adhesion mechanisms, Horobin et al. [23]

As described earlier, several theories are considered to explain this mechanism, involving mechanical theory, electrostatic (contact charging) theory, diffusion theory, wetting theory, the creation of chemical bonds, such as hydrogen, covalent, and ionic bonds, and other approaches which are fully described in numerous works [24–26]. All these theories show that the adhesion phenomena are not yet well understood. However, it should be mentioned that adhesion is governed primarily by the contact between the adhesive and the substrate (wetting and mechanical anchoring) and by founding strong bonds between the adhesive and the substrate. Therefore, the study of adhesion mechanisms allows for optimizing the performance of an adhesive joint, mainly through good surface preparation to improve "wettability" and "mechanical anchoring". The substrate surface to be glued can then be treated mechanically by sandblasting and chemically by degreasing.

1.4.4.2 Structural adhesives

Adhesive bonding must provide the assembly with sufficient mechanical strength under the environmental conditions of service [27]. Therefore, the adhesive becomes an integral part of the structure. The mechanical resistance of the assembly and its durability depend on the nature of the utilized materials, the adhesion forces that exist between these materials and the adhesive, and the behaviour of the materials constituting the structure in the external environment (in our case, the wood, the concrete, and the adhesive).

The classification of adhesives depends on the production sources, whether from natural sources or synthesized from basic hydrocarbons. The synthesized adhesives can be classified as thermoplastics, thermosetting, elastomeric, or a combination of these types. Thermoplastic adhesives do not cross-link during cure, and they can be deformed when heated and regain their rigidity when cooled without a significant change in their properties. In contrast, thermoset materials are densely cross-linked when cured and become rigid when exposed to an increase in temperature during or shortly after curing. Elastomeric materials are based on natural or synthetic developing polymers. These materials exhibit exceptional toughness and elongation, and they are designed for a broad range of applications that require high levels of flexibility and excellent peel strength [26].

Thermosetting and thermoplastic are the main categories of adhesives used in civil engineering applications; the following sections will be restricted to describe the properties of these types of adhesives

Among the thermosetting and thermoplastic families, epoxy, polyurethanes, and acrylic compounds are the most used adhesives in civil engineering structural applications [27,28]. The main characteristics and ageing properties of these different adhesives will be described hereafter. Generally, structural adhesives are characterized by excellent mechanical properties, especially mechanical strength, to guarantee joint stability. According to their characteristics, each type of adhesive has a particular role. Thus, a flexible

adhesive with a low Young's modulus is preferred for assemblies subjected to significant expansion, shocks, and vibrations. A rigid adhesive with excellent adhesion properties is recommended to ensure a near-perfect interface to secure continuity between the two bonded materials. The adhesives most commonly used to bond timber and concrete and their essential properties are described below.

- **Epoxy adhesives**

Among all the thermosetting plastic resins, epoxies are the most widely used in civil engineering compared to any other plastic due to their excellent adhesion with numerous materials and ease of application. When there are two parts (resin/hardener) systems that can cure at room temperature, mixing the two products gives rise to an exothermic reaction, allowing cross-linking. In the case of one-part systems, the base and hardener are already mixed, and the reaction takes place with extreme heating cures to improve optimum properties. They are generally used for metal-to-metal or metal-to-plastic joints that must withstand high mechanical stress, and currently, they are being used in TCC structures. They are also used to make composite materials combined with carbon fiber. These adhesives have many advantages, including good environmental resistance and high rigidity [25,26,28].

- **Polyurethane adhesives**

Polyurethane adhesives result from the condensation of an isocyanate monomer and a hydroxide or polyol monomer. Some manufacturers developed single-component polyurethane systems for processing purposes, but two-part systems are generally used. Two-part systems have higher mechanical properties due to their excellent tear and peel resistance. They are used for joining two materials, one rigid and the other flexible, e.g., metal-plastic joints. Furthermore, they are flexible and have good resistance to ageing. Thus, they are recommended for joints subjected to expansion, such as glued laminated wood. They are also excellent, resistant to shocks and vibrations, and have many uses in the naval field and transportation equipment [25,26].

- **Acrylic compounds**

Acrylic adhesives are widely used for bonding plastics, cloth, leather, and, in some cases, metal foils. They can even replace spot welding when quickly handling the joined metal parts is crucial. Acrylic adhesives are also commonly used for bonding different substrates with varying expansion coefficients, including metals and other materials. Most of the acrylic monomers used are acrylic acid, methyl acrylate, methacrylic acid, acrylamide, ethyl acrylate, and acrylonitrile. These adhesives are typically produced as two separate parts mixed just before application. They exhibit excellent mechanical resistance, especially to shearing and peeling[25,26].

Using a structural resin for the connection of wood and concrete became obvious. Indeed, this assembly is developed to serve as a structural element. The idea of connecting these two materials by glueing via a

rigid and strongly epoxy resin was born from the desire to improve the continuity of the interface compared to the usual mechanical connections [29]. In the field, the structure will be subjected to external climatic conditions and, thus, to thermo-hydric variations due to the hygroscopic properties of wood, which imply a significant expansion of the wood. A flexible adhesive tolerant of wood deformations may be a promising solution. It is then an issue to find a compromise between the mechanical strength and durability of the joint. Another critical point to consider when selecting an adhesive is that it has properties that might vary over time depending on the mechanical and climatic conditions to which it is subjected.

1.4.4.3 Ageing properties of a structural adhesive

The literature dedicated to the durability of adhesives is abundant because of their common use in the industrial field. The effects of temperature, humidity, and mechanical stress on the durability of resins, more generally of epoxy resins, have been explored [27,28].

- **Effects of temperature**

Physical ageing corresponds to the evolution of macromolecular chains initially in a non-equilibrium state. These will restructure to move toward the equilibrium state. Precisely, a resin is characterized by its glass transition temperature. The glass transition temperature (Tg) is the temperature at which the resin changes from rigid to rubber. This phenomenon is directly related to the molecular structure of the polymer for which, above the Tg temperature, intermolecular bonds weaken, forming a material with great flexibility. This change of status is accompanied by significant variations in the mechanical properties of the resin, in particular, a considerable drop in the modulus of elasticity. For a resin that polymerizes at a temperature lower than the Tg temperature, thus at a temperature for which the molecular mobility is too slow, it freezes in a non-equilibrium state. The physical ageing is then clearly related to the temperature conditions to which the polymer will be exposed. Concerning the physical ageing of a resin, many studies focus on understanding the phenomena of degradation [27,30–32]. It has been shown that thermal degradation of resins exists when they are subjected to temperatures close to the glass transition temperature. This relaxation arises more rapidly at temperatures near Tg than below Tg. Therefore, most physical ageing characterization is performed in the neighbourhood of Tg.

- **Effects of humidity**

Water can penetrate the adhesive and replace it at the bond interface. Water penetration is related to the level of the absorbed water into the free volume of adhesive nanoscopic pores; such phenomena induce wet ageing, which can also impact the polymeric matrix and reduce the mechanical properties, particularly tensile strength and elastic modulus [33]. In TCC, Moisture content in wood worsens this issue by increasing water penetration into the adhesive. This mechanism is the most common reason for reducing adhesive strength in moist environments [25]. For epoxy resin, it was revealed a plasticizing of the resin,

accompanied by a decrease in its stiffness and capacity along with an increase in its ductility after ageing in a wet climate (95% RH, 40°C), as shown in **Fig. 1-4** [34]. In our study, we will investigate the variation of moisture content levels of timber on the mechanical behaviour of adhesively bonded TCC joints.

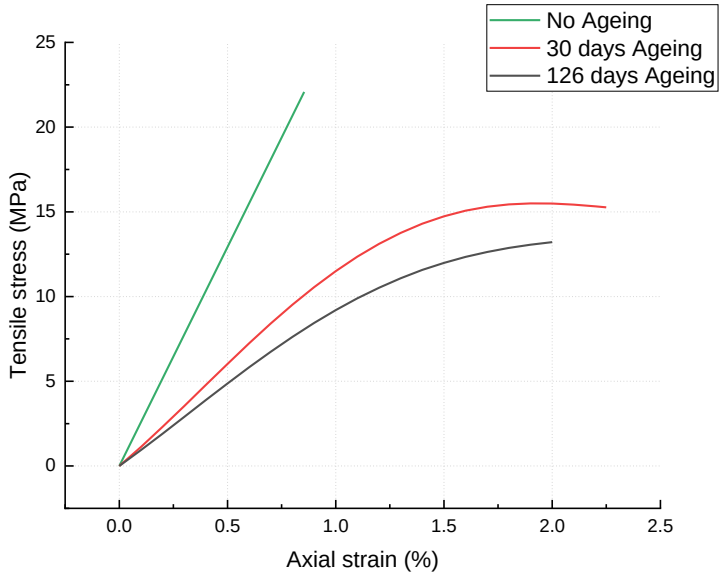

Fig. 1-4 Average tensile stress as a function of strain on unaged and wet-aged epoxy adhesive specimens at RH=95% and T= 40°, adapted from Chataigner et al. [34].

- **Effects of mechanical stresses**

Creep deformation generally occurs over a duration of time when a material is exposed to constant stress. There is a lack of fundamental knowledge on how creep affects the strength of adhesive joints. At room temperature, it is possible for polymeric materials, including adhesives, to experience creep deformation. The creep was found to be stress-dependent while the stress level increased from linear to nonlinear viscoelastic areas. In the linear viscoelastic area, the creep strain is a linear function of stress, which means the creep compliance is independent of the applied stress levels. Polymeric materials generally show linear viscoelastic behaviour at low stresses. When the stress level increases, divergence from the linearity can be found, representing a nonlinear behaviour. Furthermore, increasing stress levels reduces the time interval required to be converted into a nonlinear state [35].

1.4.4.4 Surface treatment

Proper surface treatment is essential to achieve a strong and reliable bond and avoid adhesive failures during the life of the bonded structure. The properties of the bonded surfaces directly influence the performance of the adhesive and the durability of the assembly. The main objective of surface treatment is to ensure cleanliness by removing disturbing elements, such as dust or gravel, thus promoting better

adhesion. Additionally, surface treatment increases surface roughness, which enhances mechanical bonding.

Common mechanical treatments include ultrasonic cleaning, which eliminates impurities, and sandblasting with abrasive particles to increase surface roughness, which enhances the bonding strength. Several studies[36,37] highlight the significant role of mechanical surface treatment in facilitating chemical bond formation. For instance, when sanding a wooden board, the process disrupts the bonds between wood molecules on the surface, leaving some bonds "free." During bonding, these "free" bonds can more easily bond with the resin, resulting in better adhesion. However, it is crucial to note that these free bond locations are quickly occupied by atmospheric molecules. Therefore, it is recommended to bond within 24 hours of surface treatment [36].

Consideration should also be given to the viscosity of the adhesive. Wetting refers to a drop's ability to spread on a substrate. The higher the wetting, the more the adhesive will spread, resulting in better adhesion. Even with proper surface preparation, poor wetting can lead to inadequate bonding as the resin fails to form enough physico-chemical bonds with the substrate [36].

Chemical treatments are aimed at degreasing and removing oxide layers on the surface. There are three types of treatments: solvent cleaning, alkaline cleaning with detergent, and chemical stripping with acids or bases.

Our study will investigate the effects of concrete surface sandblasting treatment on the mechanical performance of adhesively bonded TCC joints. Furthermore, we will explore the sand addition to increase the roughness between the concrete and timber surfaces.

1.4.4.5 Mechanism of bonding failure

Adhesive joints might fail due to adhesive or cohesive failure. Adhesive failure can be described as the interfacial bond mode of failure between the adherend and adhesive (**Fig. 1-5a**). In contrast, cohesive failure arises from a separation accompanied by an adhesive layer on both surfaces (**Fig. 1-5b**). When the failure of adhered happens in the first place, it is referred to as a cohesive failure in the adherend (**Fig. 1-5c**). Cohesive failure is the ideal type, whether it happens in the adhesive layer or one of the adherents. Cohesive failure allows for the ultimate strength of the components to be knocked. Bonding failure can involve several failure modes and can be assigned as a percentage of adhesive or cohesive failure. This proportion can be computed based on the rupture area of the bonding surfaces that have failed adhesively or cohesively. While failure mode is an important factor to consider when evaluating bonding joints, it should not be the only criterion used to assess their quality. The ultimate strength of the joint is a more important criterion for evaluating its quality. Some joints may fail adhesively but exhibit more strength than identical joints

with weaker adhesives that fail cohesively. However, Analyzing the failure mode can provide insights into the specific mechanisms that led to the failure, which can improve the design and construction of bonding joints. It can also provide information about the materials' behaviour under load, such as their ductility, stiffness, and strength, and help identify any potential weaknesses or defects in the joint [25,26,38].

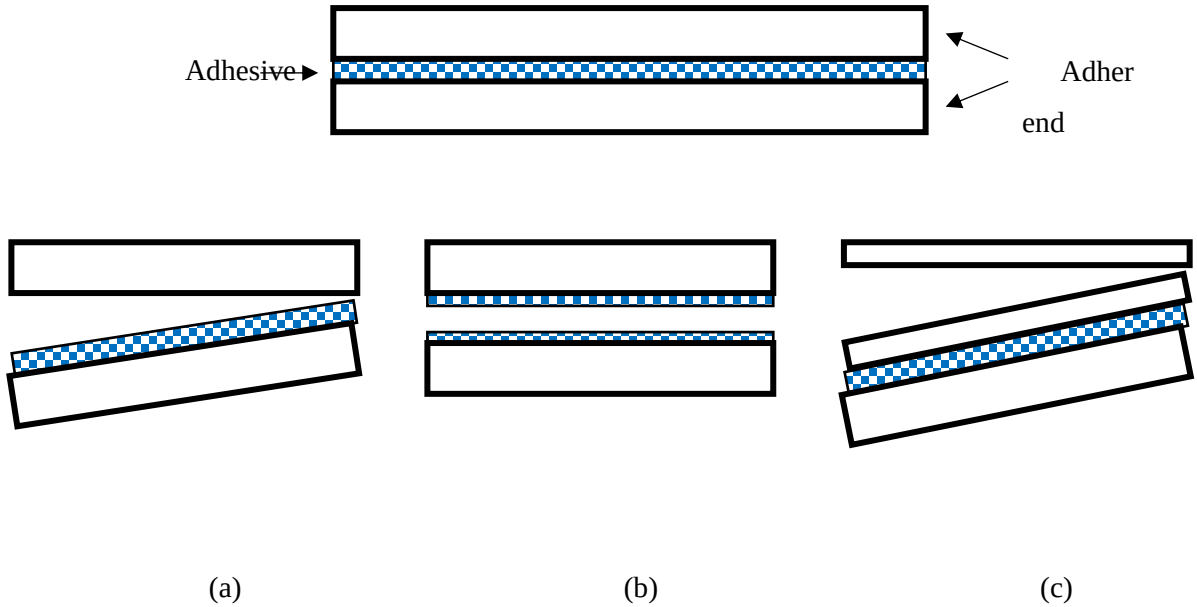

Fig. 1-5 Schematics failure modes of adhesive bonding: (a) adhesive failure, (b) cohesive failure in the adhesive layer, and (c) cohesive failure in the adherend.

1.4.4.6 Mechanical tests

The mechanical tests used to characterize the behaviour of bonded joints must represent what happens within a structure during service. Many mechanical tests exist, and there are three main modes of joint loading: normal loading, peeling, and shearing. **Fig. 1-6** shows five different types of stresses that can be present in adhesive joints, and it is possible to encounter any combination of these stresses in various adhesive applications. In the case of a bonded composite structure, the joint is generally stressed in shear. Therefore, this section will focus on mechanical shear tests, especially the most commonly used tests.

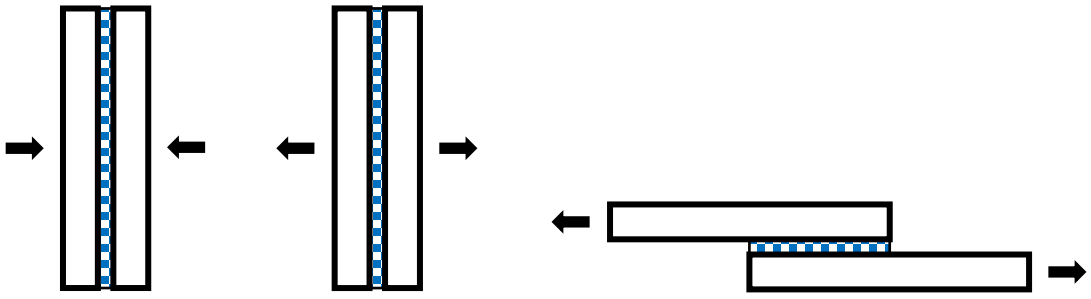

(a) (b) (c)

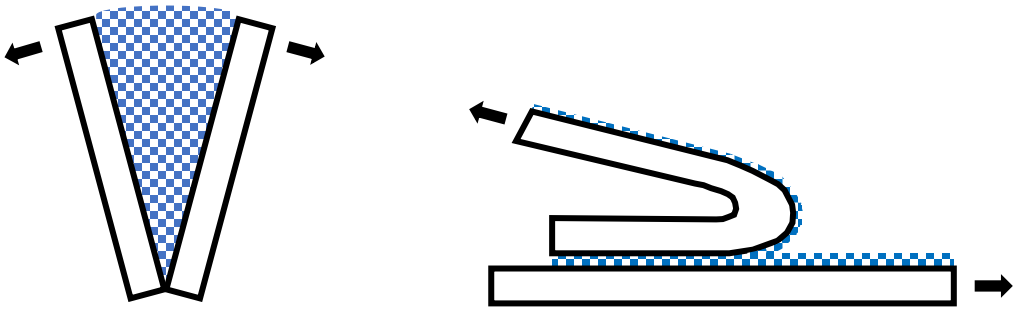

(d) (e)

Fig. 1-6 Types of stresses in adhesive joints: (a) compression, (b) tension, (c) shear, (d) cleavage, and (e) peel.

- **Shear tests**

A shear test is a mechanical test of glueing that measures the resistance of an adhesive bond to a force applied in a parallel direction to the surface. This test is commonly used to determine the shear strength of an adhesive bond, which measures the ultimate force that the bond can withstand before failure occurrence. Shear testing is commonly used in the construction field to evaluate the strength and durability of adhesive bonds. The construction of samples for shear tests is relatively simple, and they can accurately replicate the geometry and service conditions of many structural adhesives. The joints are typically made from two flat, parallel surfaces that are bonded together using the adhesive being tested. The size and shape of the samples can vary depending on the specific application. In the special cases of concrete or wood substrates, single and double overlap shear tests are the most common sample geometry, as they allow for the study of the assembly on a larger scale and do not require special devices.

- **Single lap shear tests**

Single lap joints are very frequently studied, especially with concrete substrates, because of their simplicity of implementation. The test exists in two variants: tension shear or compression-shear, where the stress is reversed, as illustrated in **Fig. 1-7**.

(a)

(b)

Fig. 1-7 Single lap shear test setup: (a) tension-shear, and (b) compression-shear.

- **Double lap shear tests**

The double lap shear test is based on the same principle as the single lap test, but the test specimen consists of two simultaneously loaded adhesive joints. The double lap shear test reduces the eccentricity of the loading compared to the single lap test, thus reducing the bending stress. This test is the standard test used for steel-concrete bonded joints in the form of push-out tests, as shown in **Fig. 1-8**. In addition to the case of glued connections to concrete or wood substrates, the double overlap shear test is used in the case of the usual wood-concrete composite connected by mechanical means. Many works are reviewed in section 1.5.5 concerning the shear tests of glue connection in the TCC systems.

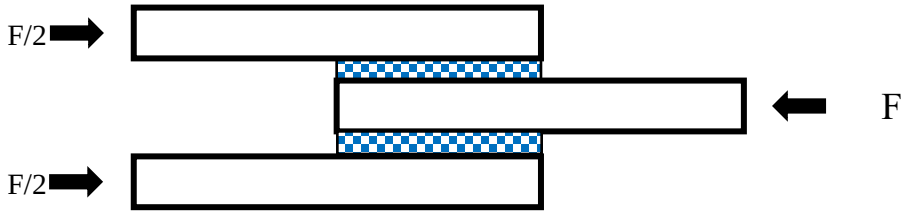

Fig. 1-8 Double lap shear test setup

1.5 Connection efficiency

In the case of Timber-Concrete Composite (TCC) construction, small-scale investigations are crucial for several reasons. Firstly, small-scale investigations can help researchers evaluate the structural behaviour of different types of TCC systems and materials. This can involve testing the strength and stiffness of individual timber and concrete components and examining how they behave when combined in a composite system. Small-scale investigations can also help optimize the design of TCC systems by identifying potential weaknesses or failure modes, refining the design to address these issues, and monitoring its response to environmental factors such as temperature and humidity. Overall, small-scale investigations are vital in developing and optimizing TCC construction systems. They provide valuable insights into the behaviour and performance of TCC components and can help to identify potential problems or limitations before moving on to full-scale testing and construction.

1.5.1 Shear connection testing

Understanding the properties and behaviour of shear connections is essential for the design and performance of timber-concrete composite systems. Shear tests can provide insight into the properties of shear connections, including slip stiffness, longitudinal shear strength, and ductility, which are essential parameters for designing TCC structures. Additionally, experimental shear tests can provide valuable data used to refine and improve FE models used to predict the behaviour of TCC structures.

The European standard EN 26891 [39] provides a testing method for determining the shear strength and stiffness of TCC joints using mechanical fasteners such as dowels or bolts and is commonly used for TCC research. Some studies have utilized this standard as a guideline for testing the shear strength of TCC with glue connections [7,40–42].

Examining how strain is distributed throughout the depth of a TCC composite section can assist in exploring how interlayer slip impacts the section stiffness. An example of this is shown in **Fig. 1-9**, which displays the distribution of strains throughout the depth of a TCC cross-section. In this figure, the strains at the concrete and timber are denoted by ε_{ct} and ε_{jb}, respectively. On the other hand, ε_s represents the strain that occurs due to slip at the bonding interface, and κ represents the curvature of the section.

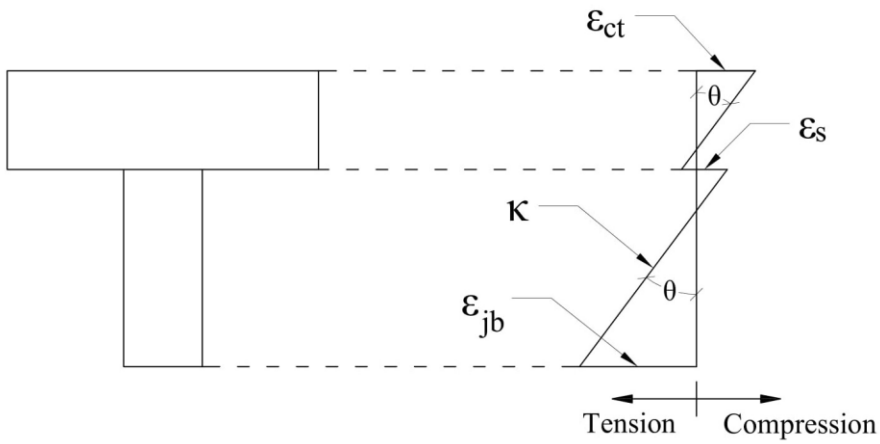

Fig. 1-9 Distribution of strains for a TCC cross-section

Identifying slip location is crucial for understanding the mechanical behaviour of the connection. It helps to determine the load transfer mechanism between the timber and concrete. Slip can occur at various locations, such as the interface between the connector and the timber, between the connector and the concrete, or within the connector itself. The type of slip that occurs depends on the characteristics of the shear connector, concrete, and timber. It can be verified through shear connector deformations or local failures in the concrete or timber. By identifying the slip location, it is possible to evaluate the shear connector's effectiveness and optimize the design of TCC joints to ensure reliable and predictable

performance. Furthermore, understanding the location of the slip is essential for accurately modeling and analyzing the behaviour of TCC systems. Various techniques, such as digital image correlation and linear variable differential transducer (LVDT) sensors, can be used to identify slip locations in TCC sections [43].

Fig. 1-10 shows the typical relationship between slip and shear force in the TCC composite structure. Slip stiffness is a measure of the resistance of the TCC system to slip or movement between the timber and concrete. It is defined as the initial slope of the linear portion of the load-slip curve representing the required shear force to cause a specific value of slip or movement. The higher the slip stiffness, the more resistant the TCC system is to slip. Additionally, the longitudinal shear strength demonstrates the maximum shear forces that the connectors can withstand before reaching failure, which is a critical measure of the connectors' strength and ability to resist slip growth under increasing loads. The ductility of the connections in TCC systems is usually described qualitatively based on the behaviour of the connections after the maximum shear strength is reached. Connections that exhibit a gradual decrease in shear strength with increasing slip are considered more ductile than those that fail suddenly after reaching their maximum strength. Additionally, the behaviour of the concrete and timber after the maximum shear strength is reached also plays a role in determining the ductility of the connection [11].

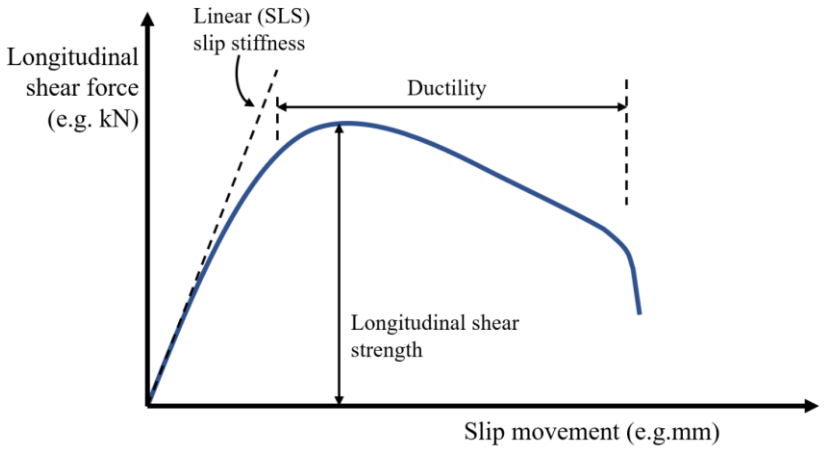

Fig. 1-10 Typical slip vs. shear stress for shear connectors in TCC systems, Dias et al. [11]

The slip stiffness value is used to calculate interlayer slip profiles, which determine the section's maximum stresses and deflection. This value is critical in assessing the success of shear connections, as a higher slip stiffness indicates a stronger connection that is better able to resist slip-induced degradation. Eq. (1.1) presents the formula used to calculate the efficiency of shear connections based on structural deflection, which was introduced by Pault et al. [44] to explain composite action in glulam timber bridge structures:

$$Efficiency = \frac{D_{NC} - D_{PC}}{D_{NC} - D_{EC}} \quad (1.1)$$

Where: D_{NC} is the deflection of the theoretically non-composite section, D_{EC} is the deflection of the theoretically entire composite section, and D_{PC} is the deflection of the (partially composite) system in question.

The definition of connection efficiency adopted by Monier et al. [45], which Piazza initially suggested in 1983, illustrated in Eq. (1.2), is an alternative approach.

$$\gamma = \frac{EI_{real} - EI_0}{EI_\infty - EI_0} \quad (1.2)$$

Where γ is the efficiency of the interlayer connection, EI_{real} is the actual section stiffness of the composite member, EI_0 is the section stiffness with no composite action, and EI_∞ is the section stiffness with a theoretical consideration of fully composite action. It was nothing that when the shear connection is very stiff, $EI_{real} \rightarrow EI_\infty$ and therefore the $\gamma \rightarrow 1$. In contrast, for a flexible shear connection, $EI_{real} \rightarrow EI_0$ and so $\gamma \rightarrow 0$.

A relatively rigid shear connector must be employed to limit the deflections in composite structures. Considering that rigidity is not the only necessary property of timber-concrete shear connectors. Notably, shear connectors must also be adequately ductile to prevent undesirable brittle failure in the composite structure [46].

Monteiro et al. [47] identified the most experimental shear test set-ups used in different studies. **Fig. 1-11** Major principal types of the testing set-up of shear tests for TCC illustrate the three primary configurations for performing TCC shear tests: double-shear, single-shear, and pure shear. Previous research studies have frequently employed these configurations to analyze the mechanical properties and shear strength of TCC connections.

In the double-shear set-up, the TCC specimen is composed of three components connected by two sets of connectors, with each component associated with a shear plane. There are two arrangements for this set-up: one where concrete is the central component, connected from each side by a timber component, and another where timber is the central component bordered by two concrete slabs. The loading is applied in the middle of the central component, and the shear forces and slip at the interfaces are measured. This setup allows for the assessment of the shear strength and slip behaviour of the connections. The single-shear configuration consists of one joist of timber connected to one concrete slab. During testing, the TCC specimen typically rests on a support beam or steel plate to prevent overturning or instability. The applied load is usually applied perpendicular to the connection plane, and the deformation and slip are measured to evaluate the connection behaviour. In contrast, the pure shear set-up consists of one timber and one concrete

slab; the set-up is designed to ensure that the load is directed coincidently with the timber-concrete interface, which means that no bending moments are introduced. This helps to eliminate the influence of any eccentricities between the load and the support, making it possible to obtain more accurate measurements of the shear strength and slip behaviour of the TCC connection.

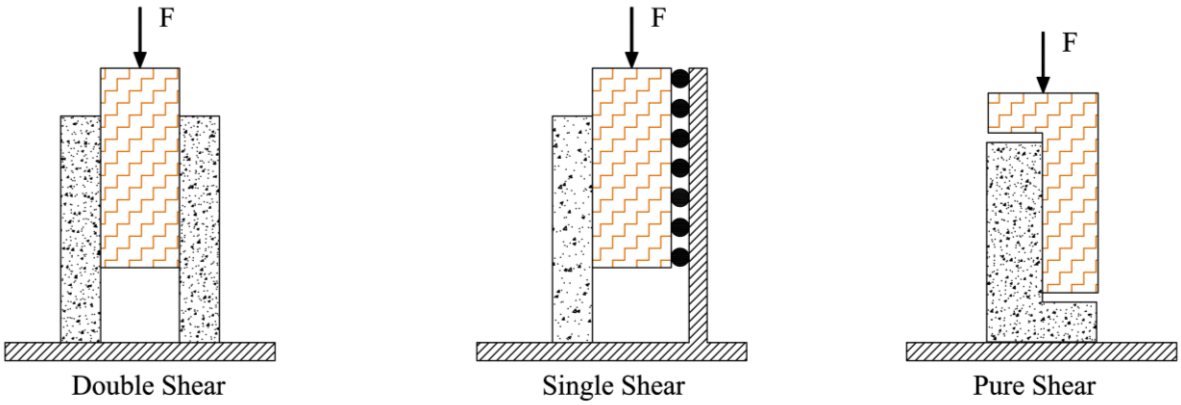

Fig. 1-11 Major principal types of the testing set-up of shear tests for TCC

The database established by Monteiro et al. [47] indicated that the double shear test setup is the most commonly used arrangement for conducting TCC shear tests, representing 52% of all tests conducted. On the other hand, the pure shear setup was utilized in only 4% of performed tests. Additionally, it was observed that the double shear set-up with a (C-T-C) arrangement had a higher frequency of usage at 64% compared to the (T-C-T) arrangement, which had a frequency of 36%. In a study carried out by Carvalho et al. [48], the influence of different arrangements of double shear test set-up on the strength and deformation of joints was investigated. The results showed that the joint configuration has a significant effect on its characteristics. (T-C-T) configuration affording smaller shear strength compared to the (C-T-C) configuration. It was also found that the ductility of the joint was affected by the arrangement of the double shear set-up, with the (C-T-C) configuration joints exhibiting higher ductility than the (T-C-T) configuration joints.

In their study, Monteiro et al. [47] observed that the connection stiffness results for variant shear test setups, including double shear, single shear, and pure shear, were similar, with less than 2.0% variances between the first setup and the other two. This finding is consistent with those of other researchers who have conducted experimental studies. Numerical results have suggested that there may be some slight differences in connection stiffness values between the double shear, single shear, and pure shear test set-ups; the differences are not considered significant. Specifically, the double shear test set-up may slightly underestimate connection stiffness compared to single shear tests and overestimate it compared to pure

shear tests. However, the slight differences in results indicate that the effects of the type of test setup used will not be significant.

1.5.2 Mechanical fasteners

Many studies have been conducted to investigate the mechanical performance of various mechanical fasteners used as shear connectors in TCC structures. These studies have explored factors such as the fasteners' type and geometry, the connectors' spacing and arrangement, the properties of the timber and concrete materials, and the loading conditions to determine the strength, stiffness, and ductility of the connections. These studies have also evaluated the failure modes of the connections, such as splitting of the timber, crushing of the concrete, pulling out of the fasteners, and bending or breaking of the connectors. Some studies have also examined the effect of environmental factors, such as moisture content and temperature, on the mechanical behaviour of the connections. Additionally, Some studies have investigated the long-term behaviour of the connections, including creep and the effect of cyclic loading on the connections' strength and durability. This section will elaborate on some of these studies. The connection properties of most papers discussed in this section are summarized in **Table 1-2**.

Table 1-2 Summary of mechanical fasteners connection properties

Source	Connectore type	Slip stfiness (kN/mm)	Shear strength (KN)
Guojing et al. [49]	Ø8 bolt with 120 mm length	7.55	27.41
	Ø12 bolt with 120 mm length	11.0	39.66
	Ø16 bolt with 100 mm length	19.96	53.01
	Ø16 bolt with 200 mm length	31.18	61.29
Khorsandnia et al. [50]	NS Series	45.0	10.9
	SFS Series	54.9	32.6
	BM Series	36.9	59.5
Sebastian et al. (2012) [51]	Bonded Iroko Dowel 40°	55.8	24.8
	Bonded Iroko Dowel 50°	37.3	33.1
	Dowelled Iroko Dowel 40°	13.5	14.2
	Dowelled Iroko Dowel 50°	11.8	22.4

Gelfi et al. [52]	Ø12 mm stud & 6Ø insertion length	31.1	11.4
	Ø16 mm stud & 6Ø insertion length	13.1	11.6
Ceccotti et al. [53]	Glued-in Ø18 mm rod	25	39.7
Auclair et al. [54]	UHPFRC + Core	20.2	17.3
Kozarić et al. [55]	10mm Lag Screw	5.2	30.9
Oudjene et al. [56]	SFS VB Screw	4.23	33.2
Branco et al. [57]	3mm Nail	5.9	5.7
	3mm Nail (+ Interlayer)	14.6	8.0
Steinberg et al. [58]	Wieland	9.9	21.7
	Tecnaria	21.0	17.9
Jiang et al. [59]	12mm Lag Screw (28-day)	11.9	26.8
Sebastian et al. [60]	12mm Coach Screw	97.7	169.6

Ahmadi et al. [61] investigated the performance of TCC by employing ultra-strength nails, bolts, and screws. The length of the fastener was between 100mm to 150mm. Fasteners were examined with static long and short-term bending by changing the anchoring depth. The results showed that the ultimate load capacity increased twice, and mid-span deflection was reduced by 80% compared to non-rigid joints. Furthermore, the performance of the TCC structure is within the acceptable criteria and regulations defined by building codes.

Meierhofer et al. [62] employed screws with variant orientations, in a straight and inclined angle at ±45°, **Fig. 1-12**, several tests have been performed to study the connectors and the TCC performance, including short-term pullout tests on concrete and wood and long-term shear and bending tests. The configuration with inclined set-up screws showed higher structural performance.

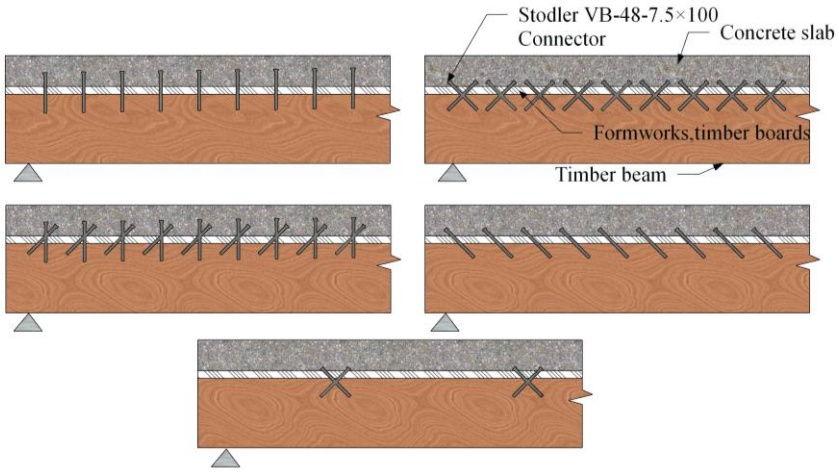

Fig. 1-12 Mechanical fasteners as shear connectors in a TCC structure, Meierhofer et al. [62]

Guojing et al. [49] investigated the mechanical properties of bolt connectors in TCC systems. Double shear push-out specimens with different bolt diameters and lengths (Ø12 bolt with 120 mm length and Ø16 bolt with 100 and 200 mm lengths) were fabricated to test shear capacity and slip modulus. The results showed that bolts were yielded with a lack of cracks in timber and concrete. The shear strength and slip modulus tend to be directly proportional to the bolt diameter. Furthermore, the shear capacity was found to be affected significantly by the strength of concrete.

Khorsandnia et al. [50] conducted an experimental campaign to investigate the strength and stiffness properties of TCC using three different types of screws, including regular screw (Ø5 and 100 mm length), SFS(Ø6 and 200 mm length with 45° inclination angle), and bird-mouth notch reinforced coach screw (Ø6 and 200 mm length, inclined at 45°), **Fig. 1-13**. The slip modulus of connections was determined through push-out tests. BM and NS have the highest and lowest shear strength among the three different connection configurations tested in this study. However, SFS has the highest slip modulus, and its stiffness was close to the BM connection.

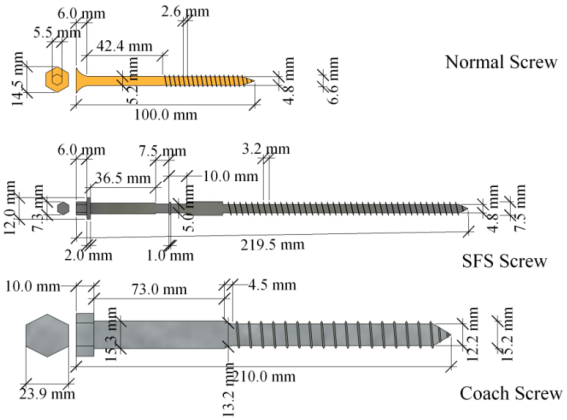

a) screw type

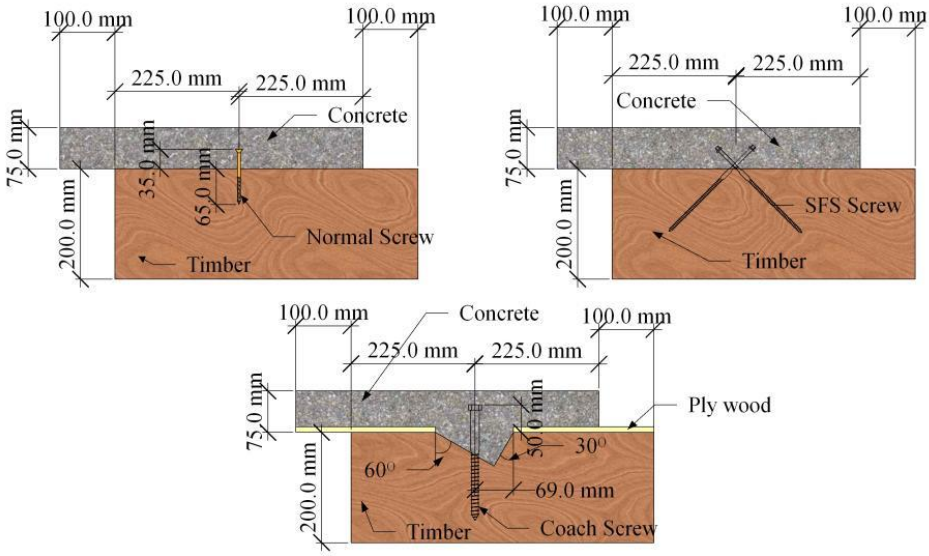

b) connection details

Fig. 1-13 Types of shear connectors and connections details studied by Khorsandnia et al. [50]

Sebastian et al. [51] investigated hardwood stud in TCC connections under load-unload-reload double-shear testing, **Fig. 1-14**. The objective was to investigate the impact of cyclic loading on the strength and stiffness of the connections. The effect of various inclination angles of the studs across the range 40-90° has been examined. The slip modulus of the bonded stud connections shows more scatter and variation with stud angle compared to the dowelled stud connections. The study found that both bonded and dowelled connections with a 50° angle performed better in terms of connection strength. However, the connections with a 40° dowel inclination had higher values for slip modulus.

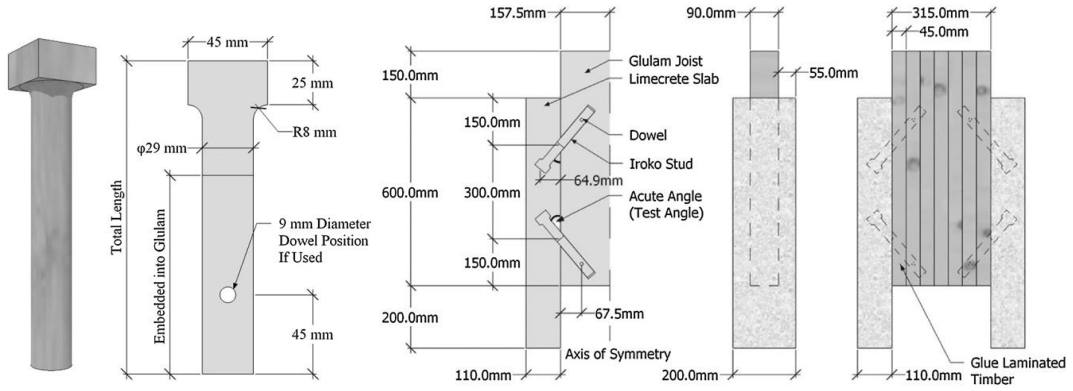

Fig. 1-14 Dowel stud connector, Sebastian et al. [51]

Gelfi et al. [52] focused on experimental investigations of strengthening and stiffening composite structures. The traditional smooth steel rods fixed into predrilled holes in the wood beam without resin were used to investigate the composite structure's local and global performance. Two methods of connections were used, including a directly contacted bond between the concrete and the timber using a Ø12 mm stud and a bond with an interposed plank installed between the concrete and the timber using a Ø16 mm stud, **Fig. 1-15**. The study concluded that both connection configurations provided adequate rigidity and flexural strength. However, they also noted that increasing the anchoring length of the stud to four times its diameter did not significantly increase the connection's rigidity and strength.

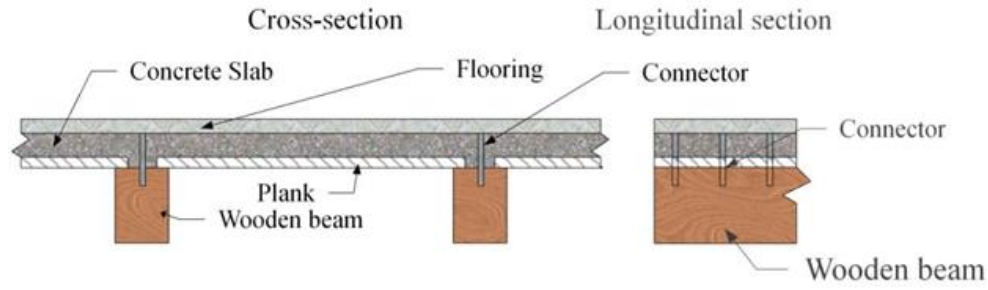

a) direct contact connection

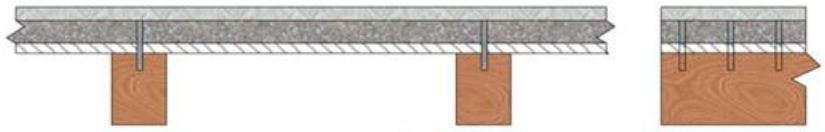

b) interposed plank connection

Fig. 1-15 Stud shear connectors for strengthening and stiffening TCC structures, Gelfi et al. [52]

In a comprehensive experimental study, Ceccotti et al. [53] used a glued-in Ø18 mm rod as a shear connector in a 6 m TCC structure. They inserted the rebars into pre-drilled holes that were filled with epoxy

adhesives, **Fig. 1-16**. Preliminary push-out tests were executed on specimens acquired from the composite beam to investigate the connection properties. Long-term tests were conducted, and the beams were exposed for five years to sustained load in outdoor conditions. The most significant parameters, such as mid-span deflection, slip, and section strains, were observed during the tests. It was found that the TCC beam showed highly stiff behaviour during the collapse tests. The collapse in the timber section under tension failure was brittle; however, no significant plasticization of the connection system happened. The deflection of TCC beams tended to increase in the first two years, while slip continued to grow throughout the test.

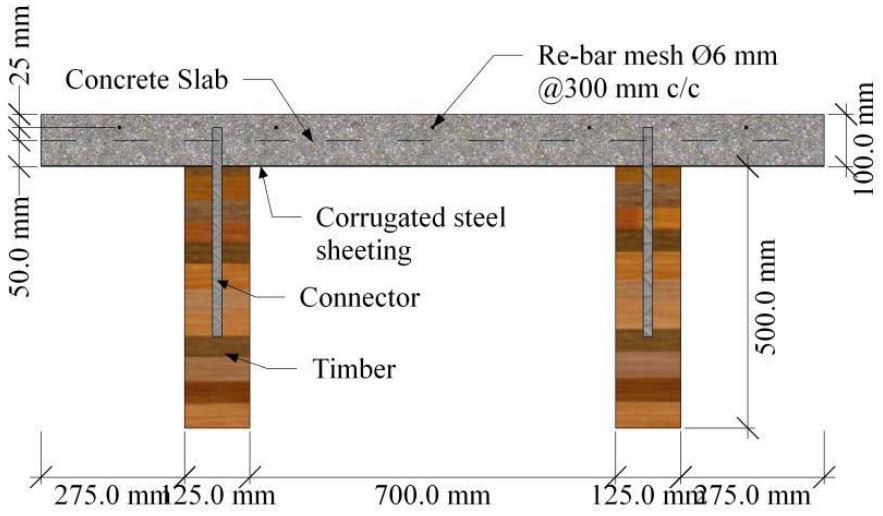

Fig. 1-16 A glued-in shear connector, Ceccotti et al. [53]

In the study by Benítez et al. [63], three types of shear connectors were investigated for designing new TCC bridges and rehabilitating old ones. The three types were a 20 mm steel plain bar with a 60° inclination angle, a circular hollow section (CHS) fixed in an identical drilled groove diameter with 150×M16 coach screws installed in the ring center, and a universal column section (UC) fixed to timber by four 75×M16 coach screws, **Fig. 1-17**. The connectors were configured to enhance the composite action performance, and their static and dynamic responses were evaluated. The results showed that the CHS and UC systems had the highest strength value, but the UC system offered full composite action and better ductility behaviour than the CHS system. The study concluded that the UC system was a more effective shear connector in terms of economic and fixation aspects.

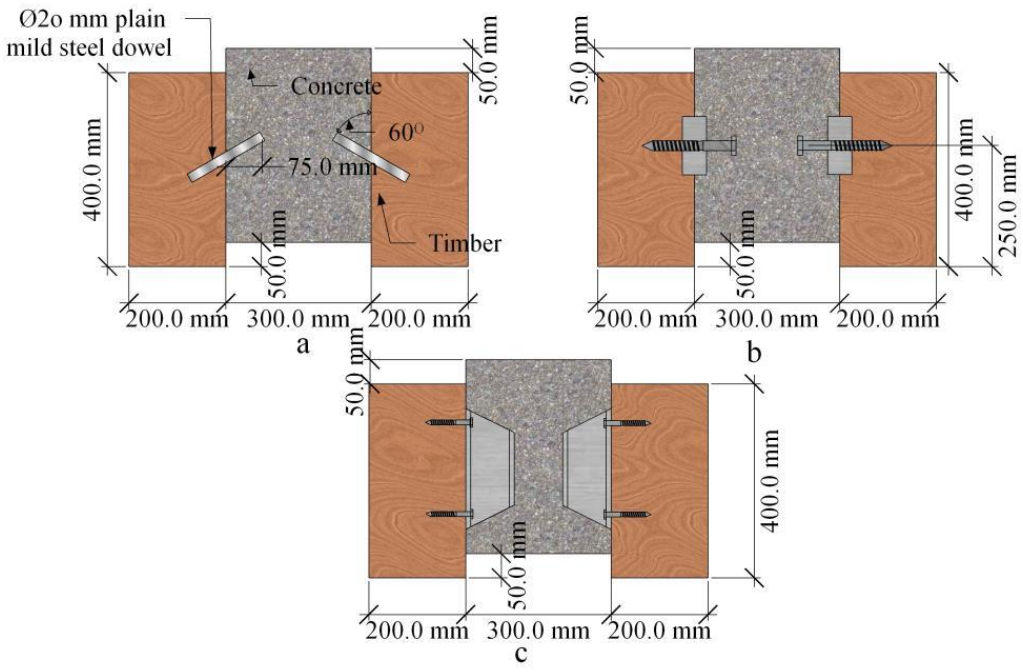

Fig. 1-17 Shear connectors to be used in TCC bridge construction and rehabilitation, Benítez et al. [63]

Auclair et al. [54] developed a composite connector for TCC structures consisting of a UHPFRC shell and a ductile cylindrical steel core, see **Fig. 1-18**. The aim was to improve the ductility behaviour and stiffness sustainability of TCC structures. The study found that the concrete shell diameter significantly impacted the connection stiffness, with increasing diameter resulting in a 67% increase in stiffness. On the other hand, the steel core diameter was found to control the connection strength, with increasing core diameter resulting in an 80% increase in resistance. The composite connector proved to be a promising solution for enhancing the performance of TCC structures.

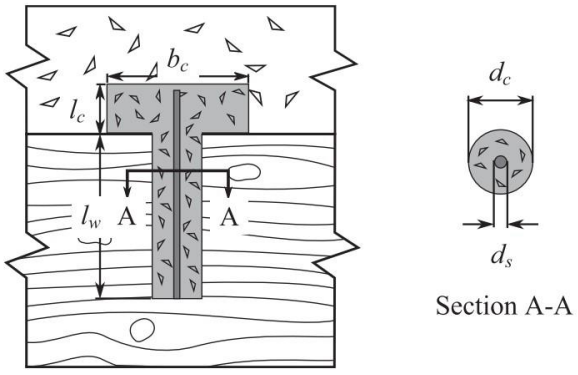

Fig. 1-18 The geometry of UHPFRC and steel core composite as a shear connector, Auclair et al. [54]

Kozarić et al. [55] experimentally examined the slip modulus of lag screw connectors (Ø10 mm and 150 mm length) as a shear connector in TCC structures. Four groups of push-out tests were conducted **Fig. 1-19**. All groups used identical cross-sections; however, each group was fabricated with a different class of lightweight concrete. The results revealed that by increasing concrete strength, the strength of the connection increased along with gaining post-yielding. The lag screws showed ductile behaviour, showing a small linear elastic behaviour before yielding and starting ductility. However, slip modulus and connection stiffness values were found to be lower than those recommended by Eurocode 5.

a) Lag screw

b) detail of a sample before concrete pouring

c) casting of the concrete

Fig. 1-19 Lag screw and testing configuration used for slip modulus testing, Kozarić et al. [55]

Oudjene et al. [56] tested the connection strength of TCC made by two round SFS-screws as a shear connector, see **Fig. 1-20**. The joints showed a small linear elastic behaviour before yielding and gaining strength. The average peak value of strength achieved by these types of connections was 33.2kN. However, this value is still lower than the values obtained by the lag screw systems analyzed by Kozarić et al. [55]. However, this type of connection offers enough ductility, with slip values above 20 mm.

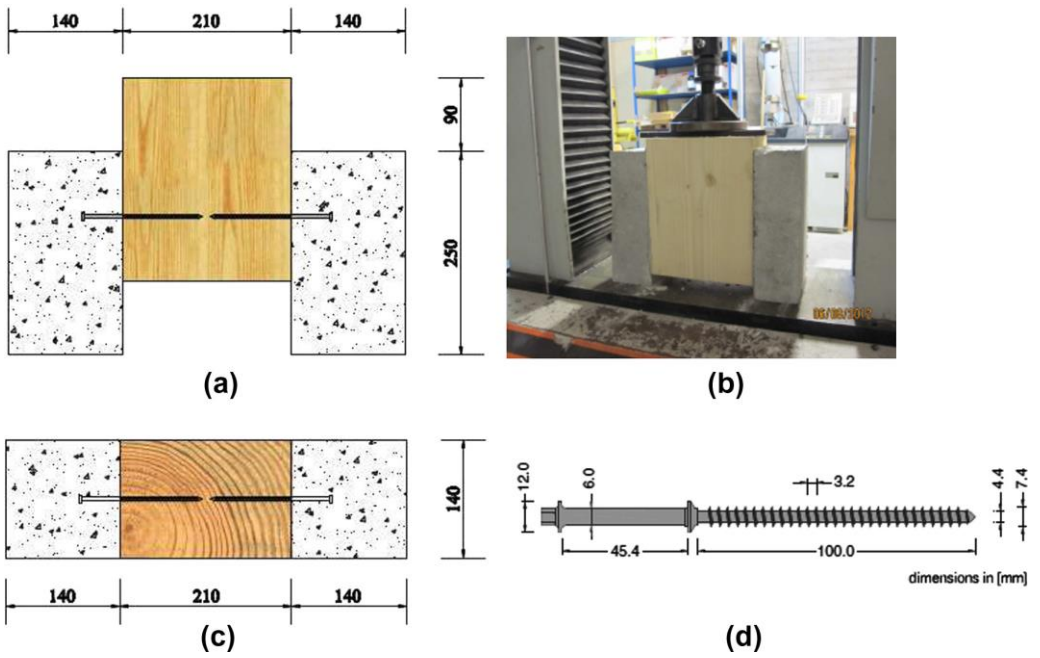

Fig. 1-20 Push-out shear test on TCC specimens: (a) specimen geometry, (b) test set-up, (c) top view, and (d) SFS-screw VB 48 7.5 100, Oudjene et al. [56]

Branco et al. [57] evaluated the performance of round nail connectors (Ø 3.4 mm and 70 mm long) in TCC, considering a lightweight aggregate type of concrete with an option of using a 2mm plywood interlayer between concrete and timber. It was found that using a 2mm interlayer with this shear connector leads to a rise in the load capacity and stiffness by 40% and 37%, respectively, see **Fig. 1-21**.

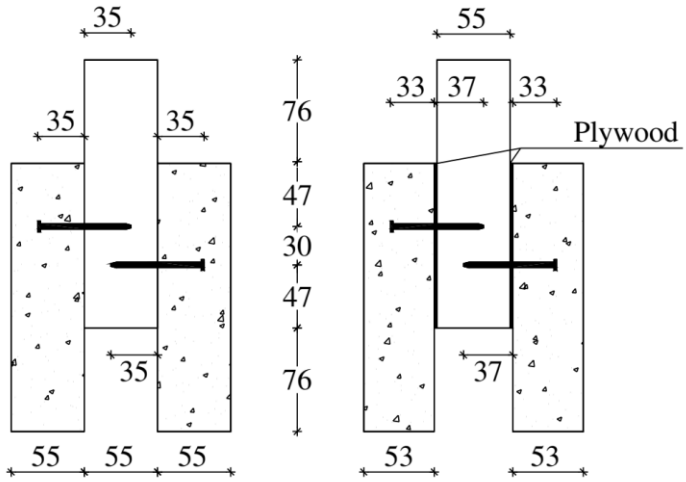

Fig. 1-21 TCC joint configuration, Branco et al. [57]

Steinberg et al. [58] conducted experiments on TCC structures with lightweight concrete using three commercially available connectors (types A through C) and two newly developed connectors (types D and

E) as shear connectors. **Fig. 1-22** illustrates these connectors. Under double-shear testing, the connectors themselves stayed approximately undamaged; few bending deformations were visible, while concrete failure was watched in all cases. However, the failure load for the specimens with type A connector was found under the ultimate failure load or 15mm slip load as recommended by EN 26891 [39]. Type B connectors achieved the highest load resistance among all connectors; however, they showed considerably low slip stiffness (9.9 kN/mm) compared to type C, which achieved the highest slip modulus (20.9 kN/mm).

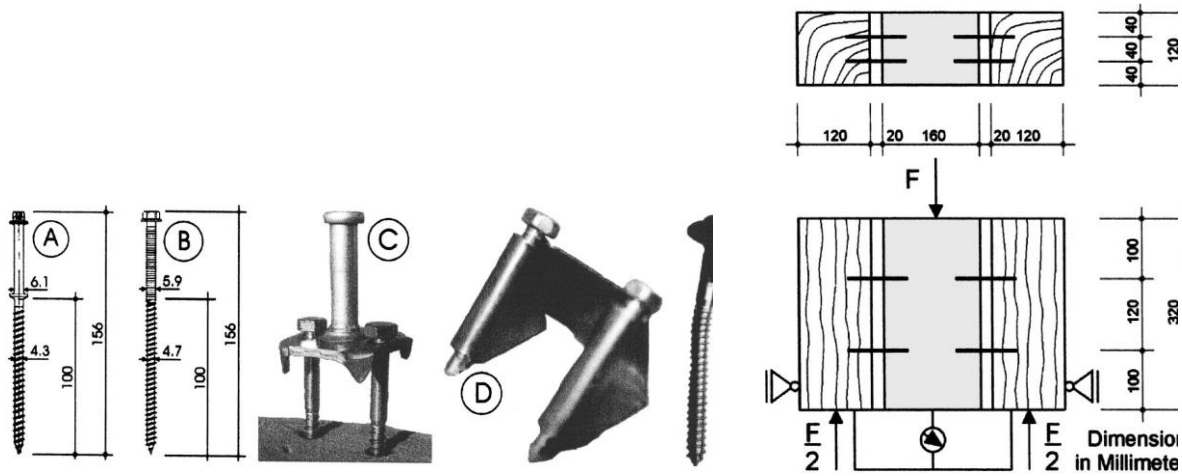

(a) (b)

Fig. 1-22 Shera connectors studied by Steinberg et al. [58]: (a) shear connectors types, and (b) Shear test arrangement

Jiang et al. [59] investigated the lag screw (Ø 2mm and 150mm long) performance as a shear connector with early-age lightweight concrete (12 h to 28 days), **Fig. 1-23**. The results showed that with an age of concrete less than seven days, both the strength and stiffness of the screw connection increased obviously with time, following the growth trend of concrete strength. Furthermore, connections shear strengths and slip modulus reached almost 100% after seven days compared to values of 28 days.

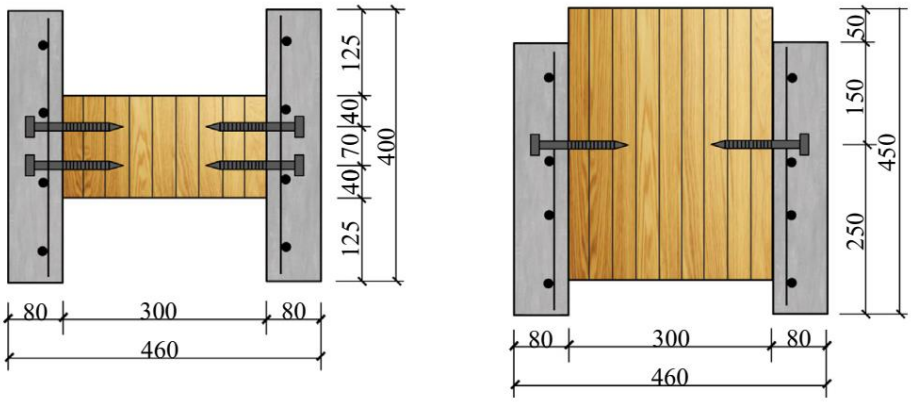

Fig. 1-23 Configuration of TCC push-out specimens with early-age lightweight concrete and lag screw as a shear connector (dimensions in mm), Jiang et al. [59]

Sebastian et al. [60] conducted double-shear experiments on beech LVL-concrete composite connections utilizing four M12 coach screw connectors that were 180 mm in length and oriented at either a 45° or 90° angle, as shown in **Fig. 1-24**. The experimental results showed that the connections with 90° oriented screws exhibited a high average slip stiffness of 97.7 kN/mm, with yielding behaviour occurring at approximately 80kN. However, significant strength was achieved after yielding, reaching a maximum load of 169.6 kN, with a slip in the range of 25-20 mm. The high strength and stiffness values observed may be attributed to the use of four coach screws along the LVL timber length.

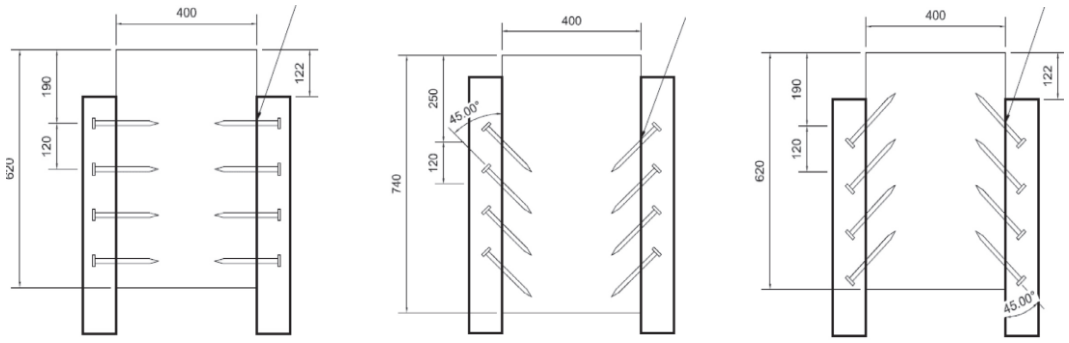

(a) (b)

Fig. 1-24 Configuration of LVL-concrete composite specimens: (a) 90° oriented angle connection details, and (b) 45° oriented angle connection details, Sebastian et al. [60]

1.5.3 Notched connections

The mechanical, geometrical interlock between the timber and concrete in notched connections is the main source of the joint's strength and stiffness. The addition of dowels can further enhance the connection's strength and stiffness, as well as improve its ductility behaviour. The dowels act as additional reinforcement, providing more support and load-bearing capacity to the joint. This makes the joint more resistant to failure under high loads or extreme conditions while maintaining its structural integrity and overall strength. The notched-dowel connection system is one of the most suitable solutions for TCC systems requiring high stiffness and ductility. A summary of the connection properties of the papers discussed in this section is illustrated in **Table 1-3**.

Table 1-3 Summary of notched connection properties

Source	Connectore type	Slip stfiness (kN/mm)	Shear strength (KN)
Gutkowski et al. [64]	Rectangular (102x25mm)	21.1	84.0
	Rectangular (127x31mm)	27.8	81.0
	Rectangular (152x38mm)	28.2	90.0
Deam et al. [65]	Round concrete plug (48.5 Ø x20mm)	83.1	13.2
	Round plug with screw (48.5 Ø x20mm)	105.9	31.4
	Round plug with pipe (48.5 Ø x20mm)	66.6	32.6
	Rectangular (50x16mm)	297.0	54.9
	Triangular 60°_30° 137l CS	145.8	84.8
Yeoh et al. [66]	Rectangular notch 300l×50d×63w CS	247.2	138.9
	Toothed metal plate 2×333l 1 mm thick staggered	463.7	139.3

Djoubissie et al. [67]	Rectangular notch (100x40mm)	155.6	164.1
	Triangular notch (40 mm depth)	38.1	54.2
Hehl et al. [68]	Longitudinal (1 groove)	84.5	74.4
	Longitudinal (2 groove)	133.0	106.9

Gutkowski et al. [69] investigated the performance of notched connections in TCC beams. The notched connection is reinforced by a threaded steel dowel bonded into the open in the wood, **Fig. 1-25**. The results showed that this shear configuration could achieve medium to high degrees of composite action in TCC beams. The composite action efficiency by the notched connection system of the TCC beam specimens ranged from 54.9% to 77.0%.

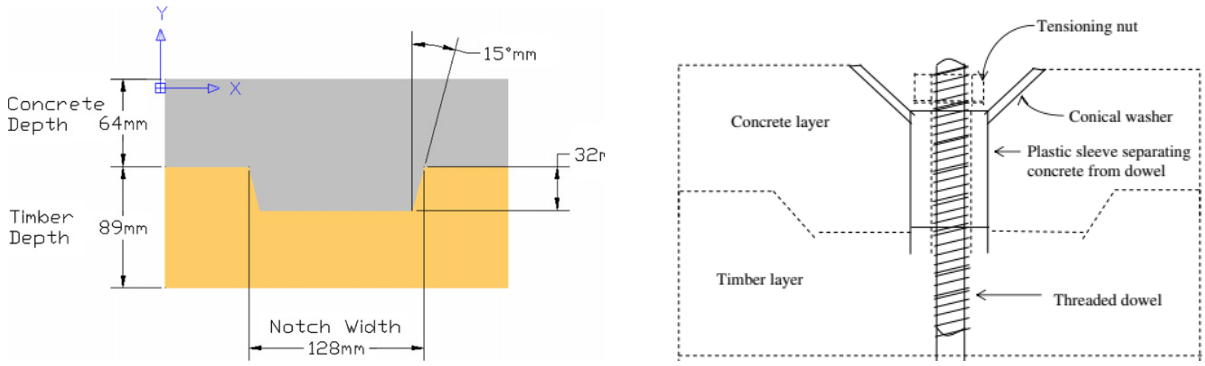

Fig. 1-25 Notched shear connection in TCC beams, Gutkowski et al. [69]

Fragiacomo et al. [70] conducted a study on the long-term behaviour of TCC beams with notched connections. In their study, they observed the specimens throughout the building and for 133 days under applied service loads. **Fig. 1-26** shows the details of the notch system used in the study. The results of the study showed that the deflection of the TCC beams with notched connections increased over time, especially under high loads. The researchers also found that concrete shrinkage had a major effect on the beam's deflection and that pre-cambering of the timber deck could help to reduce the deflection and improve the overall performance of the TCC beams. Based on these findings, the researchers recommended that if deflection limitation is required for serviceability purposes, less concrete shrinkage and the pre-cambering of the timber deck are recommended.

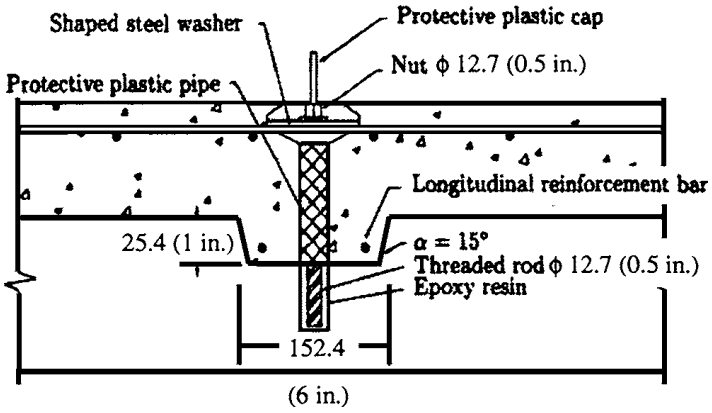

Fig. 1-26 Notched shear connection in TCC beams, Fragiacomo et al. [70]

Deam et al. [65] conducted a comprehensive study to investigate several types of shear connectors that can be used in TCC construction. The study aimed to evaluate the performance of various types of shear connectors under different loading conditions, including rectangular and round concrete cut with and without screw and steel pipe reinforcement, SFS screws, coach screws with various diameters, sheet brace anchors, and framing brackets. It was found that the rectangular concrete cut with a coach screw provided the highest strength and stiffness, **Fig. 1-27**. The author mentioned that such a system could offer a cost-effective option owing to its ability to reduce the required number of connectors along the beam (spaced at 500 mm) to achieve the intended composite action.

Plug:	50 mm length
	16.5 mm depth
Screw:	12 mm diameter
	9 mm predrilled
	150 mm length
	103 mm embedment length

Fig. 1-27 Rectangular plug with screw, Deam et al. [65]

Yeoh et al. [66] conducted a study to investigate the performance of semi-prefabricated laminated veneer lumber (LVL)-concrete composite systems. In their study, they used different types of notched cuts from the LVL joists reinforced with coach screws to ensure the connection between the two components. **Fig. 1-28** illustrates the different types of notched cuts and coach screws used in the study. The results of the study showed that the shape of the notch and bearing area significantly influenced the strength and stiffness

of the TCC structures. The researchers found that larger rectangular notches and coach screws resulted in higher strength and stiffness of the connections. The study also showed that the stiffness of the TCC structures increased with the number of coach screws used to reinforce the notched connections.

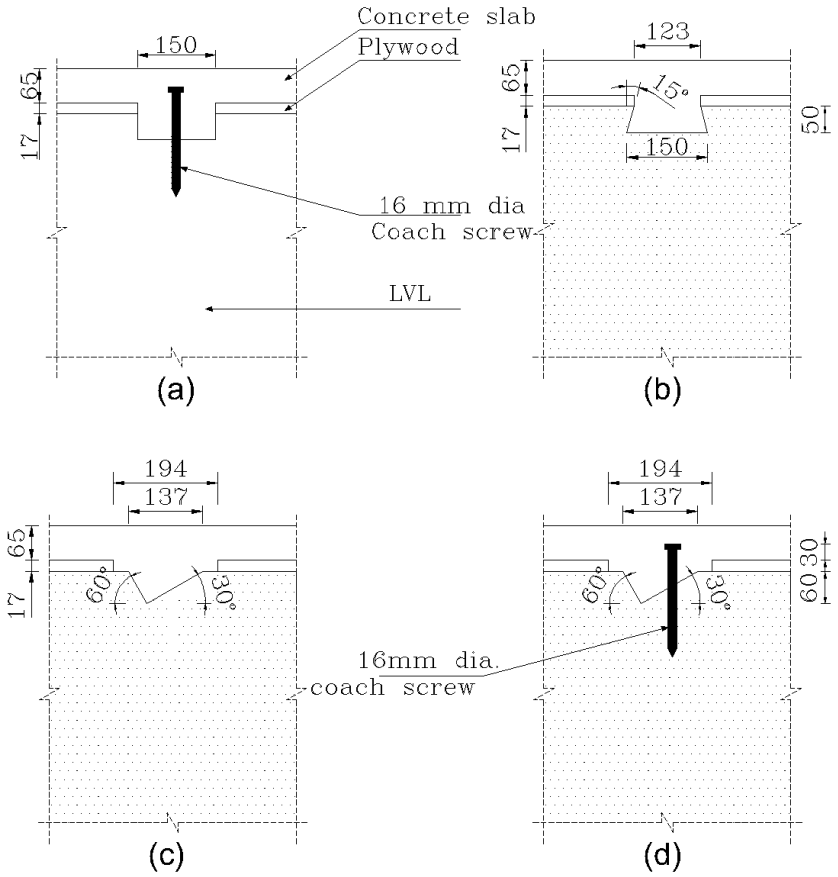

Fig. 1-28 Different types of notched connections in a TCC system (a) typical notched coach screw connection, (b) dovetail notch, (c) triangular notch, and (d) triangular notch with coach screw, Yeoh et al. [66]

Djoubissie et al. [67] performed an experimental study to analyze the behaviour of the timber-concrete connections by employing threaded steel bars and notches as a connection system. The tested configurations, as shown in **Fig. 1-29**, concerned the notch without a rod, the rod without a notch, and the notch combined with a rod. The rod consisted of an ordinary reinforcing steel bar threaded and screwed into the timber. These fasteners are combined with triangular or rectangular notches between timber and concrete. The authors conducted push-out tests on asymmetrical specimens to characterize the main mechanical parameters of this system. It was found that the joint with steel bars alone is the weakest among all the tested samples, while the connections using the inclined steel bars (120° oriented to the grain) showed higher values of stiffness in comparison with the straight bars (90° oriented to the grain).

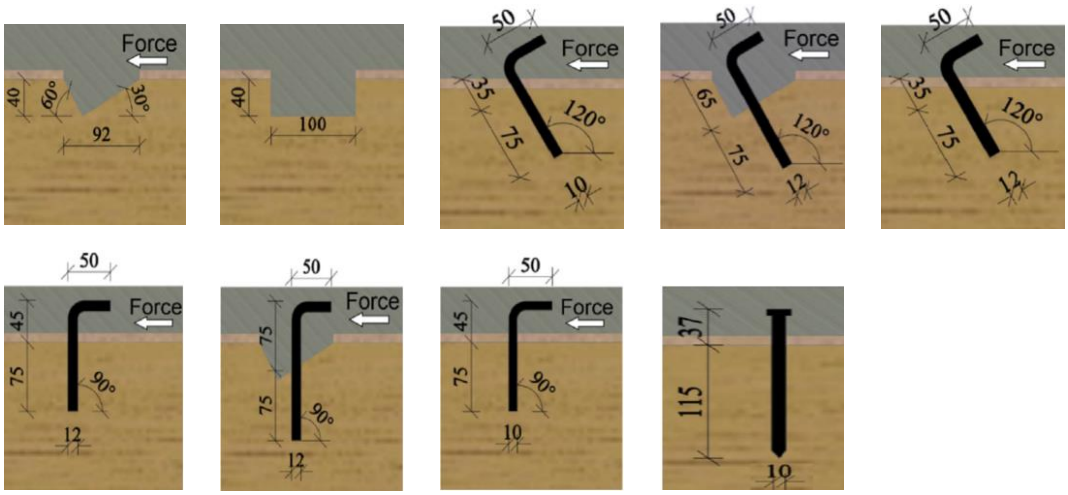

Fig. 1-29 Notched connections configurations, Djoubissie et al. [67]

Hehl et al. [68] investigated the TCC structure that used a notched connection but with a different configuration where the concrete panel was located on the bottom side instead of the top side of the specimen. This modification aimed to improve the structure's thermal and fire protection properties. **Fig. 1-30** illustrates the connection details, where a longitudinal plug into the surface of the timber joist allows for a geometrical interlock with concrete. A single shear test was performed on an 800mm long specimen under the role of three variant parameters (length, radius, and counts of the grooves). The results showed that the groove plugs were sufficiently able to transmit the shear forces and effectively connected the concrete slab vertically to the timber. Furthermore, the results showed an average of 42% less in the strength of one groove connection (74-82 kN) compared to two groove connections (107 kN).

Fig. 1-30 Notched TCC specimen tested by Hehl et al. [68]

1.5.4 Metal plate connections

The HBV (Holz-Beton-Verbundsystem) expanded steel mesh connector is the most used type of plate connection in TCC systems. The HBV requires a continuous steel mesh of which the first half is bonded by glue in a slot in the timber beam and the second half embedded into a concrete panel. Clouston et al. [71] adopted this connection system for bending and shear testing, employing several types of adhesive to secure the connection. The shear test results showed that such a system could achieve high strength, stiffness, repeatability, high ductility, and high significant composite action indicated through the bending tests. Regarding the type of adhesive required to enforce the connection, it was found that the 3MScotch-Weld™ and ® 2-Ton epoxy adhesives were the most appropriate adhesives for such a system.

Clouston et al. [43] also investigated the TCC structure using an HBV plate as a shear connector. Push-out tests and full-scale bending tests were conducted. The results showed that the average connection strength was 111 kN, with a high slip stiffness of 415.5 kN/mm. Yeoh et al. [66] also investigated the performance of the toothed metal plate connector in (LVL)-concrete composite .It was found that the connector can achieve an average connection strength of 139 kN and slip stiffness of 463.7 kN/mm.

Although extensive studies using HBV plates, Dolores et al. [72] conducted an experimental investigation into TCC connection performed by a different discrete steel mesh fastened in timber by epoxy adhesive. Three configuration systems regarding the steel rods were tested, in which rods are added longitudinally or transversally, as shown in **Fig. 1-31**. The results revealed that such a connection is satisfactory strong, rigid, and could allow for ductile failure. The connector showed slip stiffness of 838 kN/mm for the section of 180mm long without steel rods, growing to 915 kN/mm and 973 kN/mm when additional longitudinal and transverse steel rods were added, respectively.

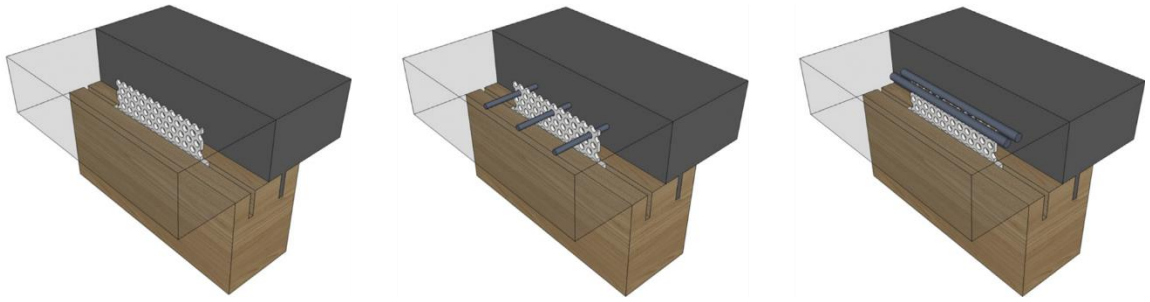

Fig. 1-31 Steel plates as a shear connector, Dolores et al. [72]

1.5.5 Glue connections

In comparison with mechanical connections, glueing connection systems can achieve an ideal interaction with full-composite behaviour between timber and concrete. In contrast, mechanical shear connectors such as screws and bolts can't offer such behaviour due to the limited stiffness of these

connectors; furthermore, mechanical shear connectors require extensive drilling and cutting, which could weaken the strength of timber elements. These inconveniences may be solved by using adhesive bonding instead of shear connectors [29,73,74]. However, it is worth mentioning that one of the main drawbacks of glued connections in TCC is the lack of ductility after the joint ruptures. As a result of rupture, the glued connection loses its load-carrying capacity, and the structure may experience brittle failure without warning signs or deformation, which could cause severe consequences.

The following reviews will illustrate the studies that used glue as a primary shear connector between the two components, meanwhile highlighting the effect of moisture content, bonding length, type of adhesives, adhesives thickness, fabricating approaches, strength and type of concrete, and surface treatment on the mechanical behaviour of the connection.

1.5.5.1 Effect of moisture content

The effect of moisture content on glued TCC can be significant, as it can affect the adhesive properties of the glue used to bond the timber and concrete elements. Moisture content can alter the surface properties of the wood and concrete, making it difficult for the adhesive to properly bond with the substrate.

Negrão et al. [41] conducted an experimental study on epoxy-bonded TCC joints to investigate the feasibility of glueing as an alternative solution to shear connectors under the role of different variables. The investigation of the effect of moisture content revealed that the behaviour of this bonding structure is dramatically affected by the increase of moisture content of timber, mainly if it occurred before the glueing process. Two groups were tested: in the reference group, joints were cured and tested at 20°C and 65% RH, while in the second group, joints were conditioned to 30°C and 95% RH after glueing. The moisture content of the wood in both groups was initially around 12%, but in the second group, it was increased to 20% at the test time. The average shear strength was 4.36 Mpa and 1.16 MPa for the reference and second groups, respectively.

While limited studies have investigated the effect of moisture content variation on glued TCC joints, they have shown that lower moisture content generally results in stronger and more durable adhesive bonds. However, studies including Frohnmüller et al. [75] emphasize the need to investigate the variable climate conditions' effect regarding moisture content on the mechanical behaviour of adhesively bonded TCC joints. Generally, Most of the studies investigated the bonding strength at an MC level of 12%. In our study, we will investigate the variation of moisture content levels of timber on the bonding performance of TCC joints, focusing on shear strength and failure modes.

1.5.5.2 Effect of bonding length

The effect of bonding length on adhesive joints, particularly in TCC joints, is a critical factor that influences the efficiency and uniformity of the bonding stress distribution, potentially affecting the overall mechanical performance of the TCC joints. Despite its importance, there is a notable scarcity of research focused on how variations in bonding length affect the mechanical behaviour of adhesively bonded TCC joints.

Fu et al. [76] conducted experimental tests and analytical derivations to investigate the shear strength of bonding lines between concrete (with a compressive strength of 24.8 MPa) and engineered wood composite using two types of epoxy, i.e., Ampreg22 and Sikadur300. The study focused on two commonly used set-ups, a double-shear test set-up with a bonding length of 50 mm and a compression-shear test set-up with a bonding length of 300 mm, to determine the shear strength of bonding lines between concrete and wood species, including cross-laminated timber and laminated veneer lumber. The study found that both tests yielded similar under-average shear strength of around 2.3 MPa, with the main failure occurring in concrete. However, the study suggested a bonding length of 50 mm to determine the shear strength of the bonding line, as a shorter bonding length leads to a more uniform distribution of shear stress.

The result by Negrão et al. [41] showed that the joints with double and triple lengths showed only a minor reduction in average shear strength attributed to the volume effect. However, the small number of tested specimens wasn't sufficient to draw firm conclusions. Given these findings, it is evident that a deeper exploration into the scale effect is essential for a more comprehensive understanding of its implications on the mechanical performance of adhesively bonded TCC joints.

1.5.5.3 Effect of adhesive type, thickness, and waiting time

Nemati Giv et al. [77] examined the shear strength of glue TCC joints between spruce wood blocks from the glulam (GL 24 h) with both cast-in-situ concrete and prefabricated concrete, as shown in **Fig. 1-32**. This study used two types of adhesives: Sikadur-330 (epoxy-based) and Sikaforce 7710- L100 (polyurethane-based). In the process of creating wet TCC joints, waiting times were established for the adhesive to cross-link before fresh concrete was poured. Three waiting times were set for each epoxy and PUR adhesive based on the gelation time of the corresponding adhesive measured through an oscillatory test. These waiting times were 0, 0.5, and 1 of t_{gel}. The experimental outcomes showed that for the wet TCC joints bonded by epoxy, the maximum average shear strength with a value of 5.67 MPa was obtained at a 0-minute waiting time; in contrast, this value was reduced by 46.7 % to reach 3.02 Mpa at 221-minutes (t_{gel}) waiting time. Whereas for the case of wet joints bonded by PUR adhesive, the average strength values were 1.80, 1.86, and 0.96 MPa at the 0-, 36-, and 72-minute (0, 0.5, and 1 of t_{gel}) waiting times, respectively. The dry TCC joints bonded with epoxy and PUR adhesives had similar average shear strength values, which

were 2.74 MPa and 2.72 MPa, respectively. Both joints also had the same failure mode, which was an adhesive failure with a small portion of concrete fracture, see **Fig. 1-33**.

The findings by Negrão et al. [41] revealed that the impact of adhesive layer thickness on shear strength was inconsistent, with thicker layers increasing strength in prefabricated specimens and decreasing it in fresh concrete specimens. The study employed two epoxy resins, ICOSIT K101-N and ICOSIT K220/60, which achieved an average shear strength of about 4.5 MPa under dry conditions, indicating good results.

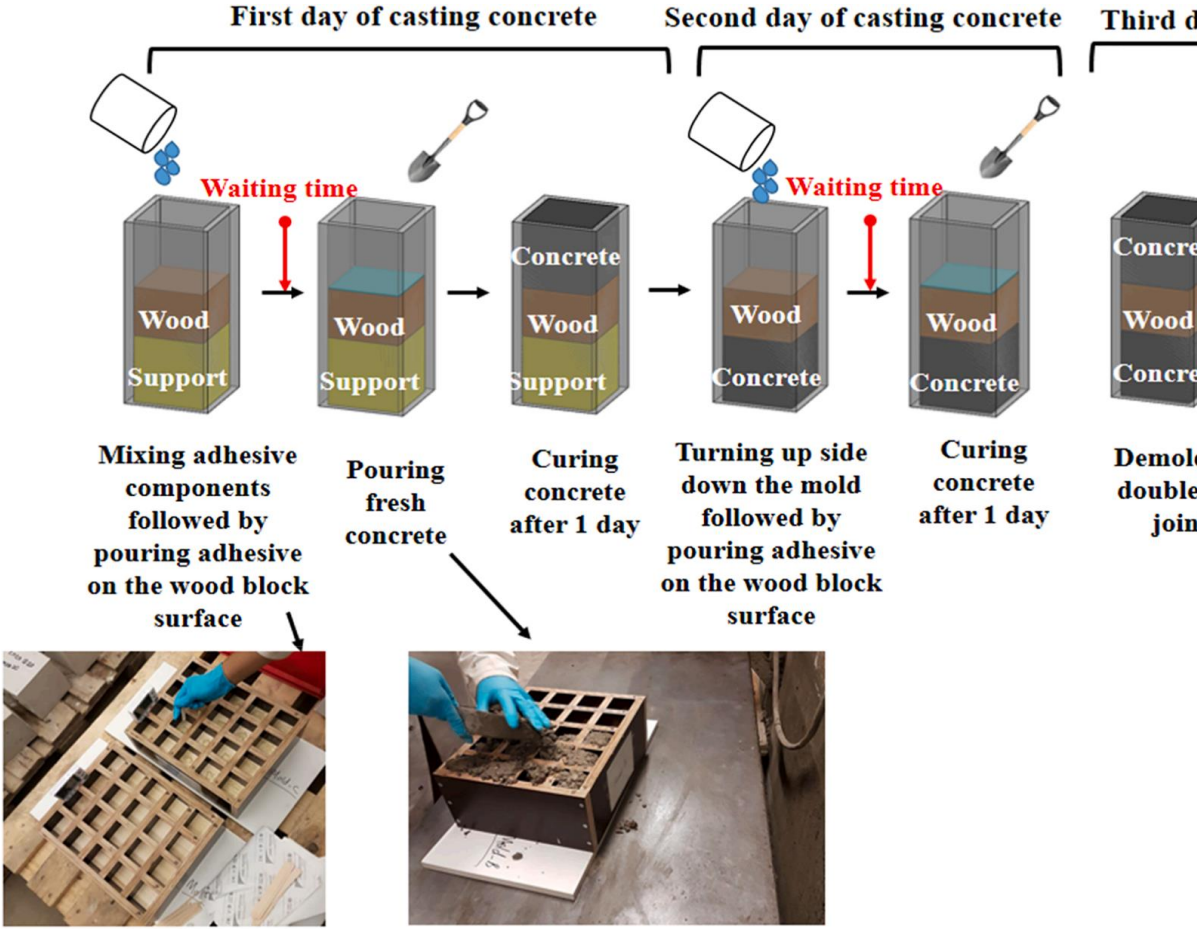

(a)

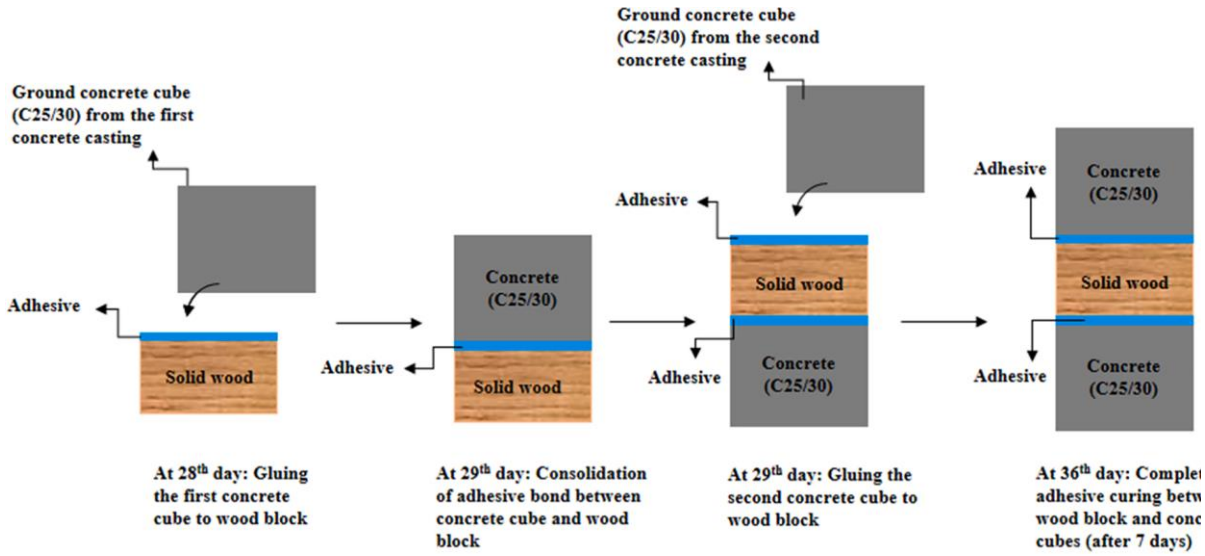

(b)

Fig. 1-32 The manufacturing process of (a) wet TCC joints and (b) dry TCC joints, Nemati Giv et al. [77]

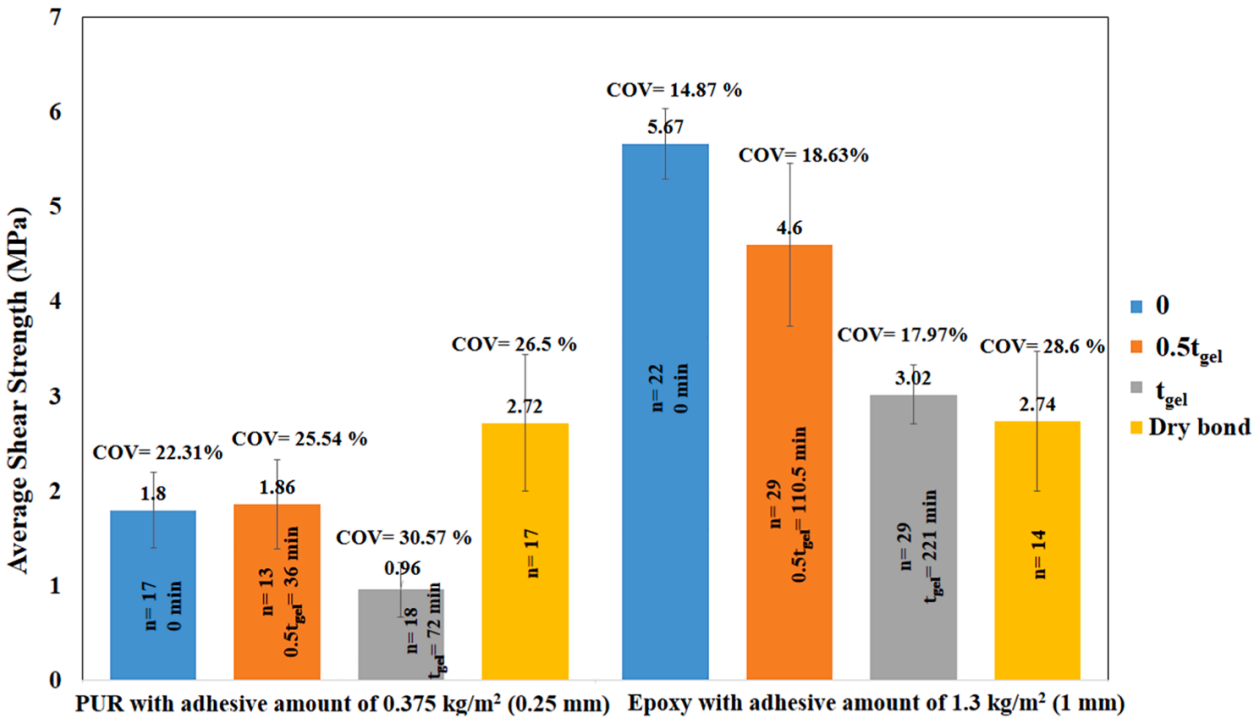

Fig. 1-33 Average shear strength of TCC dry and wet joints, Nemati Giv et al. [77]

Youssef et al. [40] Conducted a study to investigate the behaviour of the timber–concrete bonded with or without ageing using push-out tests. Investigations are conducted on four different types of adhesives: a

soft resin (polyurethane), an elastoplastic resin (modified acrylic), and two elastic and stiff resins (Epoxy) to study the influence of the adhesive stiffness on the shear strength, the ultimate capacities of connections and some local deformations. Outcomes presented a tremendous difference in results depending on the kind of adhesive: The average ultimate shear stress results of push-out tests for studied adhesives without ageing was 1.1 N/mm2 for a polyurethane, whereas two adhesives, Sikadur30 and Sikadur330, achieved 6.7 N/mm^2 and 6.6 $N/mm^{2,}$ respectively. However, the maximum average ultimate shear stress with one-year ageing was achieved by Sikadur30, represented in 4.7 N/mm^2. Additionally, The Sikadur30 had the highest ultimate capacity of 242 kN compared to 41.1 kN for polyurethane. However, these values decreased after one year of ageing. Failure modes varied, and slip vs. load plots showed a mostly linear behaviour, with specimens failing before reaching 1 mm displacement in a brittle manner.

Fu et al. [5] conducted a study to investigate the behaviour of the interfacial bonding between wood chip concrete (WCC) and timber (Cross Laminated Timber (CLT) or Laminated Veneer Lumber (LVL)) in adhesively bonded TCC systems was investigated. The WCC was produced by substituting 15% of the coarse aggregates with beech-wood chips to reduce self-weight and improve thermal insulation. The study used a double-shear specimen consisting of a WCC block in the middle and a timber block on each side, bonded by four types of constructional adhesives: epoxy, Phenol Resorcinol Formaldehyde (PRF), Polyurethane (PUR), and Urea-formaldehyde (UF). The basic properties of the four adhesives used in the study are presented in **Table 1-4**.

Table 1-4 Basic information on adhesives was used by Fu et al. [5]

	Epoxy	PRF	PUR	UF
Product name	PRIMETM 20LV	Prefere 4094	Semparoc I 12 NV	Kaurit Leim 285
Viscosity (mPa.s)	214–228	2500–5000	8000–20000	750–1000
Density (kg/m^3)	1.084	1.17	1.12	1.291–1.302
Curing time	40 h	2–3 days	7 days	6–8 days

The WCC blocks at the center of the specimens had a bonding length of 50 mm, and the preparation for the shear tests was illustrated in **Fig. 1-34**. The study involved ten samples for each type of adhesive, including epoxy, Phenol Resorcinol Formaldehyde (PRF), Polyurethane (PUR), and Urea-formaldehyde (UF), and two types of wood, i.e., CLT and LVL. Thus, a total of 80 double-bonded shear test specimens were examined.

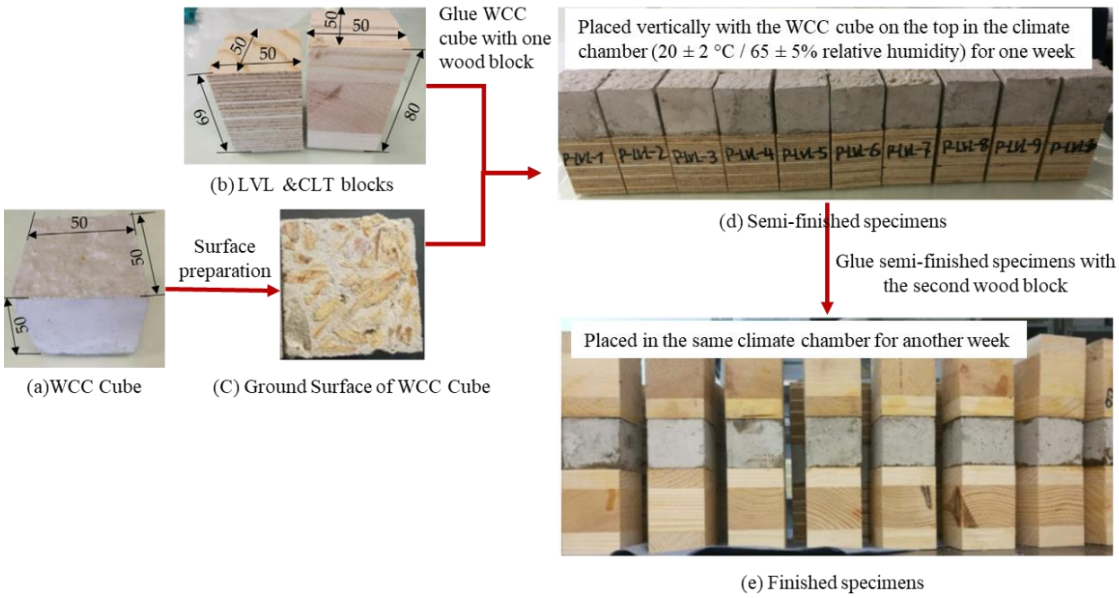

Fig. 1-34 Preparation of shear test specimens, Fu et al. [76]

PUR adhesive exhibited the highest bonding strength in both PUR-CLT and PUR-LVL specimens, with values of 0.90 MPa and 1.48 MPa, respectively. The PRF-LVL specimens showed the second-highest shear strength of 1.05 MPa, while the PRF-CLT specimens had a significantly lower strength of 0.34 MPa. This difference in shear strength between PRF-LVL and PRF-CLT could be due to their varying failure behaviour. The shear strengths of Epoxy-CLT and Epoxy-LVL were 0.79 MPa and 0.66 MPa, respectively. The UF-CLT and UF-LVL specimens had relatively low shear strengths of 0.39 MPa and 0.33 MPa, respectively, and both failed at the glue line. The low viscosity of the epoxy and UF adhesives might have caused a deficiency of the bonding at the glue lines, resulting in their low strengths. This effect was more pronounced for specimens made of epoxy-LVL and UF-LVL. However, this trend was entirely reversed for PUR and PRF specimens.

Overall, The shear bond strength of glued TCC joints is influenced by various factors, including adhesive type, thickness, and waiting time. Studies have highlighted the significant impact of these variables on the performance of adhesively bonded TCC structures. Specifically, the choice of adhesive types, such as epoxy-based or polyurethane-based, plays a crucial role in determining the shear strength of TCC joints. Additionally, the thickness of the adhesive layer and the waiting time before pouring fresh concrete onto the adhesive also affect the bonding strength. For instance, thicker adhesive layers may enhance bonding strength. Similarly, the waiting time before concrete pouring can significantly alter the shear strength of TCC joints. Further research in this area holds great potential for advancing the field of adhesively bonded TCC structures.

1.5.5.4 Effect of the fabrication process

The fabrication process plays a crucial role in determining the mechanical performance and characteristics of adhesively bonded TCC joints. Specifically, the choice between dry and wet processes significantly influences structural integrity, joint efficiency, and durability.

In the context of adhesively bonded TCC structures, the dry process involves the bonding of pre-fabricated concrete panels with timber elements. This method offers several advantages, including ease of assembly and reduced construction time. However, it also presents certain challenges, such as potential gaps between the concrete and timber components, which can affect the structural performance of the composite structure.

On the other hand, the wet process involves bonding fresh concrete with timber on-site, resulting in better integration between the two materials. This method eliminates gaps and provides superior interface continuity, enhancing the overall strength and durability of the TCC structure. Despite these advantages, the wet process introduces its own challenges, including adhesive movement during concrete pouring, water presence during adhesive cross-linking, and the heterogeneity of the concrete-wood interface.

Research studies, such as the one conducted by Nemati Giv et al. [77], have investigated the effects of different adhesive materials and fabrication processes on the mechanical performance of adhesively bonded TCC joints. The results showed that the use of epoxy resulted in higher shear strength in wet joints than in dry joints. In contrast, the use of PUR resulted in lower shear strength in wet joints than in dry joints, as shown in **Fig. 1-33**. The variance in trends observed between wet and dry TCC joints that utilize epoxy and PUR adhesives was attributed to the quantity of adhesive used. In the fabrication of these joints, the epoxy had a thickness of 1 mm, while PUR had 0.25 mm. This thicker epoxy layer offers superior mechanical interlocking in wet TCC joints compared to dry joints since adhesive can penetrate more deeply into fresh concrete than prefabricated concrete.

While both dry and wet fabrication processes have been explored to some extent, there remains a limited amount of comprehensive research on the topic. This gap presents an opportunity for further investigation and advancement in adhesively bonded TCC construction.

1.5.5.5 Effect of strength and type of concrete

The strength and type of concrete significantly affect the performance of glued connections in TCC structures. High-strength concrete has improved the load-carrying capacity and stiffness of TCC structures with glued connections. Therefore, selecting concrete type and strength should be carefully considered when designing TCC structures with glued connections to ensure optimal performance and durability.

Fu et al. [74] conducted a study investigating the bonding performance between wood and precast concrete with adhesive-bonded connection in the TCC system. Several types of TCC-bonded joints with epoxy were tested under double shear tests, as shown in **Fig. 1-35**. The test variables considered the following: i)Type of surface treatment of concrete component (i.e., sanded, sandblasted, and non-treated surfaces), ii) concrete strength (i.e., normal strength concrete (NSC), high strength concrete (HSC), and ultra-high-performance concrete (UHPC), and iii) wood type (i.e., glulam GL24 and beech wood). According to the test results, the use of sanded and sandblasted surface treatments on NSC and HSC specimens had a significant positive impact on bond shear strength, leading to a change in the predominant failure mode from facial mortar rupture to concrete substrate failures. However, UHPC joints failed mostly at the concrete/adhesive interface due to the material's low porosity, which affected the adhesive penetration process.

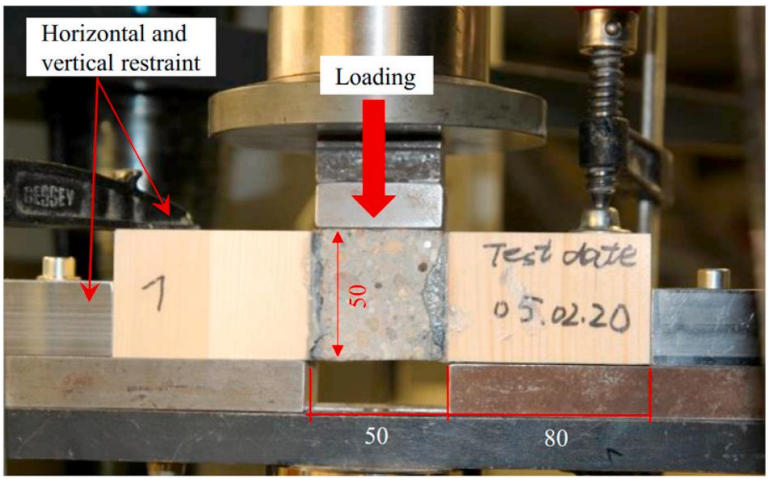

Fig. 1-35 Test setup for double-shear adhesive-bonded TCC joints, Fu et al. [74]

Kanócz et al. [78] also experimentally investigated the adhesive connection between lightweight wet concrete and vertically laminated or cross-laminated timber in two structural TCC beams. Short-term shear tests were carried out to determine the connection's shear parameters according to EN 392 [79], see **Fig. 1-36**. The shear test results showed that all failure modes of specimens were concrete shear failure and shear failure of timber fibers owed to the load eccentricity. The results showed that the adhesive connection is very effective, with an average shear strength of 5.27 MPa.

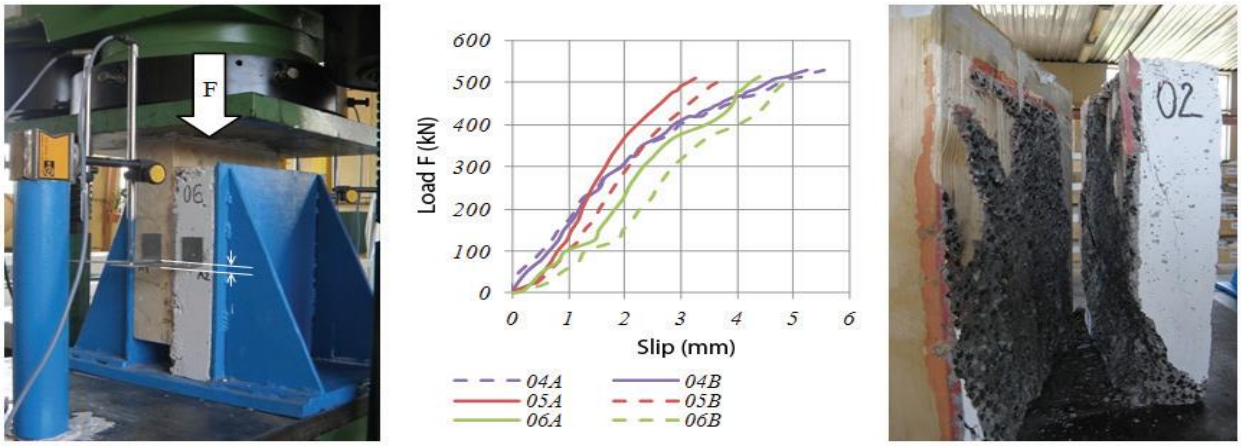

Fig. 1-36 Shear tests set-up, load–slip diagram, and failure mode, Kanócz et al. [78]

In a study by Brunner et al. [29], TCC shear test specimens were produced using a wet-on-wet method. Five specimens with each conventional concrete and self-compacting concrete were produced. Epoxy-based adhesive "Sika AG" was used with a 90-minute time interval between applying the adhesive and casting the concrete. The bonding area was 100 mm wide and 40 mm long. An evaluation of the test results showed that the average shear strength was higher when conventional concrete, instead of self-compacting concrete, was used, 2.97 N/mm2 and 2.1 N/mm2, respectively. However, these values were lower than those reported in the study by Negrão et al. [41].

There's a notable gap in research concerning the integration of self-compacting concrete (SCC) in TCC structures. The concern arises from the possibility of mechanical compaction adversely affecting bonding performance, leading to adhesive running during the wet process. Given this gap, it's crucial to prioritize investigating SCC potential in adhesively bonded TCC structures, especially in scenarios where a wet fabrication process is intended.

1.5.5.6 Effect of surface treatment

The surface treatment of concrete can have a significant effect on the glue connections in TCC. A rough and porous surface can provide better bonding with the adhesive and enhance the connection's mechanical performance. Concrete sandblasting treatment is one of the most common methods proposed in the literature.

A more recent study by Fu et al. [80] investigated the effect of concrete surface treatment on the interfacial properties of adhesively-bonded TCC joints. The study examined joints' bond strength and failure modes with three different concrete surfaces: untreated concrete, sanded concrete, and sandblasted concrete. The results showed that the surface treatment of concrete had significantly improved the bond shear strength and changed the predominant mode of failure from facial mortar rupture mode of failure into

concrete substrate failures. Furthermore, many studies by [75,77,81] found that increasing surface roughness using sandblasting or sprinkled sand plays a significant role in the bond strength of the adhesive to concrete. A rougher surface leads to a stronger bond and can improve the shear strength of the connection. Thereafter, these studies suggest that surface treatment can significantly impact the strength of glued connections in TCC. Sandblasting appears to be the most effective surface treatment for improving the strength of glued connections.

It is worth mentioning that there are limited studies on the effects of surface treatments on timber. The literature review indicates that timber can be treated by sanding to improve adhesion, as suggested by Augeard et al. [82], or by increasing surface roughness through hammering, as explored by Negrão et al. [41].

Negrão et al. [41] has investigated the use of rough interfaces of timber, which resulted in reduced shear strength, contradictory to what was expected. The reason was attributed to the weakening of the wood component during hammering.

Our study will investigate the effects of concrete surface sandblasting treatment on the mechanical performance of adhesively bonded TCC joints. Furthermore, we will explore the sand addition to increase the roughness between the concrete and timber surfaces.

1.6 Structural behaviour of TCC systems

Full-scale investigations typically involve constructing a prototype or test structure and subjecting it to loads and stresses similar to those it would experience in its intended use. This can involve applying loads to the structure to test its strength, stiffness, and deformation characteristics and monitoring its response to environmental factors such as temperature and humidity. Full-scale investigations of TCC construction are necessary to validate the results obtained from small-scale studies and to ensure the structural integrity and performance of TCC buildings in real-world conditions. Full-scale experiments of TCC structures also provide an opportunity to evaluate the durability and long-term performance of TCC systems, including their resistance to moisture, decay, and insect damage. Furthermore, it is essential to validate the accuracy of computer models used to predict the behaviour of TCC structures.

These studies can be categorized into two types: failure testing and serviceability testing. Failure testing involves subjecting TCC structures to extreme loading conditions until they fail, with the primary objective of studying structural nonlinearity and failure modes. These tests are typically used to determine the ultimate limit state of the structure, where it can no longer support the applied load. The results of these tests can be used to validate numerical models and provide design recommendations for future TCC structures. Serviceability testing, on the other hand, is used to evaluate the performance of TCC structures

under normal service conditions, such as low-level live loads and dynamic performance. The main objective of these tests is to assess the long-term behaviour of TCC structures and their ability to meet design requirements such as deflection, vibration, and durability. Experimental studies on TCC structures have employed different types of connections, including adhesive-bonded, notched, and dowel connections. Adhesive-bonded connections have gained significant attention due to their ease of installation and ability to transfer shear forces between the timber and concrete components.

1.6.1 Short-term behaviour of TCC structures

This section will consider full-scale experimental studies that have utilized glue connections.

Brunner et al. [29] used a wet-on-wet glued connection technique to produce different series of TCC slab bending test specimens with each entire or a reduced bonding area. In a reduced bonding area series, the complete contact area between the timber and the concrete was skipped with the assistance of half PVC pipes running transversal and parallel along the beam. The primary materials and parameters were used to produce the specimens: C24 Timber, C25/30 concrete, 90 min time interval between applying adhesive and casting concrete, and 2-component epoxy adhesive from SIKA. Four-point-bending tests were carried out following the standard EN 408 [83]. A decrease in bending moment capacity for the reduced area series was found compared to the complete bonding area series. With pipes running transversally, the predominant failure mode was combined with shear and compression failures in concrete. In contrast, the longitudinal series showed failure in concrete under compression.

Negrão et al. [84] investigated the effects of glue connector (Icosit K101) in full-scale TCC beams, considering cast-on-site and prefabricated tactics intended for rehabilitation simulation or the possibility of a partial or full composite action of TCC beams. An analytical model assuming fully composite action was also conducted. Furthermore, TCC beams with dowel-type shear connectors were formed and examined, aimed for comparison. The results showed that the strength is approximately similar; however, glued beams grant a more significant stiffness and, thus, slighter deflections. The results also showed that flexural tension failure was the dominant failure mode for glued prefabricated beams. In contrast, the interface shear failure mode was dominant in glued fresh concrete beams dedicated by the concrete panels. This trend may be attributed to the low quality of concrete production and inadequate compaction. Both systems showed similar results; however, fresh concrete beams had higher stiffness, while prefabricated beams showed a higher strength. Compared with experimental results tests in terms of bending strength and failure mode predicting, the numerical model was effective and accurate with a -2.1% and -5.7% margin of errors for fresh and prefabricated series, respectively.

Augeard et al. [82] established a study to investigate the mechanical behaviour of TCC beams and panels with glue connection under short-term loading. A four-point bending test was utilized according to ASTM D3737 for this purpose. GL24h Glulam, ultra-high-performance fiber-reinforced concrete (UHPFRC) or ordinary concrete (OC), carbon fiber-reinforced polymer (CFRP) or steel (HA) rebars, and Eponal 371 epoxy adhesive were used for the production of composite beams and panels. **Fig. 1-37** shows the different configurations of conducted beams; all the configurations have a constant cross-section over the length, where the length was equal to 8 m, the height was 240 or 270 mm, and the width was 80 mm. Panels have a width of 1.2 m and a height of 270 mm for the whole length L, equal to 8.15 m. Both prefabricated and fresh concrete fabrication methods were used to produce the beams, while fresh concrete was used to fabricate both panels' specimens. All fabrication methods employed an adhesive layer with sprinkled sand, as shown in **Fig. 1-38**. The results showed that the timber-UHPFRC beams enlarged the stiffness by about 70–85% higher than the reference timber section due to the high Young's modulus of concrete or rebars. Also, the ultimate capacity of the composite beam was enhanced by 36%-64% compared to timber beam (A-24 h) of the same size with 30.9 kN.m of the ultimate moment. Also, the deflection has been reduced. The mechanical behaviour of composite panels was found to be linear until a brittle failure happened. The ultimate capacity of composite panels was enhanced by 34% and 70 % for the BO-HA and BFUP-HA panels receptively compared to timber beams (A-27 h). There was no slip between concrete and wood for the BO-HA panel, while the second panel (BFUP-HA) had a slip due to using two types of concrete.

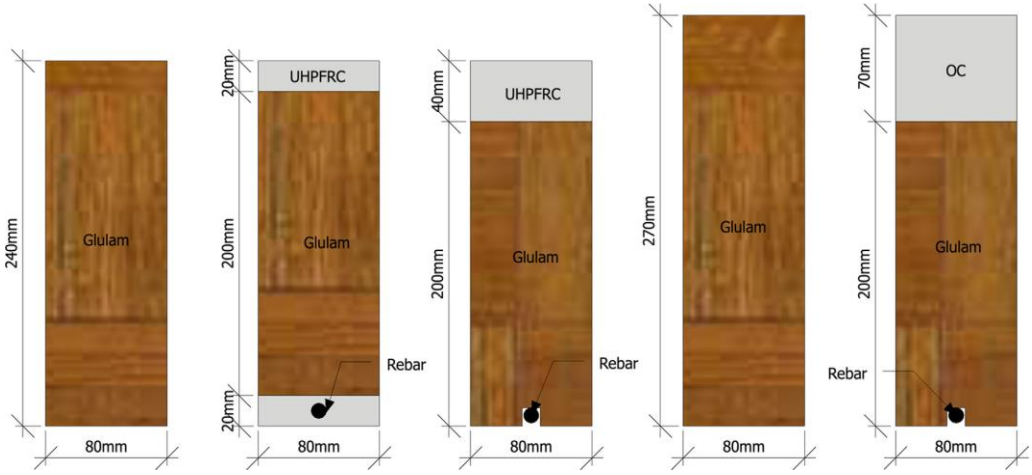

Fig. 1-37 Tested beam configurations, Augeard et al. [82]

Fig. 1-38 Specific treatment of the glulam by sprinkled sand, Augeard et al. [82]

1.6.2 Long-term behaviour of TCC structures

The serviceability limit state might be the governing factor for designing TCC floors [85]. Thermo-hygrometric changes in the environment can cause the moisture content of the wood and concrete components of TCC floors to fluctuate, leading to changes in their dimensions and mechanical properties. As a result, TCC floors can experience deflections increasing over time. Therefore, it is vital to consider the long-term performance of TCC floors when designing and to consider factors such as creep and shrinkage in the wood and concrete components and the shear connectors. Timber is subject to creep, mechano-sorptive creep, and shrinking/swelling as a function of moisture content. Mechano-sorptive creep is an additional time-dependent deformation related to humidity changes. As humidity levels fluctuate, timber absorbs or releases moisture, which leads to dimensional changes that can cause additional deformation over time. It can be particularly significant under load, where the rate of mechano-sorptive creep can be accelerated. Concrete can also experience creep and drying shrinkage. The connection systems of TCC, which might be adhesive bonding, mechanical connectors, or a combination of both, may undergo creep and mechano-sorptive creep. This phenomenon can reduce the stiffness and strength of the connections over time, which may affect the overall performance of the TCC systems [7].

The internal static indeterminacy of TCC systems means that stress in one component can cause stress in the other components due to continuous confinement. For example, the swelling or shrinking of the timber component cannot act freely because it is confined by the concrete slab, which can cause additional stress in the timber and affect the overall behaviour of the TCC system. As the TCC components experience time-dependent variations, such as creep and shrinkage, self-equilibrated stress distributions develop in the system. These stress distributions act parallel to the longitudinal axis of the components, leading to an increase in deflections over time [7]. Rigid connections are known for their higher structural effectiveness, but these connections can lead to higher internal stresses due to the possibility of internal stress redistributions [43].

Studies by Ceccotti et al. [85] and Fragiacomo et al. [70] have shown that TCC floors experience significant deflection variations on a daily and yearly scale due to changes in environmental conditions such as temperature and relative humidity. To mitigate the effects of long-term deflections in TCC systems, Fragiacomo et al. [70] suggest two potential solutions. The first is to use a type of concrete that exhibits reduced drying shrinkage, minimizing the effects of moisture-related deflection. The second solution involves protecting the TCC member against cambering, which is the excessive upward curvature of the member. By protecting the member against cambering, the effects of deflection can be minimized, improving the long-term performance of the TCC system.

The majority of research concerning the long-term performance of TCC has been investigated on TCC structures with mechanical connectors. The highest increase in deflection was discovered to happen during the first and second years of the testing period, with minor changes thereafter. In contrast, the slip at the interface of TCC structures continues to increase over the testing period of five years [85]. In order to enable the practical uses of TCC, simplified methods have been established to evaluate the rheological behaviour, e.g., Ceccotti et al. [86]. This method is based on the composite beam theory considering the creep effects. However, the effects of mechano-sorptive creep and shrinkage of concrete were added by Fragiacomo et al. [87]; in this case, the solution is created by the superposition of the hydro viscoelastic part due to sustained loading and concrete shrinkage, and the elastic part due to environment changes estimated for both yearly and daily effects. The estimated hydro-viscoelastic solution due to sustained loads is governed by an effective modulus of elasticity; in contrast, the effects of hydro-viscoelastic due to concrete shrinkage can be estimated by employing the γ-method according to Annex B of Eurocode 5. However, by applying the γ-method, it might be difficult to estimate the elastic solution for daily and yearly environmental variations; furthermore, moisture content and temperature variations effects are ignored. However, these effects can not be ignored for serviceability considerations [20].

Concerning the yearly temperature variations, the delay of internal to ambient temperature can be neglected, and for concrete and timber, the cross-section temperature can be considered to be equal to the ambient temperature. In contrast, daily variations of the temperature of concrete can be assumed to be equal to the environment owing to its high thermal conductivity; nevertheless, timber has a low thermal conductivity; therefore, the temperature of the cross-section should be adjusted. Timber moisture content should be estimated by approximating the diffusion over the cross-section as a role of several factors, such as relative humidity, ambient temperature, timber dimensions, timber species, and others. Moisture content impacts the swelling/ shrinkage of the TCC components, and it also affects mechano-sorptive creep. Moisture content can be assumed to be uniform over the cross-section, and yearly variations with a piecewise linear function can be estimated as a simplified approach [20].

Tannert et al. [7] investigated the long-term performance of adhesively bonded TCC beams, the composite beams exposed to serviceability loads for 4.5 years to investigate the effect of long-term loading on the ultimate capacity of the TCC beams. During this period, the beams were subjected to typical changes in the indoor climate conditions. The results showed that the long-term loading of about 30% of beam capacity caused no degradation of the adhesive connection with a computed efficiency of more than 95 %. The subsequent destructive tests revealed that the system's behaviour was linear until load levels approximated failure; the failure mode was brittle and happened in the concrete components only with a minor relative slip between timber and concrete.

Another study by Augeard et al. [88] was conducted to examine the mechanical behaviour of glued TCC structures under cyclic loading and material creep using four-point bending tests. Three different configurations were produced and investigated, **Fig. 1-39**. The first configuration referred to panels was made of wood, OC, and steel rebar fixed by the near-surface mounted (NSM) method. The second configuration referred to panels fabricated by two types of concrete (OC and UHPFRC). The third configuration is identical to the first, except for replacing the steel rebar with the CFRP rebar. The dimensions and fabrication procedures are similar to those used in his previous study [82]. Cycling loading was performed at least after 28 days of concrete age, utilizing a pneumatic jack supplied by an 8-bar pneumatic network. The load ranged between 4 and 20 kN, representing the dead and live loads, respectively. Sequentially, the residual resistance of the TCC members has been investigated. Bending tests with loading frequencies 0.25- 0.5 Hz were performed to determine the force and displacement of the TCC members through an installed strength sensor and a linear variable differential transformer (LVDT) sensor. Results approved that the deflection increases during the testing due to creep and fatigue. During the cycling loading, all material stresses were relatively low compared to their full capacity, with a rate of less than 50%, except for concrete under tension, which had a rate of less than 30%. May this clarify the phenomena of creep being the primary factor in the evolution of deflection with no significant influence by cycling loading. However, results showed that the residual behaviour of TCC members was reduced due to cycling loading, except for TCC members with UHPC, which was better.

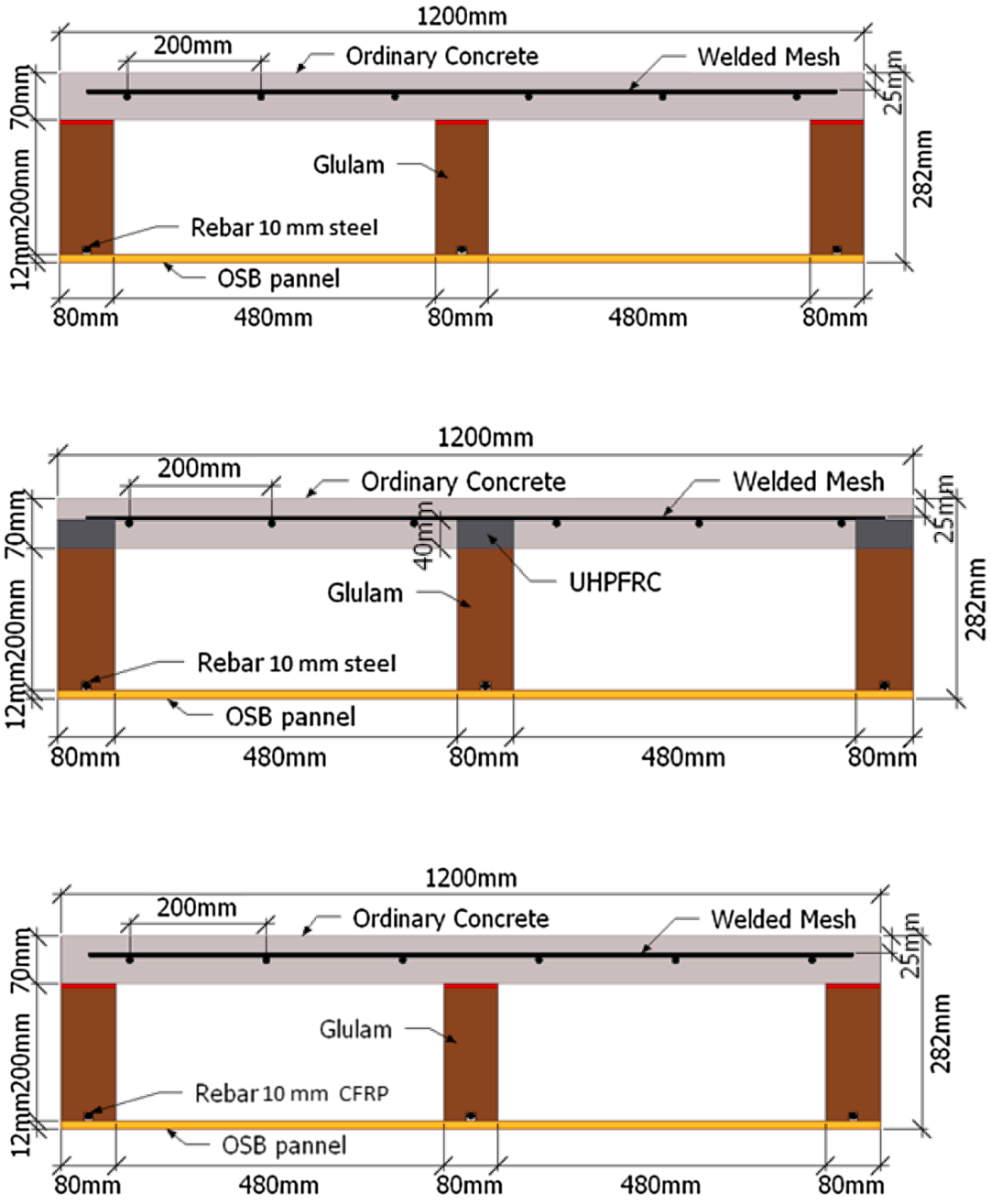

Fig. 1-39 Hybrid TCC members configurations, Augeard et al. [88]

1.7 Modeling

1.7.1 Analytical methods for TCC

Analytical modeling of the connection in timber concrete composite structures is crucial for predicting their behaviour under different loading conditions. The connection can be modeled using different methods, including discrete and continuous methods. The discrete method models each connection individually, which increases the computational complexity of the analysis, as it considers the connections as separate

entities. In this method, the behaviour of each connection is analyzed separately, and the results are combined to determine the behaviour of the entire structure [89]. On the other hand, the continuous method allows the stiffness and strength of each individual connection to be smeared along the contact area between the timber and concrete members, effectively representing the behaviour of a glued connection. In this method, the connections are treated as a continuous interface, and the behaviour of the entire interface is analyzed using an appropriate constitutive model. This method simplifies the analysis by reducing the number of discrete components that need to be analyzed and can provide a more accurate prediction of the behaviour of the entire structure. The choice between these two methods depends on various factors, such as the connector spacing, structure size, and loading conditions. A continuous connection is typically used when the connector spacing is relatively short compared to the overall beam length, whereas a discrete connection is used for larger connector spacings [90].

Analytical models have been developed to simplify the design of the slip interface in TCC beams. These models allow for relatively efficient calculations and make it possible to predict the behaviour of the TCC structures.

1.7.1.1 The Gamma method

The Gamma method is one of the analytical models provided in Annex B of Eurocode 5 for the design of timber-concrete composite structures [17]. This method is based on the theory of linear elasticity and has been developed from the differential equations of equilibrium that were derived by Möhler (1956). Initially, the method was used for mechanical connections between timber-to-timber, but it has also been adopted for use with TCCs. The linear-elastic theory assumes that all materials involved, including concrete, timber, and connection, remain within their linear-elastic range until the timber beam fails. This is generally considered applicable in many technical cases, especially for TCCs with strong and stiff connectors, such as notched connections filled with concrete. Ceccotti et al. [18] suggested that the approximate solution provided by the gamma method could be utilized for linear-elastic analysis of TCC. The method is designed to calculate effective bending stiffness considering the semi-rigidity of the shear connection and slip between the timber and concrete. To simplify the analysis, the shear connections are assumed to be evenly distributed along the span rather than being closer together near the supports and further apart toward the midspan. An effective spacing for the shear connection is used in this approach. The reduction factor γ is used to evaluate the effective bending stiffness of the timber-concrete composite section. When there is no composite action between the timber and concrete, γ is equal to zero, and the individual stiffness of the timber and concrete components determines the bending stiffness. On the other hand, when there is a full composite action, γ is equal to one, and the bending stiffness is evaluated based on the combined stiffness of the timber and concrete components. The value of γ depends on the degree of composite action and the

properties of the materials used in the TCC section. Once the effective bending stiffness is calculated, it becomes possible to determine the maximum stresses in bending, tension, and compression for both the timber and concrete elements. Eq. (2.3) for calculating the effective bending stiffness (EI_{eff}) using the gamma method is as follows:

$$EI_{eff} = \sum_{i=1,2} (E_i I_i + \gamma_i E_i A_i a_i^2) \tag{1.3}$$

Where: The symbols 1 and 2 represent concrete and timber elements, respectively, while E denotes Young's modulus of the material. A and I represent the cross-sectional area and second moment of area, respectively. Moreover, a is the distance between the element's centroid and the composite neutral axis. Finally, γ is the reduction factor for the shear connection.

Timber is a cellular and porous material that shows linear-elastic behaviour when subjected to tension and bending stresses. Timber usually fails before the concrete reaches its plastic state due to the combination of bending and tension stress [91]. The gamma method calculates the effective bending stiffness, assuming that the connection between the timber and concrete elements is linearly elastic. The gamma method will give good results if the connection remains linearly elastic and behaves according to this assumption. However, The gamma method does not account for any nonlinear behaviour, such as ductility or deformation capacity. This can be a limitation of the method in situations where the connection may experience significant deformations or nonlinear behaviour.

In the context of glued connections, the shear reduction factor (γ) is particularly critical. The current approach of determining Gamma is based on simplified assumptions and limited experimental data. A more rigorous approach is needed to determine the appropriate value of γ. This approach should incorporate probabilistic analysis considering a safety margin.

1.7.1.2 Frozen shear force method

The frozen shear force method (FSFM) is an extension of the gamma method that aims to account for the ductility of the connection. A linear model such as the gamma method cannot accurately predict the composite system's load-deflection response due to the nonlinearities in the connection at higher load levels. The frozen shear force method considers the elastic-plastic behaviour of the connection. It assumes that the connection behaves elastically until the outermost connectors yield, at which point the remaining connectors' shear force is considered "frozen." The system behaves as though there is no longer a connection between timber and concrete. This method allows for the consideration of the ductility of the connection, which is a limitation of the gamma method. The frozen shear force method allows for calculating the lower-

bound behaviour of a TCC specimen by replacing the section stiffness used in subsequent calculations with EI_{mi} instead of EI_{eff}. This method helps assess the worst-case scenario for the TCC's performance.

1.7.1.3 Elasto-plastic method

The elasto-plastic model is a simplified design methodology proposed by Frangi et al. [91] as an extension of the Frozen Shear Model. In the elasto-plastic method, the shear stiffness of the connectors is neglected, which simplifies the calculations for the load-carrying capacity of the composite system. The rigid-perfectly plastic load-slip relationship is an assumption made in some models to simplify the analysis of the connection. This assumption implies that the connectors behave as perfectly rigid until the yielding shear force is reached, at which point they become perfectly plastic and deform without additional load [91]. This method is valuable for estimating the ultimate load-carrying capacity of the composite system. However, the assumption of infinite stiffness may not be valid for all types of shear connectors, and the assumption of perfect plasticity may not hold for all connection details.

1.7.1.4 Discrete linear method

The discrete linear method, as proposed by Zhang et al. [92], is a different method for predicting the nonlinear behaviour of TCC beams. The method involves dividing the TCC beam into discrete linear segments based on the location of the connectors along the span. The load-deflection response of each segment is determined by linear analysis until the connectors at the end of the segment reach their yielding state. At this point, the connectors are treated as perfectly plastic, and the analysis is continued on the remaining linear segments until the connectors at the end of the next segment yield. This process is repeated until all connectors have reached their yielding state, and the load-deflection responses of all segments are combined to obtain the nonlinear response of the TCC beam. This approach is prescribed graphically in **Fig. 1-40**.

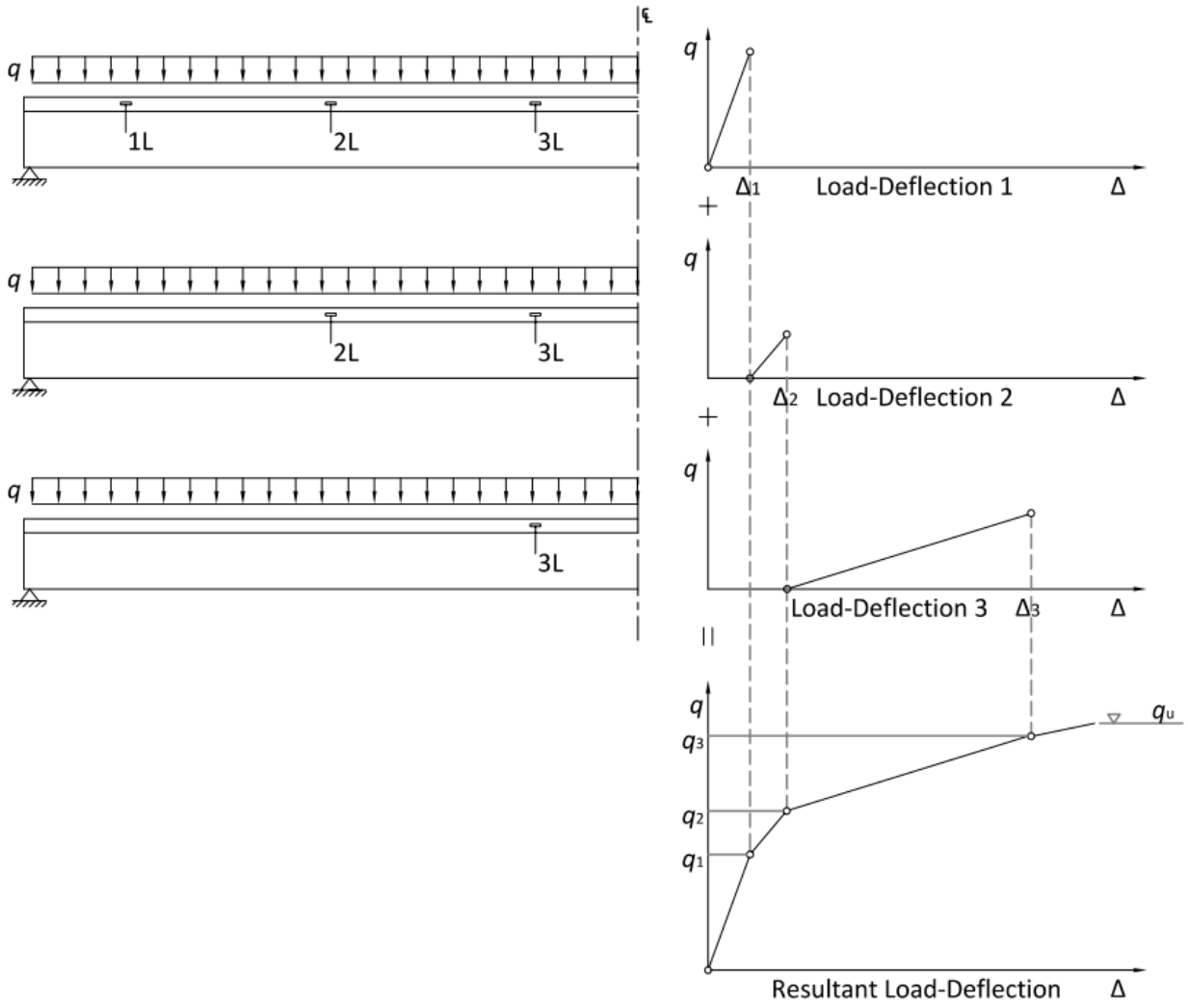

Fig. 1-40 Incremental methods for determining nonlinear load-deflection response, Zhang et al. [92]

Each of these methods has its own set of assumptions and limitations, and the choice of method to be used will depend on the specific characteristics of the connection being analyzed and the level of accuracy required. The frozen shear method is particularly useful for connections with high ductility. In contrast, the gamma method is suitable for stiff connections that remain in the linear range. The Elasto-Plastic method is more appropriate for specimens with ductile connections. It can provide a reasonable estimation of the ultimate limit state behaviour. In contrast, the discrete linear method is a newer alternative proposed by Zhang et al. [92], which uses discrete linear calculations to predict the nonlinear load-deflection response.

1.7.2 Numerical modeling of TCC

Understanding the mechanical behaviour of TCC structures and their design principles is nonetheless still under development. Finite Element Analysis (FEA) is a powerful tool that can be used to model the

behaviour of TCC connections. In addition, the FEA is still necessary for parametric analyses on TCC structures. FEA allows for a more accurate representation of the behaviour of a TCC connection than analytical methods, as it can model the non-linear behaviour of the connection and capture the effects of geometric non-linearities, material non-linearities, and boundary conditions [93].

The current FE models for TCC beams can be classified into one-dimensional (1D), two-dimensional (2D), and three-dimensional (3D). The 1D FE model for TCC beams is commonly used due to their simplicity and efficiency, which provide valuable information about the TCC's overall behaviour. In a 1D frame model, the timber beam and concrete slab are modeled by two parallel beams, and discrete nonlinear spring elements model the connections between them [90,94], **Fig. 1-41**. These spring elements are calibrated using experimental data or analytical solutions to determine the stiffness and strength of the glue or other types of connections between the timber and concrete, including any possible slip or separation at the interface. Various studies have used 1D frame models to investigate the behaviour of TCC beams under different loading conditions, such as bending, shear, and axial compression [89,93,95].

Additionally, the models can be used to evaluate the long-term behaviour of TCC beams, including creep and moisture effects. However, it is essential to note that 1D frame models have some limitations, such as their inability to accurately capture the detailed stress and strain distribution within the composite system, particularly in the transverse direction. They may also be unable to account for local effects, such as splitting, cracking, or delamination, at the interface between the timber and concrete[90,94]. Another limitation of the 1D model is that it does not consider the spatial effect of the concrete slabs. This means that the shear lag effect on the concrete slabs is ignored, which may result in relatively overestimated calculated results when a broad slab is utilized [93].

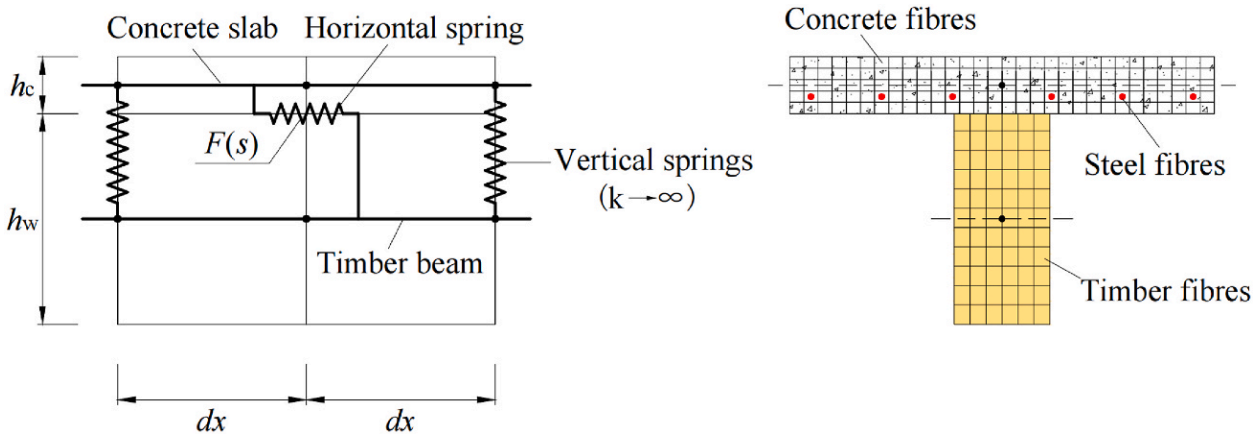

Fig. 1-41 Configuration of the 1D model used by Tao et al. [93].

The 2D FE model for TCC beams is more advanced than the 1D model, as it considers the spatial effect of the concrete slabs. In this model, the concrete slab is modeled using multi-layer shell elements. In contrast, the timber beam is modeled using fiber beam elements, and the connections between them are modeled using spring elements [96], **Fig. 1-42**. The multi-layer shell elements can capture the shear lag effect on the concrete slabs and provide more accurate stress and strain distributions compared to 1D models. The fiber beam elements can capture the detailed behaviour of the timber beam and its interaction with the concrete slab. Similar to the 1D model, the 2D FE model for TCC beams offers the advantage of easy operation and high calculation efficiency. It is considered one of the most appropriate models for analyzing TCC frame structural systems. Several research studies have shown that the 2D model provides high accuracy when compared to experimental results, particularly for composite beams with relatively large slab widths [93,97,98]. However, timber as an orthotropic material has different strength properties in different directions. The 2D model doesn't account for the orthotropic nature of timber, and this omission can result in an inaccurate representation of TCC beam behaviour.

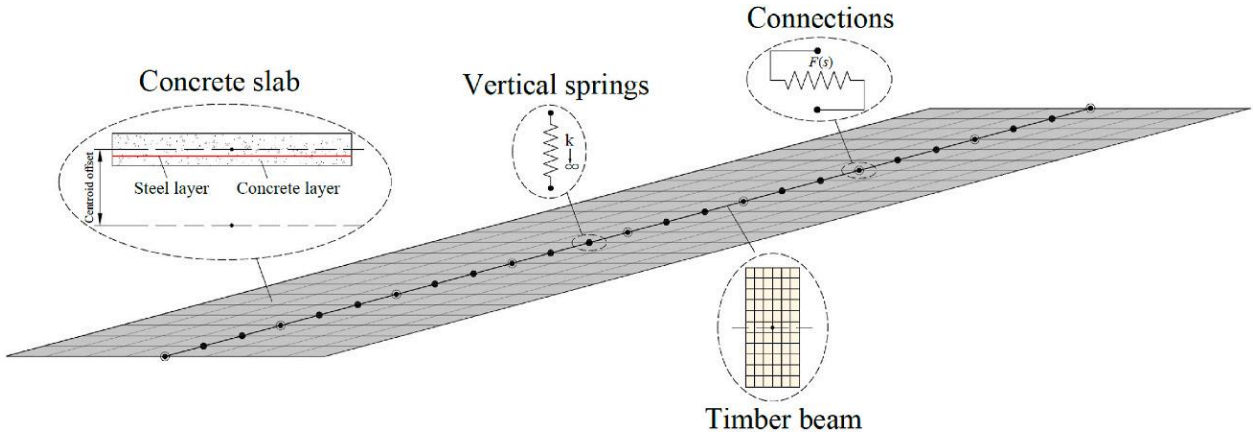

Fig. 1-42 Configuration of the 2D model used by Tao et al. [93].

The 3D finite element (FE) model for TCC beams employs solid elements to fully account for material properties and interactions between members. These solid elements come with specific definitions for stress-strain relationships and contact interactions [99,100]. This allows for a more accurate representation of the TCC beam's behaviour under different loading conditions. Multiple research studies have confirmed that the 3D model effectively captures the load-deflection behaviour, stress distribution, and slip conditions in TCC beams. This is because the 3D model considers the full geometry and material properties of the composite system, including the effects of shear lag and weak directions of the timber. It also allows for more detailed modeling of local effects, such as splitting, cracking, and delamination at the interface between the timber and concrete [100,101]. It is worth noting that the 3D model allows for out-of-plane analysis, meaning it can effectively divert loads away from the central axis of the beam. This feature is particularly valuable in scenarios where loads or external forces act in ways that induce lateral or torsional effects on the TCC beam. However, the 3D model is more complex and computationally expensive compared to the 1D and 2D models [102]. Therefore, it may not be suitable for engineering daily practices where simplicity and efficiency may be prioritized over accuracy.

1.8 Summary

This literature review has thoroughly investigated the various dimensions of TCC systems related to the theory, design, testing, and modeling of TCC structures. In terms of shear connections, glue connections are distinguished by their remarkable ability to enhance structural integrity and performance through superior strength and stiffness compared to traditional mechanical connections such as mechanical fasteners and notched or grooved joints. The adhesive bonds excel in minimizing the interface slippage between timber and concrete and optimizing the load transfer across the composite structure.

Full-scale tests help understand the load response of TCC beams and floors in addition to the influence of shear connection type on their behaviour. However, the majority of studies have focused on single T-section beam specimens with mechanical connectors, with only a few investigating glue connections. Although some studies have examined the mechanical behaviour of glue connections in TCC beams, none have provided a comprehensive insight into the mechanical behaviour of adhesively bonded TCC beams. Specifically, there is a lack of research on the strain distribution over the bending and shear sections, verification of the consistency of the neutral axis along TCC beams, failure characteristics of wet-fabricated and dry-fabricated TCC beams, quantification of interface slip between timber and concrete, and deflection response. Addressing these potential research areas is crucial for advancing the understanding and design of adhesively bonded TCC beams.

Moreover, the review has explored simplified analysis models that have been developed to replicate the observed behaviour of composite specimens. Some models assess the nonlinear load-deflection response, while others, such as the gamma method, remain within the linear regime and provide a simplified method to calculate effective section stiffnesses. Finite element modeling has been extensively utilized to simulate the behaviour of TCC structures, employing both linear and nonlinear approaches. Various modeling techniques and software have been employed, including 1D, 2D, and 3D FE models. Each modeling approach has shown proficiency in specific areas, particularly within the linear regime. The comprehensive review of modeling techniques used in previous studies will inform the selection of TCC models in this thesis. These modeling approaches will be discussed in detail in the upcoming chapters.

In conclusion, this literature review has thoroughly examined an extensive array of studies concerning the TCC system, providing a robust foundation for the research presented in this thesis. The review also justifies the selection of materials, testing methodologies, and analysis techniques used throughout this study.

Chapter 2
Glue Joints Testing

Chapter 2 Glued TCC Joints Testing

The present chapter draws upon research previously published in a journal article. *Investigation of the behaviour of adhesively bonded joints between timber and self-compacting concrete* [103].

2.1 Introduction

The shear connectors play a significant role in determining the efficiency and performance of the TCC system. Many connection systems have been developed so far. In comparison with mechanical connections, glue connections can achieve an ideal interaction with full-composite behaviour between timber and concrete [29,73,80].

The performance of the glue connection is vital for the integrity of the adhesively bonded TCC elements. Therefore, the shear bonding strength is an important mechanical property that needs to be investigated in TCC joints. Also, examining the effect of adhesive type and thickness on shear strength is essential due to limited studies in this area [104].

Manufacturing adhesively bonded TCC structures presents a unique set of challenges and advantages, particularly in the choice between dry and wet processes. In the dry process, pre-fabricated concrete panels are bonded with timber, offering ease of assembly and reducing construction time. Conversely, the wet process, which involves bonding fresh concrete with timber on-site, eliminates gaps and provides superior interface continuity. However, challenges such as adhesive movement during concrete pouring, water presence during adhesive cross-linking, and the heterogeneity of the concrete-wood interface form significant challenges to the wet process. While both processes have been studied to some extent, research on adhesively bonded TCC using dry and wet techniques remains limited [77].

Failure modes of timber-concrete joints can mainly be divided into adhesive or cohesive failure [77]. Adhesive failure includes the possibility of bond failure at the interface with concrete or wood, while cohesive failure occurs mainly within the concrete or timber. These failure modes have significant implications for the structural behaviour of TCC joints, affecting their overall ductility and load-carrying capacity [105]. The properties of the bonded surfaces directly influence the performance of the glue connections. Surface treatment is essential to achieve a robust and reliable bond in adhesively bonded TCC structures. It involves removing impurities and increasing surface roughness to promote better adhesion and prevent adhesive failures [36].

The current chapter is dedicated to double-shear push-out tests of adhesively bonded TCC joints. In this context, the authors conducted a comprehensive experimental campaign with the aim of verifying the

hypothesis that the bonding performance of wet and dry TCC joints, specifically in terms of shear strength and failure mode, is influenced by various parameters such as timber moisture content, adhesive type, adhesive layer thickness, sand addition, sandblasting of pre-fabricated concrete, and bonding scale effect.

In essence, this chapter serves a dual purpose: contributing to the knowledge base on adhesively-bonded TCC joints by informing improvements in design and manufacturing techniques. The second purpose is to provide the essential data for further analysis and modeling as part of this study, e.g., slip stiffness of the glue connections and load vs. slip profile, which are crucial outcomes for FE modeling.

2.2 Shear connection test setup

2.2.1 Test configuration

Cast-on-site and pre-fabricated concrete panels were employed for bonding with central timber beams to produce wet and dry TCC joints. This arrangement, with central timber beams and lateral concrete panels, was chosen based on its higher frequency of usage found in the literature [47]. This choice allows for better comparison with existing studies. The test configuration and TCC specimen's basic features designed for the double-shear push-out test are shown in **Fig. 2-1**. Two concrete panels are bonded on the pre-glued area of a central timber element. When it comes to wet TCC joints, the intended thickness of the epoxy adhesive layer was spread inside the bonding area on the surface of wooden elements; then, the fresh concrete was poured after permitting the stiffening time recommended by the manufacturer. In contrast, for dry TCC joints, pre-fabricated concrete panels were glued with timber components utilizing epoxy adhesives, considering zero-time intervals as a waiting time. Eventually, after curing the specimens for both the concrete hardening and targeted moisture content of timber, the test load with a parallel direction to the timber grains is performed on the top surface of the timber component to be transferred by the two bonded interfaces between timber and concrete panels. Finally, the ultimate shear strength of the glue joints should be determined, and a specimen failure will occur.

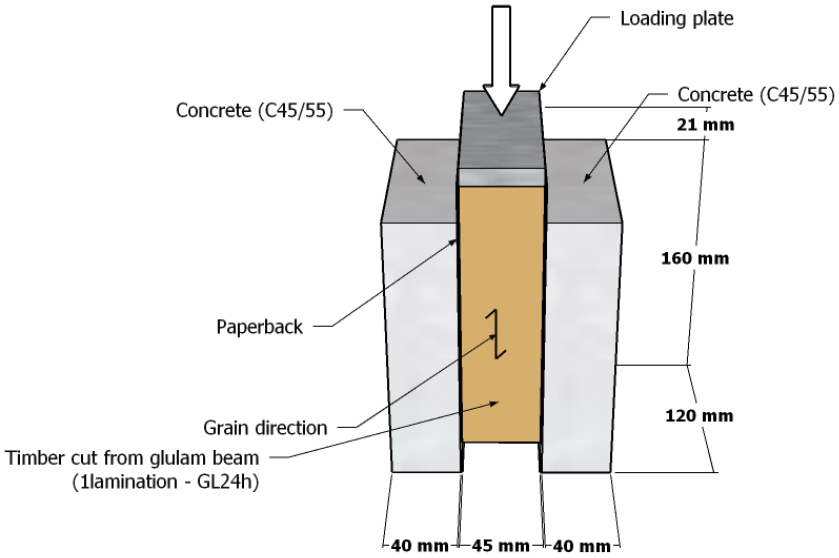

(a)

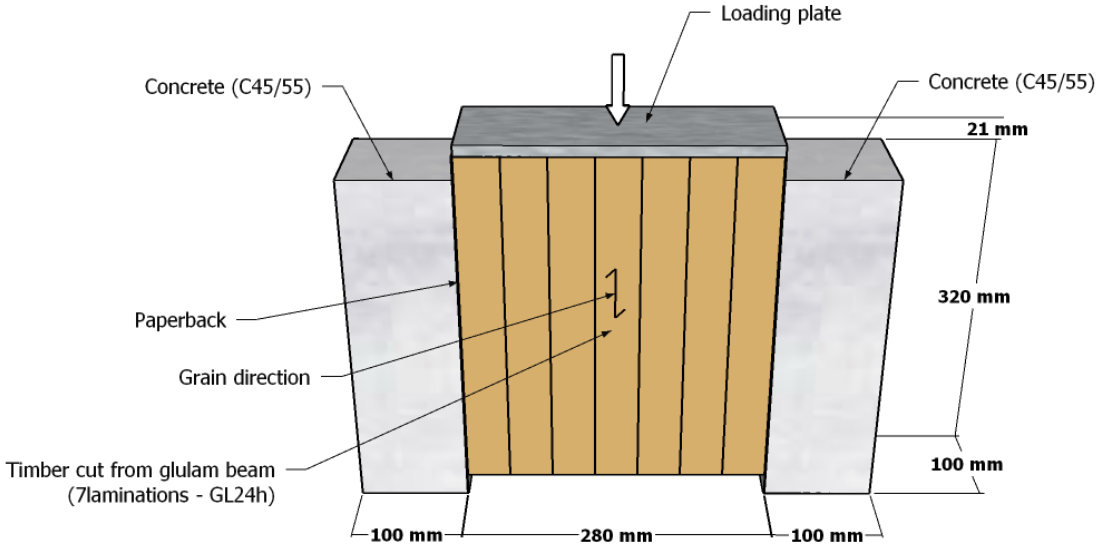

(b)

Fig. 2-1 Shear test configuration and TCC specimen's basic features, (a) standard specimen, and (b) 3X bonding length specimen

2.2.2 Loading scheme

The experimental assessments of strength and deformation properties of TCC according to the European standard EN 26891[39] are commonly used. This standard is proposed for assessing joints that use mechanical fasteners, like bolts or dowels. No standard is specified for the evaluating rule for structural glued connections. However, this standard has been utilized in several studies to test the shear strength of TCC with glue connection [7,40–42]. The procedures prescribed by EN 26891 [39] were adopted.

Compressive test machines with a capacity of 100 kN and 6000 kN were utilized to test small specimens and scaled specimens, respectively. An initial loading ramp at a rate of 10 kN/min was applied until 20 kN. After maintaining this load for 30 seconds, a second decreasing loading ramp at the same rate was performed until reaching 5 kN and held for 30 seconds. The final increasing load ramp took place at the same rate until specimen failure occurred. However, in the case of using a 6000 kN Loading machine to test scaled specimens, the preloading cycle was omitted due to the machine program shortage, see **Fig. 2-2**.

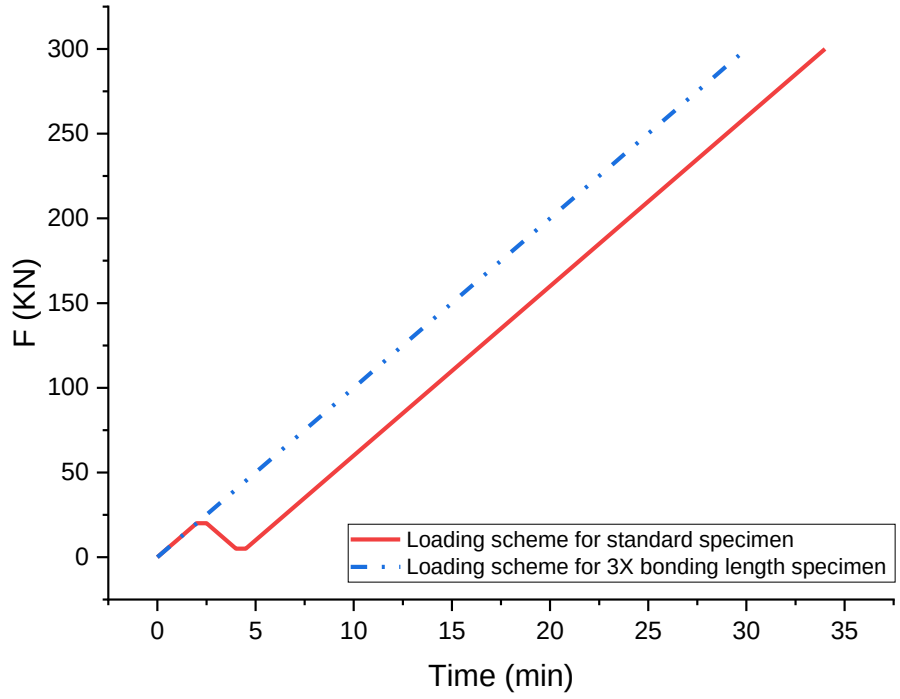

Fig. 2-2 Shear test loading scheme

2.2.3 LVDT sensors

A linear voltage displacement transducer (LVDT) sensor with a range of ±1 mm and a recording frequency of 10 Hz combined with a double-L-shaped angle was bonded on the rear surface of all specimens to measure the slip between concrete and the wood elements. The position of LVDT sensors was precisely measured and prepared for each specimen before the test, see **Fig. 2-3**.

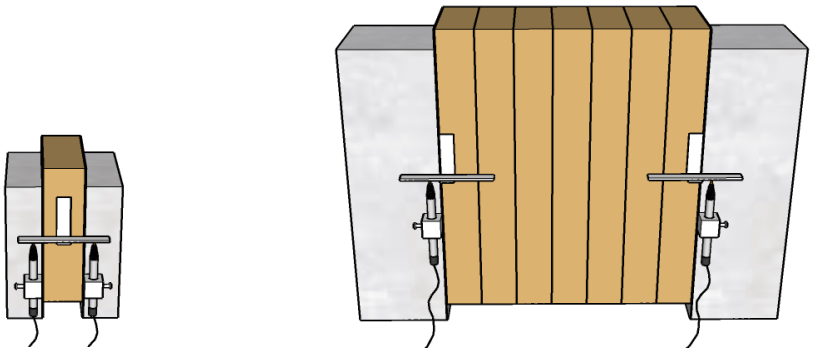

(a) (b)

Fig. 2-3 Prepared specimens with LVDT sensors, (a) standard specimen, and (b) 3X bonding length specimen

2.2.4 Digital image correlation

Digital Image Correlation (DIC) is one of the most popular optical measurement methods used to simulate and measure the deformation patterns on the surface of a sample. This measurement technique has been utilized in similar studies investigating the adhesive connection in TCC [40]. **Fig. 2-4** illustrates the measuring device used for this purpose. A black color speckle pattern was applied on the surfaces of the specimens using a black painting spray. These surfaces are observed with two high-resolution cameras (5 Megapixels), and an optical 2D setup with a pixel size of 3.45 µm is used to record the images of the samples. In the DIC setup, the cameras were positioned at a distance of 1 meter from the surface of the standard specimens and 1.5 meters from the surface of the scaled specimens. This distance was chosen to ensure an adequate field of view and capture the entire surface of the specimens. Additional lighting was employed to ensure high-quality captured images for the DIC analysis. This supplementary lighting was strategically positioned to enhance the visibility and contrast of the speckle pattern on the specimen surfaces. The Vic-3D software was used for displacement analysis and simulating the strain field development on the surface of the specimen. It is worth mentioning that the subset size and step size in the DIC post-analysis were adjusted based on the characteristics of the speckle pattern on the specimen surfaces.

(a) (b)

Fig. 2-4 Digital image correlation measuring device setup of the (a) standard specimen, and (b) 3X bonding length specimen

2.3 Materials

2.3.1 Adhesives

Epoxy resins are commonly used in structural construction and rehabilitation. Two adhesive products manufactured by SIKA AG, Sikadur®-53 and Sikadur®-32EF, were selected to be used to produce wet TCC specimens. In comparison, Sikadur®-330 and Sikadur®-31EF were used for the dry process. All adhesives are two-part epoxy-based and produced by Sika. These selections were made based on their compatibility with the intended application of creating timber-concrete composites. Notably, these selections align with known advantages of low-viscosity adhesives, such as excellent wetting and penetration behaviour into the adherents [75]. These characteristics contribute to effective and thorough bonding between materials. According to the technical data provided by the manufacturer, they are appropriate for the intended usage of timber concrete composite fabricating. The mixing ratio should be Part A: Part B = 8:1 by weight for Sikadur®-53, = 1:2 by weight for Sikadur®-32EF,= 4:1 by weight for Sikadur®-330 and = 3:1 by weight or volume for Sikadur®-31EF, as specified in the products datasheets. Some of the physical and mechanical properties of adhesives are shown in **Table 2-1**.

Table 2-1 Basic properties of adhesive products

Property	Sikadur®-53	Sikadur®-32 EF	Sikadur®-330	Sikadur®-31 EF
Density (Kg/l)	Mixed resin 2.04	Mixed resin 1.5 ± 0.1	Mixed resin 1.3 ± 0.1	Mixed resin 1.95 ± 0.1
Pot life at 20 °C (min)	30	45	60	80
Tensile Young's modulus (MPa)	4100	3800	4500	6900
Tensile strength (MPa), (7 days @ +23 °C)	20	36	30	21
Compressive strength (MPa), (7 days @ +23 °C)	70	48	-	47

2.3.2 Timber elements and bonding area

The timber glulam GL24h strength class, according to EN 1994 [106], is widely applied in TCC construction projects and is considered one of the most used types of timber in engineering construction[88,107]. For standard specimens, the timber elements were sawn from GL24h glulam beams (one lamination) 120 × 45 mm^2 in cross-section and 2.7 m reference length. In contrast, for scaled specimens with 3X bonding length, the timber elements were produced from GL24h glulam beams (7-laminations) 100 × 40 mm^2 in cross-sections and 3.5 m reference length. The use of significantly unlike cross-sections for the timber components was imposed by the estimated maximum force to be applied during the test. Two equally rectangular areas, 60 × 80 mm^2 and 60 × 240 mm^2, were determined as the bonding area, one on each opposite side of the timber element, for standard and scaled specimens, respectively. Meanwhile, the bonding lengths of 80 mm and 240 mm are parallel to the timber grains. As shown in **Fig. 2-5**, the glueing area position, dimensions, and the intended thickness of the adhesive layer were precisely ensured through the installed paperback fixed on each side of the timber element. This control can limit the differences in the shear strength outcomes of TCC joints.

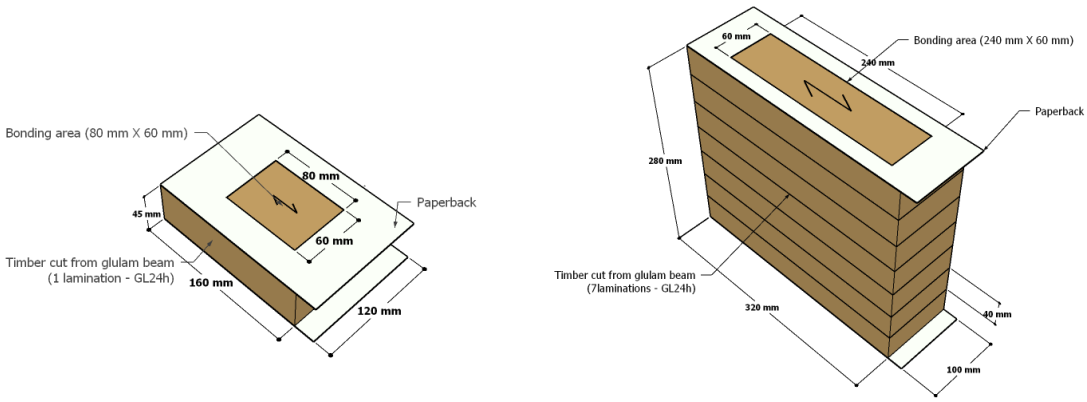

(a) (b)

Fig. 2-5 Timber element and bonding area dimensions of (a) standard specimen (b), and 3X bonding length specimen

2.3.3 Concrete elements

Concrete compacting could mechanically impact the shear strength of the glue connection due to the possibility of adhesive squeezing in the wet process. In contrast, self-compacting concrete can ensure a better fabrication of the specimens and eliminate the mechanical influence of concrete compacting on the shear strength of the connection. For both fabricating processes, self-compacting concrete to match the C45/55 strength class according to EN 1992-1:1:2004 [108] was considered. The mixing ratio of cement: water: sand (0–4 mm): and aggregates (4–16 mm) was 1:0.36:2.63:2.57 by mass. The average 28th-day compressive strength of the concrete was 74.6 MPa, based on Concrete cylinders, 110 mm in diameter and 220 mm in height.

2.4 Fabrication of specimens

2.4.1 Fabrication of wet TCC joints

Waiting times considered for both types of adhesives were different. The time interval between mixing the adhesive and casting concrete (The stiffening time) was set to 37 min and 70 min for Sikadur®-53 and Sikadur®-32EF receptively. This time interval is crucial as it allows the adhesive to achieve the desired consistency to reach a state where it is sufficiently viscous or stiffened, ensuring optimal adhesion between the timber and the wet concrete. This helps prevent the adhesive from running excessively when pouring concrete. The stiffening time is defined based on the specific properties of the adhesive being used, such as its viscosity, open time, and tackiness characteristics, considering the relative humidity and temperature conditions of the fabrication hall.

In the fabrication of wet TCC, timber elements were molded in a formwork by fixing plywood pieces to the timber elements. The concrete was cast on the pre-glued face, one face per time, **Fig. 2-6**. Pouring concrete was performed on two consecutive days. The epoxy adhesives were applied inside the bonding area with a determined thickness of 1- or 3 mm. These thicknesses fairly simulate feasible limits during the industrial fabrication process due to factory conditions and the flatness precision of glueing surfaces to guarantee an efficient connection between timber and concrete components. Subsequently, self-compacting fresh concrete was poured on the pre-glued face of the timber element. The molds were turned upside down on the second day, and the same steps that were taken on the first casting day were repeated. All specimens were de-molded on the third day and stored in an acclimatized chamber at 20 °C temperature and 65% relative humidity until they reached the intended MC of 12% at the test time, which simulates the typical value of moisture content that usually reached under service conditions for indoor structural components. Furthermore, this value of MC is the reference value specified by Eurocode for the strength of timber elements.

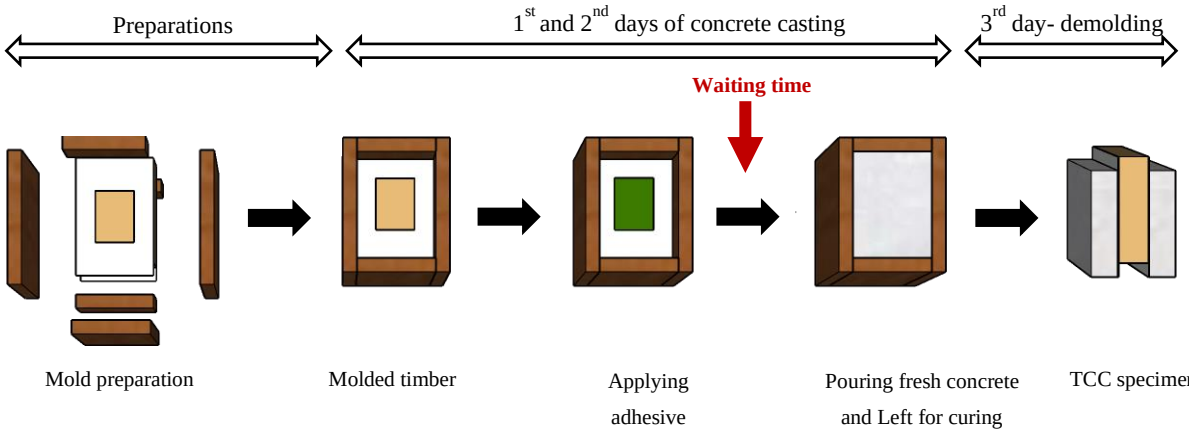

Fig. 2-6 Wet TCC specimens fabrication procedures

2.4.2 Fabrication of dry TCC joints

During this method of fabrication, concrete panels were poured inside a formwork, assembled by GA smart building company, and delivered to the lab, where the elements were fabricated. Concrete panels were left out for 28 days in room conditions. Some concrete panels were sandblasted after curing to remove the unreacted cement layer. This part was prepared to investigate the effect of sandblasting on the mean value of shear strength. The surface of the concrete panel before and after sandblasting is shown in **Fig. 2-7**. The concrete surface has a layer of mortar that was scraped off, and aggregates become visible. Timber elements were molded in a formwork by fixing plywood pieces to the timber elements to avoid misalignment that might happen between the timber and the concrete panel. Subsequently, the pre-

fabricated concrete panels were cleaned with an air blower and bonded to the pre-glued timber face with no waiting time. The composite element was left to cure for one day. Afterward, the composite element was set upside down, and the second concrete panel was glued. The concrete panels were glued to the two faces of the timber element on two days in a row of their 29th and 30th age. After fabrication, curing time was allowed, and then all composite specimens of all series were stocked in an acclimatized chamber at 20 °C temperature and 65% relative humidity until they reached the intended MC of 12% at the test time.

(a) (b)

Fig. 2-7 Pre-fabricated concrete panels (a) normal surface, and (b) sandblasted Surface.

2.5 Specimens series

2.5.1 Wet TCC joints series

All wet TCC joints tested series are illustrated in **Table 2-2**. The main series were sorted according to the moisture content of conditioned timber elements. The intended timber moisture content for each main series was assured through the acclimatized chamber. A moisture meter (Testo 606-2) was used as the control; furthermore, samples were routinely weighed until there was no significant difference between consecutive weightings.

Under each main series of standard specimens (80 mm bonding length), there are four sub-series owed to the type of adhesive used, e.g., Sikadur®-53, Sikadur®-53 mixed with sand, Sikadur®-32 EF, and Sikadur®-32 Ef mixed with sand. The grain size of the used sand was 1.5-2 mm, while the sand adhesive mixing ratio was 1:2 by weight. Four specimens were fabricated for each sub-series. It is worth mentioning that mixing sand with the adhesive aimed to increase the roughness between the concrete and timber surfaces, with the expectation of enhancing the mechanical strength of the TCC joints.

Series A2 complies with the reference conditions. The timber elements in series A2 were stored in an acclimatized chamber at 20 °C and 65% relative humidity to be conditioned to 12% MC. Simultaneously, in series A1, timber elements were dried in a 35 °C oven, while in series A3, they were stored in a wet room to reduce the required time in the acclimatized chamber. Series A1 and A3 were performed to investigate

the impact of MC variation before and after the bonding on the shear strength. They vary from series A2 only in conditioning parameters. In series A1, the timber elements were conditioned at 26 °C and 41% relative humidity to reach 8% of MC. In contrast, in series A3, they were conditioned at 20 °C and 95% relative humidity to reach 20% of MC. It is worth mentioning that the investigation into the impact of moisture content variation stems from a recognized significance highlighted in the existing literature [41,74,109], which identified moisture content as a crucial factor influencing the mechanical performance of adhesively bonded TCC joints.

A few days after performing the concrete elements as described earlier, the plywood formwork was de-molded. The Speckle pattern was applied on all composite specimens using a spray to enable digital image coloration observation. Afterward, all composite specimens of all series were stored in an acclimatized chamber at 20 °C temperature and 65% relative humidity until they reached the intended MC of 12% at the test time.

In contrast, for the 3X bonding length series A4 and A5, the two main series are sorted according to the MC of conditioned timber elements, 12% and 20%, respectively. Increasing the bonding length in the scaled specimens compared to the standard specimens is expected to have a significant effect on the bonding strength. It can influence the efficiency and uniformity of the bonding stress distribution, potentially affecting the overall mechanical performance of the TCC joints. A study by Negrão et al. [41] found that the shear strength of scaled specimens was smaller than that of the corresponding small-length specimens, attributed to the volume effect. However, the small number of tested specimens wasn't sufficient to draw firm conclusions. Therefore, further exploration of the scale effect is crucial to understanding its implications for the structural performance of adhesively bonded TCC joints.

It is worth mentioning that based on the shear strength results obtained from the first campaign, we opted to focus on MC levels of 12% and 20% rather than 8%. This decision is justified by the minor differences in shear strength between Series A1 and A2, indicating limited variation at 8% MC. Additionally, given the rarity of timber conditioned to an 8% MC level in real construction scenarios, we believe prioritising levels of MC commonly encountered in real construction scenarios is more relevant. Under each main series, there are two sub-series due to the adhesive layer thickness of 1 mm and 3 mm, and four specimens were produced for each sub-series. These two series were decided to be fabricated after the results of the standard specimens series to investigate the scale effect of bonding length and the increasing adhesive layer thickness of composite specimens made of Sikadur®-53. The timber elements of series A4 and A5 were conditioned similarly to series A2 and A3, respectively. All specimens were prepared for DIC and stored in an acclimatized chamber until they reached the intended MC of 12% at the test time.

Table 2-2 Timber- fresh concrete composite test series

Series	Sub Series	ω Cond (%)	ω Test (%)	adhesive	Bonding length (mm)	Adhesive thickness (mm)
A1	A 1.1	8	12	Sikadur®-53	80	1
	A 1.2			Sikadur®-53 + sand		
	A 1.3			Sikadur®-32EF		
	A 1.4			Sikadur®-32EF + sand		
A2	A 2.1	12	12	Sikadur®-53	80	1
	A 2.2			Sikadur®-53 + sand		
	A 2.3			Sikadur®-32EF		
	A 2.4			Sikadur®-32EF + Sand		
A3	A3.1	20	12	Sikadur®-53	80	1
	A3.2			Sikadur®-53 + Sand		
	A3.3			Sikadur®-32EF		
	A3.4			Sikadur®-32EF + sand		
A4	A 4.1	12	12	Sikadur®-53	240	1
	A 4.2					3
A5	A 5.1	20	12	Sikadur®-53	240	1
	A 5.2					3

Note: $\omega_{\_Cond}$: timber MC prior to glueing; $\omega_{\_Test}$: timber MCat test time

2.5.2 Dry TCC joints series

The tested series are illustrated in **Table 2-3**. Similar procedures have been followed for specimens made of pre-fabricated concrete of their corresponding series made of fresh concrete to ensure the intended moisture content before glueing and at the test time. However, the specificity of the fabrication process needed slight differences in the series definition. Under the B1 and B2 main series, there are four sub-series owed to the used type of adhesive and employed adhesive layer thickness of 1 mm and 3 mm. In contrast, for B3 and B4, there are two sub-series under each main series, owing to the type of adhesive utilized. Four specimens were fabricated for each sub-series. Series B1 was used as the reference series. In comparison, Series B2 was fabricated to investigate the impact of variation in MC on the shear strength before and after the bonding. Furthermore, the B3 and B4 series were produced to examine the effect of sandblasting treatment under the role of variation of MC of timber and adhesive type. Finally, 3X bonding length series B5 and B6 were manufactured to investigate the scale impact.

Table 2-3 Timber- pre-fabricated concrete composite test series

Series	Sub Series	ω Cond (%)	ω Test (%)	Sandblasted Concrete	adhesive	Bonding length (mm)	Adhesive thickness (mm)
B1	B1.1	12	12	No	Sikadur®-330	80	1
	B1.2						3
	B1.3				Sikadur®-31EF		1
	B1.4						3
B2	B2.1	20	12	No	Sikadur®-330	80	1
	B2.2						3
	B2.3				Sikadur®-31EF		1
	B2.4						3
B3	B3.1	12	12	Yes	Sikadur®-330	80	1
	B3.2				Sikadur®-31EF		
B4	B4.1	20	12	Yes	Sikadur®-330	80	1
	B4.2				Sikadur®-31EF		
B5	B5.1	12	12	No	Sikadur®-330	240	1
	B5.2						3
	B5.3				Sikadur®-31EF		1
	B5.4						3
B6	B6.1	20	12	No	Sikadur®-330	240	1
	B6.2						3
	B6.3				Sikadur®-31EF		1
	B6.4						3

Note: $\omega_{\_Cond}$: timber MC prior to glueing; $\omega_{\_Test}$: timber MCat test time

2.6 Experimental results and discussion

Fig. 2-8 illustrates the strain on the two glued interfaces just before the failure occurrence, extracted by DIC. It might be evident that both faces share the applied load equally with almost equal shear strain along the interfaces. Also, **Fig. 2-9** shows the evolution of peak shear strain as a function of the mean shear stress along the two interfaces for standard specimen and scale specimen, e.g., specimen A2.1-1 and A4.2-4. The red lines correspond to the specimens A2.1-1, while the black lines represent the scale specimens A4.2-4. The peak shear strain on the two glued interfaces of the TCC joints was measured using an artificial extensometer utility within the Vic-3D software. The extensometer was positioned along the surface of the interface to measure the deformation and strain directly and accurately. It might be seen that the peak shear strain evolution along the two interfaces looks similar, indicating satisfactory behaviour and fabrication of the specimen. However, the scale specimen shows a higher initial rigidity with less bonding strength, but

also a loss of rigidity in the course of loading. This phenomenon will be discussed in section 2.6.4. Therefore, the two glued interfaces were assumed to share the load equally as a simplification. Additionally, the interfaces were also assumed to follow a uniform distribution law of shear stress. The double-glued joints were tested until failure, as described in section 2.2.1. For general evaluations and comparisons, the shear strength of wet and dry TCC joints was calculated according to Eq. (1). For the sake of simplification, it is assumed in Eq.1 that the shear stress is uniformly distributed over the bonding area [76].

$$\tau_u = \frac{F_u}{A} \qquad \text{Equation 1}$$

Where τu is the mean shear strength, Fu is the ultimate force, and A is the bonding area.

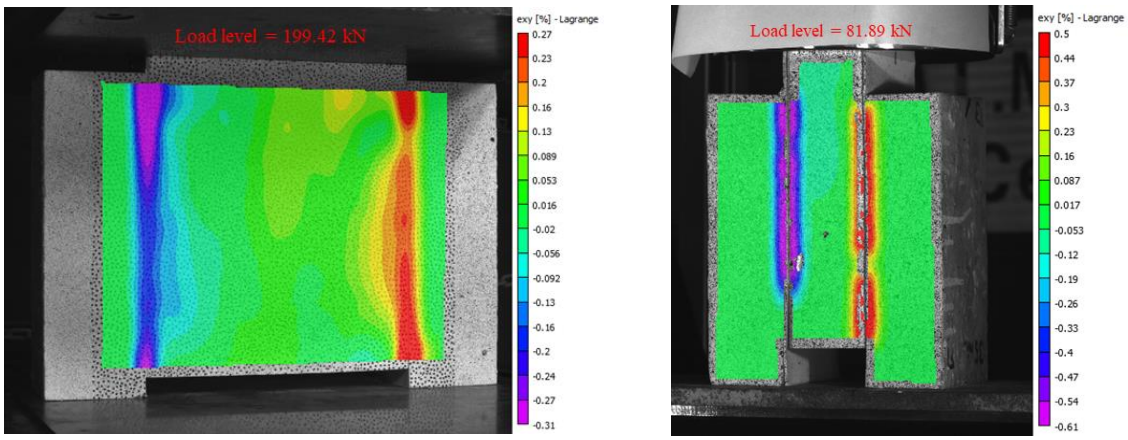

(a) (b)

Fig. 2-8 Shear strain distribution on the surface of glued interfaces extracted from DIC post-process, (a) specimen A4.2-4, and (b) specimen A2.1-1

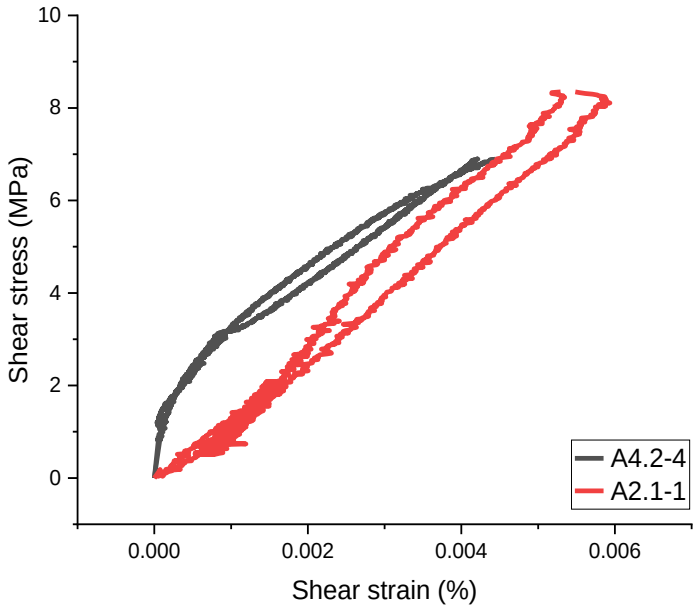

Fig. 2-9 Shear stress vs. peak shear strain along the glued interfaces extracted from DIC post-process for specimens A4.2-4 and A2.1-1

The failure mode can be purely adhesive or cohesive, and it is also possible to be a mixed failure mode between adhesive, concrete, and timber. Four types of failure modes were observed during the test campaign, as shown in **Fig. 2-10**. Generally, two or three of these failure modes may be detected for each failed face of the specimen. A percentage of each type of failure is given based on image analysis of all broken faces realized after testing.

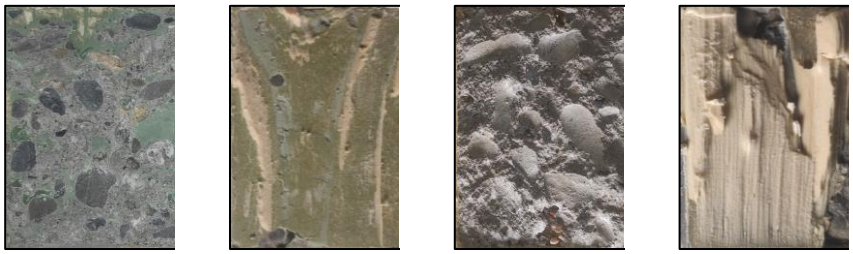

(a) (b) (c) (d)

Fig. 2-10 Types of failure modes of TCC specimens: (a) adhesive failure at the interface with concrete, (b) adhesive failure at the interface with wood, (c) cohesive failure in the concrete, and (d) cohesive failure in the timber

The shear strength of each tested series of TCC Specimens is shown in **Fig. 2-11**. Moreover, statistical parameters are evaluated for each sub-series, such as the mean value of the average shear strength (τ_{mean}), Standard deviation ($\delta\tau$), and coefficient of variation (COV). Additionally, **Fig. 2-12** illustrates the pie charts

representing the proportions of each type of failure mode for each sub-series. These figures form the base for discussing the results.

(a)

(b)

Fig. 2-11 Shear strength of all tested TCC specimens, (a) wet TCC joints, and (b) dry TCC joints

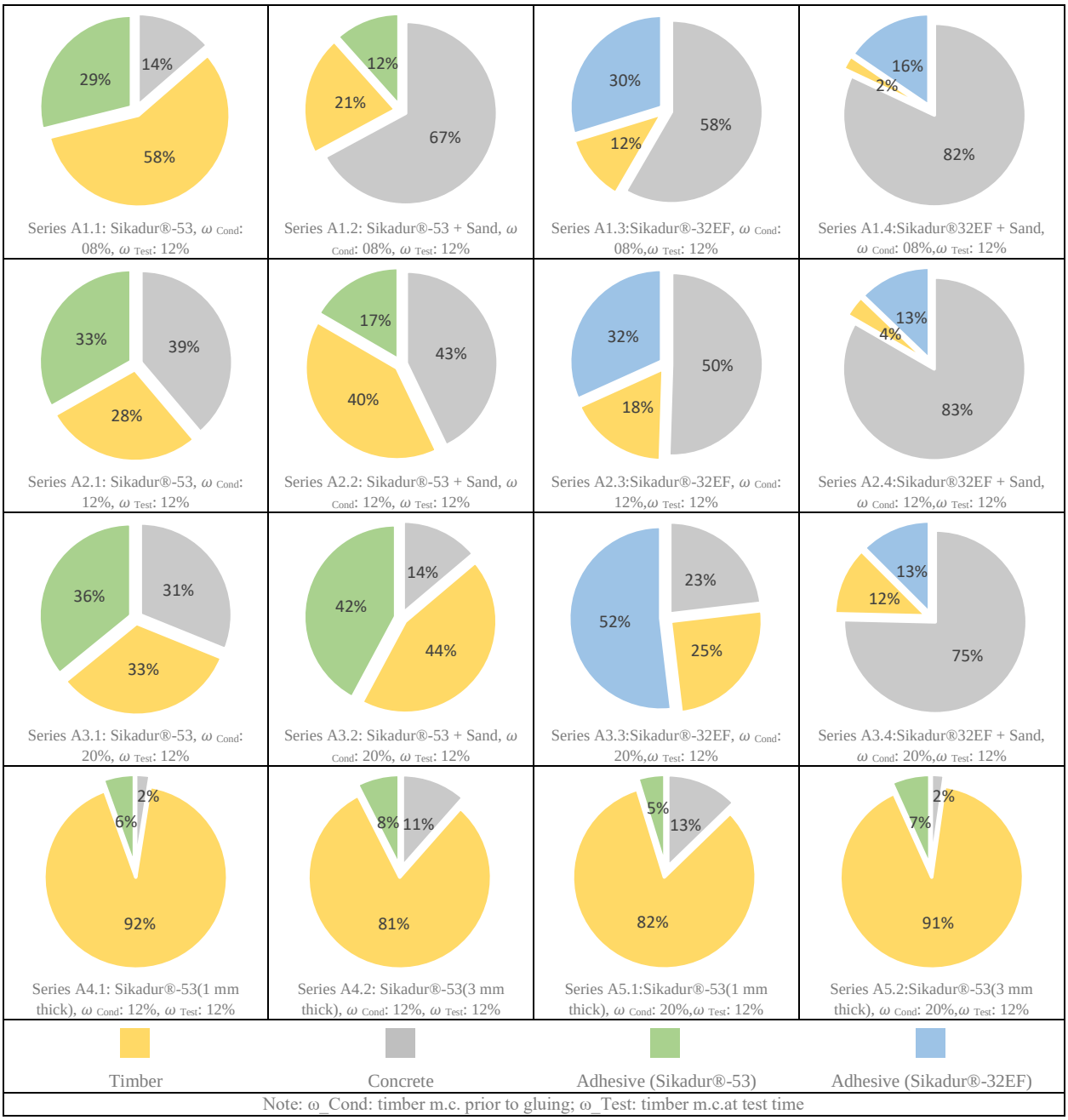
29%
14%
58%
Series A1.1: Sikadur®-53, ω Cond: 08%, ω Test: 12%
12%
21%
67%
Series A1.2: Sikadur®-53 + Sand, ω Cond: 08%, ω Test: 12%
30%
58%
12%
Series A1.3:Sikadur®-32EF, ω Cond: 08%,ω Test: 12%
16%
2%
82%
Series A1.4:Sikadur®32EF + Sand, ω Cond: 08%,ω Test: 12%
33%
39%
28%
Series A2.1: Sikadur®-53, ω Cond: 12%, ω Test: 12%
17%
43%
40%
Series A2.2: Sikadur®-53 + Sand, ω Cond: 12%, ω Test: 12%
32%
50%
18%
Series A2.3:Sikadur®-32EF, ω Cond: 12%,ω Test: 12%
13%
4%
83%
Series A2.4:Sikadur®32EF + Sand, ω Cond: 12%,ω Test: 12%
36%
31%
33%
Series A3.1: Sikadur®-53, ω Cond: 20%, ω Test: 12%
14%
42%
44%
Series A3.2: Sikadur®-53 + Sand, ω Cond: 20%, ω Test: 12%
23%
52%
25%
Series A3.3:Sikadur®-32EF, ω Cond: 20%,ω Test: 12%
13%
12%
75%
Series A3.4:Sikadur®32EF + Sand, ω Cond: 20%,ω Test: 12%
2%
6%
92%
Series A4.1: Sikadur®-53(1 mm thick), ω Cond: 12%, ω Test: 12%
8%
11%
81%
Series A4.2: Sikadur®-53(3 mm thick), ω Cond: 12%, ω Test: 12%
5%
13%
82%
Series A5.1:Sikadur®-53(1 mm thick), ω Cond: 20%,ω Test: 12%
2%
7%
91%
Series A5.2:Sikadur®-53(3 mm thick), ω Cond: 20%,ω Test: 12%
Timber
Concrete
Adhesive (Sikadur®-53)
Adhesive (Sikadur®-32EF)
Note: ω_Cond: timber m.c. prior to gluing; ω_Test: timber m.c.at test time

(a)

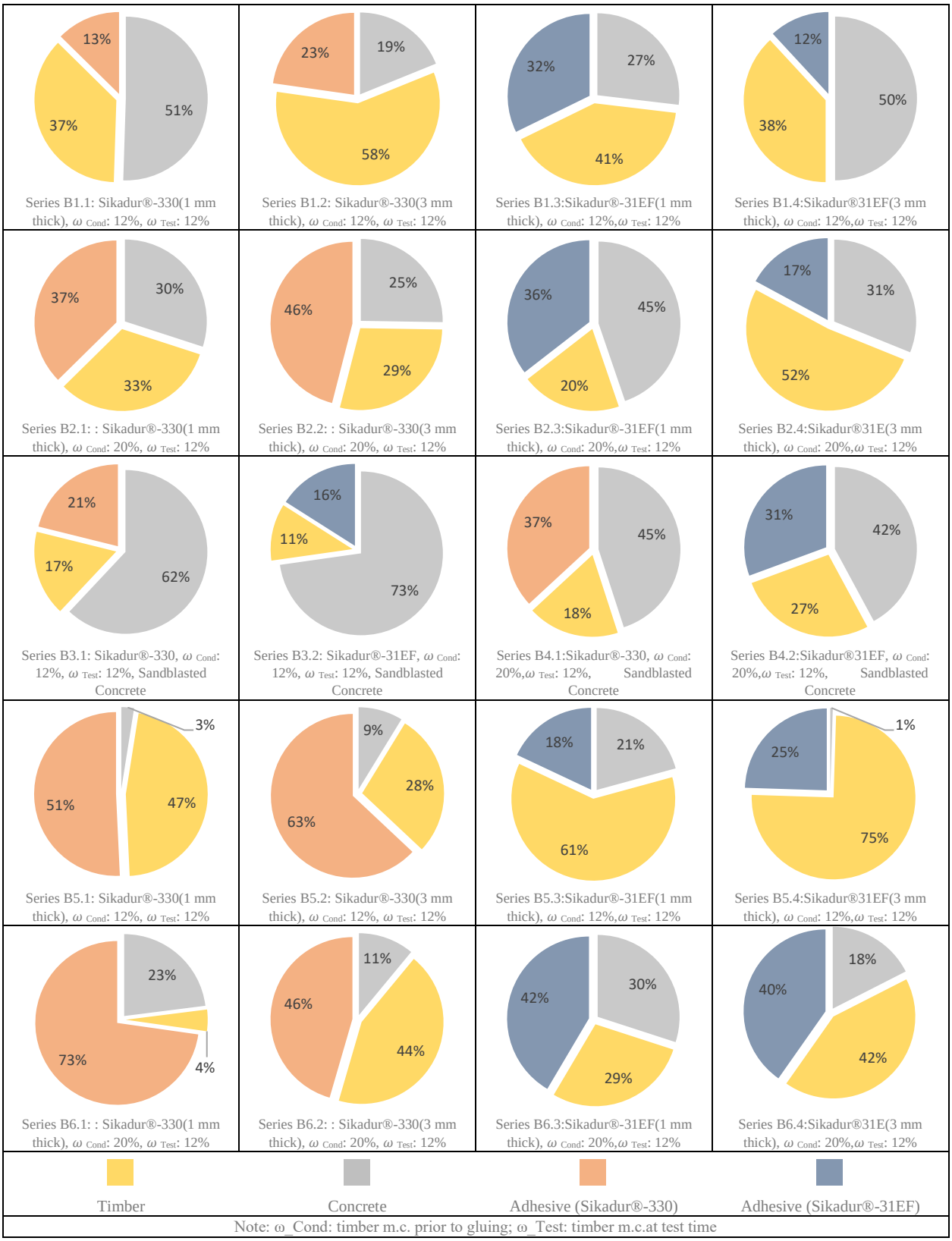

(b)

Fig. 2-12 Failure modes Proportions for (a) wet TCC joints, and (b) dry TCC joints

2.6.1 Effect of moisture content on shear strength and modes of failure

For the fresh concrete specimens series, A3 and A5 have the highest MC of the timber just before the glueing time, at 20%. In series A3, the average value of shear strength has significantly decreased compared to series A1 and A2. There is a decrease of about 10-25% in shear strength for subseries A3.1, A3.2, A3.3, and A3.4, with shear strength values of 7.41 MPa, 6.28 MPa, 4.88 MPa, and 4.59 MPa respectively, when compared to the reference subseries A2.1, A2.2, A2.3, and A2.4, with shear strength values of 8.24 MPa, 7.68 MPa, 6.38 MPa, and 5.44 MPa respectively, as shown in **Fig. 2-11**. In the case of large-scale specimens, the results showed a slight decrease in the mean value of shear strength when A5.1, i.e., 6.14 MPa, compared to series A4.1, i.e., 6.70 MPa. However, the opposite trend was observed when comparing series A5.2 to series A4.2. The mean shear strength for A5.2, i.e., 7.10 MPa, was slightly higher than that of A4.2, i.e., 7.02 Mpa. These outcomes match with those of pre-fabricated concrete series B2, B4, and B6, from which similar conclusions might be drawn. The explanation for this phenomenon might be comparable to that drawn by Negrão et al. [84], to which similar findings have been found. The water molecules adsorbed on cell walls play the role of lubricant on the intended bonding surface of the timber, reducing its bonding to the adhesive. Thus, the chemical efficiency of adhesives can be further altered by water molecules. Concerning the MC effect on the failure modes, by comparing pie charts (**Fig. 2-12**) of a series of 20% MC with their corresponding series of 12% MC, it might be seen that the influence of increasing the moisture content of the conditioned timber is more evident in a higher proportion of adhesive mode of failure. After all, the main concept to conclude from the performance of these series is that the existence of a high MC in timber elements forms a significant inconvenience for reliable glueing as a shear connector of timber concrete composite structures.

2.6.2 Effect of sand addition on shear strength and failure modes

The sand addition was attributed to the need to increase the roughness of the bonding surface between timber and concrete. The outcomes were far from those expected. The results showed that mixing sand (grain size recommended by SIKA 1.5-2 mm) and adhesive caused a slight reduction in the mean value of the shear strength in all series where sand addition was employed except A1.4. In general, there was a reduction of about 6-9 % on average by shear strength for Sikadur®-53 and Sikadur®-32EF when mixed with sand. From the pie charts (**Fig. 2-12**), It may be obvious that concrete failure is the prevailing mode of failure in the series where the sand was mixed with the adhesive, mainly for specimens made of Sikadur®-32 EF mixed with sand. One possible explanation is that the sand acts as an isolator layer since the grain size of the sand was larger than the intended adhesive layer thickness of 1 mm. Thus reducing the bonding area between adhesive and concrete. Therefore, higher stress on the concrete surfaces was produced; consequently, a higher proportion of concrete tearing up.

2.6.3 Effect of adhesive type on shear strength and failure modes

One must remark that the series made of Sikadur®-53 and Sikadur®-53+sand exhibit a substantial disparity in the mean value of shear strength compared to their corresponding series made of Sikadur®-32EF and Sikadur®-32EF+sand. As illustrated in **Fig. 2-11**, in series A2, the average shear strength of wet TCC joints made of Sikadur®-53 and Sikadur®-53+sand, i.e., 8.24 and 7.68 MPa, were 1.3 and 1.4 times those made of Sikadur®-32EF and Sikadur®-32EF+ sand, i.e., 6.38 and 5.44 MPa, respectively. One piece of evidence may conclude about the higher bonding strength of Sikadur®-53 with timber in contrast to Sikadur®-32 EF through the higher proportion of timber failure in these series, which might be due to the higher penetration depth of Sikadur®-53 into the timber element, its low-viscosity consistency may have contributed to a more effective bond compared to Sikadur®-32 EF. In contrast, in the dry process series, both Sikadur®-330 and Sikadur®-31EF showed similar results. Furthermore, these results are too similar to the results achieved by Sikadur®-53. The trend of failure modes in all 80 mm bonding length series made of Sikadur®-330 is almost identical to those made of Sikadur®-31EF. This similarity may explain the convergence of the average shear strength value achieved by both adhesives. These findings reveal the importance of adhesive selection and its compatibility with timber and concrete surfaces in achieving optimal bonding strength in TCC joints. The precise adhesive properties and mechanisms that lead to the observed variations in shear strength and failure modes can be further investigated and studied.

2.6.4 Scale effect

The results concerning the scale effect showed a significant drop in the mean value of shear strength. The mean value of shear strength of 80 mm-bonding length series A2.1 and A3.1, i.e., 8.24 and 7.41 MPa, were 1.2 times of those 240 mm-bonding length corresponding series A4.1 and A5.1, i.e., 6.70 and 6.14 MPa, respectively (see **Fig. 2-11**). Similar conclusions might be drawn to the result of large-scale dry series B5 and B6 compared to their corresponding 80 mm-bonding length series B1 and B2, respectively. This trend has been shown by Negrão et al. [41], assigning this to the volume effect. Fu et al. [76] owed this effect to the shear stress distribution. The shorter the bonding length, the more uniform the shear stress distribution. From **Fig. 2-12**, it may be clear that the timber forms the weakest elements of the connection for all large-scaled wet series. The proportion of timber failure has dramatically increased, exceeding 80% in series A4.2 and A5.1 and exceeding 90% in series A4.1 and A5.2, compared to less than 35% for their corresponding series of 80 mm bonding length. Shear failure parallel to the grain in timber elements was dominant in these series, and this phenomenon always caused one face to fail before the other. The difference observed in the scale specimens may be attributed to a higher presence of timber knots. These knots significantly increase the probability of failure initiation, particularly in larger surface areas. It is evident that during the manufacturing of timber beams, although complying with standards, the lamination

arrangement does not consider the growth speed of each lamination. A beam lamination with a rapid growth speed is weaker in terms of shear strength. Therefore, different growth speeds of the edge laminations might justify the reason that caused one face to fail before the other, as shown in **Fig. 2-13**.

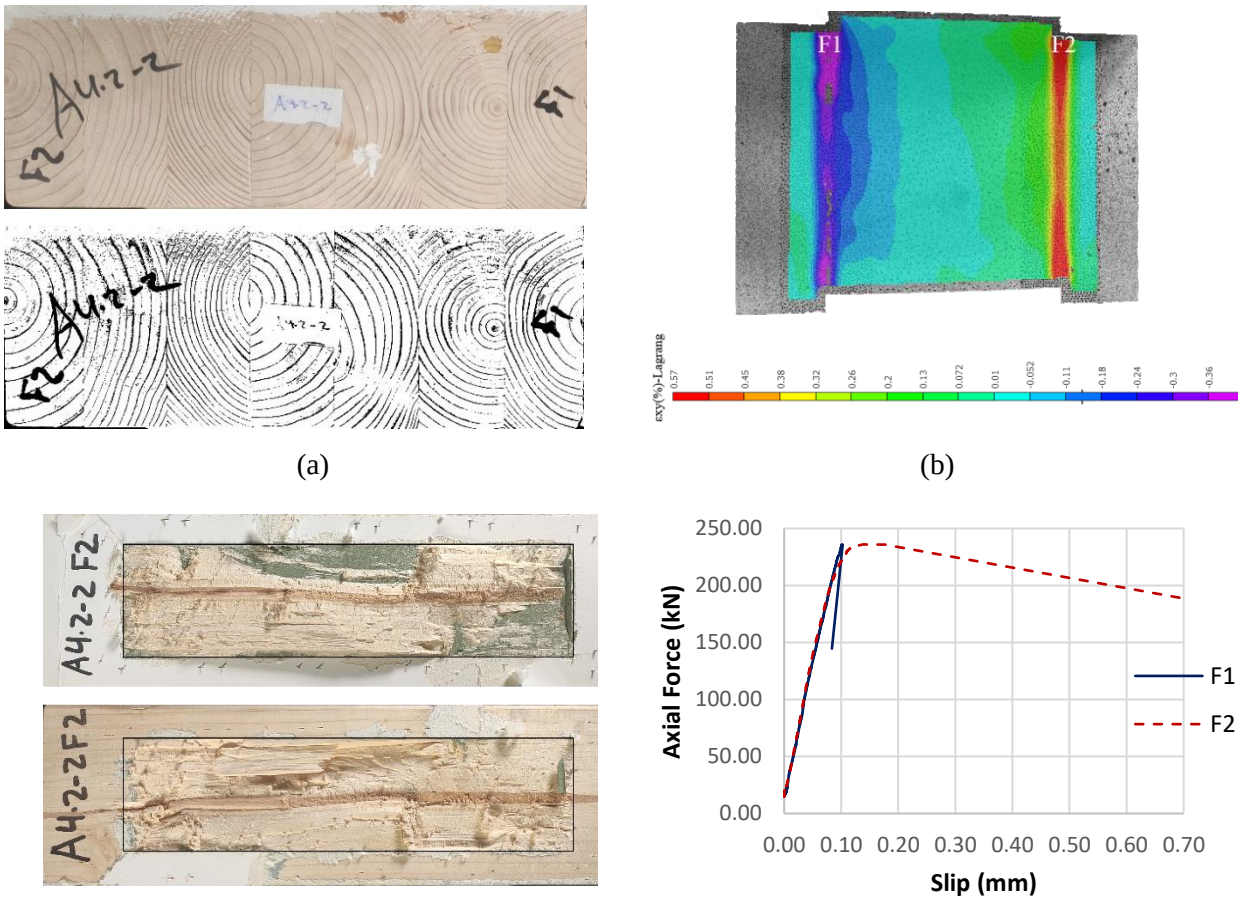

(a) (b)

(c) (d)

Fig. 2-13 Specimen A4.2-2, (a) timber element with different laminations growth speed at the edges, (b)shear strain distribution on the surface of glued interfaces just before the failure extracted from DIC post-process, (c) timber failure mode, and (d) slip at the interface extracted by the installed LVDT sensors

Fig. 2-14a illustrates the main tendency of the slip vs. shear stress curve for standard series A2.1 and scale series A4.1, respectively, extracted from the experimental curves of all specimens under each main series. Both wet series were made of Sikadure 53 at 12% MC of conditioned timber. It may be evident that the scale series A4.1 has a higher bonding rigidity with an approximated mean value of elastic slip of 0.04 mm compared with 0.45 mm for series A2.1. However, the scale series showed a more ductile mode of failure with an increase in total slip reaching approximately 0.3 mm. In contrast, for most of the standard series, a brittle mode of failure has been observed; however, the growth of slip for some cases was about

0.2 mm. The explanation for this might be that the scale series has the advantage of possibly redistributing plastic zones of the adhesive just before failure. However, this phenomenon is not possible in the case of a standard series with a smaller bonding area length. Another justification is that the failure of large-scale series happened mainly due to timber failure, as discussed earlier in this section. This could explain the ductility mode of failure of the scale series. A similar conclusion can be drawn for the dry series in which a similar behaviour was observed, e.g., series B1.1 and B1.2 in comparison with corresponding series B5.1 and B5.2, respectively, as shown in **Fig. 2-14b**.

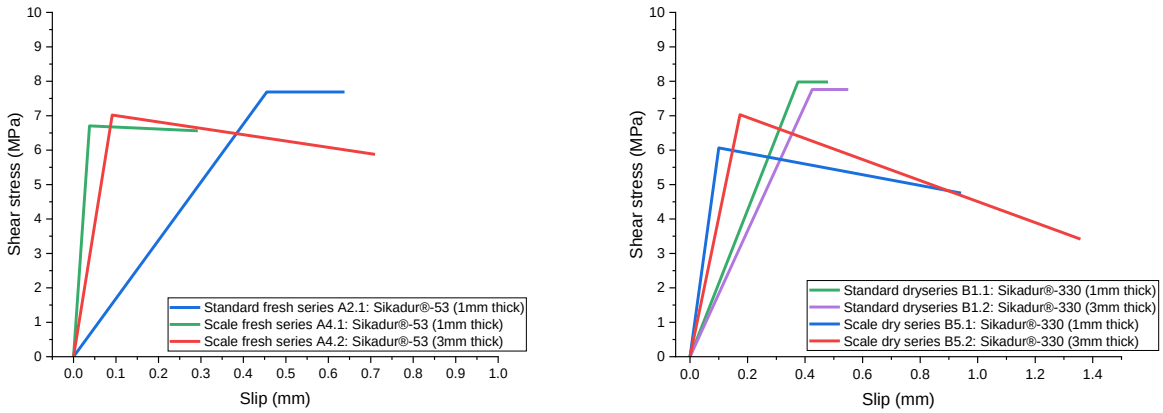

(a) (b)

Fig. 2-14 Typical Shear stress vs. slip for (a) wet series A2.1, A4.1, and A4.2, (b) dry series B1.1, B1.2, B5.1, and B5.2

2.6.5 Effect of sandblasting

Regarding the concrete sandblasting effect, the results showed a slight increase of approximately 2-5% in shear strength of all sandblasted series compared with their corresponding series except series B4.1, which showed a contradictory result with a decrease of 9.2% compared to B2.1. In Series B3 with sandblasted concrete panels, the prevailing mode of failure is concrete with more than 60% of the failure area, and this could explain the slight increase in the mean value of shear strength, where the bonding with concrete element seems much stronger, due to removal of the unreacted layer of cement generating more pours surface. Thus, more penetration paths are to be tracked by adhesive. This effect was shown by Fu et al. [74], who attributed that to the increased degree of concrete surface roughness, the larger penetration depth of the adhesive into the concrete component, and the fact that the solid substrate of concrete is stronger than the facial cover, which is easier to tear off. In contrast, in series B4, concrete is still the dominant mode of failure with less proportion than in series B3; this may be owed to the increase of adhesive failure proportion due to the increase of MC. This might explain the reason for remaining the mean value without any enhancement compared to the values from series B2. Despite the slight increase in

the mean value achieved by this mean, concrete sandblasting does not seem feasible to be used to strengthen the bond between concrete and timber higher than the corresponding value achieved without this treatment.

2.6.6 Effect of adhesive thickness on shear strength and failure modes

Increasing adhesive layer thickness to 3 mm instead of 1 mm has been investigated for only large-scale series in the case of the wet process and for all series in the case of the dry process. In the case of the wet process, the average shear strength for the 3 mm adhesive thickness series made of Sikadur®-53 A4.2 and A5.2, i.e., 7.02 and 7.1 MPa were 1.15 times of those 1 mm adhesive thickness corresponding series A4.1 and A5.1, i.e., 6.07 and 6.14 MPa, respectively (see **Fig. 2-11**). In contrast, in the dry process, the result showed an enhancement to the average value of shear strength in most cases. The average value of shear strength for 3 mm adhesive thickness series B2.2, B2.4, B5.2, B5.4, and B6.2, i.e., 7.47, 7.69, 7.03, 6.08, and 5.43 MPa were 1-1.3 times of those 1 mm adhesive thickness corresponding series B2.1, B2.3, B5.1, B5.3, and B6.1, i.e., 7.32, 6.52, 6.07, 5.99 and 4.20 MPa, respectively (see **Fig. 2-11**). These results are contradictory to findings that have been found by Negrão et al. [84]. The author concluded that the use of a thin layer of adhesives instead of a thick layer led to a significant decrease in the performance of the connection in the case of a wet process and enhanced the performance in the case of a dry process. The explanation for this might be the type of concrete used. As described in section 2.3.3, self-compacting concrete reduces the mechanical influence of concrete compacting on the connection. Therefore, there is no risk of adhesive removal or running from the bonding surface, which could cause significant differences in the results due to the uncertainty of the residual adhesive thickness, as in the case of mechanically compacted concrete.

In the case of the dry process with an 80 mm bonding length made of 3 mm adhesive layer thickness of Sikadur®-330, the proportion of adhesive failure has been approximately doubled compared with their corresponding series; however, a contradictory trend happened for those series made of Sikadur®-31EF, where the proportion of adhesive failure has been approximately reduced to one half (see **Fig. 2-12**). In contrast, in the case of large-scale specimens, a different trend might be drawn, where the proportions of timber failure have been increased in most cases except series B5.2 (see **Fig. 2-12**). One possible justification for this is the increasing penetration depth of adhesive into timber due to increased adhesive layer thickness; therefore, mechanical bonding with timber is enhanced. Nemati Giv et al. [105] showed that increasing the adhesive thickness leads to altering the mode of failure from bonding failure to wood-adhesive interface failure and concrete failure, thus increasing the bonding strength. Furthermore, Increasing the adhesive layer thickness seems to magnify the ductility behaviour of the mode of failure. The approximated total slip of, e.g., fresh series A4.2 (0.71 mm) was 2.36 times of A4.1 (0.3 mm), see **Fig. 2-14a**. Similar behaviour can be detected for standard and scale dry series, as shown in **Fig. 2-14b**.

ıncreasing the adhesive layer thickness from 1 mm to 3 mm seems feasible to enhance the mean value of the shear strength, especially in the case of 20% MC of conditioned timber before glueing. Furthermore, this aspect is crucial when considering applications on a larger scale, where ensuring a consistent adhesive thickness of 1mm across the entire bonding surface of timber elements may not be feasible. Comparison between the dry and wet TCC joints

2.6.7 Comparison between the dry and wet TCC joints

The comparison between the mean value of shear strength of wet and dry TCC joints at 12% and 20% MC of conditioned timber with 80 mm bonding length and 1 mm adhesive thickness can be observed in **Fig. 2-15a** and **b**. The average shear strength between TCC joints using Sikadur®-53 for the wet process compared with Sikadur®-330 and Sikadur®-31EF for the dry process is significantly similar based on an ANOVA: Single Factor test, with a P-value equal to 0.91 and 0.21 (α=0.05) for 12% and 20% MC of conditioned timber respectively, in contrast, the average shear strength of wet TCC joints made of Sikadur®-32EF is significantly different than their corresponding TCC joints based on post-hock test. One possible explanation for a higher mean value of shear strength achieved by the wet process series made of Sikadur®-53 is the higher penetration depth into fresh concrete than the non-sandblasted pre-fabricated concrete panels. However, in the sandblasted series, the mean values of shear strength are almost identical to their corresponding series made of Sikadur®-53 due to mechanical interlocking enhancement, which is described in section 2.6.5. In contrast, the comparison between large-scale series of wet and dry TCC joints at 12% and 20% MC of conditioned timber with 240 mm bonding length and 1 mm adhesive thickness is illustrated in Fig. 12c and d. Similarly to small-scale specimens, the average value of shear strength between wet and dry TCC joints is significantly similar based on an ANOVA: Single Factor test, with a P-value equal to 0.31 (α=0.05) for 12% MC of conditioned timber. However, the same ANOVA test showed a significant difference in the average value of shear strength with a P-value equal to 0.015 (α=0.05) for 20% MC of conditioned timber. The results of the series made of Sikadur®-330 are significantly less than their corresponding TCC joints made of Sikadur®-53 based on the POST-Hock test. A similar conclusion can be drawn in the case of 3 mm adhesive thickness instead of 1 mm. Although the differences in the mean values on some occasions when the results of wet and dry processes are compared, these findings are contradictory to what was found by Nemati Giv et al. [105]. The author revealed that the mean shear strength of wet joints made of Sikadur330 with 1 and 3 mm thicknesses (5.7 and 6.7 MPa, respectively) were 2.2 and 3 times those of dry joints (2.6 and 2.2 MPa).

Wet and dry TCC joints have some similarities and differences in failure modes, as illustrated in **Fig. 2-12**. The trend and proportion of failure modes in the small-scale wet series made of Sikadur®-53 are similar to their corresponding dry series made of Sikadur®-330 and Sikadur®-31EF. This similarity may

explain the convergence of both fabrication techniques' average shear strength values, as prescribed in section 2.6.3. In the case of the large-scale, unlike the wet-process series, where timber failure was the dominant failure mode as specified in section 2.6.4. The prevailing mode of failure is almost adhesive in all dry series made of Sikadur®-330. However, the trend of failure modes in the dry series B5.3 and B5.4 made of Sikadur®-31EF is almost similar to those in wet series A4.1 and A4.2 made of Sikadur®-53.

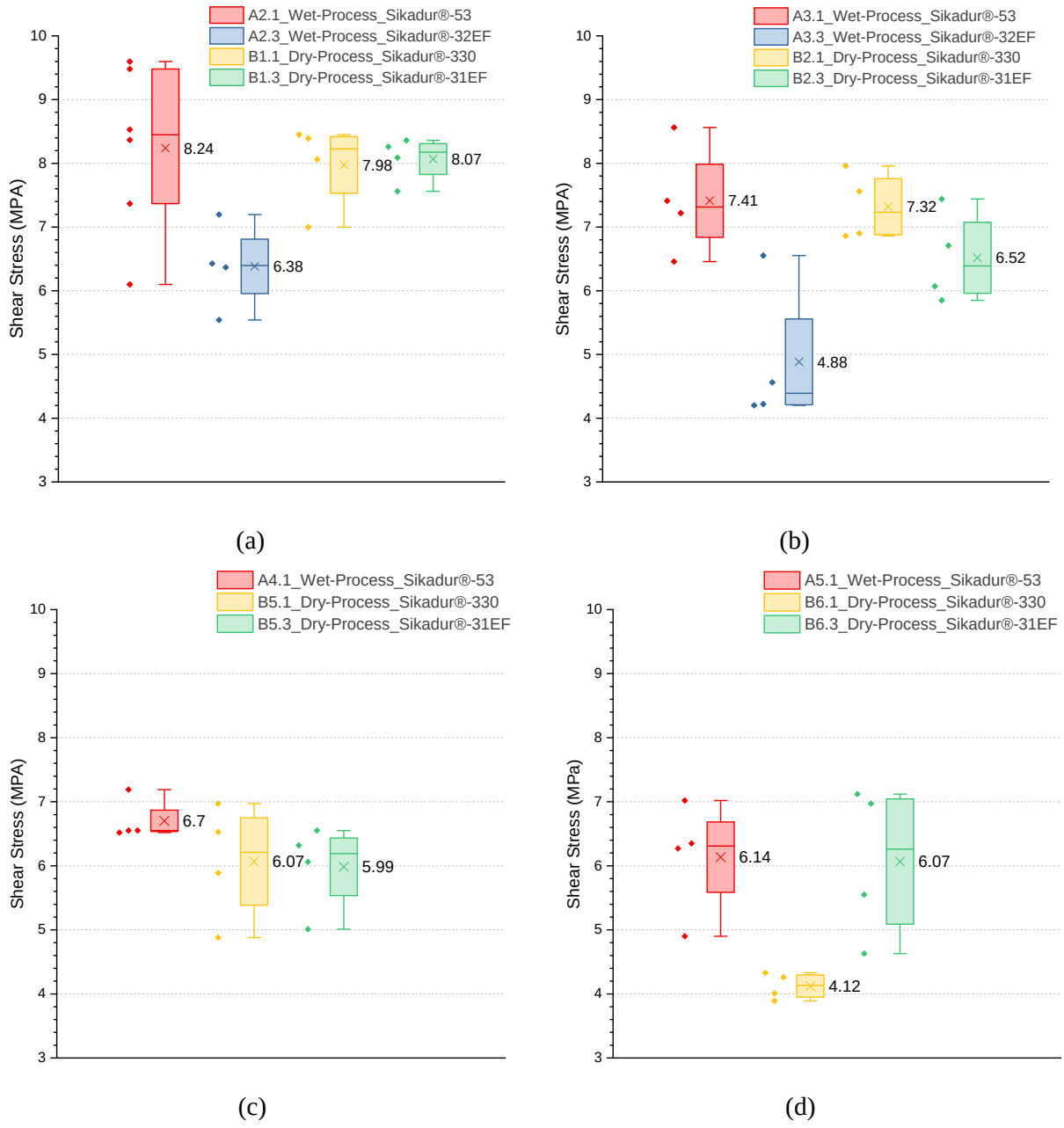

Fig. 2-15 Comparison between wet and dry TCC joints, in case of 1 mm adhesive thickness of (a) standard series at 12% MC of conditioned timber, (b) standard series at 20% MC of conditioned timber, (c)

large-scale series at 12% MC of conditioned timber, and (d) large-scale series at 20% MC of conditioned timber

After all, the radar diagram in **Fig. 2-16** illustrates a synthesized comparison for evaluating the most suitable method of TCC fabrication in terms of shear strength, sensitivity to MC, the sensitivity of adhesive thickness (geometrical uncertainty), and ease of implementation. Each of these factors represents one branch of the diagram, while the scale of each axis ranges from one (worst) to five (best). As Shown, Sikadur®-53 with wet process forms the best option to be selected for TCC fabrication with the highest ranks among the other options. In contrast, the Sikadur®-32 EF with the wet process is the worst option. In comparison, both adhesives Sikadur®-330 and Sikadur®-31EF with dry process achieved almost equivalent ranks with some deviations on the same branch.

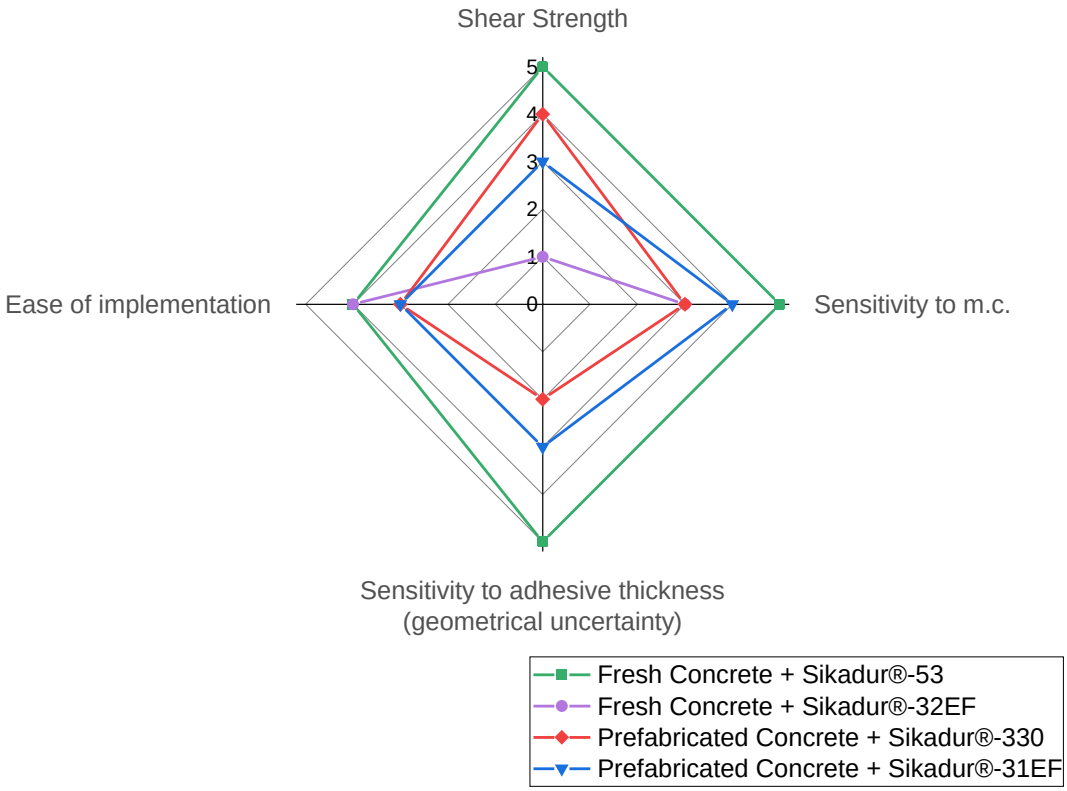

Fig. 2-16 Radar diagram for evaluating the most suitable method of TCC fabrication

2.7 Summary

This chapter investigates the bonding performance of wet and dry TCC joints. The study in this chapter was guided by a pre-defined hypothesis, which sought to explore the impact of moisture content variation

of the timber, adhesive type, adhesive film thickness, sand addition, sandblasting of the pre-fabricated concrete surface, and bonding scale effect on the shear strength and failure modes of the joints.

The findings suggest that glueing seems to be a possible option as a shear connector for producing both dry and wet TCC joints. In the case of the wet process, both Sikadur-53 and Sikadur-32EF epoxy resins used in this study led to the average shear strength of about 8.24 MPa and 6.38 MPa, respectively, at 12% MC of timber and 1 mm adhesive layer thickness. In contrast, dry joints using Sikadur-330 and Sikadur-31EF led to a mean value of shear strength of about 8 MPa under the same conditions; furthermore, both adhesives achieved about a mean value of 6 MPa of shear strength in the case of scale series under 12% MC of timber and 1mm adhesive layer thickness, and these results look similar to the results achieved by Sikadur®-53 in wet-process with a mean value of 6.7 MPa of shear strength.

Under dry conditions of timber elements, the mean value of shear strength is considered high and is primarily affected by a failure in the concrete and timber parts. In contrast, the results showed that the performance of this bonding system is significantly reduced by increasing the MC of timber before the glueing process. Therefore, careful moisture control and pre-bonding conditioning of timber are recommended to ensure optimal bonding performance.

The results indicate that concrete sandblasting does not significantly enhance the strength of the connection between concrete and timber compared to joints without the sandblasting treatment. Furthermore, contrary to what was expected, sand addition appears to cause a slight reduction in the average value of the shear strength in most series where it was employed.

Increasing the adhesive layer thickness from 1 mm to 3 mm enhances the average value of the shear strength, especially in the case of a series made of Sikadur®-330 conditioned at 20% before glueing. However, despite the contradictory trend in results due to increasing the adhesive layer thickness up to 3 mm in some series, this solution still seems reasonable to guarantee the intended minimum adhesive thickness along the surface of timber elements, especially in the case of full-scale TCC beams.

These results obtained in this experimental campaign, where realistic conditions of industrial fabrication regarding wood MC, adhesive layer thickness, and glueing surface were imitated, indicate that adhesive bonding can provide satisfactory shear strength for TCC joints and can be considered as an alternative to mechanical connectors in TCC structures.

By understanding and emphasizing the significant impact of moisture content, adhesive type, and bonding techniques on the shear strength and failure modes of TCC joints, this chapter lays the groundwork for a deeper analysis of the structural performance of adhesively bonded TCC beams in **Chapter 3**.

Chapter 3
TCC Beams Testing

Chapter 3 TCC Beams Testing

The present chapter draws upon research previously published in a journal article. *Experimental investigation on adhesively bonded timber-self-compacting concrete composite beams with a thin slab* [110].

3.1 Introduction

Given the necessity to limit the carbon footprint of constructions, it becomes essential to seek a consistent proportion of material that considers both environmental and structural requirements. This approach not only reduces the demand for clinker production, which is known for its high carbon footprint, but also takes advantage of timber's lower carbon footprint compared to traditional industrial building materials. Additionally, timber acts as a carbon sink, effectively absorbing and storing CO2 emissions from the atmosphere [111]. In this pursuit, achieving a relatively higher ratio of timber to concrete in the cross-section of the floor system could be targeted. However, this attempt must ensure that it does not compromise the structural performance, which is often reached when both materials are pushed to their limits. While acknowledging the complexity of achieving the optimal trade-off between climate impact and structural performance. Studies by [111,112] have demonstrated the significant role of replacing traditional building materials such as concrete with timber in reducing the construction industry's carbon footprint while maintaining structural integrity. The present chapter approaches this challenge by utilizing a thin concrete slab connected to a timber beam. This geometric configuration is another crucial motivation for employing SCC in fabricating concrete slabs in both wet and dry processes.

The stiffness and performance of the mechanical connection are some of the key points intensively investigated and discussed [3,16,18,20]. Due to its local aspect, at least for most of the usual connection systems, the mechanical connection cannot provide a continuous flexural strain diagram between the two materials, and the existing relative slip leads to an additional deflection. In the same way, the flexural failure can generally be due to a combined effect of plasticization of metal connectors, concrete crushing around the connector heads, and pull-out of connectors either in wood or concrete. This means that in such TCC floor systems, failure rarely occurs in timber beams, panels, or concrete slabs because of an exceedance of the equivalent flexural strength of the materials [20], which limits mechanical performance. TCC floor systems with adhesive connections were developed to overcome this limitation under ultimate and serviceability conditions [6,20–25].

As the cross-sectional height increases, especially in heavily loaded or large-span TCC beams and slabs, there is an increased demand for high-shear strength connections such as adhesive bonding [74]. Consequently, high-strength concrete in adhesively bonded TCC floor systems is highly recommended for

optimizing material efficiency and reducing overall weight [74,113]. In addition to its favourable bonding shear strength, adhesive bonding offers several advantages, making it a promising solution for TCC structures. Adhesive bonding can provide a rigid bonding between timber and concrete components, ensuring efficient load-shared contribution and enhancing the overall stiffness of the composite system [7]. The even distribution of stresses along the bond line improves load-bearing capacity and enhances structural integrity compared to traditional mechanical connectors. Furthermore, adhesive bonding eliminates the need for drilling and cutting, avoiding the potential weakening of the timber elements [16]. This advantage also simplifies the construction process, leading to faster assembly of TCC structures [16].

Previous studies [7,29,41,75,84] have demonstrated two main bonding processes for TCC structures: wet and dry. The wet-bonding process involves applying adhesive to the timber surface and subsequently pouring fresh concrete directly onto it. On the other hand, the dry-bonding process involves using pre-fabricated concrete slabs glued to the timber component. This approach has shown promise in streamlining construction timelines and minimizing moisture impacts on timber surfaces. Additionally, it allows for the separate fabrication of timber and concrete elements, enabling optimized logistics and construction efficiency [75].

In the previous chapter, we investigated the mechanical behaviour of TCC joints bonded with epoxy resin adhesives, focusing on the bonding process under both dry and wet conditions. This involved conducting double push-out shear tests on adhesive-bonded TCC joints and considering several key variables. The findings from our previous chapter were enlightening. Under dry conditions, the shear strength is within a mean value range of 6-8 MPa. Additionally, cohesive failure in concrete and timber primarily influences the predominant failure mode.

Building upon the insights gained from the previous chapter, One of the key challenges in adhesively bonded TCC structures is achieving a full bond between timber and concrete. The bond between these two materials is essential for the composite action to take place, ensuring that they work together efficiently and carry loads effectively. Achieving a full bond can be particularly challenging due to differences in material properties and surface conditions.

After testing the connection under shear in the previous, the logical next step in pursuing an efficient TCC floor system with high industrial feasibility is to evaluate the structural behaviour of the composite elements. This chapter presents the findings derived from the experimental work on full-scale TCC beams. This involved the complete process of designing, fabricating, and testing six full-scale TCC beams, employing both wet and dry fabrication methods. The chapter aims to extend the current state-of-the-art in adhesive-bonded TCC structures by comprehensively evaluating the load-bearing capacity, stiffness,

interface slip, and deformation. By doing so, we aim to contribute significantly to advancing knowledge in this field, offering a nuanced and comprehensive understanding of the mechanical behaviour and performance of adhesively bonded TCC structures. Additionally, through this investigation, we aim to identify and promote innovative solutions that align with the global objective of a low-carbon footprint construction.

3.2 The manufacturing process and specimens series

The manufacturing process of the TCC specimens involved two distinct processes: the wet and dry fabrication processes. A total of six full-scale TCC beams were produced and labeled based on their fabrication process, as shown in **Table 3-1**. In the wet fabrication process, the timber elements were precisely prepared by molding them within a formwork. Metallic L-shaped pieces were attached to the timber elements to ensure precise alignment and positioning. The adhesive chosen for this process was Sikadur®-53, a two-part epoxy-based adhesive manufactured by SIKA AG. The adhesive was applied to the full width of the timber elements with a controlled adhesive thickness of 3 mm by adjusting the position of two metallic L-shaped sides. The top surface of timber elements was not rectified before bonding, allowing for potential unevenness in the timber surfaces. It is worth mentioning that the GL timber beams are produced with geometrical tolerances. According to EN 14080 [114], the maximum allowable deviation of longitudinal warping for GL timber, measured over a length of 2 m, is 4 mm. The variations in the moisture content of timber from the time of fabrication to the time of concrete bonding might contribute to the geometrical imperfections of the bonding surface. The incorporation of a controlled 3mm thick adhesive layer aims to mimic real-world construction scenarios where uneven surfaces of timber elements may be encountered during adhesive application. This approach remains justified in achieving the minimum thickness required for full bonding along the surface of timber elements. Moreover, it is worth noting that our previous study revealed a notable improvement in average shear strength by increasing the adhesive layer thickness from 1 mm to 3 mm in some occasions [103]. A reinforcement mesh of type ST25C was carefully incorporated into the flange. The next step involved pouring self-compacting fresh concrete onto the pre-glued face of the timber element. The timing between the adhesive application and concrete pouring, referred to as the "stiffening time", was set to 37 minutes to ensure optimal adhesion between timber and wet concrete, as shown in **Fig. 3-1**.

On the other hand, in the dry fabrication process, concrete panels with nominal dimensions of 3.20 m in length, 400 mm in width, and a thickness of 60 mm were poured inside a formwork. Following the pouring process, these concrete panels underwent a curing period of three days under room conditions. Next, timber elements were securely positioned and fixed to ensure precise alignment between the timber and the concrete panels. Subsequently, the pre-glued timber surface was prepared, referring to the timber element

surface with an adequate layer of adhesive (3 mm thick) to guarantee complete bonding along the beam. Afterward, pre-fabricated concrete slabs were cleaned using an air blower and immediately bonded to the pre-glued timber surface without any waiting period.

The moisture content of wood during the fabrication process was not controlled, as it cannot be in an industrial hall where many other prefabricated concrete components are produced simultaneously. However, in compliance with the regulations and standards for fabricating glue-laminated timber and considering the ongoing conditions in the industrial hall during the fabrication process, the wood moisture content was estimated to fall within the range of 12%-14%.

Post-bonding, all composite beams underwent a curing period of 14 days. After that, composite beams were transferred from GA company's manufacturing site to the LMDC (Laboratoire Matériaux et Durabilité des Constructions) laboratory, where they underwent further curing under room conditions until the designated test date. Throughout this period, the moisture content of the wood experienced a reduction and stabilized at a value closely aligned with the 12% recommended for structural testing, as indicated in **Table 3-1**.

Table 3-1 Specimens series

Fabrication Process	Specimen ID	Adhesive	Timber			Concrete			Timber MC. at test
			L	W	H	L	W	H	
			[mm]			[mm]			[%]
Wet-process	WB1	Sikadur®-53	3200	118	236	3200	400	58	12.23
	WB2							58	12.27
	WB3							55	12.18
Dry-process	DB1	Sikadur®-330	3200	118	236	3200	400	63	12.24
	DB2							62	12.27
	DB3							60	12.04

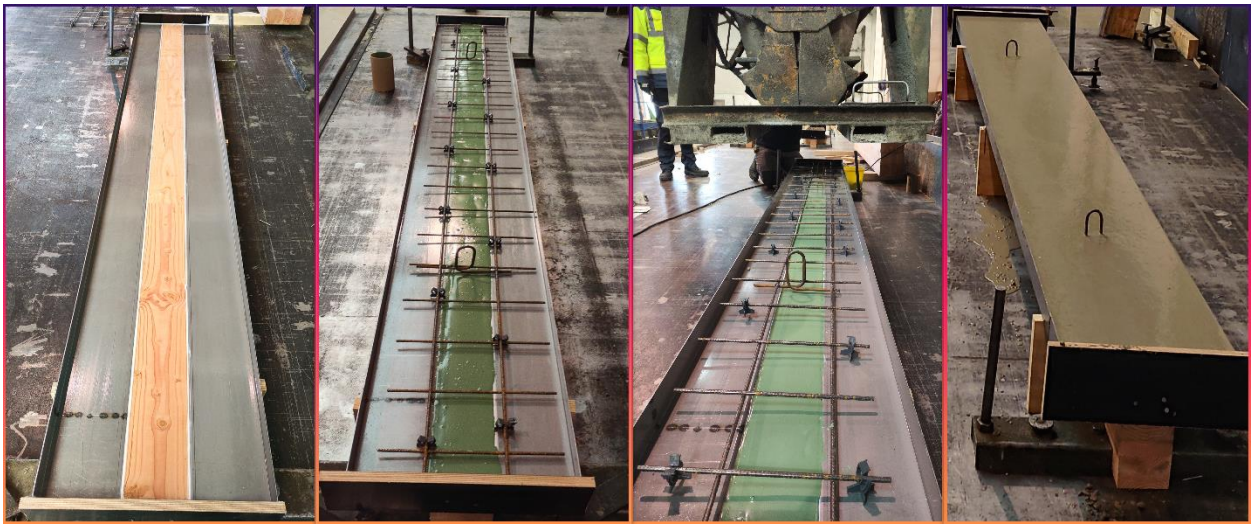

Fig. 3-1 Wet process of TCC beam manufacturing

3.2.1 Strain gauges and LVDT sensors

Strain gauges were employed to capture and analyze strain distributions within the concrete and timber components at the mid-span of the TCC beam. These strain gauges were strategically positioned at the rear mid-centerline of the TCC beam to monitor and accurately measure strain variations in both materials. To capture and quantify the slip occurring at the bonding interface between concrete and the wood components precisely, a linear voltage displacement transducer (LVDT) sensor was employed. This LVDT sensor has a measurement range of ±1.5 mm and was configured to record data at a frequency of 10 Hz. For optimal positioning and accurate measurements, the LVDT sensor was glued to the rear surface of the TCC beam using a double-L-shaped angle. The placement of the LVDT sensors was meticulously set at a distance of 40 cm from the edge of the beam. Additionally, an LVDT sensor was employed to determine the midspan deflection of the beam. All strain gauges and LVDT sensors were integrated with the Dewetron device to enable data acquisition and recording, as illustrated in **Fig. 3-2**.

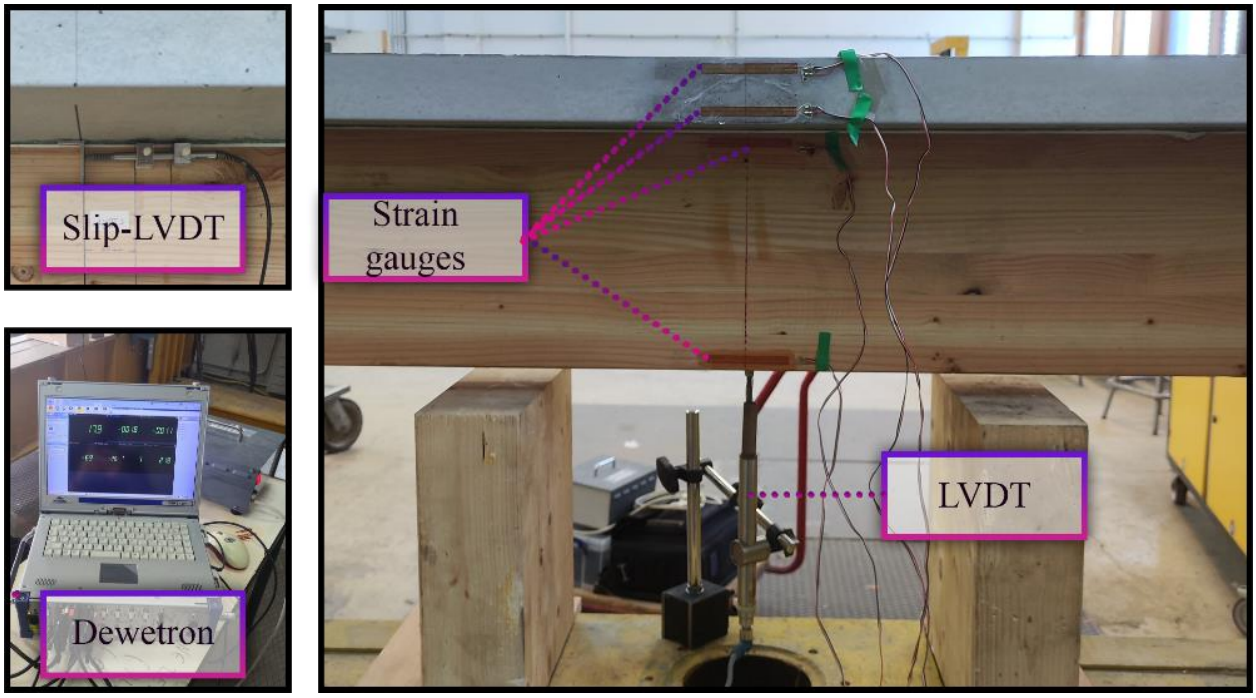

Fig. 3-2 Strain gauges and LVDT sensors arrangement

3.2.2 Digital image correlation

Fig. 3-3 illustrates the measuring device used for this purpose. To enhance the accuracy of measurements, a black-colored speckle pattern, characterized by a diameter size of 5.08 mm, was applied onto the surfaces of the specimens. This pattern was achieved using a specialized speckle kit, which ensured the uniform and controlled application of the speckle pattern. These surfaces are observed with two high-resolution cameras (5 Megapixels), and an optical 2D setup with a pixel size of 3.45 µm is used to record the images of the samples. In the DIC setup, the cameras were positioned at a distance of 3.6 meters from the surface of the TCC beams. Furthermore, the separation distance between the two cameras was maintained at 1.3 meters. These distances were chosen to ensure an adequate field of view and capture the entire surface of the specimens. Similar to push-out tests, additional lighting was employed to ensure high-quality captured images for the DIC analysis. Also, the Vic-3D software was used for displacement analysis and simulating the strain field development on the surface of the specimen. The subset size was set at 19, while the step size was configured at 6.

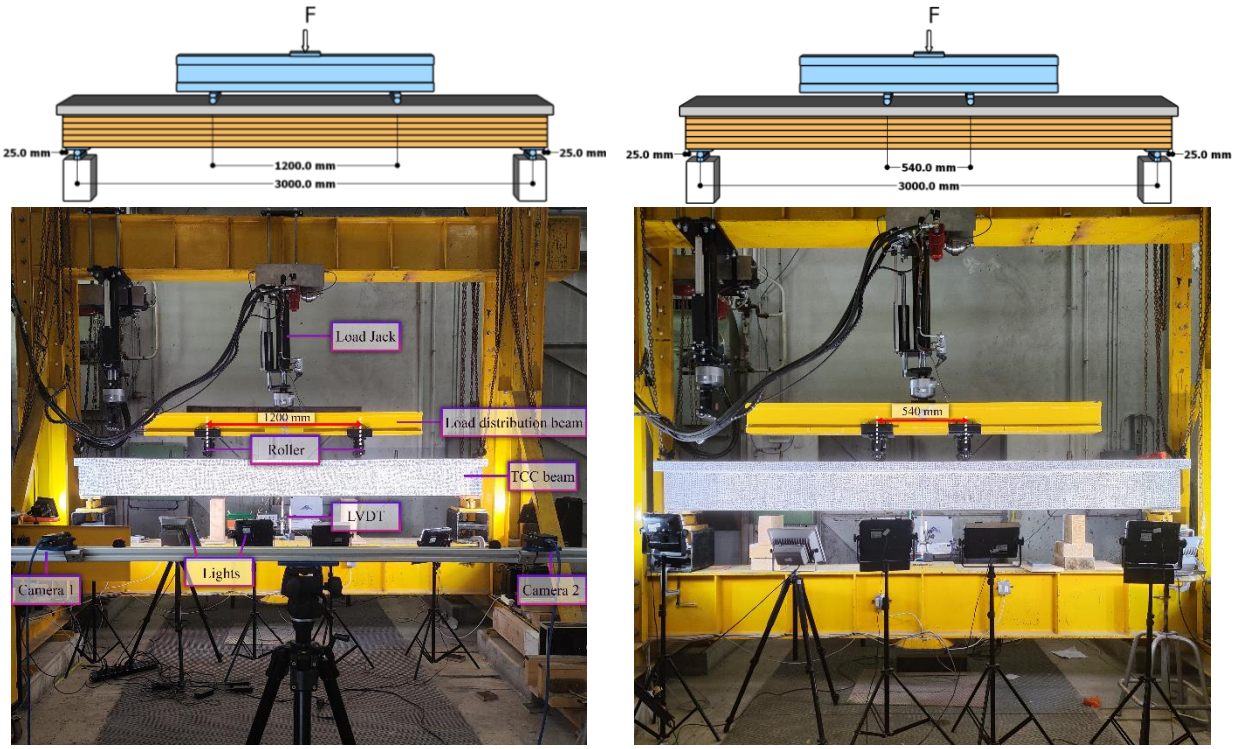

(a) (b)

Fig. 3-3 Test configuration and digital image correlation measuring device setup, (a) configuration 1, and (b) configuration 2

3.3 Materials

3.3.1 Adhesives

For the fabrication of timber-concrete composite (TCC) beams, careful consideration was given to selecting suitable adhesives to ensure optimal performance. In the wet TCC beam production, Sikadur®-53, a product manufactured by SIKA AG, was chosen. Conversely, the dry process involved the use of Sikadur®-330. Both adhesives are two-part epoxy-based and produced by Sika. These selections were driven by the results of the push-out tests conducted in the previous chapter and their compatibility with the intended application of bonding TCC. To provide insight into the adhesive properties, **Table 2-1** presents certain physical and mechanical characteristics sourced from the product data-sheet.

3.3.2 Timber

The timber elements were fabricated from GL24h glulam beams consisting of 6 laminations. These lamination beams were characterized by a cross-sectional dimension of 120 × 40 mm² and a reference length of 3.2 meters. Detailed information regarding the mechanical strength and stiffness of the timber elements can be found in **Table 3-2**, where hypothetical mean values were estimated from characteristic values.

Table 3-2 Mechanical strength and stiffness of used timber and concrete

Material	Property	Parameters	Value
Timber (GL24 h)	Mean value of modulus of elasticity	E [MPa]	11000[a]
	Mean value of shear modulus	G [MPa]	720[a]
	Mean bending strength	f_m [MPa]	31.50[b]
	Mean tensile strength	f_t [MPa]	21.32[b]
	Mean shear strength	f_v [MPa]	3.43[b]
Concrete (C45/55)	Mean value of modulus of elasticity	E_c [MPa]	36283[c]
	Mean value of shear modulus	G [MPa]	14513[c]
	Mean compressive strength	f_{cm} [MPa]	53[c]
	Mean tensile strength	f_{ctm} [MPa]	3.8[c]
	Mean surface's tensile strength	$f_{ctm,surf}$ [MPa]	2[d]

[a] According to EN 1194 [115]

[b] Calculated from characteristic values in EN 1194 [115], assuming a lognormal distribution with COV 15% [116]

[c] According to EN 1992-1:1:2004 [108]

[d] According to Frohnmüller et al. [75]

3.3.3 Concrete

In the dry process of timber-concrete composite (TCC) fabrication, an essential factor influencing the quality of the bond is the evenness of the concrete plate's surface intended for glueing. Any deviations such as unevenness, irregularities, or imperfections on the concrete surface can hinder the effective adhesion and bonding of the concrete to the timber. These divergences have the potential to create weak points within the composite structure, compromising its overall integrity. Contrary to the literature suggesting the sandblasting process for the bottom surfaces of the pre-fabricated concrete, in contact with the formwork, as a recommendation for adhesively bonded surfaces to eliminate oils, release agents, and potential surface weaknesses [75], this procedure was not carried out due to manufacturing restrictions prohibiting work beneath a concrete surface. Instead, the bottom surface of the pre-fabricated concrete was cleaned with compressed air, ensuring compliance with safety regulations, as workers were not positioned beneath the concrete slab. On the other hand, in the wet process, the mechanical behaviour of adhesive bonding can be affected by concrete compacting. This is due to the possibility of the adhesive being squeezed or displaced during the concrete compaction process. In contrast, the utilization of self-compacting concrete offers the advantage of facilitating improved surface specimen fabrication, simultaneously mitigating the mechanical impact of concrete compacting on the behaviour of the connection. For both fabricating processes, SCC

was considered to match the C45/55 strength class as outlined in EN 1992-1:1:2004 [108]. The concrete slabs integrated into the composite beams were precisely manufactured to have full-length and cross-section nominal dimensions of 0.4 x 0.06 x 3.2 m^3. A reinforcement mesh of ST25C was carefully incorporated into the concrete slabs not only to enhance their durability and prevent potential damage during transportation or handling but also to connect the concrete flange to the composite concrete-wood beam web. This reinforcement serves multiple purposes, including securing the composite beam web and reinforcing the lateral concrete surfaces between the flange and the center part of the concrete deck. **Table 3-2** provides an overview of the concrete material's mechanical strength and stiffness properties.

3.4 Test configuration

The specimens were tested in a four-point bending configuration, according to EN 408 [83]. It's worth mentioning that this standard is primarily oriented to determine the bending strength of glued laminated timber. Despite its primary orientation, many researchers have adopted this standard for testing TCC structures under four-point bending conditions, where the timber element is mainly subjected to bending stresses. However, this standard EN 408 [83] doesn't specifically define a loading procedure. Various researchers have employed different approaches within this framework. For instance, Negrão et al. [84] tested glued TCC beams according to EN 408 [83] using the time-load curve prescribed by EN 2689 [39]. Their objective was to maximize the stress on the timber-concrete interface at a similar level of push-out tests. Their load rate was 98.1 N/s, transitioning from force-controlled to displacement-controlled after reaching 70% of the estimated ultimate load. Similarly, Frohnmüller et al. [75] subjected TCC beams to four-point bending according to EN 408 [83]. In their quasi-static procedure, the specimens were subjected to loading at a constant velocity of 0.1 mm/s until reaching a peak load of 200 kN. The subsequent steps included a reduction in load to 50 kN, and then the load increased again. This loading cycle was iterated seven times before loading the TCC beams to their ultimate load-carrying capacity. Notably, some authors have used displacement control instead of load control. For example, Augeard et al. [82] employed a four-point bending test to study the mechanical behaviour and determine the moment-curvature curve of hybrid beams. A hydraulic jack with a capacity of 500 kN was utilized, with the test being controlled in displacement at a fixed speed of 4 mm/min.

In line with these considerations, this study deliberately chose to stress the timber-concrete interface to the greatest level possible, similar to the TCC push-out test in the previous study [103]. The loading process was conducted statically, with a gradual and continuous increase in load until failure was reached. For this purpose, a hydraulic jack with a capacity of 200 kN was employed. The loading speed was maintained at a rate of 10 kN/min, consistent with the loading speed used in the push-out tests. The experimental setup involved conducting four-point static bending tests on simply supported TCC beams. All test beams shared

a total length of 3200 mm and a clear span of 2850 mm. The chosen length of the TCC beam was also influenced by the capabilities of the current loading machine available in our lab. The dimensions of the cross-section of TCC beams were carefully selected to ensure that the neutral axis is positioned in the timber element close to the bonding interface and complies with the testing machine's maximum load capacity. These dimensions were submitted for verification to ensure compliance with ultimate limit states (ULS) and serviceability limit states (SLS).

Furthermore, considerations were made to account for transverse compression at the support. The computation of transverse compression stresses was anticipated to reach a maximum value of 3.2 MPa. This value accounts for almost 80% of the mean strength of transverse compression for the timber used in our study. Additionally, lateral bulking was thoroughly assessed. According to ASTM D3737, lateral supports are necessary to prevent lateral-torsional buckling if the depth-to-width ratio exceeds 3. In this study, the depth-to-width ratio is 2.5, and the beams' cross-section was found to be capable of resisting lateral bulking, as the critical bending moment required to induce lateral bulking was determined to be 2781 kN·m. Two different configurations were employed to vary the bending moment distribution between the two loading points. The first configuration featured a length of 1200 mm between the loading points, while the second configuration exhibited a length of 540 mm, as shown in **Fig. 3-3**. After testing two of each wet and dry TCC beam under test configuration 1, the decision was made to reduce the distances between the loading points (configuration 2). This adjustment aimed to increase the concentration of the bending moment at the mid-span of the TCC beams, aiming for a failure mode governed by pure bending and tension failure, and to eliminate the observed tilting behaviour in the first configuration. It is worth mentioning that the distances between the loading points in both configurations were within the maximum allowable margin for adjustment of the loading machine. Specifically, the first configuration used the maximum allowable distances between the loading points, while the second configuration used the minimum allowable distances.

3.5 Experimental results and discussion

3.5.1 Load and mid-span deflection response

Fig. 3-4 illustrates the load-to-mid-span deflection curves for all tested specimens, providing insights into how the applied load relates to the deflection at the mid-span of each composite beam. Additionally, **Fig. 3-5** presents the bending moment vs. curvature curves at the mid-span cross-section of the tested beams, offering insights into the local flexural behaviour. Comparing both global and local bending behaviour observed in **Fig. 3-4** and **Fig. 3-5**, respectively, it becomes evident that the volume does not impact the bending performance of TCC beams. On the other, **Fig. 3-6** presents the load response deflection

along the tested TCC beams, offering a comprehensive view of the load-deflection behaviour of the entire set of beams. It is worth mentioning that the fully composite lines in **Fig. 3-4** refer to the anticipated analytical load-deflection behaviour assuming full composite action ($\gamma = 1$). Conversely, the non-composite lines are calculated assuming the absence of composite action ($\gamma = 0$), as detailed in **Chapter 4**

Fig. 3-4a and **b** show that both wet and dry fabricated TCC beams exhibited nearly identical load-to-mid-span deflection responses up to a certain point. Before the occurrence of bonding failure at the interface in the dry beams (section 3.5.2), both wet and dry TCC beams displayed similar load-to-mid-span deflection responses, indicating consistent behaviour and alignment with the fully composite behaviour under the applied loads. However, after the failure occurred in the dry beams, their load-to-deflection response deviated from the fully composite behaviour still observed in the wet beams. The compromised shared contribution mechanism in the dry beams disturbed the composite action, changing their structural response under the applied loads.

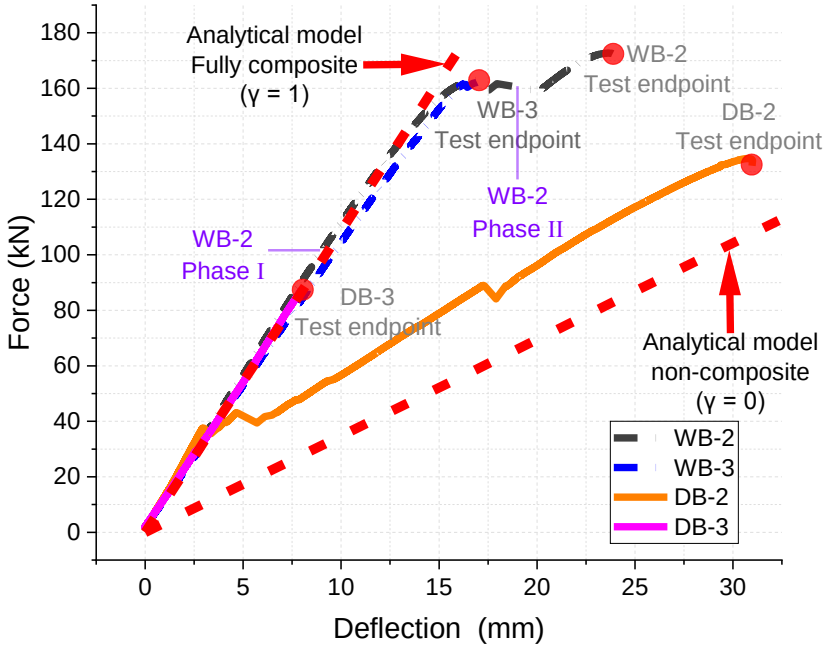

(a)

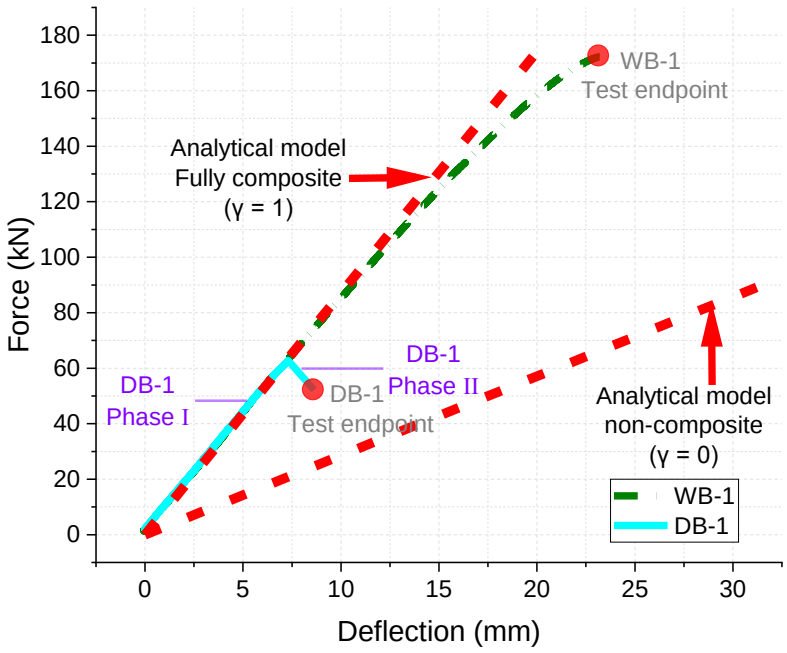

(b)

Fig. 3-4 Load and mid-span deflection response curves of tested beams, (a) configuration 1, and (b) configuration 2.

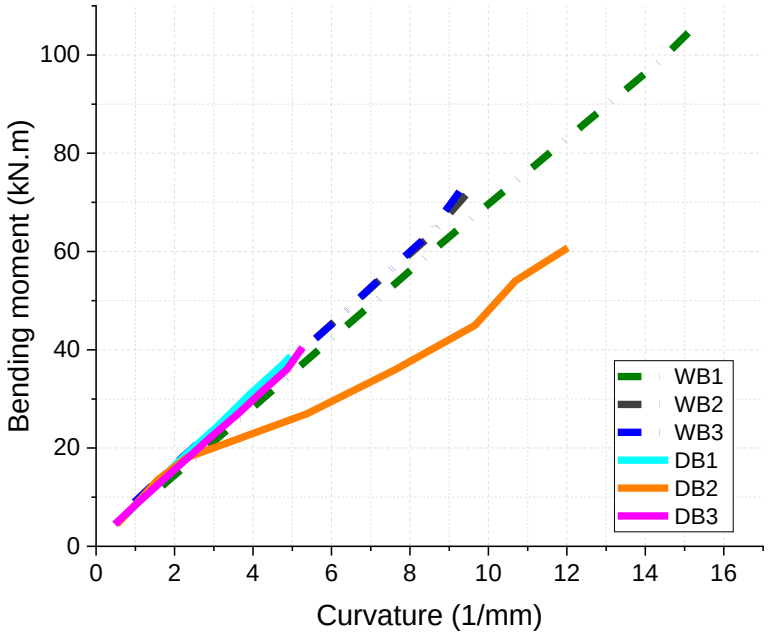

Fig. 3-5 Bending moment vs. curvature curves at the mid-span cross-section of tested beams.

The load-to-mid-span deflection response can be divided into two distinct phases. The first phase of the load-to-mid-span deflection response reflects the beam's capacity to undergo elastic deformation. During this phase, there is a continuous increase in the applied load until it reaches the approximate elastic peak

value, known as the first peak. Simultaneously, there is a proportional increase in the deflection at the mid-span of the composite beam, as depicted in **Fig. 3-4**.

The second phase represents a sudden drop in the applied load and an increase in the mid-span deflection, and this behaviour is particularly noticeable in case DB-1. However, in some cases of wet-fabricated beams (e.g., WB-2), in the second phase, the deflection response exhibits a non-synchronous increase, indicating a nonlinear behaviour of the composite beam. This response was followed by a subsequent rebound effect, ultimately leading to the load reaching its maximum value, as shown in **Fig. 3-4**. The increase in non-synchronous displacement suggests that different parts of the beam experience varying levels of deformation and may respond differently to the applied load. This phase is often associated with the beginning of yielding or localized damage within the beam. The transverse compressive stress vs. strain curves at the support extracted from DIC analysis indicate that both edges of the beam underwent non-elastic behaviour when the stress level exceeded approximately 3 MPa, as illustrated in **Fig. 3-7**. These deviations from the linear elastic behaviour suggest that the beams exhibited some degree of plastic deformation. The observed response at the right edge is slightly different from that at the left edge. This discrepancy could be attributed to differences in the level of settlement at the support. For instance, at a load level of 163.7 kN, the right edge experienced a total settlement of 4.6 mm compared to 2.5 mm at the left edge, as shown in **Fig. 3-6**. It is worth mentioning that the inclusion of wood confinement above the support, secured with screws, could have strengthened the beams and potentially limited the settlement. The wood confinement would have likely prevented or minimized the wood crushing that was not anticipated due to it's supposed strength.

Fig. 3-6 illustrates a noticeable trend in these wet series of TCC beams. The increase in deflection along the beams is observed to be consistently proportional to the increase in the applied load level up to the point of reaching the ultimate load-carrying capacity of the beam. Once the beams approach their ultimate load-carrying capacity, a significant change in the beam's behaviour occurs. At this point, the deflection rate along the beam significantly escalated, indicating a rapid increase in deformations and displacements within the beam.

On the other hand, noteworthy behaviour was observed in the case of dry fabricated TCC beams, particularly in specimen DB-1, as shown in **Fig. 3-4b**. This behaviour is characterized by a sudden drop in the applied load and a simultaneous increase in the mid-span deflection. The sudden drop in the applied load suggests that the beam may have reached a critical load level. This drove an evident adhesion failure at the interface between the timber and concrete components, as described in section 3.5.2. This adhesion failure at the interface is a significant factor contributing to the sudden drop in the applied load and the increase in deflection. In the case of DB-2, a significant change in the beam's behaviour was observed after

the bonding failure occurred at a load level of 37 kN, as shown in **Fig. 3-4a**. This bonding failure led to a deviation from the fully composite response, and the beam's behaviour started aligning with the fully-non composite response. Furthermore, the deflection along the DB-2 beam after the failure exhibited a notable difference compared to the pre-failure behaviour, as evident from **Fig. 3-6**. The deflection after the failure showed a rapidly increased growth rate, indicating the effect of the compromised composite action on the observed behaviour of TCC beams.

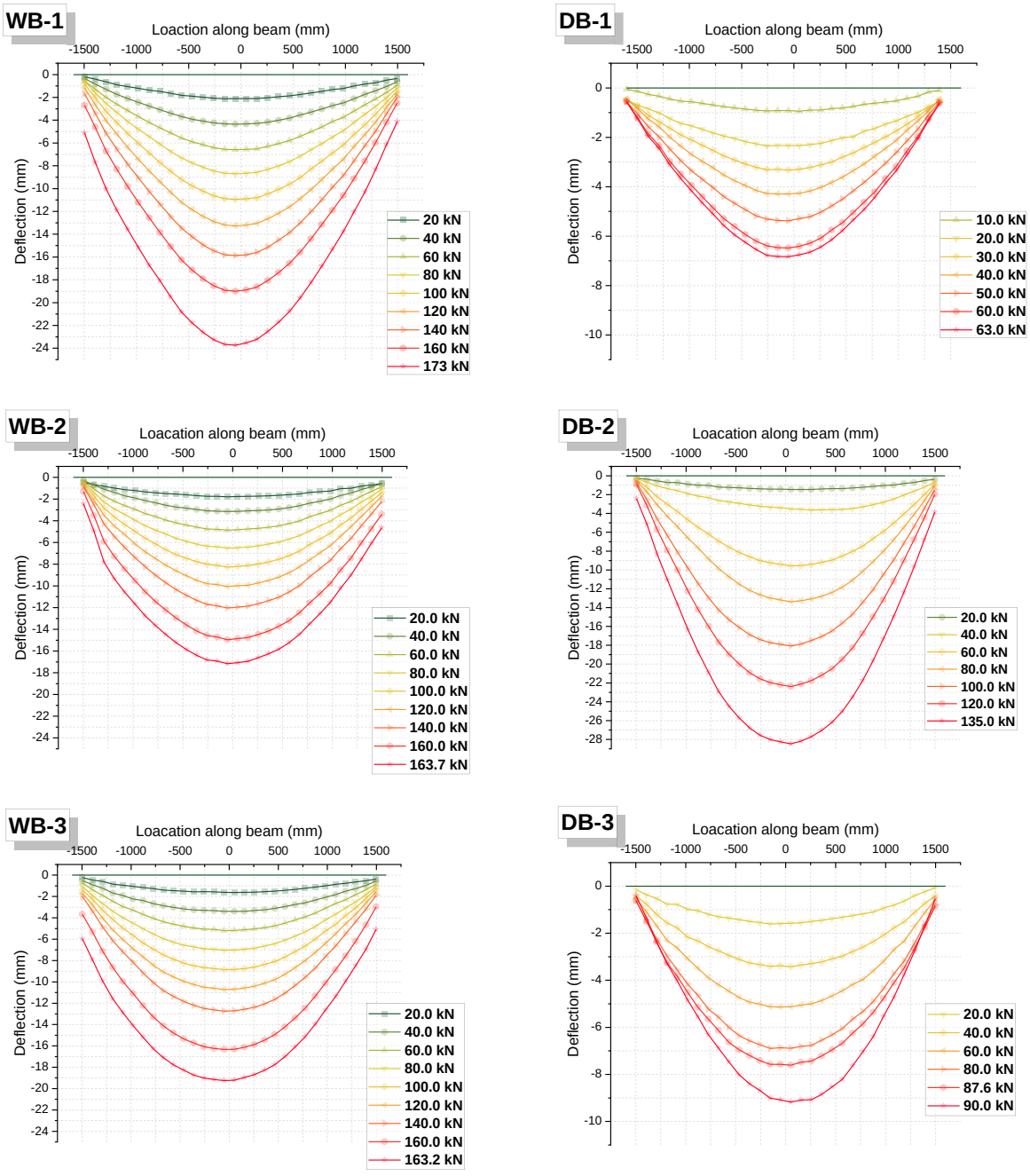

Fig. 3-6 Load response deflection along tested TCC beams

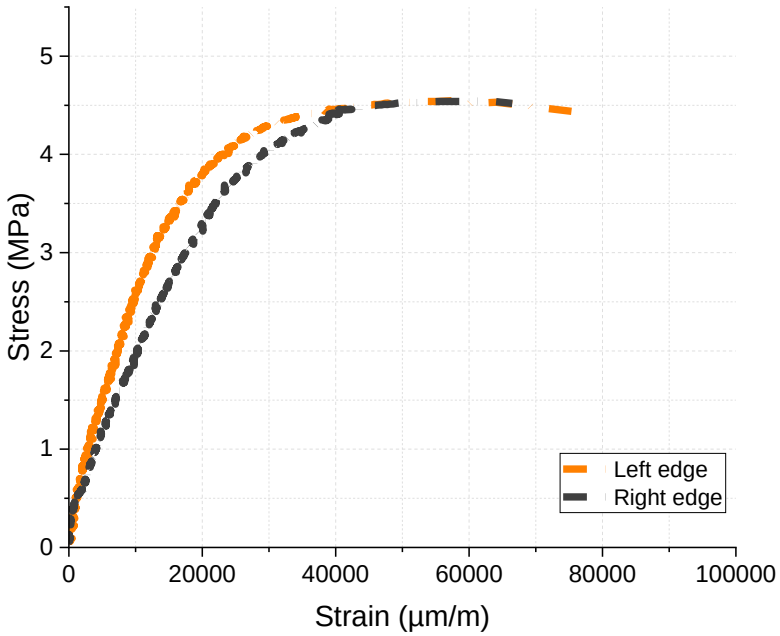

Fig. 3-7 Transverse compressive stress vs. strain curves at the support extracted from DIC analysis of beam WB-2.

3.5.2 Failure characteristics

The fabrication method impacts the failure behaviour and characteristics, specifically whether the composite beams were wet-fabricated or dry-fabricated. Based on their damage characteristics, composite beams' failure modes can be classified into two groups: the wet-fabricated group and the dry-fabricated group.

3.5.2.1 Dry TCC beams

All tested dry-fabricated beams showed identical failure modes. **Fig. 3-8** shows the connection damage at the interface. A complete separation between the composite beam's concrete slab and glue layer is apparent. The failure occurred mainly due to adhesion failure at the interface. One possible explanation for this failure mode is the imperfect connection between the pre-fabricated concrete slabs and timber elements. The quality or effectiveness of the connection between these two components may have been compromised during the dry fabrication process. This imperfect connection resulted in a significant drop in the ultimate load-carrying capacity of the composite beams compared to both the wet-fabricated beams and the expected ultimate load-carrying capacity predicted by the analytical model using the γ-method developed for evaluating the behaviour of timber-concrete composite beams as per Eurocode 5.

After the test, further investigations involved studying fracture surfaces, delamination patterns, interface failure, or any other visible damage characteristics captured by the high-resolution camera to better

understand the observed failure modes. One notable finding from these investigations is that the concrete slab was partially or entirely separated from the glued interface along the beam. This delamination or separation between the concrete slab and the glued interface indicates an adhesion failure mechanism in the composite beams. The separation between the concrete slab and the glued interface can be attributed to various factors, such as inadequate adhesive bonding, improper surface preparation, or other fabrication-related issues. These factors may have compromised the bond strength and integrity between the concrete and the glued interface, resulting in the observed delamination. In this context, it is worth mentioning that some connection defects were noticed at the early age of dry specimens, particularly more intensely at the edges of the composite beam. These defects indicate potential issues or weaknesses in the connections between beam components, which may have occurred during the fabrication or drying. This phenomenon was also observed by Arendt et al. [117]. The observation that the defects are more dominant at the edges of the beam indicates that there may be challenges in achieving consistent and uniform connections throughout the entire beam length during fabrication. The effects of shrinking and difficulties in attaining proper pressure distribution at the edges can indeed play a role in forming these defects. Shrinkage, both drying shrinkage and autogenous shrinkage, can exert forces on the components, potentially causing separation or weakening of the bond between the concrete surface and the adhesive layer. The consequence would be that glueing should occur after the concrete has fully developed its strength or is fully cured to minimize the impact of shrinkage on the bonding quality. Moreover, the presence of oil residuals on the bottom surface of the concrete slab results from the concrete fabrication process. While some precautionary measures were taken, including cleaning and air blowing to mitigate their effects, this issue remains an important consideration. Oil residuals can act as a barrier, inhibiting proper bonding between the concrete surface and the adhesive layer. This weakens the adhesive bonding and can contribute to the observed connection defects and failure mode.

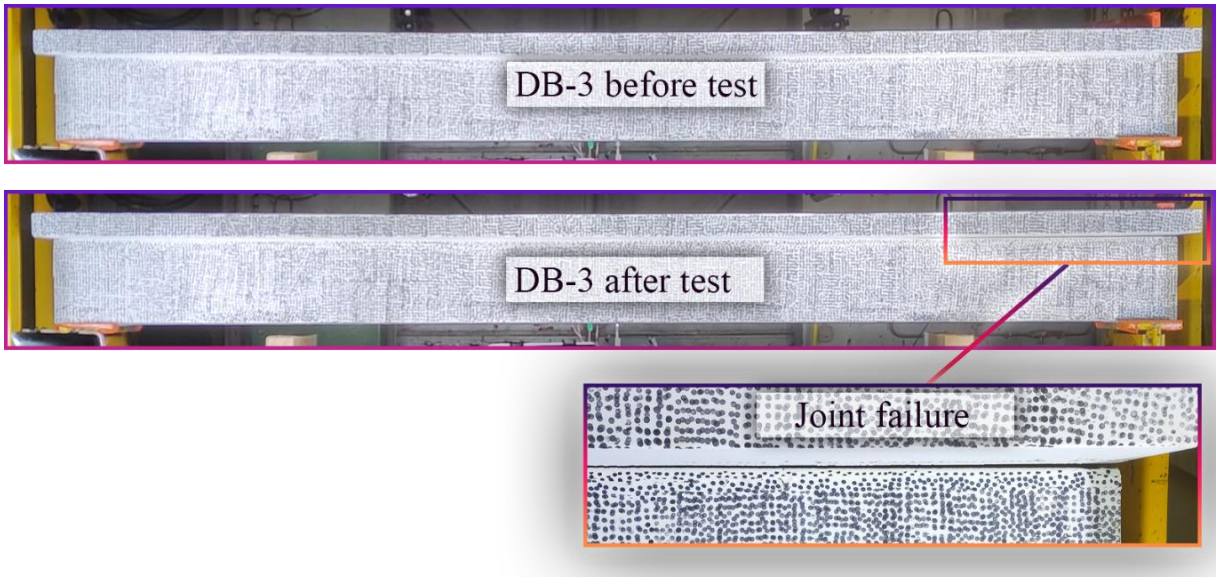

Fig. 3-8 Adhesion failure in dry TCC beams

3.5.2.2 Wet TCC beams

The significant observation of minor bottom cracks near the mid-span and horizontal cracks on the timber element in wet-fabricated beams indicates potential failure modes. Bottom cracks around knots near the mid-span suggest localized tensile and bending stresses that may exceed the capacity of the timber component, which aligns with the findings from Frohnmüller et al. [75] and Negrão et al. [84] observations for dry-fabricated beams, where the ultimate load-carrying capacity was governed by bending and tension failure in the timber, and contrasts the predominant shear failure at the interface in the case of wet-fabricated beams. This failure mode is depicted in **Fig. 3-9**, revealing areas where the timber has failed. Horizontal cracks on the timber signify shear failure, which is particularly influential between the support and loading point. Fracture sounds around 90% of the full load indicate considerable stress, potentially nearing the timber's failure point. Additionally, as the load approached the full load level, the beam exhibited tilting towards the front side. The tilting behaviour as the load approached full load level can be attributed to initial geometrical imperfections, amplified by the initiation of crushing and plasticization of timber in compression perpendicular to the grain above the contact area with the support. Notably, no cracks in the concrete component were observed, contrary to the signs of compression failure in concrete, as demonstrated by Frohnmüller et al. [75].

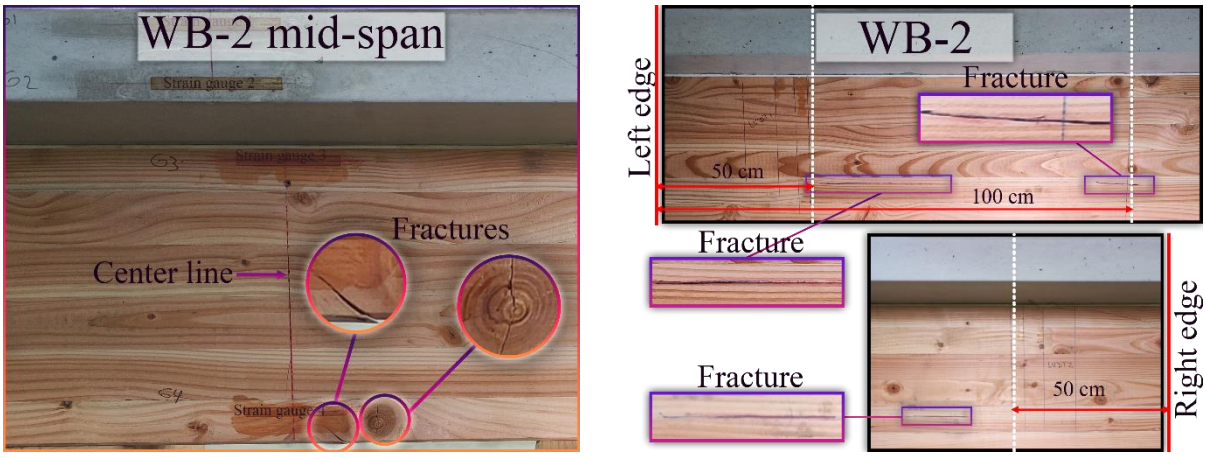

(a) (b)

Fig. 3-9 Failure mechanism in wet TCC beams, e.g., WB-2 at (a) mid-span and (b) beam edges

3.5.3 Interface slip

Interface slip between a concrete slab and timber is a crucial phenomenon that influences the structural behaviour and performance of composite beams. As external loads are applied to the beam, relative movement occurs between the concrete slab and the timber, leading to interface slip. In this study, slip measurements for the interface between the concrete slab and timber at a distance of 40 cm from both edges of the TCC beam were obtained from LVDT sensors for wet and dry fabricated beams. **Fig. 3-10** illustrates the slip at the interface for all tested beams in the study.

The investigation uncovered semi-symmetrical slip patterns on both sides of TCC beams, which remained consistent in most cases until the point of failure. The slip behaviour exhibited distinctive characteristics when comparing wet and dry TCC beams. It might be evident from the curves depicted in **Fig. 3-10** that the slip curves demonstrate a noticeable trend in the case of wet TCC beams. After the applied load is released at the end of the test, the slip curves return close to their original points. This phenomenon suggests the robustness and resilience of the adhesive bonding in wet TCC beams and the absence of significant interface failure during the testing process.

On the other hand, the behaviour of dry TCC beams differs significantly. In this case, all beams exhibited a pronounced increase in slip values as the test approached its end. This distinct change in slip behaviour strongly indicates an interface failure in dry TCC beams at varying load levels.

Reducing the distance between the points of loading, e.g., 540 mm, as demonstrated in the case of WB-1, led to higher values of interface slip at the same load level compared to the corresponding TCC beams, e.g., WB-2 and WB-3. The wet beam (WB-1) exhibited an average interface slip of 0.16 mm at a load level of 160 kN. In contrast, the other test configuration with an expanded distance between the loading points

(e.g., 120 cm) resulted in a slightly lower interface slip of an average value of 0.12 mm and 0.13 mm in the case of WB-2 and WB3, respectively. Similar conclusions can be drawn for dry beams, highlighting the consistency of the observed slip behaviour. The key reason behind this behaviour can be attributed to the shear stress distribution along the beam. With a reduced distance between the loading points, the shear stress affects a more extended beam section, leading to higher relative displacements between the timber and concrete components.

The case of DB-2 indicates a notable change in beam behaviour after the occurrence of an interface failure. This change can be attributed to the separation of the connection between the timber and concrete components, disrupting the shared contribution mechanism at the interface. As a consequence of this imperfect connection, several factors come into play. Localized deformations may occur at the point of failure, leading to localized stress concentrations and potential weaknesses in the beam's structure. The compromised shared contribution mechanism also escalates the slip between the concrete slab and timber.

In **Fig. 3-11a**, it might be apparent that there is no variation in flexural longitudinal strains between the points of loading, as found by DIC post-process. This suggests a consistent pattern of constant bending moments in this region. The zero shear stress (green zone in **Fig. 3-11b**) at the mid-span of the TCC beam further supports the fact that no relative movement or deformation is occurring between the concrete slab and timber in this region.

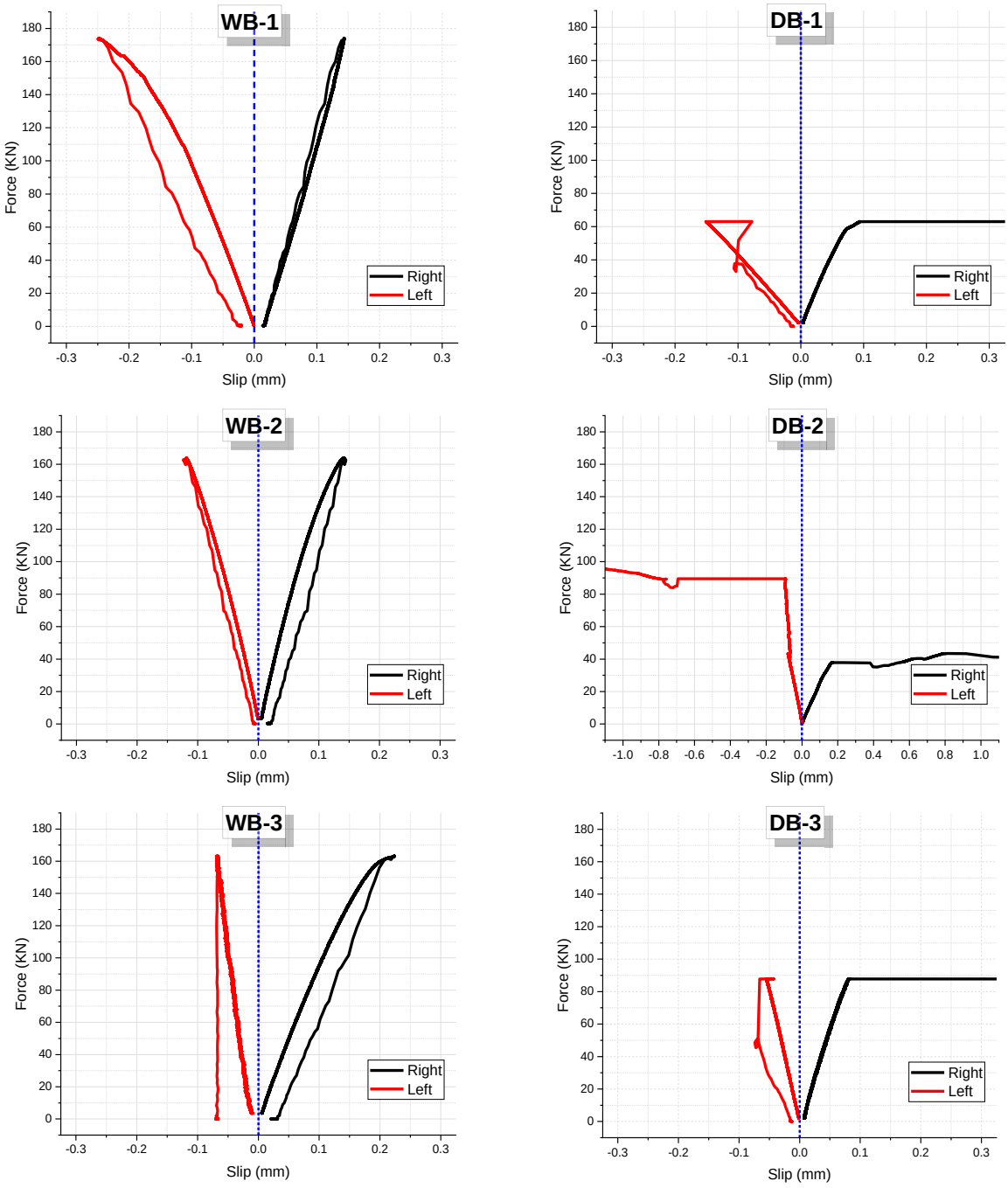

Fig. 3-10 Interface slip in shear zone

3.5.4 Strain distribution

The pure bending segment, isolated from other external loads, enables a thorough examination of the beam's behaviour under bending stresses alone. In order to allow for this investigation, strain gauges were strategically placed along the depth of the composite beams at the mid-span to measure the strains induced by the applied load. Furthermore, analytical models were utilized to predict the strain distribution at the

pure bending segment of timber-concrete composite (TCC) beams. Additionally, DIC was employed to measure the bending strain at beam segments where the shear stress is acting, e.g., ± 1000 mm from the center line, see **Fig. 3-11**, which illustrates an example of the bending strain and shear strain distribution extracted by DIC post analysis. It is worth mentioning that while the bending strain is increasing and reaching its maximum value at the bottom of the mid-span cross-section of the TCC beam, the shear strain further increases. However, the shear strain reaches its maximum at the position of the flexural neutral axis value along the shear span between the loading point and the support. The increase in downward shear strain at the supports could be attributed to the concentrated loadings, causing higher shear stress at these points.

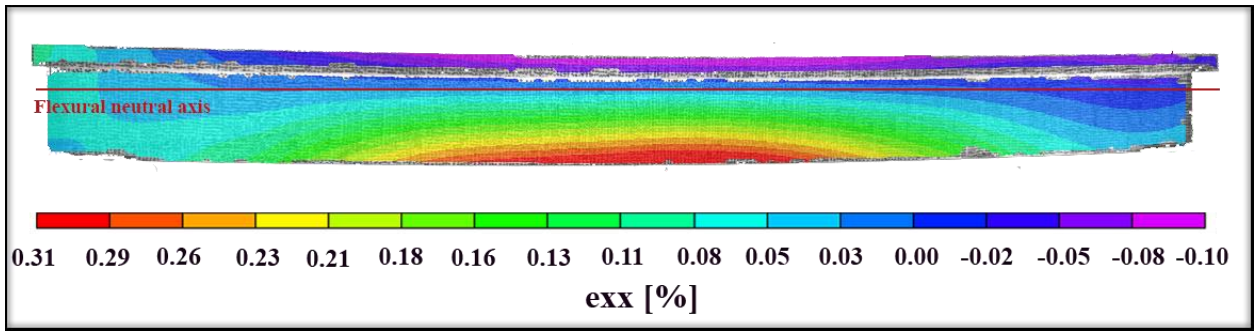

(a)

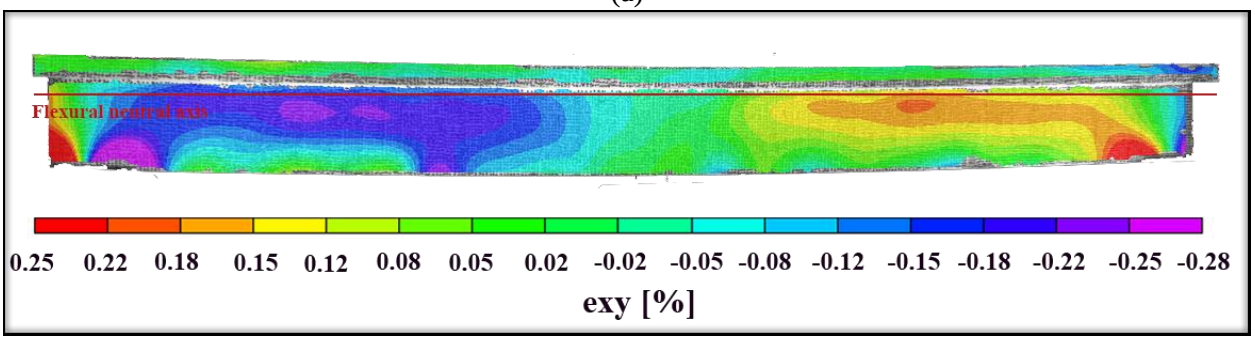

(b)

Fig. 3-11 Strain distribution on the surface of WB-1 extracted from DIC post-process at a load level of 173 kN, (a) bending strain, and (b) shear strain

Fig. 3-12 shows the bending strain distribution at the mid-span cross-sections of the composite beams. The continuous lines on the graph represent the actual bending strain measured experimentally, while the dashed lines represent the predicted bending strain obtained from the analytical model. Additionally, the dashed horizontal red lines represent the theoretical neutral axis location within the cross-section. From the analysis, it is evident that the actual neutral axis is located inside the timber components (very close to the timber/concrete interface) in all cases of the composite beams, as depicted in **Fig. 3-12**. This alignment closely matches the position of the theoretical neutral axis, indicating an effective load distribution between the timber and concrete components and reinforcing the effectiveness of the timber-concrete composite

beams design. This configuration is desirable as it efficiently utilizes each material's strength and properties, resulting in a well-balanced load distribution and optimal performance of the composite beams. Thus, the timber is primarily responsible for the tensile bending stresses, while the concrete component takes up the compressive bending stresses.

WB-1 and DB-1, which have a smaller distance between the load points, experienced higher bending stress at the same load level than their corresponding beams in the other load configuration, e.g., WB-1, WB2, and WB3 exhibited bending strain at a load level of 160 kN of 2915.67, 1900.17, and 1867.04 μm/m, respectively. The closer distance of the load points in WB-1 and DB-1 concentrates the bending stress over a shorter span of the beams, leading to higher stress levels at the mid-span cross-section. In contrast, at the same level of applied load, the other load configuration with a larger distance between load points distributes the bending stress over a wider span, resulting in lower bending stress values at the mid-span.

As mentioned in section 3.5.2, DB-2 exhibited a significant change in beam behaviour after reaching a load of 37 kN, coinciding with bonding failure at the interface. In **Fig. 3-12**, it is evident that the bending stress distributions deviated from the predictions of the analytical model after the bonding failure occurred. The deviation indicates a change in the load-carrying mechanism and the effectiveness of the composite action. Upon analyzing the behaviour of the composite beam, it was observed that the neutral axis in the timber shifted to the mid-section of the timber. This means half of the timber is subjected to compression stress while the second half is under bending stress. Before the bonding failure, the beam exhibited a consistent load-deflection response behaviour in line with the theoretical limit of a fully composite response. However, after the bonding failure took place, the beam's behaviour deviated from the fully composite response and started aligning more closely with the theoretical limit (lower limit) of a fully-non composite action, as shown in **Fig. 3-4a**.

By comparing the bending stress distribution at the pure bending section of the composite beams, as shown in **Fig. 3-12**, with the bending stress at a distance of ±1000 mm from the center line, as shown in **Fig. 3-13** and **Fig. 3-14**, a notable observation arises regarding the behaviour of the wet fabricated TCC beams. The results indicate that the wet fabricated TCC beams exhibit a consistent neutral axis location within the cross-section along the beam's span. This consistency suggests a rigid and full-bonded connection between the components. However, when the composite beams were close to reaching their ultimate load-carrying capacity, certain beams exhibited variations in the location of the neutral axis, particularly on one side of the beam, e.g., WB-1 and WB-3 showed a disruption in the position of the neutral axis on the right section of the beams at load level exceeding of 140 kN, as shown in **Fig. 3-13**. This observation suggests that the connection's performance between the timber and concrete may have been compromised, likely due to the high level of shear stress experienced by the beam at this location.

In contrast to the wet-fabricated TCC beams, the dry-fabricated TCC beams exhibited less consistency in their neutral axis location along the beam. The neutral axis location within the right and left sections in the dry beams showed more significant variability compared to their mid-span cross-section, especially when approaching their ultimate load-carrying capacity. The presence of bonding defects at the interface in some dry beams, as discussed in section 3.5.2, could be a contributing factor to this variability in the neutral axis location along the beam. **Fig. 3-14** shows a notable example in the case of DB-1, where the neutral axis position at distances of -1000 mm from the center line shifted towards the concrete components when the beam was close to reaching its ultimate load-carrying capacity. However, the right section (at distances of +1000 mm from the center line) of DB-1 exhibited a more consistent neutral axis location with the mid-span cross-section, suggesting a better-shared contribution mechanism in the right section. The observed inconsistency in the neutral axis location along the dry-fabricated TCC beams highlights the impact of bonding defects on the overall behaviour of the composite beams.

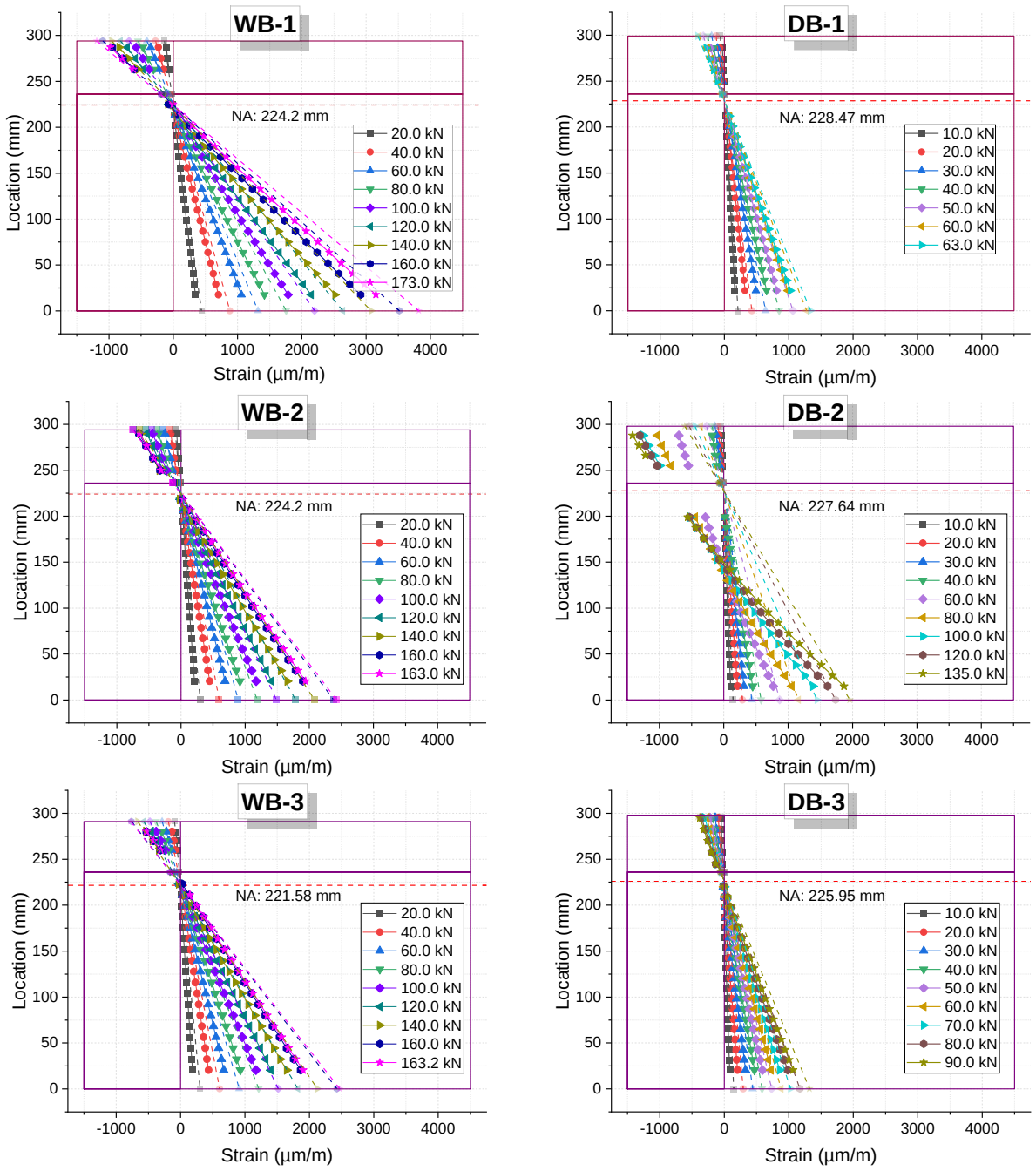

Fig. 3-12 Bending strain distribution of the composite beams at the mid-span cross-section

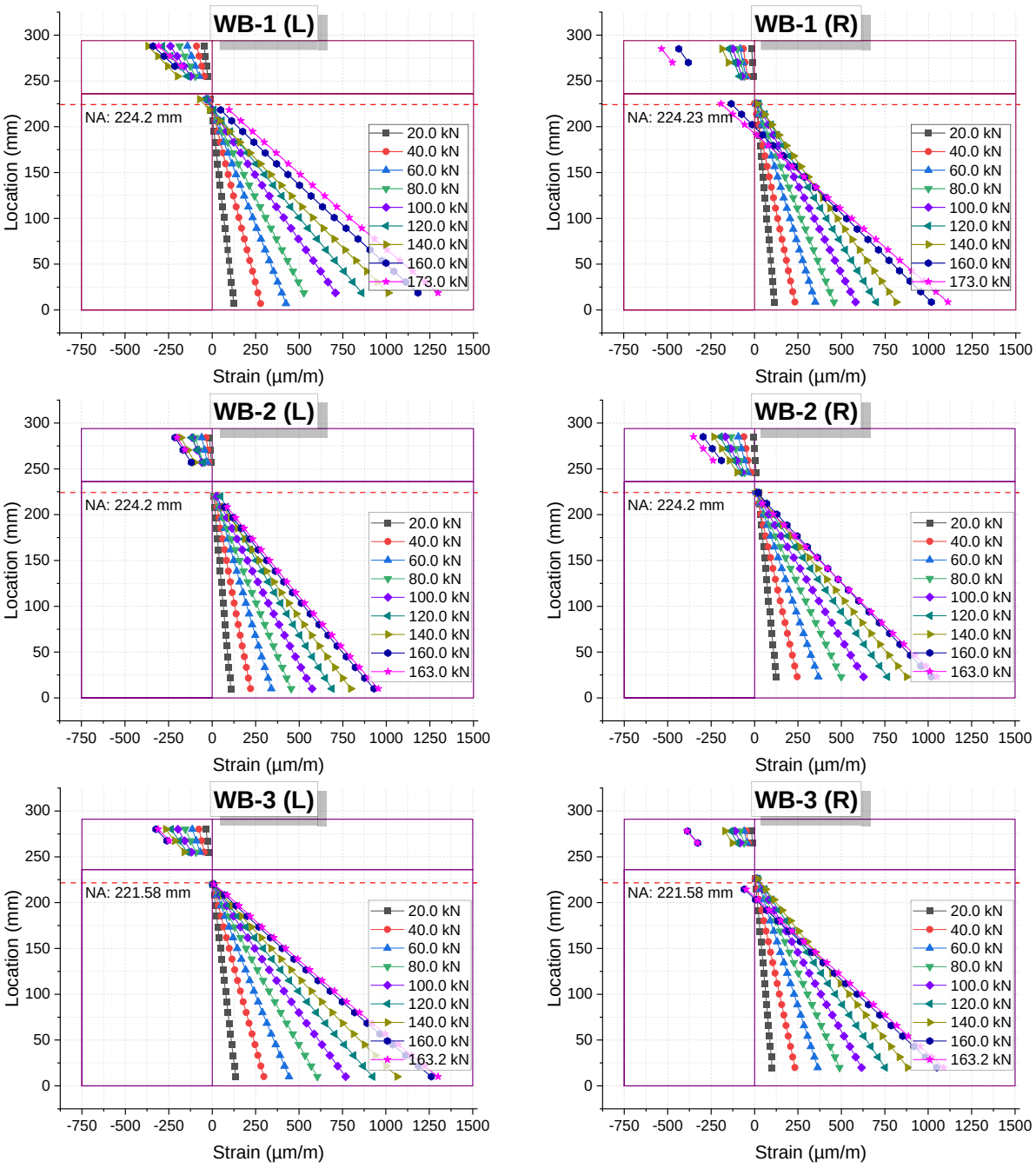

Fig. 3-13 Bending strain distribution of the wet composite beams at distances -1000 mm (L) and +1000 mm (R) from the center line

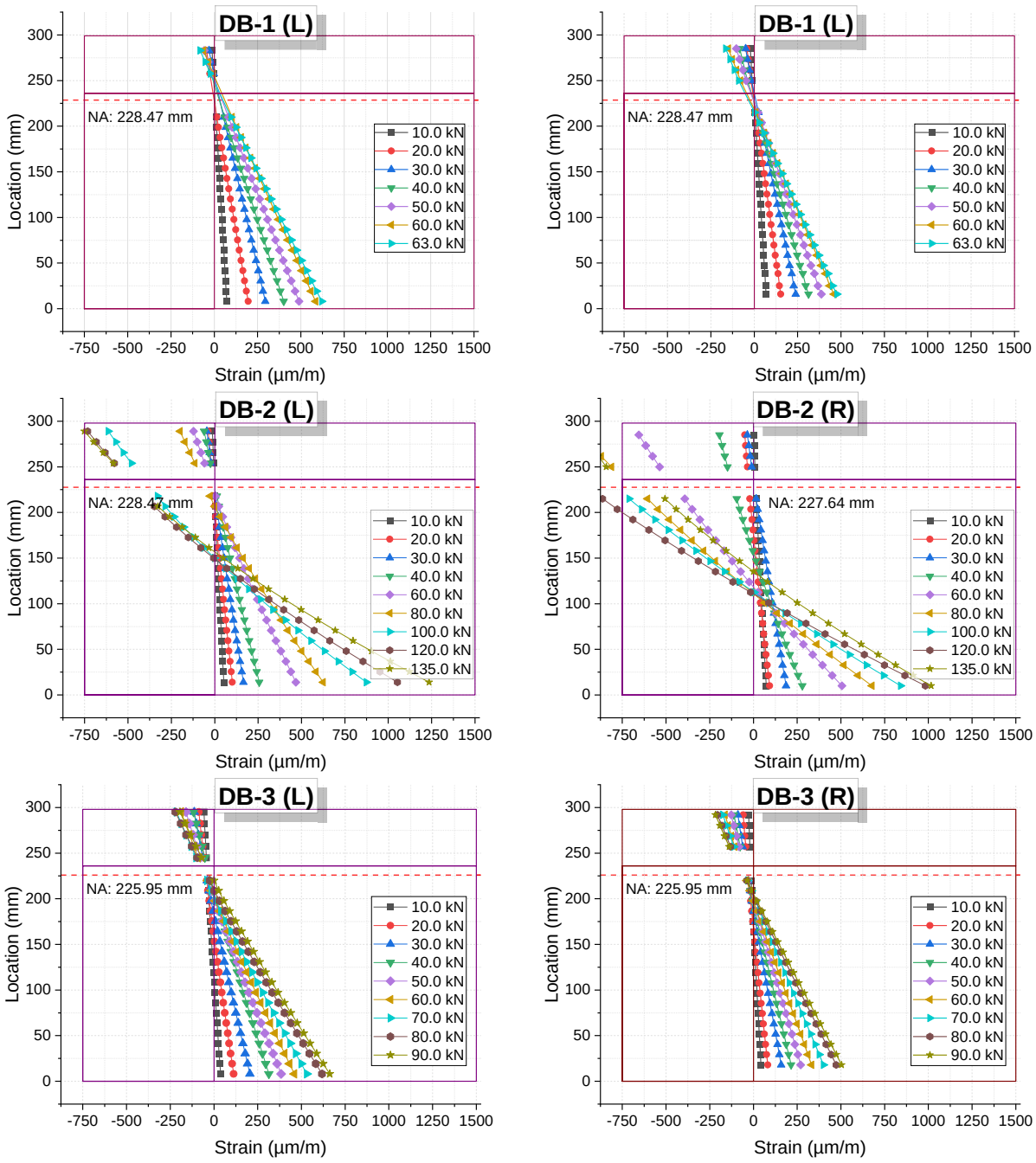

Fig. 3-14 Bending strain distribution of the dry composite beams at distances -1000 mm (L) and +1000 mm (R) from the center line

3.6 Summary

This chapter has presented the outcomes of an extensive experimental investigation on a 3.2 m span of adhesively bonded TCC beams. The comprehensive test outcomes provide valuable insights into the behaviour and performance of TCC structures, offering essential knowledge for further advancements in the field of TCC and adhesive bonding techniques. Based on the outcomes of this study, the following main conclusions can be drawn:

The findings underscore the importance of proper bonding techniques and material selection in TCC structures. The outcomes provide valuable evidence of the reliability and efficiency of glue connections in TCC beams, particularly in wet series. This highlights a stable and well-functioning composite action achieved through a full rigid connection between components.

The investigation into the failure characteristics of the TCC beams revealed a pronounced influence of the fabrication method on the resulting failure modes. The analysis identified two distinct groups of failure modes, each associated with the wet or dry fabrication method.

Dry-fabricated beams exhibited failure modes characterized by adhesion failure at the interface, attributed to imperfect connection during the dry fabrication process. This failure mode significantly reduced the ultimate load-carrying capacity of dry-fabricated TCC beams compared to wet-fabricated beams. Shrinkage-related forces and oil residuals on the concrete slab surface were identified as contributing factors to the observed connection defects and failure modes.

One notable recommendation arising from the previous finding is the importance of sandblasting treatment on the concrete surface before bonding. Sandblasting can serve as a valuable technique to remove oil residuals and create a roughened surface, promoting stronger adhesive bonding between the concrete slab and the timber component.

Wet-fabricated TCC beams exhibited favourable characteristics, including well-bonded connections, consistent neutral axis alignment, and efficient load distribution. Various failure modes interact at the point of their tested ultimate load-carrying capacity, including bending cracking and shear failure in the timber.

The strain distribution analysis confirmed the effectiveness of the composite action in wet-fabricated TCC beams. At the same time, the load-deflection response showed consistent behaviour up to the ultimate load-carrying capacity. However, in certain cases near ultimate load-carrying capacity, deviations in the neutral axis position indicated potential bonding challenges under high shear stress. In contrast, dry-fabricated beams exhibited deviations, especially near ultimate load-carrying capacity, implying

compromised load-shared contribution and highlighting the impact of bonding defects on overall structural behaviour.

The interface slip analysis revealed semi-symmetrical slip patterns on both sides of TCC beams, with notable differences between wet and dry beams. Wet TCC beams exhibited robust adhesive bonding, with slip curves returning close to their original positions after load release, indicating minimal interface failure. In contrast, dry TCC beams showed a pronounced increase in slip values, signifying interface failure at varying load levels.

Chapter 4
Analytical and FE Modeling

Chapter 4 Analytical and FE Modeling

The present chapter draws upon research previously published in a journal article *Experimental investigation on adhesively bonded timber-self-compacting concrete composite beams with a thin slab* [110], and *Finite element modeling of full-scale adhesively bonded timber-concrete composite beams* [118].

4.1 Introduction

Properly understanding and accurate prediction of the behaviour of TCC beams are essential to ensure their safe and efficient implementation in real-world applications. Analytical modeling provides valuable insights into the structural performance of composite beams. The γ-method in Eurocode 5 is a widely used approach for evaluating the behaviour of timber-concrete composite (TCC) beams. It offers a practical and efficient way to estimate essential parameters such as effective bending stiffness, maximum stresses, and deformation characteristics in TCC structures. This chapter investigates the realm of analytical modeling, shedding light on its role in predicting the behaviour of adhesive-bonded TCC beams.

While the analytical model offers valuable insights, it is limited by several factors. It simplifies the complex behaviour of TCC structures, particularly in capturing adhesive bonding behaviour, material heterogeneity, and local failure mechanisms. It may not fully represent the actual behaviour of experimental specimens due to its assumptions and idealizations. The analytical model does not account for certain factors, such as material nonlinearity, geometric irregularities, and boundary conditions, that are better addressed by numerical modeling. These limitations impose the use of Finite Element (FE) to provide a more accurate representation of the structural behaviour of TCC beams.

This chapter also employs FE modeling to comprehensively explore the adhesive bonding within TCC systems, thus enhancing the comprehension of outcomes drawn from the experimental investigations detailed in **Chapter 2** and **Chapter 3**. Within this chapter, a detailed methodology of the modeling methodology is provided, incorporating the theoretical framework, underlying assumptions, and data sources used for the research. The methods adopted for model calibration and validation are elaborated upon, ensuring the model's consistency in representing the precise behaviour of the experimental specimens.

4.2 Analytical modeling

4.2.1 Bending stiffness and maximum stress

In the initial stages of our analysis, we employed a straightforward analytical model to calculate bending deformations and stresses within the cross-section of the TCC beam. This approach relies on fundamental mechanical principles grounded in linear elasticity, considering the composite section's behaviour. The utilization of linear-elastic analysis is justified by the assumed rigid connection of timber and concrete facilitated by the adhesive bond at the interface.

As specified in Eurocode 5, the formulation for determining the effective bending stiffness, denoted as (EI)eff, is provided by Eq. (4.1). It is worth mentioning that this approach has been adopted by many studies in the analysis of TCC structures [7,75,119].

$$(EI)_{eff} = E_1 I_1 + \gamma E_1 A_1 a_1^2 + E_2 I_2 + E_2 A_2 a_2^2 \tag{4.1}$$

Fig. 4-1 illustrates all the geometrical dimensions of the TCC composite beams. In this context, Ei, Ii, and Ai represent the elastic modulus, the second moment of area, and the cross-sectional area of the individual components, concrete slab (1) and timber joist (2), respectively; γ signifies the reduction factor of shear connection; ai represents the distance between the neutral axis of the entire composite section and those of the individual components.

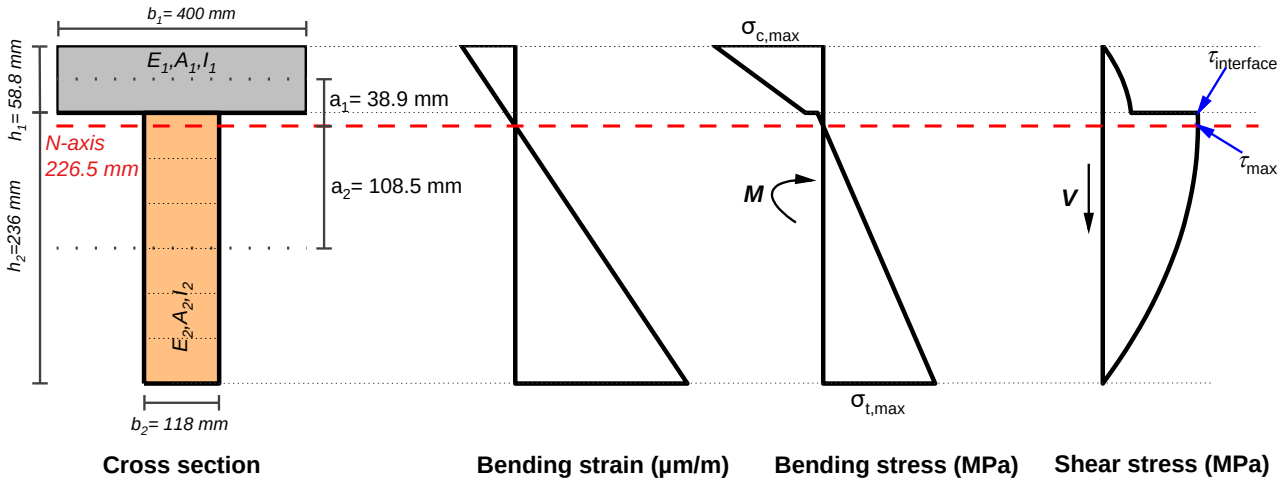

Fig. 4-1 Definition of geometrical dimensions and stress distribution within the cross-section of a TCC beam.

It is important to mention that the parameter γ holds important significance in composite action. When γ = 0, it indicates the absence of composite action, representing the lower limit where the two components, timber and concrete, act independently. On the other hand, when γ = 1, it signifies full composite action,

representing the upper limit where the timber and concrete work together as a fully integrated composite system, resulting in optimal composite behaviour, as shown in **Fig. 3-4**. In this study, γ is assumed to be equal to 1 since timber and concrete are rigidly coupled due to the adhesive bond. This assumption allows for the calculation of the effective bending stiffness in the adhesively bonded TCC beams.

Upon obtaining the value for the bending stiffness $(EI)_{eff}$ (e.g., 6.57 x 10^{12} N.mm^2), the bending stresses at various locations within the cross-section can be calculated under the assumption of elastic structural behaviour for the TCC beam. The equations for the maximum normal stresses on the top of the concrete ($\sigma_{c,t}$) and bottom of the timber ($\sigma_{t,b}$) components are expressed as follows,

$$\sigma_{c,t} = -\frac{a_1 E_1 M}{(EI)_{ef}} - \frac{h_1 E_1 M}{2(EI)_{ef}} \tag{4.2}$$

$$\sigma_{t,b} = +\frac{a_2 E_2 M}{(EI)_{ef}} + \frac{h_2 E_2 M}{2(EI)_{ef}} \tag{4.3}$$

The determination of the beam's maximum bending moment (M) involves a straightforward calculation: multiplying the shear span by half of the ultimate axial load ($F_u/2$) applied to the TCC beam. Additionally, the location (ordinate of the fiber) where the maximum shear stress occurs is characterized by a zero value of normal stress, and it can be calculated according to Eq (4.4).

$$\tau_{max} = \frac{V E_2 (0.5h_2 + a_2)^2}{2(EI)_{ef}} \tag{4.4}$$

Where: V represents the maximum shear force in the TCC beam

4.2.2 Failure criteria

Failure criteria play a crucial role in assessing the structural integrity of TCC beams. In the context of TCC beams, where timber and concrete interact through rigid coupling, distinct failure modes need to be considered due to the different mechanical behaviour of these materials. In this study, the chosen static system is a single-span beam, as shown in **Fig. 4-2**.

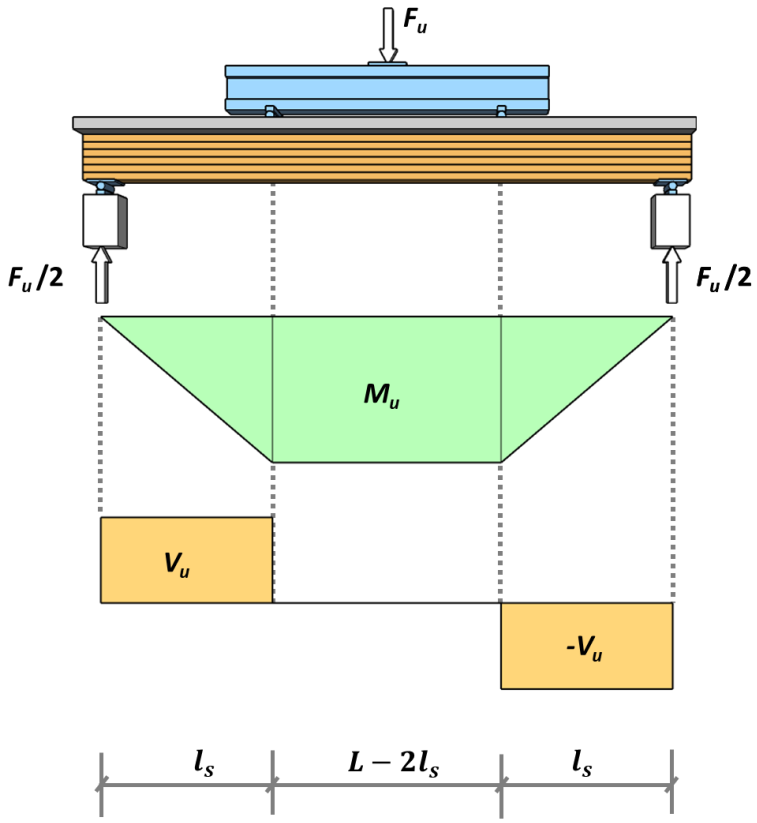

Fig. 4-2 Test setup 4-point bending

As a result of the composite action and the chosen static system, the concrete part of the TCC beam mainly experiences compression stresses. In contrast, the timber part undergoes bending and tension stresses. Linear-elastic stress-strain relationships are utilized to analyze and understand the stress distributions in the TCC beam. These stress distributions are shown in **Fig. 4-3**. The continuous lines on the graph represent the actual bending strain measured experimentally, while the dashed lines represent the predicted bending strain obtained from the analytical model. Additionally, the dashed horizontal red lines represent the theoretical neutral axis location within the cross-section.

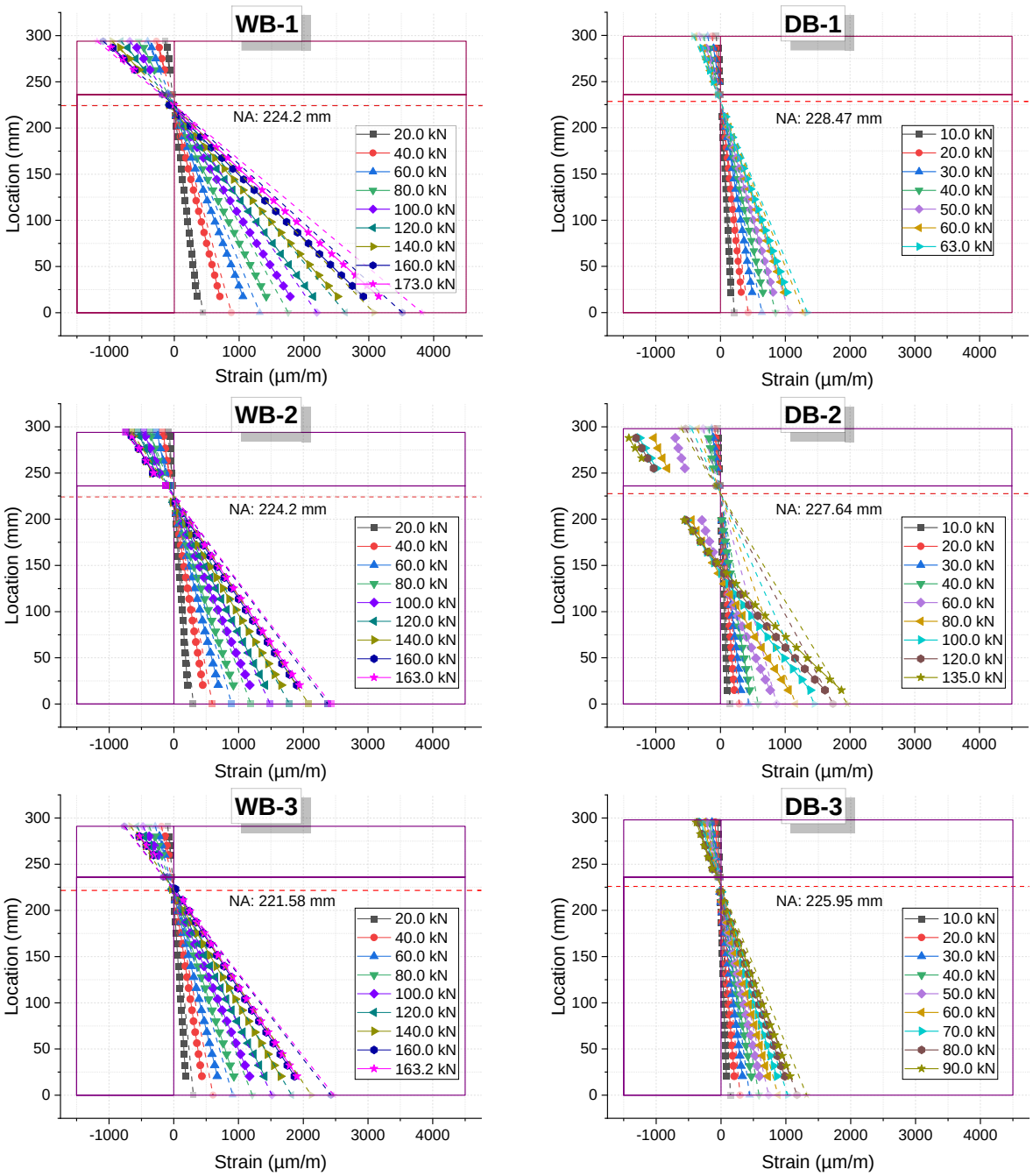

Fig. 4-3 Bending strain distribution of the composite beams at the mid-span cross-section.

By incorporating the failure criteria into the analytical model, it becomes possible to predict potential failure modes and assess the structural integrity of adhesive-bonded TCC beams under various loading conditions. It's worth mentioning that these failure criteria used in the analytical model are derived from the principles of TCC structural design prescribed by Eurocode 5 [17]. The failure criteria in the analytical model include the following:

a. Compression failure of the concrete: where maximum compression stress ($\sigma_{c,\,max}$) exceeds the concrete's compressive strength (f_c), $\sigma_{c,\,max} / f_c \geq 1$.
b. Bond failure of the joint: where shear stress exceeds ($\tau_{interface}$) the shear strength of the adhesive bond (f_{bond}), $\tau_{interface} / f_{bond} \geq 1$.
c. Shear failure of the timber: where maximum shear stress (τ_{max}) exceeds the timber's shear strength (f_v), $\tau_{max} / f_v \geq 1$.
d. Tension and bending failure of the timber: this criterion considers the combined effects of tension and bending stresses in the timber. If the combined effect exceeds the tensile and bending strengths of the timber, it suggests a possibility of failure in the timber component due to both tensile and bending stresses, $\sigma_{t,n} / f_t + \sigma_{t,m} / f_m \geq 1$.

4.2.3 Prediction of the ultimate capacity

Predicting the failure load in adhesive-bonded TCC beams involves assessing the critical load level at which the structure reaches its ultimate capacity and may experience failure. The methodology to predict the ultimate capacity of the TCC beam involves determining the ultimate section forces, bending moment (M), and shear force (V). This is accomplished by incorporating the material strength values into the relevant equations, as outlined in Eqs. (4.1) to (4.4), with detailed strength values provided in **Table 4-1**. Once the ultimate section forces are obtained, the next step is to calculate the loading for each failure criterion separately. Finally, the failure load, Fu, can be evaluated by considering the loading from each failure criterion. The failure load corresponds to the smallest value among all the calculated failure loads based on different failure criteria, as outlined in Eq. (4.5).

Table 4-1 Mechanical strength and stiffness of used timber and concrete

Material	Property	Parameters	Value
Timber (GL24 h)	Mean value of modulus of elasticity	E [MPa]	11000[a]
	Mean value of shear modulus	G [MPa]	720[a]
	Mean bending strength	f_m [MPa]	31.50[b]
	Mean tensile strength	f_t [MPa]	21.32[b]
	Mean shear strength	f_v [MPa]	3.43[b]
Concrete (C45/55)	Mean value of modulus of elasticity	E_c [MPa]	36283[c]
	Mean value of shear modulus	G [MPa]	14513[c]
	Mean compressive strength	f_{cm} [MPa]	53[c]

Mean tensile strength	f_{ctm} [MPa]	3.8[c]
Mean surface's tensile strength	$f_{ctm,surf}$ [MPa]	2[d]

[a] According to EN 1194 [115]

[b] Calculated from characteristic values in EN 1194 [115], assuming a lognormal distribution with COV= 15% [116]

[c] According to EN 1992-1:1:2004 [108]

[d] According to Frohnmüller et al. [75]

$$F_u = min\begin{Bmatrix} F_{u,c} \\ F_{u,b} \\ F_{u,v} \\ F_{u,m+t} \end{Bmatrix} \quad (4.5)$$

Where: $F_{u,c}$, $F_{u,b}$, $F_{u,v}$, and $F_{u,m+t}$ represent the predicted failure load of compression failure of the concrete, bond failure of the joint, shear failure of the timber, and tension and bending failure of the timber, respectively.

$$F_{u,c} = \frac{\sigma_{c,max} \times 2 \times (EI)_{ef}}{(0.5h_1 + a_1) \times l_s \times E_1} \quad (4.6)$$

$$F_{u,b} = \frac{2\,\tau_b\, b_2 (EI)_{ef}}{E_1\, b_1 h_1 a_1} \quad (4.7)$$

$$F_{u,v} = \frac{4\,\tau\,(EI)_{ef}}{E_2 (0.5h_2 + a_2)^2} \quad (4.8)$$

$$F_{u,m+t} = \frac{2\,(EI)_{ef}}{l_s \times E_2 (\frac{0.5h_2}{f_m} + \frac{a_2}{f_t})} \quad (4.9)$$

Where: l_s is the shear span, τ_b represents the mean shear strength of the glue joint determined from the previous study of the pushout test, f_m and f_t are the mean bending and tensile strength of timber, respectively.

Shear deformations can affect the overall stiffness and behaviour of the composite beam, leading to changes in its load-deflection response and stress distribution. Considering both shear and bending deformations in the analytical model could significantly improve the accordance between the model's predictions and the experimental results [75]. The bending and shear midspan deflection of the TCC beams can be calculated using Eq. 4.10 and 4.11, respectively. It is worth mentioning that the method used by Frohnmüller et al. to calculate the shear deformation was adopted [75].

$$w_m = \frac{1}{2} \times \frac{-F_u l_s (3L^2 - 4{l_s}^2)}{24(EI)_{ef}} \quad (4.10)$$

$$w_v = \frac{F_u l_s}{(GA)} \quad (4.11)$$

$$(GA) = \sum G_i \,.\, A_i \,.\, \delta_i \tag{4.12}$$

Where: (GA) represents the shear stiffness of the composite beam.

The factor δ_i in the equation represents the portion of the cross-section that is affected by the mean value of the shear stress $\overline{\tau_\iota}$, which is related to the total shear stress in the composite beam. The mean shear stress ($\overline{\tau_\iota}$) is calculated using shear stress values at the top edge ($\tau_{i,t}$) and lower edge ($\tau_{i,l}$) of the computational layer, as outlined in Frohnmüller et al. [75]. **Fig. 4-4** illustrates the analytical shear stress distribution at different load levels over the cross-section of the TCC beam. Notably, the timber component significantly dominates the effective shear stiffness, constituting 94.7% of the total, compared to 86.8% of the total effective shear stiffness by the employed cross-section (e.g., $A_{timber}/A_{concrete}$ = 4.9) in the study by Frohnmüller et al. [75]. In contrast, the concrete part makes a comparatively minor contribution, accounting for approximately 5.3%. The combined effect results in an overall shear stiffness, denoted as GA, determined to be 3.71×10^7 N·mm²/mm².

$$\delta_i = \frac{\overline{\tau_\iota}}{\sum \overline{\tau_\iota}} = \frac{\frac{\tau_{i,t} + \tau_{i,l}}{2}}{\sum \overline{\tau_\iota}} \tag{4.13}$$

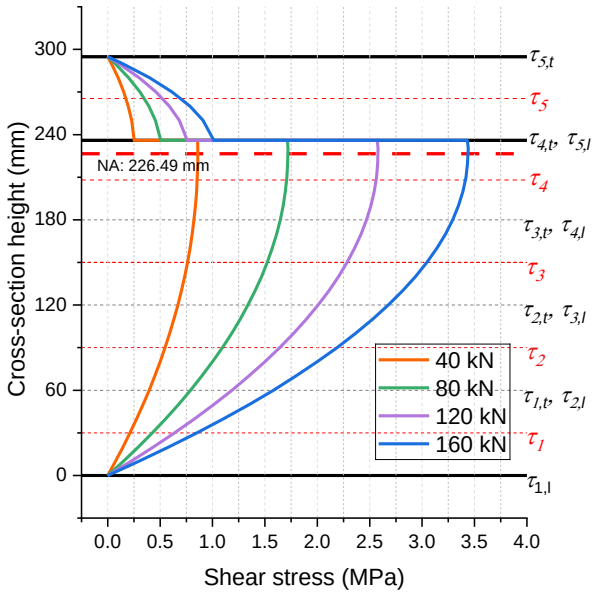

Fig. 4-4 Analytical shear stress distribution over the cross-section at different load levels

4.2.4 Model validation

The success of the model's validation lies in its ability to accurately predict the structural behaviour of the TCC composite beams under different loading conditions. Comparing the analytical models to experimental results is a crucial step in the validation process. Various critical parameters were measured

and recorded during the experimental testing, including load-deflection responses, bending strain distributions, and load-bearing capacity. These data were collected at different stages of loading, allowing for a detailed analysis of the TCC beams' structural behaviour.

4.2.4.1 Deformation behaviour

The deformation behaviour and stiffness of the TCC beams can be effectively visualized through load-displacement curves, presented in **Fig. 4-5**. These curves illustrate how the TCC beams respond to applied loads and how their deflection changes as the load increases. In **Fig. 4-5**, the load-displacement curves show the relationship between the applied load and the mid-span deflection of the TCC beams.

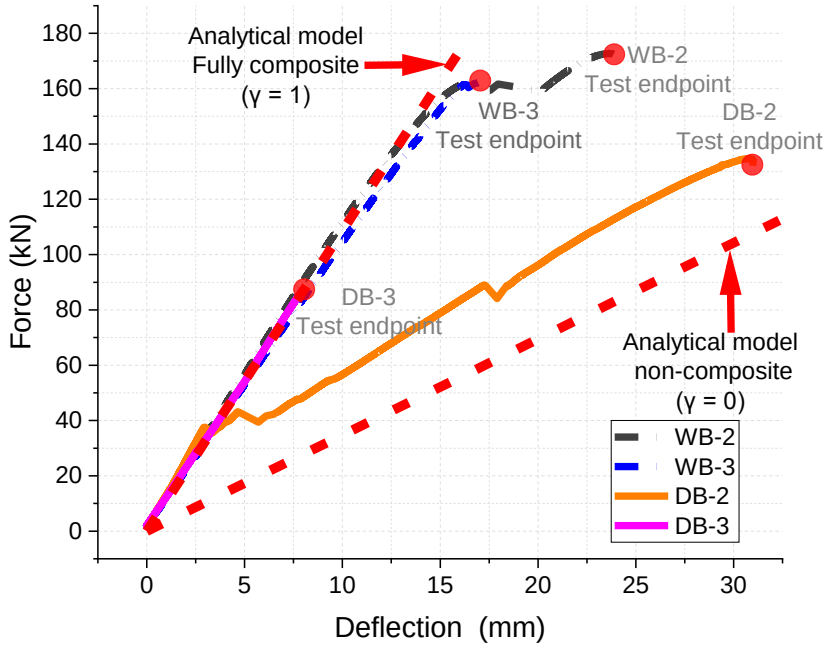

(a)

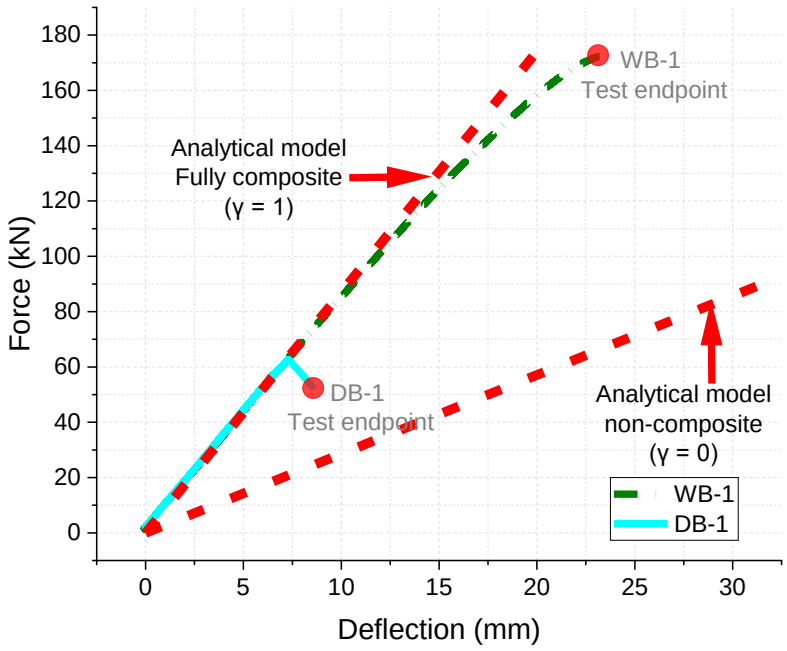

(b)

Fig. 4-5 Load and mid-span deflection response curves of tested beams, (a) configuration 1, and (b) configuration 2.

Table 4-2 presents the calculations of the deflection characteristics (Δw) of the TCC composite beams within the 15 kN to 60 kN load range, representing approximately 10% to 40% of the predicted ultimate failure load, respectively. It is worth mentioning that considering shear deformation and bending deformations influences the overall characteristics of deformation. The results showed a discrepancy ranging from 2% to 5%, signifying a consistent and high level of accordance between the predicted and measured midspan deflections. These results aligned with outcomes demonstrated by Frohnmüller et al. [75], emphasizing the significance of shear stiffness in the design of TCC beams.

Table 4-2 Comparison between the analytical model and experimental results

Test configuration	Beam N.o.	Analytical model predictions							Experimental results		$\frac{\Delta w_{exp}}{\Delta w_{comp}}$	$\frac{F_{u,exp}}{F_{u,comp}}$
		$\Delta w_{comp} = \Delta w_m + \Delta w_v$		$F_{u,c}$	$F_{u,b}$	$F_{u,v}$	$F_{u,m+t}$	$F_{u,comp}$	Δw_{exp}	$F_{u,exp}$		
		Δw_m	Δw_v									
		[mm]	[mm]	[kN]	[kN]	[kN]	[kN]	[kN]	[mm]	[kN]		
Config. 1	WB-2	3.05	1.09	311.94	286.34	159.6	150.19	150.19	4.07	163.00	0.98	1.08
	WB-3								4.35	163.20	1.05	1.08
	DB-2								-	37.56	-	-
	DB-3								4.28	90.00	1.03	-
Config. 2	WB-1	3.68	1.49	228.25	286.34	159.6	109.89	109.89	5.35	173.00	1.03	1.57
	DB-1								5.40	63.00	1.04	-

4.2.4.2 Bending stress distribution

Fig. 4-3 illustrates the bending strain distribution at the mid-span cross-sections of the composite beams. The graph compares the actual bending strain measured experimentally (represented by continuous lines) and the predicted bending strain obtained from the analytical model (represented by dashed lines). The bending stress distribution predicted by the analytical model generally aligns well with the experimental stress distribution in all tested beams, particularly before the levels of load that induced beam failure. This close agreement between the predicted and experimental bending stress distributions demonstrates the overall accuracy and reliability of the analytical model in simulating the beam's behaviour. This consistency highlights the validity of the analytical model as a valuable tool for designing and analyzing timber-concrete composite structures. However, it might be said that the analytical model provides conservative values for the bending stress distribution at the mid-span cross-section. The fact that the analytical model provides conservative values suggests that the model tends to predict slightly higher bending strains than the experimental measurements.

4.2.4.3 Ultimate capacity and failure mode

A comparison has been made between the ultimate failure loads obtained from the bending tests ($F_{u,exp}$) and the failure loads calculated ($F_{u,comp}$) using the analytical model. This comparison is essential to assess the accuracy and reliability of the analytical model in predicting the beam's ultimate capacity and failure behaviour. It is important to exclude the dry TCC beams from this comparison, as their failure was primarily attributed to the imperfect connection between the timber and concrete components, as discussed in section 3.5.2. By excluding these beams, we can focus on the performance of the analytical model for the wet TCC beams, which exhibit a more consistent behaviour.

The comparison between $F_{u,exp}$, and Fu,comp in Table 4-2 reveals good accordance with a ratio of 1.08 in the case of test config 1, e.g., WB-2 and WB-3. This suggests that the analytical model's calculated failure loads are in close agreement with the average experimental failure loads. The deviation of 8% indicates that the model provides accurate predictions of the ultimate failure loads for the TCC composite beams tested in this study. It also confirms that the model's estimations are consistent with the actual performance observed during the experimental tests. However, in configuration two, particularly in the case of WB-1, where the load points were positioned closer to each other, a significant difference was observed between the experimental results and the predicted failure force obtained from the analytical model. The observed discrepancy between the experimental and predicted failure loads in config. 2 (e.g., WB-1) can be partly attributed to the estimated beam capacity concerning tension and bending failure. In the analytical model, the estimation of the beam capacity relies on using a determined mean value obtained from the characteristic values of the GL24H timber element.

The combination of observed bending and shear failures in the timber component in the wet TCC beams indicates that multiple failure modes compromised the structural behaviour of TCC beams, as discussed in section 3.5.2. This observation provides further evidence to support the hypothesis that the beam capacity concerning tension and bending failure is less estimated in the case of WB-1 (config. 2). In contrast, the predicted capacity concerning shear failure aligns well with the actual failure load, highlighting the analytical model's accuracy in capturing the composite beams' shear behaviour. The comparison between the calculated failure modes and the experimental results shows good accordance. The calculations consistently predict that the failure will occur in the timber component of the wet TCC beams, indicating that the analytical model effectively predicts the failure behaviour of the TCC beams.

4.3 FE modeling

4.3.1 Model development

ABAQUS is a widely used commercial finite element software package that provides a powerful platform for solving complex engineering problems involving nonlinearities, material behaviour, and other advanced features. The ABAQUS/standard (version 2022) finite element software was adopted to develop and analyze the 3D models in this study.

The following sections will provide an overview of the development of the Abaqus numerical model. The first step in developing the numerical model was to define the geometry of the physical system, which represents a detailed 3D model of the system, including all relevant geometric features and boundaries. After that, the model was meshed. The material properties of the system were then defined by specifying the elastic, plastic, and other material properties. Next, the loading conditions for the system were defined, specifying the type and magnitude of the external loads and constraints that would be applied to the system during the simulation. Next, the numerical model was solved using Abaqus' advanced analysis. Finally, the simulation results were analyzed using Abaqus' post-processing utilities, which involved creating visualizations of the system behaviour, such as in terms of stress and strain distributions, displacement vectors, and other relevant metrics. It’s worth mentioning that the developed model does not account for the long-term behaviour influenced by the creep and shrinkage of both concrete and timber.

4.3.2 Model definition and geometry

The 3D FE model for TCC beams uses solid elements to ensure that material properties and interactions between the members are fully considered. These solid elements have specific definitions of stress-strain and contact relations, which results in a more accurate representation of the TCC beam's behaviour under different loading conditions. The decision to use a 3D solution for the analysis was motivated by the fact that the 3D model allowed for a more detailed analysis of the interaction between the different layers of the

structure and provided insights into the mechanisms that control slip behaviour, transverse distributions of support reactions and bending moments. Moreover, the decision to employ a 3D model was influenced by its capability for out-of-plane analysis. This feature allows the model to effectively simulate and assess the impact of loads deviating from the central axis of the beam. In the case of our tests, this can be due to uncertainty in positioning the loading system.

The C3D8R solid element is a commonly used 8-node linear brick element in ABAQUS that is well-suited for modeling complex three-dimensional geometries. Hourglassing is a common issue in finite element analysis where spurious deformations occur in certain elements due to their deformation mode. The C3D8R brick element has been shown to be less exposed to hourglassing than other element types, making it a good choice for modeling high-stress regions [120]. In addition, the C3D8R brick element uses reduced integration, which means that the integration points are reduced from the total number of nodes in the element. This reduces the computational running time and memory requirements of the analysis, especially for 3D analyses where the number of elements can be very large [98]. In this context, The C3D8R solid elements were used to specify the timber beam, concrete slab, loading beams, and steel supports. Appropriate, cohesive zone parameters were selected based on the experimental results. The COH3D8 element has six degrees of freedom at each node and models the behaviour of an adhesive layer between two surfaces. It allows for modeling the cohesive behaviour of materials that can be described by a traction-separation law. In this case, the COH3D8 elements were used to model the behaviour of the adhesive layer between the timber and concrete in the TCC connections.

The global coordinate system was established such that the x-axis aligns with the span direction of the beam, the y-axis is perpendicular to the plane of the concrete slab, and the z-axis is oriented in the transverse-span direction. As a result, length, width, and depth will correspond to the x, y, and z coordinates, respectively. The dimensions of the parts used in the model are typically based on those of the experimental tests and are chosen to be representative of the actual system being modeled. The dimensions of the parts used in the model are detailed in **Table 4-3**.

Table 4-3 Parts dimensions utilized in the TCC model

Model configuration	Element	Length (mm)	Width (mm)	Depth (mm)
Push-out model (Scaled specimen)	Timber	280	100	320
	Concrete	100	100	320
	Cohesive	240	60	1
	Loading plate	280	100	20

	Steel support	100	100	100
4-Points bending model	Timber	3200	120	240
	Concrete	3200	400	60
	Cohesive	3200	120	1
	Loading plate	300	60	20
	Steel support	150	120	100

4.3.3 Materials constitutive model

4.3.3.1 Concrete

The concrete damage plasticity (CDP) model provided by Abaqus was used to simulate the behaviour of concrete. The CDP model incorporates both elastic and inelastic material responses to capture the complex behaviour of concrete under various loading conditions. Concrete is assumed to be an isotropic and homogeneous material. It considers two main mechanisms: damage and plasticity. The model combines concepts from plasticity theory and damage mechanics to capture concrete's non-linear, inelastic, and deteriorating response.

The stress-strain relations for the three-dimensional multiaxial condition are given by the scalar damage elasticity equation:

$$\sigma = (1 - d)D_0^{el} : (\varepsilon - \varepsilon^{pl}) \tag{4.14}$$

where $D_0^{el}$is the initial (undamaged) elasticity matrix; d is the scalar stiffness degradation variable, which can take values in the range from zero (undamaged material) to one (fully damaged material); ε is the total strain rate, and ε^{pl} is the plastic part of the strain rate.

The uniaxial compressive and tensile behaviour of concrete in one dimension is shown in **Fig. 4-6** and expressed as Eq. (4.15). It's essential to note that concrete behaves accordingly in the other two dimensions.

$$\begin{aligned} \sigma_c &= (1 - d_c)E_c(\varepsilon_c - \varepsilon_c^{pl,h}) \\ \sigma_t &= (1 - d_t)E_t(\varepsilon_t - \varepsilon_t^{pl,h}) \end{aligned} \tag{4.15}$$

Where E_0 is the initial elastic stiffness of concrete; ε_c and ε_t represent the strains corresponding to the compression and tension strengths, respectively. The plastic hardening strain in compression and tension, denoted as $\varepsilon_c^{pl,h}$ and $\varepsilon_t^{pl,h}$, and concrete damage in compression and tension, denoted as, d_c and d_t are expressed as in Eq. (4.16) and Eq. (4.17), respectively, for the post-peak behaviour. Additionally,

Table 4-4 shows the concrete material properties utilized in the finite element model.

$$\varepsilon_c^{pl,h} = \varepsilon_c^{in,h} - \frac{d_c}{(1-d_c)}\frac{\sigma_c}{E_0}$$
$$\varepsilon_t^{pl,h} = \varepsilon_t^{in,h} - \frac{d_t}{(1-d_t)}\frac{\sigma_t}{E_0} \quad (4.16)$$

$$d_c = 1 - \frac{\sigma_c}{\sigma_{cu}}$$
$$d_t = 1 - \frac{\sigma_t}{\sigma_{tu}} \quad (4.17)$$

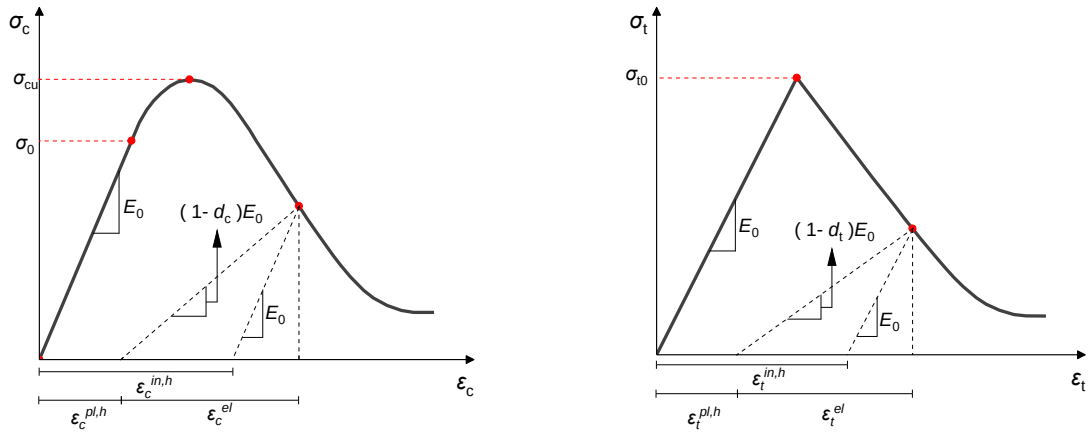

(a) (b)

Fig. 4-6 Uniaxial stress-strain responses of concrete: (a) compressive loading and (b) tensile loading

Table 4-4 Concrete material properties

Parameters		Value
Elasticity properties [108]	Young's modulus (MPa)	36283
	Poissons' ratio	0.2
Plasticity properties [121,122]	Dilation angel	40
	Eccentricity	0.1
	f_{b0}	1.16
	K	0.6667
	Viscosity parameter	0.001
Compression behaviour definition	Compression yield stress (MPa)	53
Tension behaviour definition	Tension yield stress (MPa)	3.8

4.3.3.2 Timber

ABAQUS user subroutine was used to define the 3D elastic-plastic damage constitutive model of the timber similar to the model done by Tao et al. [93]. The decision to employ this model is motivated by its superior ability to simulate the complex behaviour of timber, particularly brittle failure in shear and tension modes not adequately addressed by pre-built models in ABAQUS. The radial and tangential directions were set to correspond with the Y and Z directions at every material point of the timber, as illustrated in **Fig. 4-7**. The orthotropic stress-strain relation shown in Eq. (4.18) was used to describe the behaviour of the timber. The model considers shear and tension damage factors, which can have values of either zero or one, demonstrating the exclusive consideration of brittle damage failure modes.

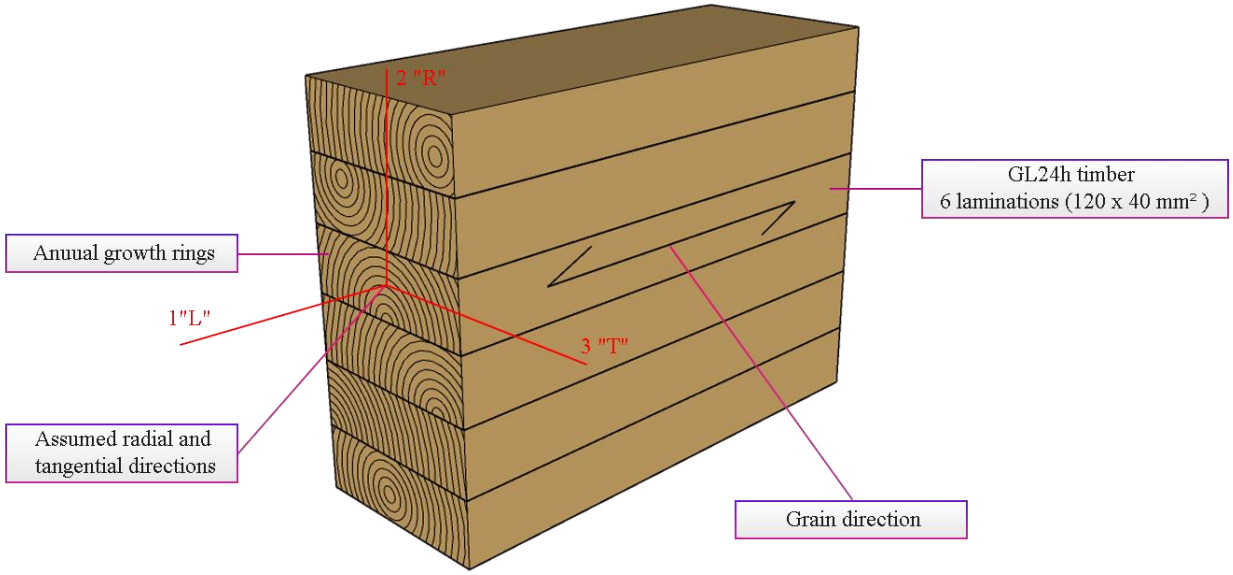

Fig. 4-7 GL24h timber beam cross-section

$$\begin{bmatrix}\sigma_{11}\\ \sigma_{22}\\ \sigma_{33}\\ \sigma_{12}\\ \sigma_{23}\\ \sigma_{13}\end{bmatrix} = \begin{bmatrix} C_{d1111} & C_{d1122} & C_{d1133} & & & \\ C_{d1122} & C_{d2222} & C_{d2222} & & & \\ C_{d1133} & C_{d2233} & C_{d3333} & & & \\ & & & C_{d1212} & & \\ & & & & C_{d2323} & \\ & & & & & C_{d1313} \end{bmatrix} \begin{bmatrix}\varepsilon_{11}\\ \varepsilon_{22}\\ \varepsilon_{33}\\ \varepsilon_{12}\\ \varepsilon_{23}\\ \varepsilon_{13}\end{bmatrix} \tag{4.18}$$

In which:

$$\begin{cases} C_{d1111} = E_1(1-d_1)(1-v_{23}v_{32}(1-d_2)(1-d_3))/T_d \\ C_{d2222} = E_2(1-d_2)(1-v_{13}v_{31}(1-d_1)(1-d_3))/T_d \\ C_{d3333} = E_3(1-d_3)(1-v_{12}v_{21}(1-d_1)(1-d_2))/T_d \\ C_{d1122} = E_1(1-d_1)(1-d_2)(v_{21}+v_{31}v_{23}(1-d_3))/T_d \\ C_{d1133} = E_3(1-d_3)(1-d_1)(v_{13}+v_{12}v_{23}(1-d_2))/T_d \\ C_{d2233} = E_2(1-d_2)(1-d_1)(v_{32}+v_{12}v_{31}(1-d_1))/T_d \\ C_{d1212} = (1-d_{12})G_{12} \\ C_{d2323} = (1-d_{23})G_{23} \\ C_{d1313} = (1-d_{13})G_{13} \\ T_d = 1-v_{12}v_{21}(1-d_1)(1-d_2)-v_{23}v_{32}(1-d_2)(1-d_3)-v_{31}v_{13}(1-d_3)(1-d_1)-2v_{21}v_{32}v_{13}(1-d_2)(1-d_3)(1-d_1) \end{cases} \quad (4.19)$$

Where σ_{ij} and ε_{ij} represent stress and strain components, respectively; E_i stands for the modulus of elasticity in the I direction; G_{ij} is the shear modulus in the i-j plane; subscript 1 corresponds to the direction parallel to the timber grain (L); subscript 2 represents radial direction (R) of timber; subscript 3 denotes the timber tangential direction (T); υ_{ij} is the Poisson's ratio, which satisfies $E_i/\upsilon_{ij} = E_j/\upsilon_{ji}$; d_i and d_{ij} are factors related tension and shear damage factors, respectively.

The strength criteria provided by Yamada et al. [123] were utilized to evaluate the strength of the timber elements as represented by Eq. (4.20).

$$\begin{cases} L\ direction: \dfrac{\sigma_{11}^2}{f_{t,1}^2}+\dfrac{\sigma_{12}^2}{f_{v12}^2}+\dfrac{\sigma_{13}^2}{f_{v13}^2}=\ell^2 \\ R\ direction: \dfrac{\sigma_{22}^2}{f_{t,2}^2}+\dfrac{\sigma_{12}^2}{f_{v12}^2}+\dfrac{\sigma_{23}^2}{f_{v23}^2}=\ell^2 \\ T\ direction: \dfrac{\sigma_{33}^2}{f_{t,3}^2}+\dfrac{\sigma_{23}^2}{f_{v23}^2}+\dfrac{\sigma_{13}^2}{f_{v13}^2}=\ell^2 \end{cases} \quad (4.20)$$

$$and \begin{cases} \ell \geq 1\ failure \\ \ell \leq 1\ non-failure \end{cases}$$

Where $f_{t,1}$, $f_{t,2}$, and $f_{t,3}$ are the uniaxial strength in the L, R, and T directions; $f_{v\,ij}$ is the shear strength of the i-j plane.

Based on the defined 3D constitutive model, the stress-strain relationships for tension and shear behaviour of the timber are illustrated in **Fig. 4-8**. The variables $f_{t,i}$ and $\varepsilon_{t,i}$ represent the tensile strength and fracture strain in the i-direction. Similarly, $f_{v,ij}$ and γ_{ij} denote the shear strength and failure strain in the i-j plane, respectively. The user subroutine was developed to calculate the stress component increments in timber elements at each incremental step using Eq. (4.18). Subsequently, the yield or damage of the elements was then estimated using Eq. (4.20). If the elements failed in tension or shear, the corresponding damage factors are set to 1 to indicate failure.

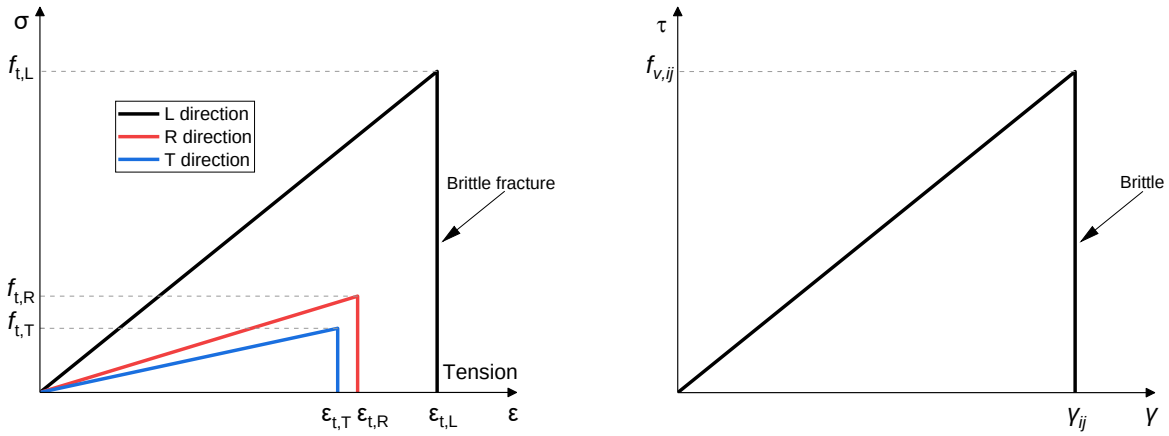

(a) (b)

Fig. 4-8 Stress-strain relation of the timber, (a) tension behaviour, and (b) shear behaviour, adopted from Tao et al. [93]

Timber elastic parameters and strength properties used in this study are shown in **Table 4-5** and **Table 4-6**. It should be mentioned that these values were estimated based on the strength characteristics and stiffness properties of GL24h available in standard EN 1194 [115]. The timber material's elastic modulus in R and T directions were assumed to be identical. This assumption was based on the precedent set by others [124]. The mean values for $f_{c,1}$, $f_{b,1}$, and $f_{t,1}$ were extracted, assuming a lognormal distribution with COV 14% [116,125]. Conservative values have been assumed for the compression and tension strength in the R or T directions, respectively. The shear failure in the T-L and R-L planes of the timber in TCC beams is expected to occur similarly during bending tests. In the T-L plane, the shear strength can be considered identical to the estimated strength of the R-L plane parallel to the grain. In the R-T plane, where shear failure is less likely to occur, the shear strength can be conservatively estimated as 20% of the measured strength in the R-L plane [93].

It's noteworthy that the γ-method accounts for the combined effects of tension and bending stresses in the timber as a criterion for potential failure of the timber. This criterion considers the combined effects of tension and bending stresses in the timber. If the combined effect exceeds the tensile and bending strengths of the timber, it suggests a possibility of failure in the timber component due to both tensile and bending stresses. Given this consideration, adopting an approach in the FE models that utilizes the average value between the mean value of bending strength and the mean value of tension strength seems reasonable. This decision aligns the FE model more closely with the principles embedded in Eurocode 5, ensuring that the FE models adhere to the same criteria for predicting potential failure modes.

Table 4-5 Timber elastic parameters

Parameters	E_1 (MPa)	E_2 (MPa)	E_3 (MPa)	G_{12} (MPa)	G_{13} (MPa)	G_{23} (MPa)	v_{12}	v_{13}	v_{23}
Value	11000	900	600	750	750	80	0.35	0.29	0.29

Table 4-6 Timber strength properties

Parameters	$f_{c,1}$ (MPa)	$f_{b,1}$ (MPa)	$f_{t,1}$ (MPa)	$f_{c,2}$ (MPa)	$f_{t,2}$ (MPa)	$f_{c,3}$ (MPa)	$f_{t,3}$ (MPa)	f_{v21} (MPa)	f_{v31} (MPa)	f_{v23} (MPa)
Value	36.8	31.5	21	7	2	7	2	3.42	3.42	0.70

Where 1, 2, and 3 denote L, R, and T directions, respectively.

4.3.3.3 Glue shear connection

When modeling TCC structures using finite elements, one of the most important steps is defining the connections between the elements. Connections are vital in transferring shear forces between the timber and concrete components, guaranteeing structural integrity and load-carrying capacity. A precise and reasonable representation of connections is essential to capture the mechanical behaviour and performance of TCC structures accurately.

The material model used for the adhesive layers in composite structures is typically Elastic/Traction and Quads Damage [126]. This material model accounts for both the elastic behaviour and the damage evolution of the adhesive under loading conditions. The elastic behaviour is represented by the traction response of the adhesive, describing its stiffness and ability to transmit forces. The stress-strain relations for traction behaviour are as follows:

$$\begin{Bmatrix} t_n \\ t_s \\ t_t \end{Bmatrix} = \begin{bmatrix} E_{nn} & & \\ & E_{ss} & \\ & & E_{tt} \end{bmatrix} \begin{Bmatrix} \varepsilon_n \\ \varepsilon_s \\ \varepsilon_t \end{Bmatrix} \tag{4.21}$$

The quantities t_n, t_s, and t_t represent the nominal tractions in the normal and the two local shear directions, respectively; while the quantities E_{nn}, E_{ss}, and E_{tt} represent the corresponding stiffness and the quantities ε_n, ε_s, and ε_t represent the corresponding nominal strains.

By referencing the manufacturer's data sheet, the elastic properties of the adhesive can be incorporated into the finite element analysis of the TCC structure. The data sheet typically provides information on the adhesive's modulus of elasticity in tension, tensile strength, and other relevant mechanical properties. However, the shear modulus has been estimated based on the experimental pushout tests conducted in our previous study [103].

The Quads Damage model incorporates the damage evolution, simulating the initiation and propagation of cracks or delamination within the adhesive layers. By utilizing this model, the finite element analysis can capture the behaviour of the adhesive layers and their interaction with the timber and concrete components in the TCC structure. Damage is assumed to initiate when a quadratic interaction function involving the nominal stress ratios (as defined in the expression below) reaches a value of one. This criterion can be represented as

$$\left\{\frac{\langle t_n \rangle}{t_n^o}\right\}^2 + \left\{\frac{t_s}{t_s^o}\right\}^2 + \left\{\frac{t_t}{t_t^o}\right\}^2 = 1 \tag{4.22}$$

t_n^o, t_s^o, and t_t^o represent the peak values of the nominal stress when the deformation is either purely normal to the interface or purely in the first or the second shear direction, respectively.

The nominal stress in the first and second shear directions has been assumed to be equal to the shear strength obtained from experimental pushout tests [103]. The shear strength measured in these tests provides a reliable estimate of the stress levels experienced by the TCC structure in those directions.

The damage evolution law describes the rate at which the material stiffness is degraded once the corresponding initiation criterion is reached. It involves the utilization of a scalar damage variable denoted as D, which serves as an indicator of overall damage in the material and captures the combined effects of all the active mechanisms. It initially has a value of 0. When damage evolution is accounted for, D monotonically evolves from 0 to 1 upon further loading after the initiation of damage. The stress components within the traction-separation model are affected by this damage according to Eq. (4.23).

$$\begin{aligned} t_n &= \begin{cases} (1-D)\bar{t}_n, \bar{t}_n > 0 \\ \bar{t}_n, otherwise\ (no\ damage\ to\ compressive\ stiffness) \end{cases} \\ t_s &= (1-D)\bar{t}_s \\ t_t &= (1-D)\bar{t}_t \end{aligned} \tag{4.23}$$

Where $\bar{t}_n$, $\bar{t}_s$, and $\bar{t}_t$ are the stress components predicted by the elastic traction-separation behaviour for the current strains without damage.

When modeling progressive delamination in TCC structures, different approaches can be used to describe the delamination process. Two common methods are displacement-based and energy-based approaches, which are available as suboptions under the damage evolution feature in the Abaqus software.

In the displacement-based approach, the delamination is characterized based on the relative displacement between the timber and concrete components. As the delamination progresses, the separation or opening of the crack interface is tracked by monitoring the relative displacements. This approach

typically involves defining a critical displacement criterion, such as a maximum allowable separation, at which the delamination is considered to have occurred. The model then simulates the separation and subsequent behaviour of the delaminated region. On the other hand, in the energy-based approach, the delamination is described in terms of the energy dissipation or release associated with the crack propagation. The model tracks the accumulation of energy in the delaminated region and determines the critical energy release rate at which delamination initiates or progresses. This approach focuses on the energy balance and the fracture mechanics principles to simulate the delamination process accurately.

In this study, a linear softening energy approach of damage evolution has been utilized. This choice of approach is notably influenced by the observed plateau in experimental push-out tests, which can be attributed to the phenomenon of timber plasticization. Within the context of linear softening, as illustrated in **Fig. 4-9**, Abaqus utilizes an evolution equation for the damage variable, denoted as D, given by Eq. (4.24).

$$D = \frac{\delta_m^f \left(\delta_m^{max} - \delta_m^0\right)}{\delta_m^{max} \left(\delta_m^f - \delta_m^0\right)} \tag{4.24}$$

Where $\delta_m^f = 2G^C/T_{\text{eff}}^0$ with T_{eff}^0 as the effective traction at damage initiation. δ_m^{max} refers to the maximum value of the effective displacement attained during the loading history.

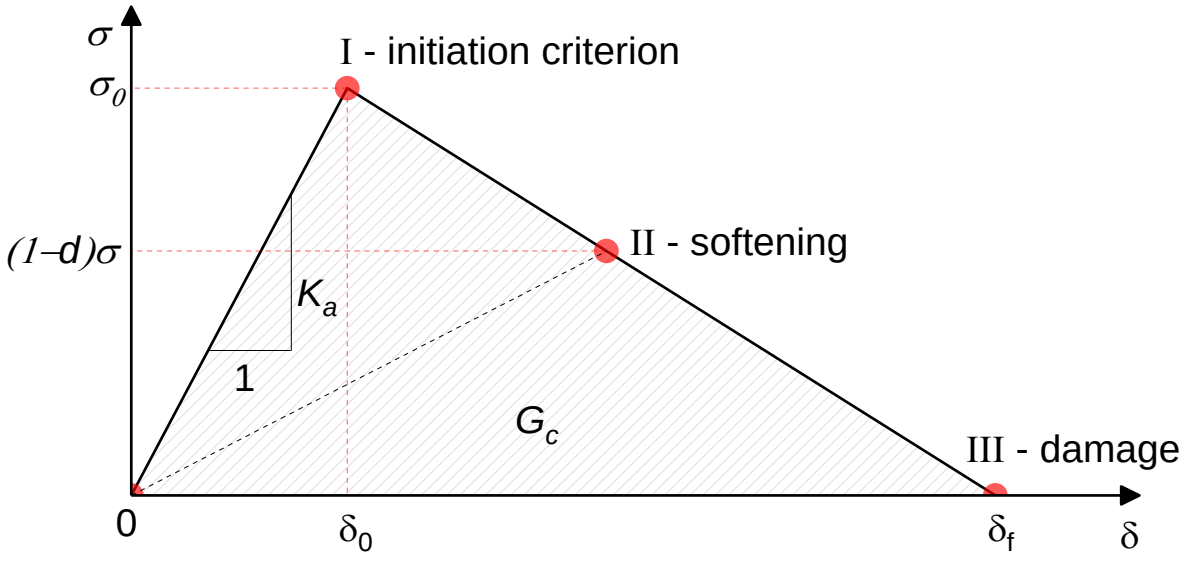

Fig. 4-9 Elastic-linear softening constitutive model of adhesive

Setting a viscosity coefficient is indeed important to stabilize the material in a softening regime, particularly when using the suboptions/damage stabilization cohesive approach in finite element modeling.

The viscosity coefficient (χ) represents a numerical parameter used to control the rate of material softening and prevents numerical instabilities that can occur during the simulation. In a study conducted by Demir et al. [127], the influence of the viscosity coefficient on the analysis results was analyzed in detail. Different values of the viscosity coefficient were tested to determine the optimal value for stabilizing the material behaviour. The study found that a viscosity coefficient of $\chi = 0.0005$ provided the best results in terms of stabilizing the material and producing accurate simulation outcomes. **Table 4-7** illustrates the defined parameters of the glue connection used in the numerical analysis.

Table 4-7 Glue connection parameters

Parameter	Value
Elastic modulus (E)	4100 MPa
Shear modulus (G)	1675 MPa
Damage initiation shear stress (σ_0)	6.7 MPa
Fracture energy (G_c)	40000 J/m^2
Viscosity coefficient (χ)	0.0005

Fig. 4-10 shows the finite element model (FE) of push-out tests, and **Fig. 4-11** illustrates the shear vs. slip curves for FE compared to the experimental results of push-out tests from series A4.1, as detailed in **Chapter 3.** The experimental data represent a range of tests conducted with Sikadur®-53 adhesive, having an adhesive thickness of 1 mm. It is apparent that the FE results fall within the range of the experimental curves, affirming the accuracy of the glue shear connection modeling.

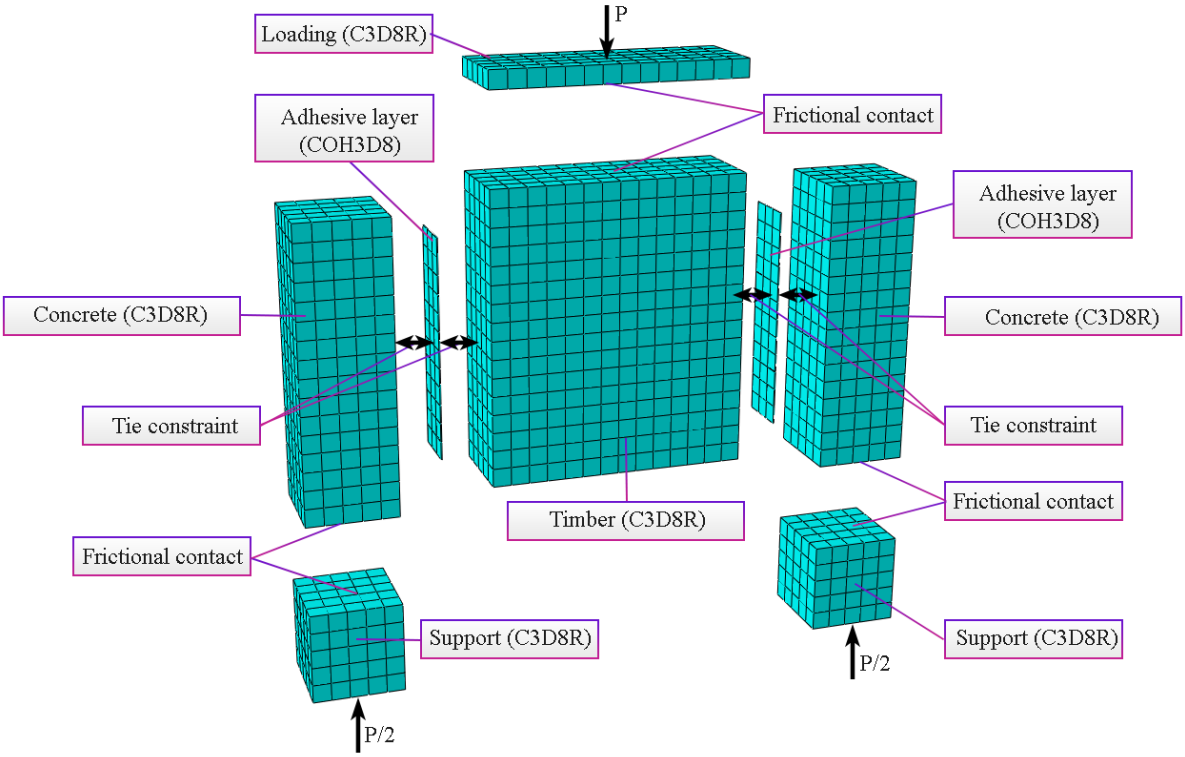

Fig. 4-10 Assembly of the 3D FE model of push-out tests

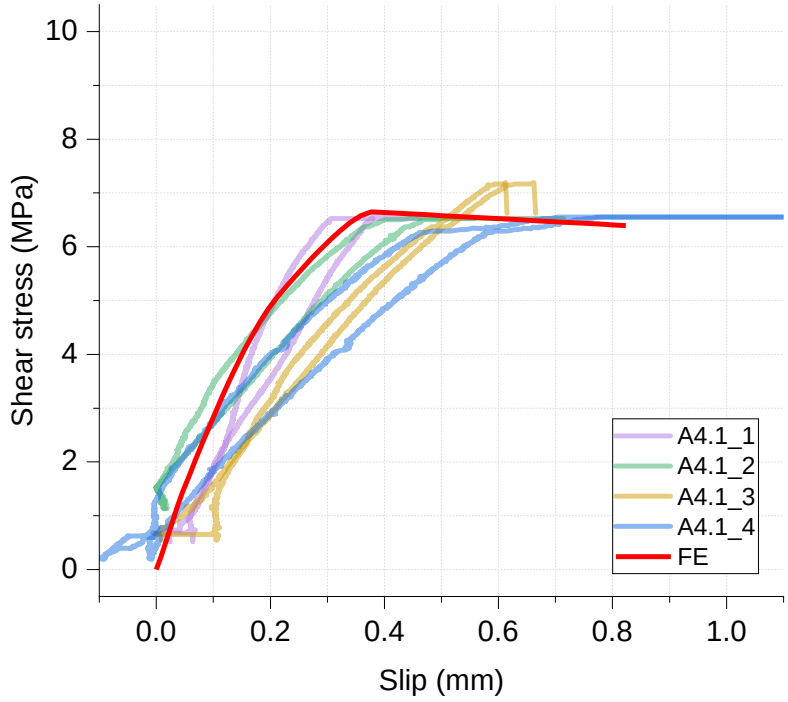

Fig. 4-11 Glue shear connection validation for scale specimen of pushout tests

4.3.3.4 Steel

In the finite element modeling of the TCC structure, the support and loading plates are assigned a material definition with a very high stiffness compared to other materials in the model. This step ensures that the support and loading plates remain rigid and do not deform under the applied loads and defined boundary conditions. The support and loading plate components were defined as steel material with an elastic modulus of 200 GPa.

4.3.4 Model assembly

The tie constraint is a commonly used approach to simulate adhesive bonding in finite element analysis, providing a convenient and efficient way to model the interaction between different components in a bonded assembly. By setting the tie constraint, the relative displacements and rotations between the bonded surfaces are constrained based on the contact conditions. This allows for the simulation of adhesive bonding behaviour, including the transfer of shear and normal forces, as well as the ability to model delamination or separation if the bond fails. In this context, a tie constraint has been established between the glued components (timber and concrete) and the adhesive layer, setting the adhesive layer surface as "slave" and the glued component surfaces as "master,". It is crucial to follow this order and set the appropriate master-slave relationship to avoid errors or incorrect handling of delamination behaviour, see **Fig. 4-12**.

A surface-to-surface contact interaction was defined between each loading and support plate and its corresponding timber or concrete component. The contact interaction was established using a "hard contact" formulation for normal behaviour and a " penalty friction" formulation with a friction coefficient of 0.35 for tangential behaviour. The coefficient of friction used is sourced from available literature for modeling wood-steel contact [128–130]. The "hard contact" formulation means that the contact between the surfaces of the plates and the timber or concrete components is considered to be rigid and non-deformable. On the other hand, the friction formulation accounts for the resistance to sliding or relative motion between the contact surfaces.

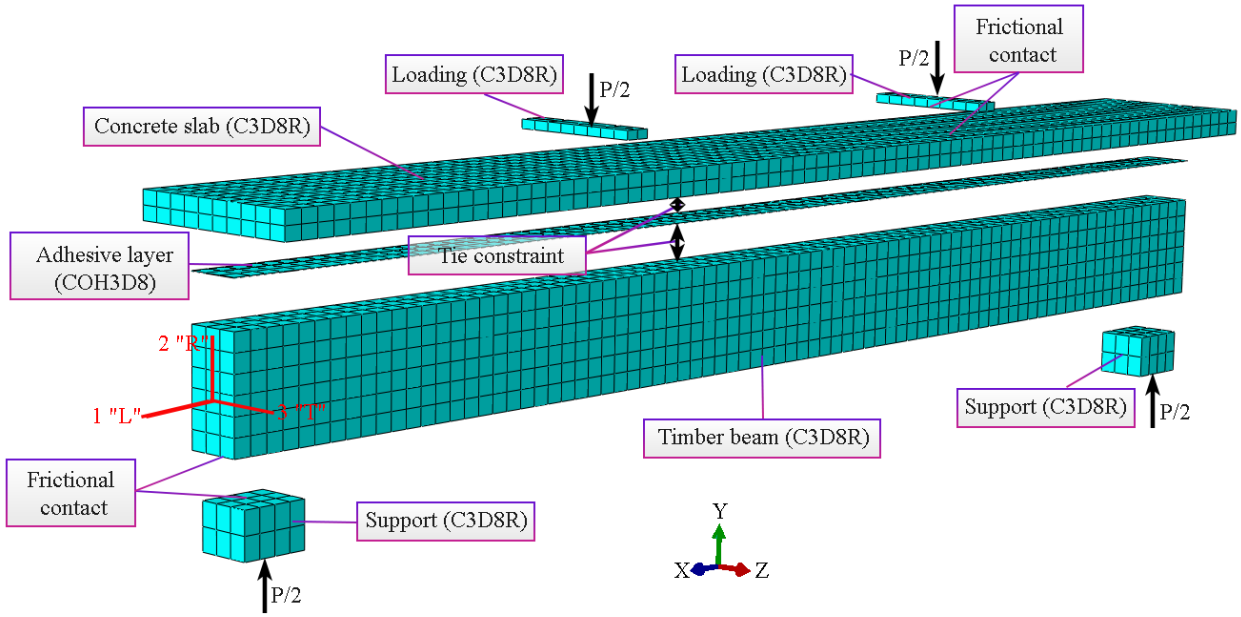

Fig. 4-12 Assembly of the 3D FE model

4.3.5 Boundary conditions

Boundary conditions refer to the constraints or restrictions imposed on the structure at its boundaries or edges. Two types of boundary conditions have been applied to the underside of the support plates. The first support has been set as roller support. The support plate is constrained against the translational movement in the vertical direction (perpendicular to the support plate), but it is allowed to translate horizontally freely along the surface of the support plate without considering any rotational constraints. In contrast, the second support has been assigned as pinned support. Therefore, the support plate is constrained against the translational movement in all directions (vertical and horizontal) with no rotational constraints.

4.3.6 Loading producers

The displacement-controlled analysis is often considered easier to converge compared to the load-controlled method in finite element analysis. Displacement-controlled analysis involves specifying the desired displacements or deformations at certain locations or nodes in the model, and the analysis is iteratively performed until the desired displacements are achieved. The advantage of displacement-controlled analysis is that it provides direct control over the deformation behaviour of the structure. By prescribing the displacements, it is relatively straightforward to track the progress of the analysis and monitor the convergence of the solution. In contrast, load-controlled analysis involves specifying the applied loads on the structure and solving for the resulting displacements. Load-controlled analysis can sometimes be more challenging to converge, especially when the structure undergoes large deformations

or exhibits non-linear behaviour. Moreover, the reduction in load that typically occurs with such deformations becomes notably challenging to manage. In this context, the displacement-controlled analysis has been utilized in this study. Loading applied to the specimen is based on a specified displacement assigned to the upper surface of the loading plate.

In the simulation of complex tasks, non-linear effects can introduce challenges that may require more iterations to achieve convergence. The default options provided in Abaqus software are typically conservative and may not be sufficient for solving such problems. To address this issue, the convergence criteria and the allowable number of iterations in the simulation settings have been adjusted, ensuring that the solution adequately captures the non-linear behaviour of the system.

4.3.7 Elements meshing

Meshing is a fundamental step in finite element analysis (FEA), where the geometry of a structure is discretized into smaller elements. These elements collectively form a mesh, and their interactions simulate the behaviour of the entire structure under various conditions. In Abaqus, as in most FEA software, elements are the basic building blocks of the mesh. Different types of elements are available, each suited for specific types of geometries and behaviours.

Once the geometry was defined, the next step was to generate a mesh of interconnected elements that discretized the physical domain. This involved selecting an appropriate element type (linear, quadratic, or cubic), specifying the mesh density, and applying any necessary constraints to ensure the mesh was well-formed and appropriate for the analysis. It's important to note that the choice of element types, element size, and mesh quality can significantly impact the accuracy and efficiency of analysis. The mesh size was determined through an iterative mesh refinement process, aiming for mesh convergence where further refinement results in negligible changes in stress and deformation outcomes without increasing computational demands. **Table 4-8** illustrates the types of elements and more detailed properties used in the model.

Table 4-8 FE mesh and element types used in the FEA model

Material	Element type	Element size	Mesh density	Mesh Controls
Adhesive	COH2D4	40 mm	Uniform	Sweep
Concrete	C3D8R	40 mm	Uniform	Structured
Timber	C3D8	40 mm	Uniform	Structured
Steel supports	C3D8R	40 mm	Uniform	Structured
Loading plates	C3D8R	40 mm	Uniform	Structured

4.3.8 Model validation

Finite Element (FE) modeling offers a powerful tool to simulate complex structural behaviour, such as those exhibited by TCC beams. In this section, we seek into the process of validating the FE models by comparing their predictions with the outcomes of experimental tests. This critical assessment involves a comprehensive analysis of key parameters, including load-deflection responses, bending strain distributions, and load-bearing capacity, which were precisely measured and recorded during experimental trials.

4.3.8.1 Deformation behaviour

In the context of deformation behaviour, the experimental testing and numerical simulation provided valuable insights into how the TCC beams respond to different loading conditions. This section investigates the observed deformation behaviour of the TCC beams, highlighting the comparison between experimental results and FE model predictions.

The load-deflection curves for the TCC beams, obtained through both numerical simulations and experimental tests, are visually presented in **Fig. 4-13**. It can be that the model's performance is highly satisfactory within the linear regimes, accurately predicting deflections for wet and dry fabricated TCC beams. However, an exception is noted for DB-2, where a distinct shift in the beam's behaviour occurred following the bonding failure at a load level of 37 kN. **Table 4-9** displays the computed deformation characteristics (Δw) for the TCC composite beams across a load range of 15 kN to 60 kN. This range corresponds to approximately 10% to 35% of the anticipated ultimate failure load in test configuration 1. The findings indicate an 11% to 19% variance between the predicted and measured midspan deflections.

Fig. 4-13 illustrates that both wet and dry fabricated TCC beams initially showed almost identical load-to-mid-span deflection behaviour. This similarity continued until the point of bonding failure at the interface in the dry beams, as discussed earlier in **Chapter 3**. However, the key deviation occurred when bonding failure happened in the dry beams. This unexpected specific change in the behaviour of the dry TCC beams was not predicted by the FE model, although the assumptions describing interfaces and interactions meet the results of the push-out tests. Early bonding failure in the dry beams could result from various factors, such as inadequate adhesive bonding, improper surface preparation, or internal pre-cracking due to differential deformation between the wood and the concrete, which is linked in particular to shrinkage.

The FE numerical results regarding the degree of composite action (DCA) are presented in **Table 4-9**. The calculation of DCA follows the methodology proposed by Gutkowski et al. [131], as expressed by Eq. (4.25).

$$DCA = \frac{\Delta_N - \Delta_C}{\Delta_N - \Delta_F} \quad (4.25)$$

In this equation, Δ_N stands for the projected non-composite action deflection; Δ_C is the observed deflection of the test specimens, and Δ_F denotes the projected deflection under fully composite action, all at the same load level of 40% of the ultimate capacity.

The results demonstrated a high level of agreement between the predicted DCA derived from the FE model and the corresponding experimental measurements. This close alignment indicates that the FE model effectively captures the bending behaviour and deflection of the composite beams and accurately predicts their composite action. It is important to note that within the FE model, the failure mode observed was attributed to timber failure. The specifics of the failure modes will be discussed in detail in the coming sections.

In **Fig. 4-13**, the FE model maintains a worthy alignment with both the analytical model and the experimental results, which is especially noticeable at the beginning of the load vs. deflection curves. However, a notable contrast becomes apparent towards the end of the curves concerning the expected behaviour of the TCC beams, as predicted by the FE model and the analytical model (γ-method). As per the analytical model (depicted by dotted lines in **Fig. 4-13**), the beams were expected to exhibit fully composite action with a narrower range of discrepancy, ranging from 0.02% to 0.05%. Nevertheless, the FE model's predictions deviate from this anticipated behaviour, showcasing an increased range of discrepancy compared to analytical results.

Table 4-9 Comparison between the FE model and experimental results

Test configuration	Beam N.o.	FE-model predictions			Experimental results			$\frac{DCA_{exp}}{DCA_{FE}}$	$\frac{\Delta w_{exp}}{\Delta w_{FE}}$	$\frac{F_{u,exp}}{F_{u,FE}}$
		DCA_{FE}	Δw_{FE} [mm]	$F_{u,FE}$ [kN]	DCA_{exp}	Δw_{exp} [mm]	$F_{u,exp}$ [kN]			
Config. 1	WB-2	0.9	3.66	176	0.9	4.07	163.00	1	1.11	0.93
	WB-3				0.88	4.35	163.20	0.98	1.19	0.93
	DB-2				0.94	-	37.56	1.04	-	-
	DB-3				0.88	4.28	90	0.98	1.17	-

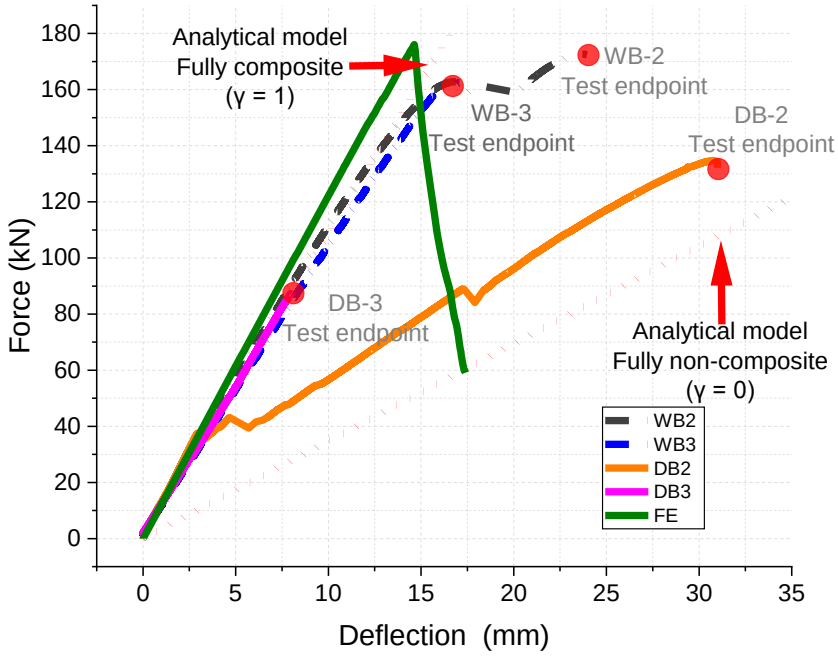

Fig. 4-13 Load and mid-span deflection response curves of tested TCC beams (config.1) vs. FE

4.3.8.2 Bending stress distribution

Fig. 4-14 presents the numerical strain distribution at the midspan of the TCC beams obtained from FE simulations. This visualization provides insights into how strains are distributed across the cross-section of the beams as they undergo different loading levels. The comparison between the FE results and the experimental data demonstrates a strong correspondence, particularly in the lower section of the beams. This alignment signifies a high level of agreement, providing confidence in the reliability and validity of the FE model to capture deformation, strain distribution, the interaction between timber and concrete, and overall load distribution.

The observed slight discrepancy in the strain distribution at the top of the concrete section could be attributed to several factors, such as composition, curing conditions, and material variability, that can influence concrete's behaviour. Suppose the properties used in the FE model do not precisely match the actual behaviour of the concrete used in the experiments. In that case, it can lead to some differences in strain distribution.

Comparing the bending stress distribution predictions from the analytical model (illustrated in **Fig. 4-3**) and the FE model, it becomes evident that the FE model offers results more closely aligned with the experimental test outcomes. The increased alignment between the FE model predictions and the experimental results suggests that the FE model considers a wider range of factors that influence the

structural behaviour of the TCC beams. This might include more precise material properties, a more accurate representation of the adhesive bond, and a more comprehensive consideration of load distribution effects.

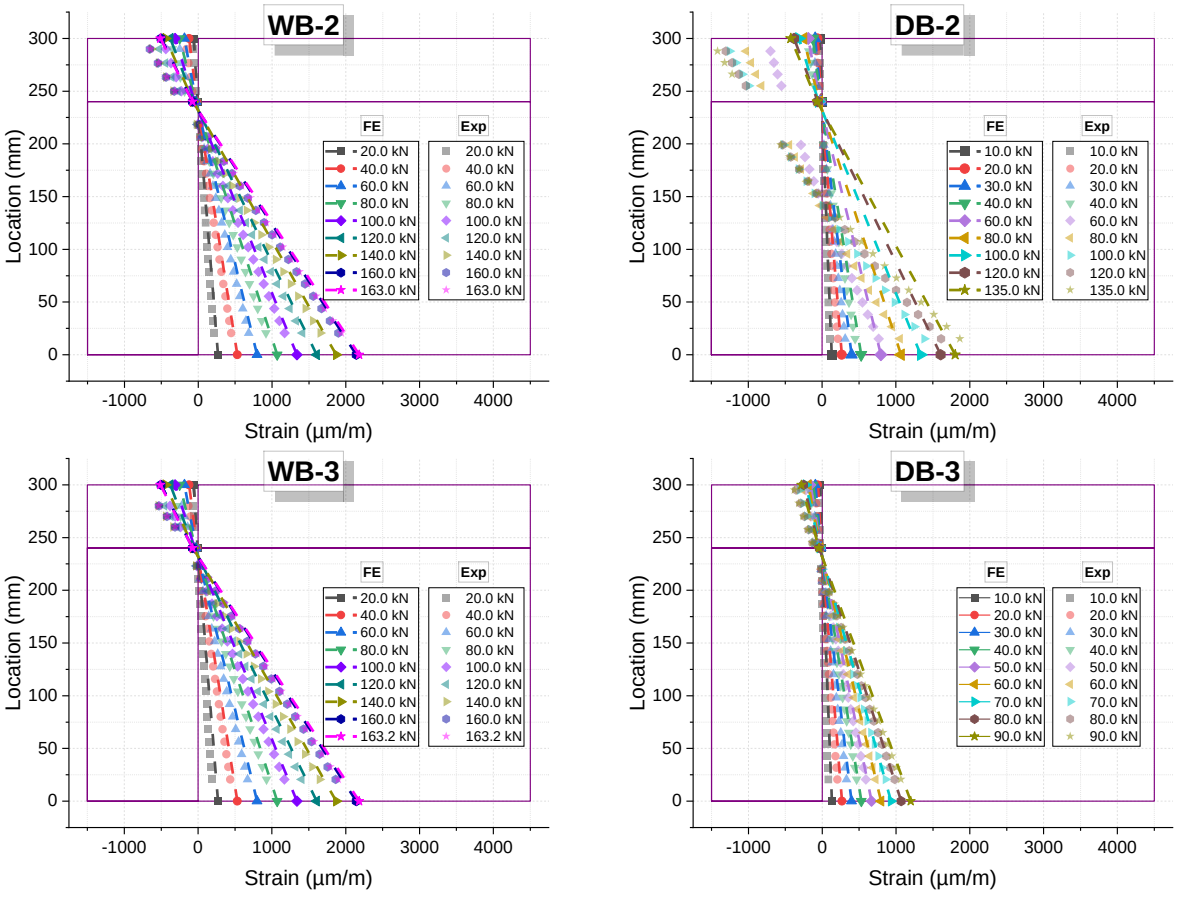

Fig. 4-14 Strain distribution at the mid-span of the TCC beams

4.3.8.3 Ultimate capacity

A validation procedure was undertaken for the FE model by comparing its predictions with the experimental results. Just as in the analytical model validation, the primary objective was to evaluate the accuracy and reliability of the FE model in capturing the behaviour of the TCC composite beams under varying loading conditions. The ultimate failure loads obtained from the experimental bending tests ($F_{u,exp}$) were compared with the corresponding failure loads calculated ($Fu,_{FE}$) using the FE model. This comparison assessed the FE model's capability to predict the beams' ultimate capacity and failure behaviour.

Similar to the analytical model validation, specific considerations were made in the comparison process. The dry TCC beams, which exhibited failures attributed primarily to the imperfect connection between timber and concrete components, were excluded from the comparison. The evaluation focused on the

performance of the FE model for the wet TCC beams, which displayed a more consistent and reliable behaviour.

The comparative analysis in **Table 4-9** between the experimental ultimate failure loads ($F_{u,exp}$) and the predicted failure loads ($F_{u,FE}$) using the FE model demonstrates promising results. This alignment is evident from the close ratio of 0.93, signifying a remarkable correspondence by a 7% deviation between the model's predicted failure loads and the average experimental results, validating its effectiveness in predicting their ultimate failure loads.

4.3.8.4 Failure modes

The validation process of the FE model, particularly in terms of failure modes, stands as a strong affirmation of its accuracy and reliability. The consistent correspondence between the failure modes predicted by the FE model and those observed in the experimental results serves as a vital validation criterion. The FE model effectively simulates the initiation and progression of failure modes, closely mirroring the actual behaviour exhibited by the adhesively bonded TCC beams during experimental testing.

In the experimental investigations, the presence of bottom cracks (in the neighborhood of knots) near the mid-span indicates localized tensile and bending stresses that may exceed the capacity of the timber component. Furthermore, the experience of horizontal cracks on the timber in the region between the support and loading point signifies the development of shear failure in the timber element, as depicted in **Fig. 4-15**.

Fig. 4-16 illustrates the beam's bending and shear stress distribution at the predicted ultimate capacity (e.g., 176 kN). Notably, the FE model correctly captures the sequence of failure initiation, starting with shear failure in the shear zone between the support and loading point, followed by bending failure at the bottom of the timber element, as shown in **Fig. 4-17**. These markers serve as precise positions where the timber element has reached its ultimate limit and experienced failure, according to the strength criteria expressed by Eq. (4.20). The absence of concrete failure indications in the FE model, consistent with the experimental results, further highlights the model's precision in simulating the composite action between the materials and their failure modes. This convergence between FE predictions and experimental outcomes underscores the model's capability to provide a comprehensive and reliable analysis of TCC beams' behaviour.

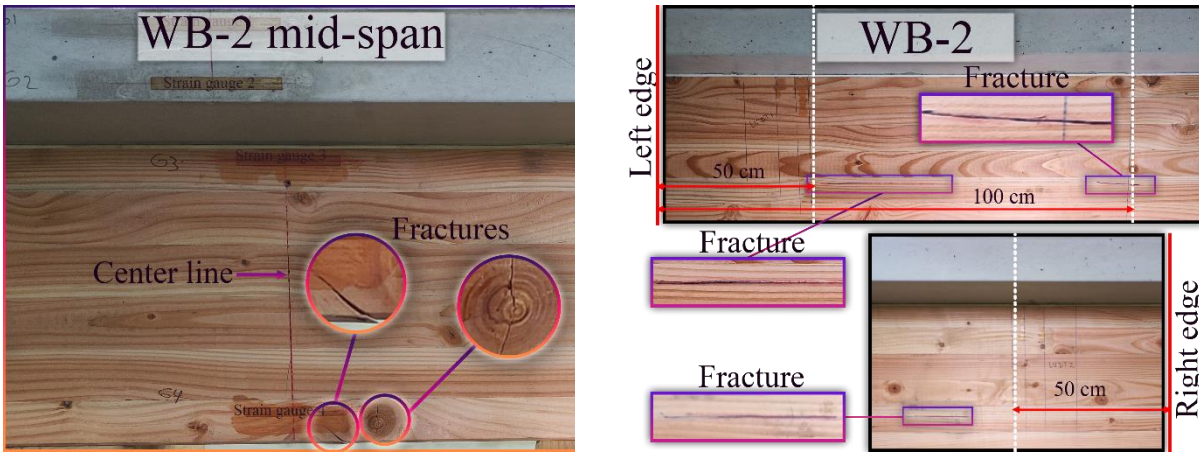

(a) (b)

Fig. 4-15 Failure mechanism in wet TCC beams, e.g., WB-2 at (a) mid-span and (b) beam edges

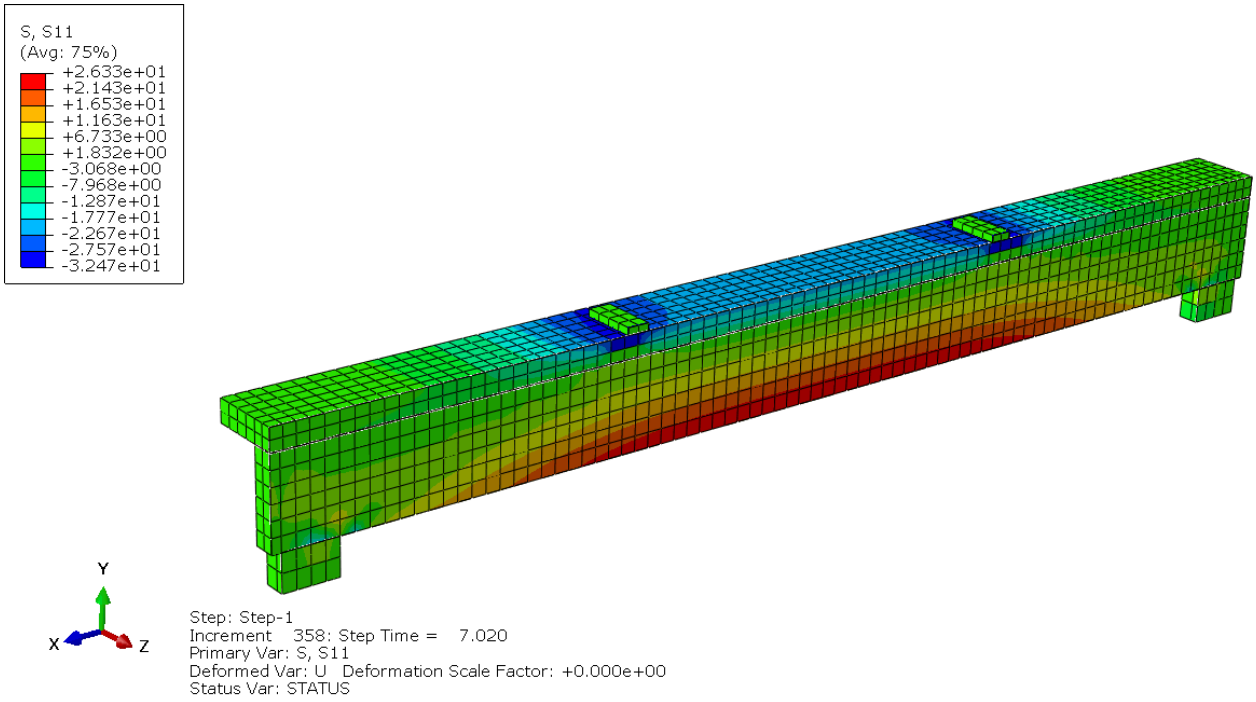

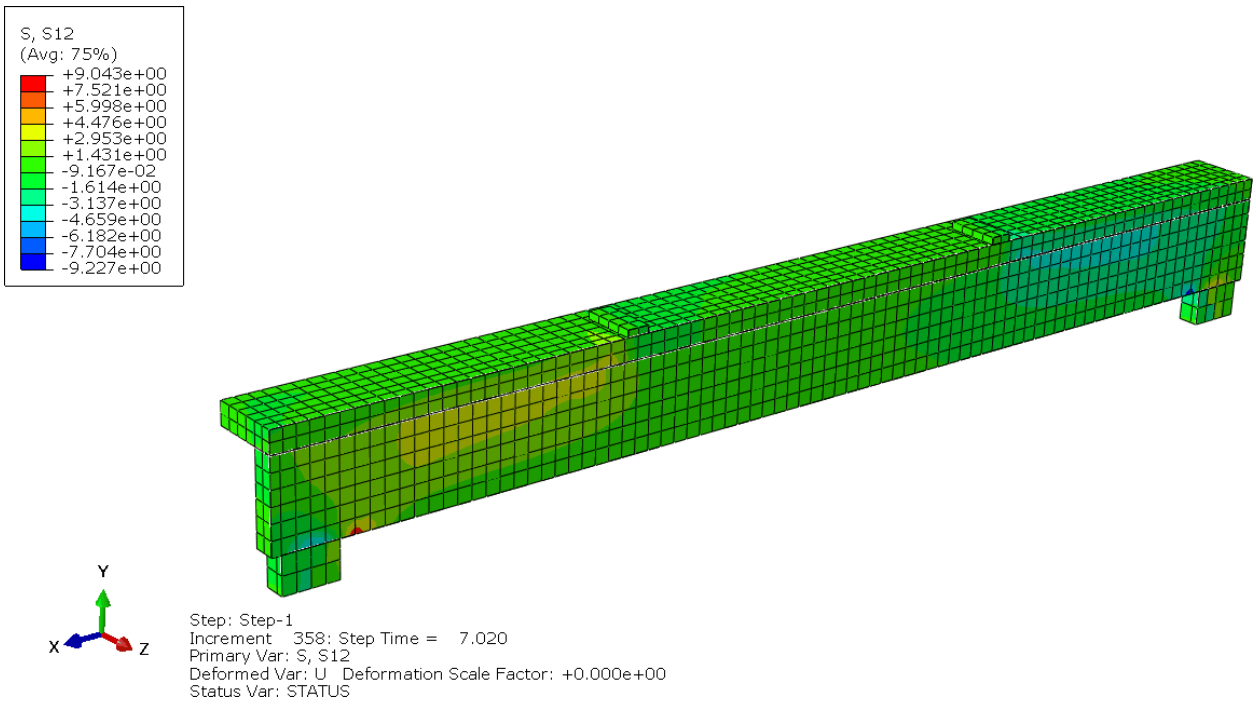

Fig. 4-16 Stress distribution derived from the 3D FE model_applied load is 176 kN

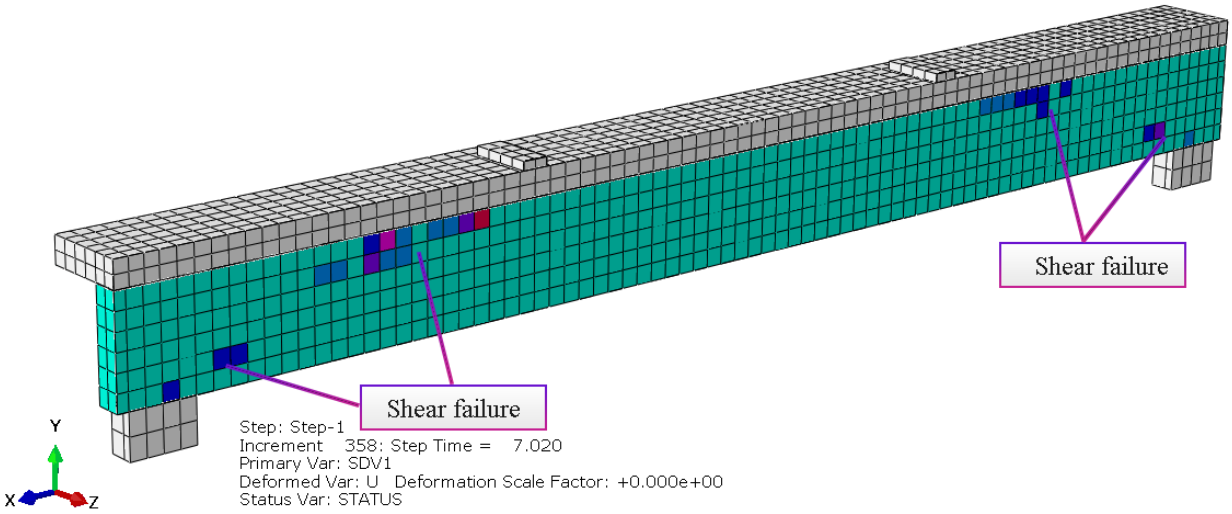

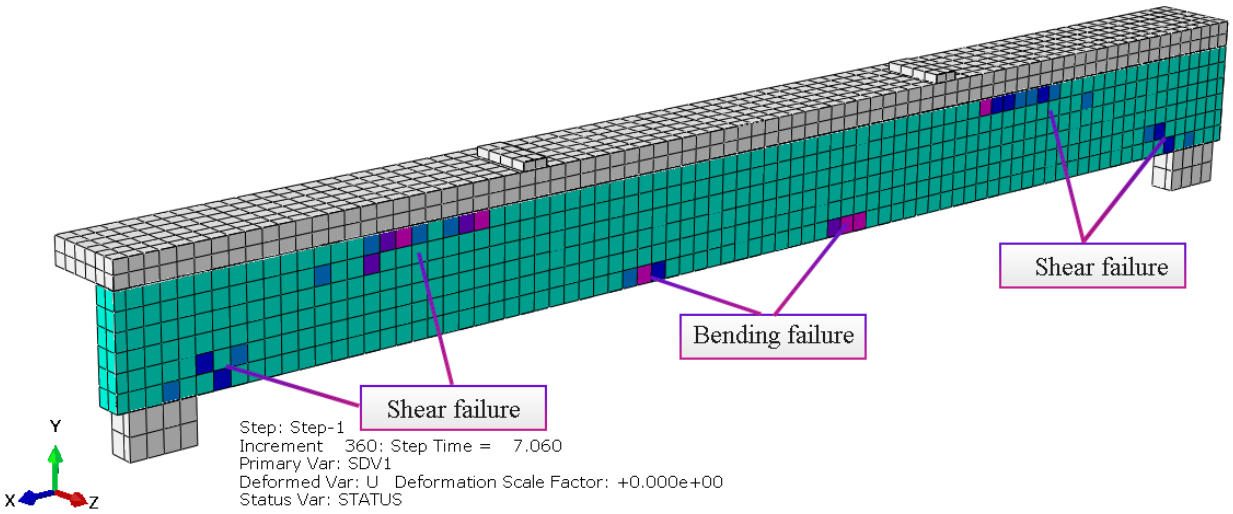

Fig. 4-17 Main failure modes derived from the 3D FE model_applied load1 is 176 kN

4.4 Summary

The Analytical modeling focuses on the accurate prediction and understanding of the behaviour of TCC beams using analytical methods. The γ-method from Eurocode 5 is introduced as a widely employed approach for evaluating TCC beams' behaviour. This method simplifies the analysis by considering two extreme limits of working conditions and provides essential insights into parameters like effective bending stiffness, maximum stresses, and deformation characteristics. The chapter presents the calculation of effective bending stiffness using a basic analytical beam model based on linear elasticity. This approach is suitable due to the rigid coupling of timber and concrete through the adhesive bond. Formulas are provided to calculate effective bending stiffness and maximum stresses on the components of the TCC beam, including concrete and timber, under various loading conditions. Various failure criteria are discussed to assess different types of failure, considering the loading conditions experienced by each material. The chosen static system and linear-elastic stress-strain relationships are integrated into the analytical model to predict potential failure modes and evaluate structural integrity. The prediction of the ultimate capacity is detailed, involving calculations of ultimate section forces and considering failure criteria separately. The analytical model's validity is tested through comparison with experimental results, with a focus on load-deflection responses, bending stress distributions, and load-bearing capacity. Despite some discrepancies between analytical predictions and experimental results, especially in specific loading configurations, the developed analytical model provides a practical and efficient tool for designing and analyzing adhesive-bonded TCC beams. The validation of the analytical model through a comparison with experimental results has highlighted its reliability and accuracy. The model successfully captures load-deflection responses, bending strain distributions, and ultimate failure loads, demonstrating its ability to predict the behaviour of

TCC beams. Moreover, incorporating shear deformations into the model has further improved the accuracy of load-deflection predictions, enhancing its practical applicability.

This chapter also presented a comprehensive analysis of adhesively bonded TCC beams through 3D non-linear FE modeling and a comparative analysis of the experimental results. The findings bring several significant insights and contributions to TCC structures. The 3D non-linear FE model developed for adhesively bonded TCC beams proved valuable for simulating and analyzing their behaviour. The model accurately predicted various structural responses, highlighting its effectiveness in capturing deformation behaviour, bending stress distribution, ultimate capacity, and failure characteristics. A noteworthy agreement is observed between the FE model predictions and experimental outcomes, particularly in the linear regimes of TCC beam behaviour. It emphasizes its capability to align with experimental measurements and predict the degree of composite action. Identifying a critical deviation point during bonding failure underscores the complex nature of TCC structures, where the performance is not exclusively determined by the inherent properties of timber and concrete but is highly influenced by the quality of the adhesive bond. The investigation into bending stress distribution reveals a strong correspondence between the FE simulations and experimental data, especially in the lower sections of the beams. However, slight divergences were observed in the strain distribution at the top of the concrete section. The FE model demonstrates remarkable alignment in predicting the ultimate capacity of wet TCC beams. Lastly, the FE model effectively captures the initiation and progression of failure modes in TCC beams. This precision in simulating the sequence of failure initiation, from shear failure to bending failure, confirms the reliability of the developed model.

General Conclusion

General Conclusion

1. Summary of the work done

The research conducted in this thesis has been primarily focused on investigating the mechanical behaviour and performance of adhesively bonded TCC joints and beams. Through a series of experimental tests, analytical modeling, and finite element (FE) simulations, valuable insights were gained into the durability, bonding performance, and structural behaviour of TCC joints and beams.

In order to achieve this objective, the following methodologies were implemented:

Experimental Tests:

The study began with exploring the bonding performance of wet and dry TCC joints. This investigation aimed to understand the impact of moisture content variation, adhesive type, adhesive thickness, surface treatment of concrete, and bonding scale effect on the shear strength and failure modes of TCC joints. To conduct this investigation, both cast-on-site and pre-fabricated concrete panels were utilized for bonding with central timber beams, resulting in wet and dry TCC joints. Several series of specimens were manufactured and tested to evaluate the effects of the mentioned parameters on the shear strength and failure modes of the joints. The test load with a parallel direction to the timber grains was performed on the top surface of the timber component, which was to be transferred by the two bonded interfaces between timber and concrete panels. During testing, linear voltage displacement transducer (LVDT) sensors were employed to measure the slip between the concrete and wood elements. Additionally, to enhance the analysis, the digital image correlation technique (DIC) was utilized for displacement analysis and simulating the strain field development on the surface of the specimens.

Following the investigation of bonding performance, an extensive experimental investigation on a 3.2 m span of adhesively bonded TCC beams was performed. This comprehensive study aimed to analyze the failure characteristics, interface slip, strain distribution, and load-deflection response of adhesively bonded TCC beams under a four-point bending configuration, as per EN 408 [83] standards. The manufacturing process of the TCC specimens involved two distinct fabrication methods: wet and dry processes. A total of six full-scale TCC beams were produced and labeled based on their fabrication process. During testing, strain gauges were strategically positioned within the concrete and timber components at the mid-span of the beams to capture and analyze strain distributions accurately. An LVDT sensor was employed to capture and quantify the slip occurring at the bonding interface between concrete and the wood components precisely. Additionally, an LVDT sensor was employed to determine the midspan deflection of the beam. Similar to the approach used in the Pushout tests, DIC was employed for displacement analysis, providing

insights into strain field development on the specimen's surface. This measurement technique enhanced the analysis by providing detailed information on strain variations, load response deflection along the beam, and slip behaviour at the bonding interface.

Analytical and Numerical Modeling:

The analytical modeling focuses on the accurate prediction and understanding of the behaviour of TCC beams using analytical methods. The primary aim was to develop a practical tool for designing and analyzing adhesive-bonded TCC beams. A basic analytical beam model based on linear elasticity, specifically the γ-method from Eurocode 5, was employed to calculate effective bending stiffness and maximum stresses on the concrete and timber components. The prediction of the ultimate capacity is detailed, involving calculations of ultimate section forces and considering failure criteria separately. To validate the analytical model, comparisons were made with experimental results, focusing on key parameters such as load-deflection responses, bending stress distributions, and load-bearing capacity. Through these comparisons, the reliability and accuracy of the analytical model were assessed.

Numerical modeling delves into a comprehensive analysis of adhesively bonded TCC beams through 3D non-linear finite element (FE) modeling using Abaqus software and comparative analysis with experimental results. The primary objective was to develop a detailed understanding of the behaviour and performance of TCC beams using advanced numerical simulations. The modeling methodology employed in **Chapter 4** combines theoretical frameworks, underlying assumptions, and data sources to develop and validate a 3D non-linear finite element (FE) model for adhesively bonded TCC beams. The validation process involves comparing simulated predictions with experimental outcomes, focusing on key parameters like load-deflection responses, bending strain distributions, and load-bearing capacity.

The primary results obtained from the research can be summarized as follows:

On experimental aspects:

Push-out shear test findings reveal adhesive bonding as a viable shear connector for both dry and wet TCC joints. In wet processes, Sikadur-53 and Sikadur-32EF epoxy resins showed satisfactory shear strengths of approximately 8.24 MPa and 6.38 MPa, respectively, at 12% timber moisture content and 1 mm adhesive layer thickness. Conversely, dry joints using Sikadur-330 and Sikadur-31EF achieved mean shear strengths of about 8 MPa under similar conditions. However, increasing timber moisture content before glueing significantly reduced bonding system performance, highlighting the need for moisture control and pre-bonding conditioning. Surprisingly, concrete sandblasting did not notably enhance connection strength, and sand addition caused a slight reduction in shear strength in most series.

Nevertheless, increasing the adhesive layer thickness to 3 mm enhanced shear strength, particularly in series with a high moisture content of the timber before glueing.

The investigation on adhesively bonded TCC beams emphasizes the significance of proper bonding techniques and material selection for TCC structures, showcasing the reliability of glue connections, especially in wet series. It reveals distinct failure modes in TCC beams, revealing adhesion failure in dry-fabricated beams due to imperfect connection, and identified contributing factors like shrinkage forces and oil residuals. Sandblasting is recommended to enhance adhesive bonding. Wet-fabricated TCC beams exhibit well-bonded connections and efficient load distribution. Strain distribution analysis confirms composite action effectiveness in wet beams. The comparative analysis highlights the advantageous positioning of our TCC cross-section design for sustainable construction.

On analytical and numerical aspects:

The developed analytical model serves as a practical and efficient tool for designing and analyzing adhesive-bonded TCC beams. The model successfully captures load-deflection responses, bending strain distributions, and ultimate failure loads. Incorporating shear deformations has improved the accuracy, enhancing its practical applicability.

The developed 3D nonlinear FE model for adhesively bonded TCC beams provided valuable insights into their behaviour. It accurately predicted structural responses such as deformation, bending stress distribution, ultimate capacity, and failure characteristics. The model demonstrated high agreement with experimental data, particularly in linear regimes of TCC beam behaviour, and effectively captured failure mode initiation and progression. Overall, the FE model proved to be a reliable tool for simulating TCC beam behaviour and can contribute to optimizing design and analysis processes in TCC structures.

2. Perspectives

Future studies can be proposed to continue this work:

On experimental aspects:

- Conducting shear and bending tests while considering the ageing effect of the connection induced by continuous or cyclic hydric loads over an extended period. This approach would provide valuable insights into the long-term performance and durability of adhesively bonded TCC joints and beams. By subjecting these connections to realistic environmental conditions over time, researchers can observe how the adhesive properties evolve and how the structural integrity of the joints and beams is affected.

- By conducting full-scale tests (> 9 m span) of adhesively bonded TCC beams with multiple timber joists, analyzing the response of the composite beams to different loads, and monitoring factors such as deflection, strain distribution, and failure modes, researchers can gain valuable insights into the behaviour of TCC structures in real-world applications.

On analytical and numerical aspects:

- Developing a predictive model for estimating the shear strength of adhesively bonded TCC joints based on the mechanical properties of the component materials is essential. Such a model would eliminate the need for conducting pushout tests, providing a convenient and efficient means of assessing adhesive performance. The model can accurately predict shear strength by utilizing material properties, including timber and concrete characteristics and adhesive properties. This tool would streamline the adhesive selection process, allowing designers to choose the most suitable adhesive from a wide range of options available in the market.
- Conducting a parametric study to investigate the effect of changing material properties and specimen design details on the response of adhesively bonded TCC specimens is essential. This study will analyze the influence of changing concrete grade and timber elastic modulus and grade on the behaviour of these specimens. By systematically varying these parameters and observing their impact on factors such as load-bearing capacity, stiffness, and failure modes, researchers can gain valuable insights into the optimal material selection and design considerations for enhancing the performance and durability of TCC structures.
- Utilize the complete 3D model to analyze additional full-scale TCC structures and evaluate the model's performance against the obtained results. This comprehensive analysis will validate the model's predictive capabilities and enhance confidence in its use for future design and optimization of TCC structures.
- Conduct a comprehensive investigation into the long-term behaviour of TCC structures, integrating factors such as material creep properties and adhesive ageing. By incorporating these considerations into the calculations, researchers can more accurately estimate the structural lifespan and assess potential degradation mechanisms over time.

References

References

[1] The key role of forest and landscape restoration in climate action, 2022. https://doi.org/10.4060/cc2510en.

[2] P. Quintana Gallo, D.M. Carradine, R. Bazaez, State of the art and practice of seismic-resistant hybrid timber structures, Eur. J. Wood Wood Prod. 79 (2021) 5–28. https://doi.org/10.1007/s00107-020-01556-3.

[3] A. Ceccotti, Composite concrete-timber structures, Prog. Struct. Eng. Mater. 4 (2002) 264–275. https://doi.org/10.1002/pse.126.

[4] D. Yeoh, M. Fragiacomo, B. Deam, Experimental behaviour of LVL-concrete composite floor beams at strength limit state, Eng. Struct. 33 (2011) 2697–2707. https://doi.org/10.1016/j.engstruct.2011.05.021.

[5] Q. Fu, L. Yan, T. Ning, B. Wang, B. Kasal, Interfacial bond behavior between wood chip concrete and engineered timber glued by various adhesives, Constr. Build. Mater. 238 (2020) 117743. https://doi.org/10.1016/j.conbuildmat.2019.117743.

[6] T. Ghanbari Ghazijahani, H. Jiao, D. Holloway, Composite Timber Beams Strengthened by Steel and CFRP, J. Compos. Constr. 21 (2017) 1–11. https://doi.org/10.1061/(asce)cc.1943-5614.0000714.

[7] T. Tannert, B. Endacott, M. Brunner, T. Vallée, Long-term performance of adhesively bonded timber-concrete composites, Int. J. Adhes. Adhes. 72 (2017) 51–61. https://doi.org/10.1016/j.ijadhadh.2016.10.005.

[8] M.L.R. van der Linden, H.J. Blass, Timber-concrete composite floor systems, Doctoral Thesis, Delft University Press, 1996. https://repository.tudelft.nl/view/tno/uuid:5d7420d0-1e28-4491-8a70-e8cf17a480ac.

[9] P. Müller, Patent DE334431C: Decke aus hochkantig stehenden Holzbohlen oder Holzbrettern und Betondeckschicht, Patentschau Aus Dem Betonbau Und Den Damit Verwandten Gebieten. Auszuge Aus Den Patentschriften. Bet. Und Eisen, H. XVII, S 244 (1921).

[10] J. Poštulka, Holz-Beton-Verbunddecken, 36 Jahre Erfahrung". Bautecknic 74., (1997).

[11] A.M.P.G. Dias, Mechanical behaviour of timber-concrete joints. PhD thesis, University of Coimbra Portugal, 2005.

[12] Rilem TC111 CST, Behaviour of timber concrete composite load-bearing structures. Proceedings of ACMAR-Ravenna International Symposium, Dept. of Civil Engineering, University of Florence, Italy., (1992).

[13] M. Natterer, J., Herzog, T., and Volz, Construire en Bois 2. 2nd edition, Presses polytechniques et universitaires romandes, Switzerland., (1998).

[14] U. Kuhlmann, J. Schänzlin, Grooves as shear connectors for timber-concrete composite decks, Proc., RILEM Conf. Joints Timber Struct. (2001) 283–290.

[15] E. Baas, M. Riggio, A.R. Barbosa, I. Mugabo, E.J. Baas, E.L. Schmidt, Living Lab at Peavy Hall: Structural Health Monitoring of Mass Timber Buildings, Shatis (2019). https://www.researchgate.net/publication/338612314.

[16] D. Yeoh, M. Fragiacomo, M. De Franceschi, K. Heng Boon, State of the Art on Timber-Concrete

Composite Structures: Literature Review, J. Struct. Eng. 137 (2011) 1085–1095. https://doi.org/10.1061/(asce)st.1943-541x.0000353.

[17] BSI, BS EN 1995-1-1: 2004+ A2: 2014. Eurocode 5: Design of timber structures–Part 1–1: General–Common rules and rules for buildings, (2014). https://doi.org/10.3403/03174906U.

[18] A. Ceccotti, Composite concrete-timber structures, Prog. Struct. Eng. Mater. 4 (2002) 264–275. https://doi.org/10.1002/pse.126.

[19] M. Fragiacomo, A. Ceccotti, Long-Term Behavior of Timber–Concrete Composite Beams. I: Finite Element Modeling and Validation, J. Struct. Eng. 132 (2006) 13–22. https://doi.org/10.1061/(asce)0733-9445(2006)132:1(13).

[20] M. Fragiacomo, J. Schänzlin, Proposal to Account for Concrete Shrinkage and Environmental Strains in Design of Timber-Concrete Composite Beams, J. Struct. Eng. 139 (2013) 162–167. https://doi.org/10.1061/(asce)st.1943-541x.0000605.

[21] S.T. Deresa, J. Xu, C. Demartino, G. Minafò, G. Camarda, Static Performances of Timber- and Bamboo-Concrete Composite Beams: A Critical Review of Experimental Results, Open Constr. Build. Technol. J. 15 (2021) 17–54. https://doi.org/10.2174/1874836802115010017.

[22] A. Dias, Design of timber-concrete composite structures: A state-of-the-art report by COST Action FP1402/WG 4, 2018.

[23] R.W. Horobin, Theory of staining and its practical implications, Theory Pract. Histol. Tech. (2002) 109–138.

[24] S. Bharti, Adhesives and Adhesion Technologies: A Critical Review, Am. J. Polym. Sci. Technol. 4 (2018) 36. https://doi.org/10.11648/j.ajpst.20180401.13.

[25] S. Ebnesajjad, A.H. Landrock, Adhesives Technology Handbook, 2014. https://doi.org/10.1016/B978-0-323-35595-7.00023-1.

[26] P. Cognard, Handbook of Adhesives and Sealants: Volume 1, McGraw-Hill Education, 2005. http://www.sciencedirect.com/science/article/pii/S1874569502800045%5Cnhttp://linkinghub.elsevier.com/retrieve/pii/S1874569502800045.

[27] R.A. Pethrick, Design and ageing of adhesives for structural adhesive bonding-A review, Proc. Inst. Mech. Eng. Part L J. Mater. Des. Appl. 229 (2015) 349–379. https://doi.org/10.1177/1464420714522981.

[28] J. Michels, R. Widmann, C. Czaderski, R. Allahvirdizadeh, M. Motavalli, Glass transition evaluation of commercially available epoxy resins used for civil engineering applications, Compos. Part B Eng. 77 (2015) 484–493. https://doi.org/10.1016/j.compositesb.2015.03.053.

[29] M. Brunner, M. Romer, M. Schnüriger, Timber-concrete-composite with an adhesive connector (wet on wet process), Mater. Struct. Constr. 40 (2007) 119–126. https://doi.org/10.1617/s11527-006-9154-4.

[30] L. Barral, J. Cano, J. Lopez, I. Lopez-Bueno, P. Nogueira, M.J. Abad, C. Ramirez, Physical aging of an epoxy/cycloaliphatic amine resin, Eur. Polym. J. 35 (1999) 403–411. https://doi.org/10.1016/S0014-3057(98)00132-3.

[31] D. Cangialosi, Physical Aging of Polymers, 2018. https://doi.org/10.1002/0471440264.pst015.pub2.

[32] J.M. Hutchinson, Physical aging of polymers, Prog. Polym. Sci. 20 (1995) 703–760.

https://doi.org/10.1016/0079-6700(94)00001-I.

[33] P. Nogueira, C. Ramírez, A. Torres, M.J. Abad, J. Cano, J. López, I. López-Bueno, L. Barral, Effect of water sorption on the structure and mechanical properties of an epoxy resin system, J. Appl. Polym. Sci. 80 (2001) 71–80. https://doi.org/10.1002/1097-4628(20010404)80:1<71::AID-APP1077>3.0.CO;2-H.

[34] S. Chataigner, M. Rabasse, M. Quiertant, K. Benzarti, C. Aubagnac, Durability of adhesively bonded composite reinforcements for concrete structures, in: 3rd Int. Fib Congr. Exhib. Inc. PCI Annu. Conv. Bridg. Conf. Think Glob. Build Locally, Proc., 2010: p. sp.

[35] M. Miravalles, I.I.P. Dharmawan, The creep behaviour of adhesives A numerical and experimental investigation, (2007) 100.

[36] J. Custódio, J. Broughton, H. Cruz, A review of factors influencing the durability of structural bonded timber joints, Int. J. Adhes. Adhes. 29 (2009) 173–185. https://doi.org/10.1016/j.ijadhadh.2008.03.002.

[37] J.R.J. Wingfield, Treatment of composite surfaces for adhesive bonding, Int. J. Adhes. Adhes. 13 (1993) 151–156. https://doi.org/10.1016/0143-7496(93)90036-9.

[38] G. Critchlow, General introduction to surface treatments, 2018. https://doi.org/10.1007/978-3-319-55411-2_7.

[39] BSI, BS EN 26891:1991 Timber structures. Joints made with mechanical fasteners. General principles for the determination of strength and deformation characteristics, (1991). https://doi.org/10.3403/00248652.

[40] G. Youssef, L. Loulou, S. Chataigner, S. Caré, A. Flety, R. Le Roy, M. Bornert, C. Aubagnac, Analysis of the behaviour of a bonded joint between laminated wood and ultra high performance fibre reinforced concrete using push-out test, Constr. Build. Mater. 53 (2014) 381–391. https://doi.org/10.1016/j.conbuildmat.2013.10.074.

[41] J.H.J. de O. Negrão, C.A. Leitão de Oliveira, F.M. Maia de Oliveira, P.B. Cachim, Glued Composite Timber-Concrete Beams. I: Interlayer Connection Specimen Tests, J. Struct. Eng. 136 (2010) 1236–1245. https://doi.org/10.1061/(ASCE)ST.1943-541X.0000228.

[42] J.H. Negrão, F.M. Oliveira, C.L. Oliveira, Investigation on timber-concrete glued composites, 9th World Conf. Timber Eng. 2006, WCTE 2006 1 (2006) 327–334.

[43] P. Clouston, L.A. Bathon, A. Schreyer, Shear and Bending Performance of a Novel Wood–Concrete Composite System, J. Struct. Eng. 131 (2005) 1404–1412. https://doi.org/10.1061/(asce)0733-9445(2005)131:9(1404).

[44] J. Pault, R. Gutkowski, Composite action in glulam timber bridge systems. Structural Research Report No. 17B, Colorado State University, Civil Engineering Department, 1977.

[45] V. Monier, G. Duchanois, J.C. Bignon, Optimized generation of non-standard wood structures based on native irregular components, Struct. Archit. New Concepts, Appl. Challenges (2013) 2209–2216. https://doi.org/10.1201/b15267-303.

[46] M. Ballerini, R. Crocetti, M. Piazza, An experimental investigation on notched connections for timber-concrete composite structures, 7th World Conf. Timber Eng. (2002) 171–178.

[47] S.R.S. Monteiro, A.M.P.G. Dias, J.H.J.O. Negrão, Assessment of timber-concrete connections made with glued notches: Test set-up and numerical modeling, Exp. Tech. 37 (2013) 50–65.

https://doi.org/10.1111/j.1747-1567.2011.00804.x.

[48] E.P. Carvalho, E.V.M. Carrasco, Influence of test specimen on experimental characterization of timber-concrete composite joints, Constr. Build. Mater. 24 (2010) 1313–1322. https://doi.org/10.1016/j.conbuildmat.2009.12.036.

[49] G. He, L. Xie, X. (Alice) Wang, J. Yi, L. Peng, Z. Chen, P.J. Gustafsson, R. Crocetti, Shear Behavior Study on Timber-Concrete Composite Structures with Bolts, BioResources 11 (2016) 9205–9218. https://doi.org/10.15376/biores.11.4.9205-9218.

[50] N. Khorsandnia, H.R. Valipour, K. Crews, Experimental and analytical investigation of short-term behaviour of LVL-concrete composite connections and beams, Constr. Build. Mater. 37 (2012) 229–238. https://doi.org/10.1016/j.conbuildmat.2012.07.022.

[51] W. Sebastian, S. Thompson, Indicative comparisons between bonded and dowelled hardwood studs for limecrete-spruce connections under load-unload-reload double-shear testing, Eng. Struct. 45 (2012) 151–165. https://doi.org/10.1016/j.engstruct.2012.06.008.

[52] P. Gelfi, E. Giuriani, Behaviour of stud connectors in wood-concrete composite beams, Struct. Stud. Repairs Maint. Hist. Build. Vi 6 (1999) 565-578\r907. https://www.witpress.com/elibrary/wit-transactions-on-the-built-environment/42/5645.

[53] A. Ceccotti, M. Fragiacomo, S. Giordano, Behaviour of a timber-concrete composite beam with glued connection at strength limit state, 9th World Conf. Timber Eng. 2006, WCTE 2006 1 (2006) 343–350.

[54] S.C. Auclair, L. Sorelli, A. Salenikovich, A new composite connector for timber-concrete composite structures, Constr. Build. Mater. 112 (2016) 84–92. https://doi.org/10.1016/j.conbuildmat.2016.02.025.

[55] L. Kozarić, D. Kukaras, A. Prokić, M. Bešević, M. Kekanović, Slip modulus of screws in timber and lightweight concrete composite structures, BioResources 13 (2018) 6021–6032. https://doi.org/10.15376/biores.13.3.6021-6032.

[56] M. Oudjene, E.M. Meghlat, H. Ait-Aider, J.L. Batoz, Non-linear finite element modelling of the structural behaviour of screwed timber-to-concrete composite connections, Compos. Struct. 102 (2013) 20–28. https://doi.org/10.1016/j.compstruct.2013.02.007.

[57] J.M. Branco, P.J.S. Cruz, M. Piazza, Experimental analysis of laterally loaded nailed timber-to-concrete connections, Constr. Build. Mater. 23 (2009) 400–410. https://doi.org/10.1016/j.conbuildmat.2007.11.011.

[58] E. Steinberg, R. Selle, T. Faust, Connectors for Timber–Lightweight Concrete Composite Structures, J. Struct. Eng. 129 (2003) 1538–1545. https://doi.org/10.1061/(asce)0733-9445(2003)129:11(1538).

[59] Y. Jiang, W. Hong, X. Hu, R. Crocetti, L. Wang, W. Sun, Early-age performance of lag screw shear connections for glulam-lightweight concrete composite beams, Constr. Build. Mater. 151 (2017) 36–42. https://doi.org/10.1016/j.conbuildmat.2017.06.063.

[60] W.M. Sebastian, M. Piazza, T. Harvey, T. Webster, Forward and Reverse shear transfer in beech LVL-concrete composites with singly inclined coach screw connectors, Eng. Struct. 175 (2018) 231–244. https://doi.org/10.1016/j.engstruct.2018.06.070.

[61] B.H. Ahmadi, M.P. Saka, Behavior of Composite Timber-Concrete Floors, J. Struct. Eng. 119 (1993) 3111–3130. https://doi.org/10.1061/(ASCE)0733-9445(1993)119:11(3111).

[62] U. Meierhofer, A Timber/Concrete Composite System, Struct. Eng. Int. 3 (1993) 104–107. https://doi.org/10.2749/101686693780612529.

[63] M.F. Benítez, Development and testing of timber / concrete shear connectors, 51st Int. Conv. Pof Soc. Wood Sci. Technol. (2008) 1–13.

[64] R.M. Gutkowski, K. Brown, A. Shigidi, J. Natterer, Investigation of Notched Composite Wood–Concrete Connections, J. Struct. Eng. 130 (2004) 1553–1561. https://doi.org/10.1061/(asce)0733-9445(2004)130:10(1553).

[65] B.L. Deam, M. Fragiacomo, A.H. Buchanan, Connections for composite concrete slab and LVL flooring systems, Mater. Struct. Constr. 41 (2008) 495–507. https://doi.org/10.1617/s11527-007-9261-x.

[66] D. Yeoh, M. Fragiacomo, A. Buchanan, C. Gerber, Preliminary research towards a semi-prefabricated LVL-concrete composite floor system for the Australasian market, Aust. J. Struct. Eng. 9 (2009) 225–240. https://doi.org/10.1080/13287982.2009.11465025.

[67] D.D. Djoubissie, A. Messan, E. Fournely, A. Bouchaïr, Experimental study of the mechanical behavior of timber-concrete shear connections with threaded reinforcing bars, Eng. Struct. 172 (2018) 997–1010. https://doi.org/10.1016/j.engstruct.2018.06.084.

[68] S. Hehl, T. Tannert, R. Meena, T. Vallee, Experimental and Numerical Investigations of Groove Connections for a Novel Timber-Concrete-Composite System, J. Perform. Constr. Facil. 28 (2014). https://doi.org/10.1061/(asce)cf.1943-5509.0000549.

[69] R. Gutkowski, K. Brown, A. Shigidi, J. Natterer, Laboratory tests of composite wood-concrete beams, Constr. Build. Mater. 22 (2008) 1059–1066. https://doi.org/10.1016/j.conbuildmat.2007.03.013.

[70] M. Fragiacomo, R.M. Gutkowski, J. Balogh, R.S. Fast, Long-Term Behavior of Wood-Concrete Composite Floor/Deck Systems with Shear Key Connection Detail, J. Struct. Eng. 133 (2007) 1307–1315. https://doi.org/10.1061/(asce)0733-9445(2007)133:9(1307).

[71] P. Clouston, S. Civjan, L. Bathon, Experimental behavior of a continuous metal connector for a wood-concrete composite system, For. Prod. J. 54 (2004) 76–84.

[72] D. Otero-Chans, J. Estévez-Cimadevila, F. Suárez-Riestra, E. Martín-Gutiérrez, Experimental analysis of glued-in steel plates used as shear connectors in Timber-Concrete-Composites, Eng. Struct. 170 (2018) 1–10. https://doi.org/10.1016/j.engstruct.2018.05.062.

[73] M. Smilovic, D. Cubela, J. Radnic, A. Harapin, Experimental testing of wood-concrete and steel-concrete composite elements in comparison with numerical testing, Materwiss. Werksttech. 44 (2013) 562–570. https://doi.org/10.1002/mawe.201300026.

[74] Q. Fu, L. Yan, N.A. Thielker, B. Kasal, Effects of concrete type, concrete surface conditions and wood species on interfacial properties of adhesively-bonded timber – Concrete composite joints, Int. J. Adhes. Adhes. 107 (2021) 39–43. https://doi.org/10.1016/j.ijadhadh.2021.102859.

[75] J. Frohnmüller, J. Fischer, W. Seim, Full-scale testing of adhesively bonded timber-concrete composite beams, Mater. Struct. Constr. 54 (2021). https://doi.org/10.1617/s11527-021-01766-y.

[76] Q. Fu, L. Yan, B. Kasal, Testing methods for shear strength of bond line between concrete and different types of engineered wood, Int. J. Adhes. Adhes. 102 (2020) 102671. https://doi.org/10.1016/j.ijadhadh.2020.102671.

[77] A. Nemati Giv, Q. Fu, L. Yan, B. Kasal, Interfacial bond strength of epoxy and PUR adhesively bonded timber-concrete composite joints manufactured in dry and wet processes, Constr. Build. Mater. 311 (2021) 125356. https://doi.org/10.1016/j.conbuildmat.2021.125356.

[78] J. Kanócz, V.V. Bajzecerová, Timber - Concrete composite elements with various composite connections part 3: Adhesive connection, Wood Res. 60 (2015) 939–952.

[79] BSI, BS EN 392:1995 Glued laminated timber. Shear test of glue lines, (1995).

[80] Q. Fu, L. Yan, N.A. Thielker, B. Kasal, Effects of concrete type, concrete surface conditions and wood species on interfacial properties of adhesively-bonded timber – Concrete composite joints, Int. J. Adhes. Adhes. 107 (2021). https://doi.org/10.1016/j.ijadhadh.2021.102859.

[81] K. Kong, E. Ferrier, L. Michel, A. Agbossou, Experimental and analytical study of the mechanical behavior of heterogeneous glulam-UHPFRC beams assembled by bonding: Short- and long-term investigations, Constr. Build. Mater. 100 (2015) 136–148. https://doi.org/10.1016/j.conbuildmat.2015.09.022.

[82] E. Augeard, L. Michel, E. Ferrier, Experimental and analytical study of the mechanical behavior of heterogeneous glulam–concrete beams and panels assembled by a specific treatment of wood, Constr. Build. Mater. 191 (2018) 812–825. https://doi.org/10.1016/j.conbuildmat.2018.10.038.

[83] BSI, BS EN 408:2010+A1:2012 Timber structures. Structural timber and glued laminated timber. Determination of some physical and mechanical properties, 2011. https://doi.org/doi.org/10.3403/30159970.

[84] J.H.J. de O. Negrão, F.M. Maia de Oliveira, C.A. Leitão de Oliveira, P.B. Cachim, Glued Composite Timber-Concrete Beams.II: Analysis and Tests of Beam Specimens, J. Struct. Eng. 136 (2010) 1246–1254. https://doi.org/10.1061/(ASCE)ST.1943-541X.0000251.

[85] A. Ceccotti, M. Fragiacomo, S. Giordano, Long-term and collapse tests on a timber-concrete composite beam with glued-in connection, Mater. Struct. Constr. 40 (2007) 15–25. https://doi.org/10.1617/s11527-006-9094-z.

[86] A. Ceccotti, Timber-concrete composite structures, Timber Eng. Step 2 (1995) E13.

[87] M. Fragiacomo, Long-Term Behavior of Timber–Concrete Composite Beams. II: Numerical Analysis and Simplified Evaluation, J. Struct. Eng. 132 (2006) 23–33. https://doi.org/10.1061/(asce)0733-9445(2006)132:1(23).

[88] E. Augeard, E. Ferrier, L. Michel, Mechanical behavior of timber-concrete composite members under cyclic loading and creep, Eng. Struct. 210 (2020) 110289. https://doi.org/10.1016/j.engstruct.2020.110289.

[89] N. Khorsandnia, H. Valipour, S. Foster, K. Crews, A force-based frame finite element formulation for analysis of two- and three-layered composite beams with material non-linearity, Int. J. Non. Linear. Mech. 62 (2014) 12–22. https://doi.org/10.1016/j.ijnonlinmec.2014.02.001.

[90] E. Lukaszewska, M. Fragiacomo, H. Johnsson, Laboratory Tests and Numerical Analyses of Prefabricated Timber-Concrete Composite Floors, J. Struct. Eng. 136 (2010) 46–55. https://doi.org/10.1061/(asce)st.1943-541x.0000080.

[91] A. Frangi, M. Fontana, Elasto-Plastic Model for Timber-Concrete Composite, Struct. Eng. Int. 1 (2003) 47–57.

[92] C. Zhang, P. Gauvreau, Timber-Concrete Composite Systems with Ductile Connections, J. Struct.

Eng. 141 (2015) 1–12. https://doi.org/10.1061/(asce)st.1943-541x.0001144.

[93] H. Tao, H. Yang, J. Zhang, G. Ju, J. Xu, B. Shi, Nonlinear finite element analysis on timber-concrete composite beams, J. Build. Eng. 51 (2022) 104259. https://doi.org/10.1016/j.jobe.2022.104259.

[94] M. Fragiacomo, A finite element model for long-term analysis of timber-concrete composite beams, Struct. Eng. Mech. 20 (2005) 173–189. https://doi.org/10.12989/sem.2005.20.2.173.

[95] M. Fragiacomo, Experimental behaviour of a full-scale timber-concrete composite floor with mechanical connectors, Mater. Struct. Constr. 45 (2012) 1717–1735. https://doi.org/10.1617/s11527-012-9869-3.

[96] R. Crocetti, T. Sartori, R. Tomasi, Innovative Timber-Concrete Composite Structures with Prefabricated FRC Slabs, J. Struct. Eng. 141 (2015) 1–10. https://doi.org/10.1061/(asce)st.1943-541x.0001203.

[97] P. Agel, K. Klajmonová, A. Lokaj, R. Fojtík, Carrying Capacity of Semi-Rigid Joint of Timber-Concrete Beams, in: Proc. 2015 Int. Conf. Mater. Environ. Biol. Eng., Atlantis Press, 2015: pp. 301–305. https://doi.org/10.2991/mebe-15.2015.72.

[98] S.R.S. Monteiro, A.M.P.G. Dias, S.M.R. Lopes, Bi-dimensional numerical modeling of timber–concrete slab-type structures, Mater. Struct. Constr. 48 (2015) 3391–3406. https://doi.org/10.1617/s11527-014-0407-3.

[99] M. Fragiacomo, J. Balogh, L. To, R.M. Gutkowski, Three-Dimensional Modeling of Long-Term Structural Behavior of Wood-Concrete Composite Beams, J. Struct. Eng. 140 (2014) A4014006. https://doi.org/10.1061/(asce)st.1943-541x.0000909.

[100] Y. Wei, Z. Wang, S. Chen, K. Zhao, K. Zheng, Structural behavior of prefabricated bamboo-lightweight concrete composite beams with perforated steel plate connectors, Arch. Civ. Mech. Eng. 21 (2021) 1–21. https://doi.org/10.1007/s43452-021-00176-9.

[101] M. Oudjene, E.M. Meghlat, H. Ait-Aider, P. Lardeur, M. Khelifa, J.L. Batoz, Finite element modelling of the nonlinear load-slip behaviour of full-scale timber-to-concrete composite T-shaped beams, Compos. Struct. 196 (2018) 117–126. https://doi.org/10.1016/j.compstruct.2018.04.079.

[102] C. O'Loinsigh, M. Oudjene, E. Shotton, A. Pizzi, P. Fanning, Mechanical behaviour and 3D stress analysis of multi-layered wooden beams made with welded-through wood dowels, Compos. Struct. 94 (2012) 313–321. https://doi.org/10.1016/j.compstruct.2011.08.029.

[103] M. Shehada, Z.I. Djamaï, F. Duprat, Investigation of the behaviour of adhesively bonded joints between timber and self-compacting concrete, Eur. J. Environ. Civ. Eng. 0 (2023) 1–22. https://doi.org/10.1080/19648189.2023.2276132.

[104] T. Vallée, T. Tannert, S. Fecht, Adhesively bonded connections in the context of timber engineering–A Review, J. Adhes. 93 (2017) 257–287. https://doi.org/10.1080/00218464.2015.1071255.

[105] A. Nemati Giv, Q. Fu, L. Yan, B. Kasal, The effect of adhesive amount and type on failure mode and shear strength of glued timber-concrete joints, Constr. Build. Mater. 345 (2022) 128375. https://doi.org/10.1016/j.conbuildmat.2022.128375.

[106] BSI, Eurocode 4 : Design of composite steel and concrete structures - BS EN 1994-1-1:2004, 3 (2009). https://doi.org/10.3403/BSEN1994-1.

[107] Y. Sousseau, M. Chaplain, S.M. Elachachi, T. Catterou, C. Faye, P. Garcia, Timber connection

behaviour characterisation based on similitude laws, Eur. J. Environ. Civ. Eng. (2023) 1–21. https://doi.org/10.1080/19648189.2023.2206886.

[108] BSI, BS EN 1992-1-1:2004 Eurocode 2: Design of concrete structures. General rules and rules for buildings, (2004). https://doi.org/10.3403/03178016.

[109] L. Eisenhut, W. Seim, S. Kühlborn, Adhesive-bonded timber-concrete composites – Experimental and numerical investigation of hygrothermal effects, Eng. Struct. 125 (2016) 167–178. https://doi.org/10.1016/j.engstruct.2016.05.056.

[110] M. Shehada, Z.I. Djamaï, F. Duprat, Experimental investigation on adhesively bonded timber-self-compacting concrete composite beams with a thin slab, Eng. Struct. 309 (2024) 118108. https://doi.org/10.1016/j.engstruct.2024.118108.

[111] L. Tupenaite, L. Kanapeckiene, J. Naimaviciene, A. Kaklauskas, T. Gecys, Timber Construction as a Solution to Climate Change: A Systematic Literature Review, Buildings 13 (2023). https://doi.org/10.3390/buildings13040976.

[112] J. Jussila, E. Nagy, K. Lähtinen, E. Hurmekoski, L. Häyrinen, C. Mark-Herbert, A. Roos, R. Toivonen, A. Toppinen, Wooden multi-storey construction market development – systematic literature review within a global scope with insights on the Nordic region, Silva Fenn. 56 (2022). https://doi.org/10.14214/sf.10609.

[113] M. Schäfers, W. Seim, Development of adhesive bonded timber-UHPC composites - Experimental and theoretical investigations, in: 11th World Conf. Timber Eng. 2010, WCTE 2010, 2010: pp. 591–600.

[114] BSI, BS EN 14080:2013 Timber structures. Glued laminated timber and glued solid timber. Requirements, (2014). https://doi.org/10.3403/30236370.

[115] BSI, BS EN 1194:1999 Timber structures. Glued laminated timber. Strength classes and determination of characteristic values, (1999). https://doi.org/https://doi.org/10.3403/01544431.

[116] J. Köhler, J.D. Sørensen, M.H. Faber, Probabilistic modeling of timber structures, Struct. Saf. 29 (2007) 255–267. https://doi.org/10.1016/j.strusafe.2006.07.007.

[117] S. Arendt, M. Sutter, M. Breidenbach, R. Schlag, V. Schmid, Neue Forschungsergebnisse zu Nass-in-Nass geklebten Holz-Beton-Verbunddecken, Bautechnik 99 (2022) 56–65. https://doi.org/10.1002/bate.202200068.

[118] M. Shehada, Z.I. Djamaï, F. Duprat, Finite element modelling of adhesively bonded timber-concrete composite beams, Eur. J. Environ. Civ. Eng. 0 (2024) 1–20. https://doi.org/10.1080/19648189.2024.2340634.

[119] J. Kanócz, V. Bajzecerová, Timber - Concrete composite elements with various composite connections part 3: Adhesive connection, Wood Res. 60 (2015) 939–952.

[120] C.G. Chiorean, S.M. Buru, Practical nonlinear inelastic analysis method of composite steel-concrete beams with partial composite action, Eng. Struct. 134 (2017) 74–106. https://doi.org/10.1016/j.engstruct.2016.12.017.

[121] J. Lee, G.L. Fenves, Plastic-Damage Model for Cyclic Loading of Concrete Structures, J. Eng. Mech. 124 (1998) 892–900. https://doi.org/10.1061/(asce)0733-9399(1998)124:8(892).

[122] J. Lubliner, J. Oliver, S. Oller, E. Oñate, A plastic-damage model for concrete, Int. J. Solids Struct. 25 (1989) 299–326. https://doi.org/10.1016/0020-7683(89)90050-4.

[123] S.E. Yamada, C.T. Sun, Analysis of Laminate Strength and Its Distribution, J. Compos. Mater. 12 (1978) 275–284. https://doi.org/10.1177/002199837801200305.

[124] A.M.P.G. Dias, J.W. Van de Kuilen, S. Lopes, H. Cruz, A non-linear 3D FEM model to simulate timber-concrete joints, Adv. Eng. Softw. 38 (2007) 522–530. https://doi.org/10.1016/j.advengsoft.2006.08.024.

[125] A. Zona, M. Barbato, M. Fragiacomo, Finite-Element Model Updating and Probabilistic Analysis of Timber-Concrete Composite Beams, J. Struct. Eng. 138 (2012) 899–910. https://doi.org/10.1061/(asce)st.1943-541x.0000509.

[126] B. Kawecki, J. Podgórski, Numerical model of glulam beam delamination in dependence on cohesive strength, AIP Conf. Proc. 1922 (2018). https://doi.org/10.1063/1.5019059.

[127] A. Demir, H. Ozturk, K. Edip, M. Stojmanovska, A. Bogdanovic, Effect of Viscosity Parameter on the Numerical Simulation of Reinforced Concrete Deep Beam Behavior, Online J. Sci. Technol. 8 (2017) 50–56. https://www.tojsat.net/journals/tojsat/articles/v08i03/v08i03-09.pdf.

[128] H. Eslami, L.B. Jayasinghe, D. Waldmann, Nonlinear three-dimensional anisotropic material model for failure analysis of timber, Eng. Fail. Anal. 130 (2021) 105764. https://doi.org/10.1016/j.engfailanal.2021.105764.

[129] D. Čizmar, D. Damjanović, K. Pavković, V. Rajčić, Ductility analysis of laminated timber beams of small section height, J. Croat. Assoc. Civ. Eng. 66 (2014) 395–406. https://doi.org/10.14256/JCE.874.2013.

[130] C. Sandhaas, A.K. Sarnaghi, J.W. van de Kuilen, Numerical modelling of timber and timber joints: computational aspects, Springer Berlin Heidelberg, 2020. https://doi.org/10.1007/s00226-019-01142-8.

[131] R. Gutkowski, K. Brown, A. Shigidi, J. Natterer, Laboratory tests of composite wood-concrete beams, Constr. Build. Mater. 22 (2008) 1059–1066. https://doi.org/10.1016/j.conbuildmat.2007.03.013.